ANALYSIS, DESIGN OPTIMIZATION AND VIBRATION SUPPRESSION OF SMART LAMINATED BEAMS

Abolghassem Zabihollah

A Thesis

in

The Department

Of

Mechanical and Industrial Engineering

Presented in Partial Fulfillment of the Requirements

For the Degree of Doctor of Philosophy at

Concordia University

Montreal, Quebec, Canada

August 2007

Your file Votre référence
ISBN: 978-0-494-31133-2
Our file Notre référence
ISBN: 978-0-494-31133-2

ABSTRACT

Analysis, Design Optimization and Vibration Suppression of Smart Laminated Beams

Abolghassem Zabihollah, Ph.D.

Concordia University, 2007

A general frame work is developed for the sensitivity analysis and design optimization of smart laminated composite beams with capability to suppress the vibration under random excitations. The smart structure consists of a host laminated composite beam with embedded/surface bonded piezoelectric sensors/actuators. A layerwise displacement model including the electro-mechanical coupling is utilized to account for the strong inhomogeneities through the thickness and to develop the finite element model. To perform the sensitivity analysis of the smart structure for different design parameters, analytical gradients based on developed layerwise finite element model for both static and dynamic problems are proposed. The developed sensitivity gradients provide an efficient way to predict the behavior of responses of smart structure without re-analysis.

A design optimization algorithm based on developed analytical gradients and layerwise finite element model is then developed to determine the optimal design of the smart laminated beams for a variety of objective and constraints functions, including inter-laminar stresses, weight and natural frequencies.

The smart laminated beam design based on the developed optimization algorithm is used in the dynamic analysis and vibration control. An optimal control strategy, Linear Quadratic Regulator (LQR) is used to design the feedback control gain and to control the vibration response of system under deterministic loads. Effects of laminate configuration and sensor/actuator location are investigated in controlled response. An in-house experimental set-up is designed to demonstrate the performance and functionality of the proof-of-concept of smart composite beam. In many practical applications, including aerospace and automotive industries, smart laminated structures are exposed to random loading, considering this, an optimal control algorithm is developed to suppress the vibration response of the smart beam under random excitations. Different types of random loadings, including Gaussian white-noise, band limited and narrow-band excitations are investigated.

ACKNOWLEDGEMENTS

I would like to express my appreciation to my supervisors, Dr. Ramin Sedaghati and Dr. Rajamohan Ganesan for their guidance and supports. Advises I received from my supervisors concerning the scope and direction of this dissertation have been invaluable. The faculty members of the department of mechanical and industrial engineering, in particular, my committee members also deserve my sincere thanks.

I owe the biggest debt of gratitude to my wife. Her understanding, love, and companionship have allowed me to preserve and flourish during this time. It is to her that I would like to dedicate this dissertation, with love.

TABLE OF CONTENTS

NOMENCLATURE

Latin symbols	Nomenclature
C_{ij}	Material elasticity coefficients
$\overline{Q}_{ij}$	Plane stress-reduced stiffness
E_i	Young's moduli in i direction
G_{ij}	Shear moduli in the ij plane
ν_{ij}	Poisson's ratio
u	Displacement in x-direction
w	Deformation in the thickness direction
b	Width of the beam
f_j	Body forces per unit volume
D_i	Electrical displacement
Q	Electrical charge applied on the surface
$[\bar{e}]$	The transformed piezoelectric coupling matrix
$[\bar{g}]$	The transformed permittivity matrix
h	Height of the beam
l	Length of the beam
T	Kinetic energy
U	Strain energy
$[q]$	Modal matrix
$[K]$	Stiffness matrix
$[C]$	Damping matrix

$[M]$	Mass matrix
$\{F\}^e$	Element force vector
N	Total number of plies in the laminate
$\{E\}$	Electric field vector
d_{ij}	Piezoelectric constant
$R_X(\tau)$	Autocorrelation function
$R_{X_1X_2}(\tau)$	Cross-correlation function
$S_X(\omega)$	Spectral density
$S_{X_1X_2}(\omega)$	Cross-spectral density
n_p	Number of piezoelectric layers in the laminate
$V^{(k)}$	Applied voltage
F^P	Bending force due to the piezoelectric actuator

Greek symbols	**Nomenclature**
σ_{ij}	Stress components
ε_{ij}	Strain components
θ	Angle between fiber orientation and the reference axis
ρ	Density
ψ	Electric potential
Φ	Interpolation functions though the thickness
$\varphi_i(x)$	Interpolation functions along the length

$\{\eta\}$	Modal coordinates
ξ	Damping coefficient
ω	Natural frequency
μ_X	Mean-value

Math symbols	**Nomenclature**
[ ]	Matrix
{ }	Vector
| |	Determinant

LIST OF FIGURES

LIST OF TABLES

CHAPTER 1

INTRODUCTION AND LITERATURE REVIEW

1.1 Motivation

Recent advances in design and manufacturing of laminated composite structures have greatly enhanced the use of these novel structural materials in various applications, including aerospace, automotive and civil industries. Laminated composite materials offer great potential advantages compared to their standard metallic counterparts, including high strength-to-weight ratio, high corrosion and impact resistance, and excellent fatigue strength. Today, laminated structures are being widely used in satellite, aircraft components, automotive construction, helicopter blades, marine constructions, and civil structures. Excessive vibration in these structures may result in instability and/or poor functionality of the system and consequently may lead to uncomfortable environment, structural fatigue and unpredicted failure. In order to control the stability and enhance the functionality of the laminated structures during operation, conventional laminated composite structures can be combined with sensing and actuating capabilities of piezoelectric materials and a controller, to create a novel type of structural elements, so called, *smart laminated structures*. These structures have the capability to adapt their response to external stimuli such as load or environmental changes. These new structures have opened new challenges in research communities. Contrary to the conventional isotropic materials, laminated composites can be tailored according to desired

performance and functionality. Combining electrical effects and mechanical fields increase the number of parameters to be considered in design and manufacturing of laminated smart structures, requiring a robust optimization algorithm for the design optimization of the system.

The potential of using piezoelectric elements for vibration control of metallic structures has been demonstrated in variety of experiments. However, the use of piezoelectric element for vibration suppression in laminated composite structures is limited to simple cases. There are many issues, which require to be resolved to make realistic smart laminated structures with suitable sensing and actuation capability to achieve the desired response.

Further, in many applications such as aerospace and automotive, the structural elements are under random loading. Therefore, it is extremely important to investigate the functionality of these novel smart systems under stochastic excitations and also determine the optimum location of actuators and sensors for optimal performance.

In the following sections, a brief introduction and literature survey of different aspects of the present subject are provided in systematic way. The literature survey is limited to available works in English that were mainly presented in the last two decades.

1.2 Composite Materials

Development of composite materials is one of the great technological advances of the last half of the twentieth century. Composites refer to materials created by the synthetic assembly of two or more organic or inorganic components, in order to obtain specific characteristics and properties such as high directionable strength, high mechanical modulus and low weight. Selected materials to create a composite material are a reinforcing component and a compatible matrix binder. Composite materials are usually subdivided into the following classes according to the structural constituents: (i) laminar: composed of layers or laminar constituents; (ii) particulate: the dispersed phase consists of small particles; (iii) fibrous: the dispersed phase consists of fibers; (iv) flake: the dispersed phase consists of flat flakes.

Fiber reinforced composites are the most common materials used in aerospace, construction and automotive industries. In fibrous composite materials, the fibers provide virtually all strength and stiffness while the matrix is to bind the reinforcements together and keep them in proper orientation, to transfer the load to and between them and distribute it evenly, to protect the fibers from hazardous environments and handling, to provide resistance to crack propagation and damage, to provide all the inter-laminar shear strength of the composite, and to offer protection from high temperature and corrosion. The key point behind the fibrous composite is that the individual fibers are stiffer and stronger than the same material in bulk form whereas matrix materials have their usual bulk-form properties . By changing the orientation of the fibers, we can optimize the composite material for strength, stiffness, fatigue, heat and moisture resistance. Fiber

reinforced composite materials for structural applications are often made in the form of a thin layer, which is called *lamina.*

The structural elements, such as bars, beams and plates are made by stacking together several plies of fiber reinforced layers in different or similar angles to achieve the desired properties. The different layers of lamina are permanently bonded together usually by the matrix material under heat and pressure using a hot press, vacuum bag or autoclave[1].

1.3 Smart Materials and Technology

Smart materials may be defined as the materials which adapt themselves to respond to environmental changes. In the following, some of the most common smart materials are introduced and their advantages and disadvantages as sensing and actuating elements in laminated composite structures are reviewed.

1.3.1 Electrostrictive materials

Electrostrictive materials such as lead magnesium niobate compounds (PMN) and lead-titanate enriched lead magnesium niobates (PMN-PT) deform when exposed to an electric field. Electrostrictive materials are lightweight and can generate relatively significant strain when used as actuators. These materials have potential applications in micropositioners, deformable mirrors, precision laser systems and tools[2]. Electrostrictive materials have been used in adaptive optic systems, scanning tunneling microscopes and precision micropositioners[3].

Yang *et al*[4] designed a smart cantilever structure with self-sensing and self-actuating capability for vibration control using PMN-PT. However, due to the temperature-dependent nature, Electrostrictive materials have limited application in aerospace applications, including laminated composite structures.

1.3.2 Magnetostrictive materials

Magnetostrictive materials such as Terfenol-D change their shape when subjected to an applied magnetic field. Potentially, sensing can also be accomplished by measuring the variation in magnetic field resulting from changing the shape. However, due to the excellent capability of generating strains and forces, magnetostrictive materials are commonly used as actuators in many applications, including, ultrasonic transducers, positioners, sonar projectors and vibration control[5]. Magnetostrictive transducers are relatively heavy compared to piezoelectric materials, which limit their application in laminated structures, since they can significantly alter the passive dynamics of the system[6].

1.3.3 Electrorheological fluids

Electrorheological (ER) Fluids are characterized by a considerable variation of their rheological behavior when subjected to external electric fields[7]. In the absence of an electric field, the strain rate of ER fluids is directly proportional to the applied stress. Application of an electric field may significantly increase the viscosity, damping capability and shear strength of ER fluids. This characteristic makes ER fluids attractive

for providing a rapid response interface in controlled mechanical devices. Kamath and Werley[8] utilized ER fluids to design an active damping mechanism.

ER fluids have some shortcomings such as low yield strength, low operating temperature range, high operating voltage and intolerance of common impurities (such as water) picked up during manufacturing or use. In addition, modeling of ER fluids is difficult since the interdisciplinary understanding of rheology and dielectric is required to develop an accurate model of the system.

1.3.4 Magnetorheological fluid

Magnetorheological (MR) fluids are a class of new intelligent materials whose rheological characteristics change rapidly and can be controlled easily in the presence of an applied magnetic field[9]. They are stable suspensions of noncolloidal very fine ferromagnetic particles in an insulating carrying medium exhibiting controllable rheological behavior in the presence of applied magnetic field. MR fluids have been utilized in various applications, including, dampers, brakes and clutches, polishing devices, hydraulic valves, seals, and flexible fixtures. Recently, the application of MR fluids in vibration control has been attracted by many researchers[10]. However, due to the nature of MR fluids, it is very difficult to integrate them with thin laminated composite structures.

1.3.5 Shape memory alloys

Shape memory alloys (SMAs) are a class of metal compounds which posses the capability of sustaining and recovering relatively large strains, approximately ten percent, without undergoing plastic deformation. Nickel-titanium alloy (Nitinol, Ni: Nickel, ti: titanium, nol: Noval ordnance Laboratory) and copper zinc aluminum (CuZnAl) alloys are commercial examples of SMAs. These materials possess many potential applications in aerospace and automotive industries as fire detector, sensors/actuators in air conditioners, etc.

SMAs materials have slow response time compared to other smart materials, for example, while electrical heating sources allow the materials to respond within seconds, cooling often takes on the order of minutes. In addition, relatively high energy is required for actuating shape memory alloys, and the effects are very limited to a certain thermal range, requiring very precise actuation[1]. Thus, SMAs materials are not good candidates to be used in laminated structures for vibration control.

1.3.6 Piezoelectric materials

In 1880, Pierre and Jacques Curie observed that a piezoelectric material generates an electric voltage when stressed mechanically, called *direct effect*. Gabriel Lippman predicted, a year later[11] , that piezoelectric materials change dimensions when subjected to an applied voltage, called *converse effect*. This observation indicated that piezoelectric materials, potentially, can be used as sensors and actuators. The piezoelectric effect is a property that exists in many materials. The name is made up of two parts; piezo, which is

derived from the Greek word for pressure, and electric for electricity. The rough translation is, therefore, pressure - electric effect.

Natural crystals, such as quartz, Rachelle salts, tourmaline and lithium sulfate, were the first known and commercially used piezoelectric materials. A quartz transmitter was used for sonar application in 1916[12].

In 1940s it was discovered that the ceramic materials such as barium titanate could be induced to exhibit piezoelectric properties. Today, Piezoceramic of lead Zirconate Titanate (PZTs) and piezopolymers of PolyVinyliDene Fluorides (PVDFs) are the most common piezoelectric materials[13], being widely used in commercial applications. Piezopolymers are used mostly as sensors because they require extremely high actuating voltage whereas piezoceramics are extensively used both as sensors and actuators, since they require lower actuating voltages and are used for wide range of frequencies.

It should be noted that these ceramics are not actually piezoelectric but rather exhibit a polarized electrostrictive effect. A material must be formed as a single crystal to be truly piezoelectric. Ceramic is a multi crystalline structure made up of large numbers of randomly orientated crystal grains. The random orientation of the grains results in a net cancellation of the effect. Thus, the ceramic must be polarized to align a majority of the individual grain effects. Today, the term piezoelectric has become interchangeable with polarized electrostrictive effect in most literature[10]. Piezoelectric ceramic materials, as stated earlier, are not piezoelectric until the random ferroelectric domains are aligned.

This alignment is accomplished through a process known as *poling*. Poling consists of inducing a D.C. voltage across the material (See Figure 1.1). The ferroelectric domains partially align to the induced field resulting in macroscopic polarization, which facilitate the electromechanical coupling. The number of domains that align depends upon the poling voltage, temperature, and the time the voltage is held on the material. During the poling, the material permanently increases in dimension between the poling electrodes and decreases in dimension parallel to the electrodes. Thus, due to this coupling, piezoelectric materials will deform when exposed to an electric filed, actuation, or sense mechanical stresses by measuring the variation of electric field due to dipole rotations[14]. The material can be depoled by reversing the poling voltage, increasing the temperature beyond the material Currie point, or by inducing a large mechanical stress.

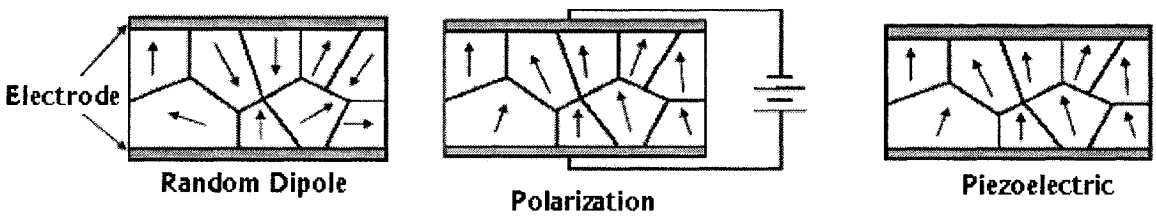

Figure 1.1 Creating piezoelectric from piezoelectric ceramic[12]

Piezoelectric materials have exhibited many advantages compared to other smart materials, particularly for dynamic application. They have linear behavior at low electric field (~300 volts), and show very low sensitivity to temperature when employed below transition temperature, called *Curie temperature*. The variation of piezoelectric strain tensor of a standard piezoceramic material under a constant load is less than 12 percent over a temperature range of 120 ^{o}C[15]. These characteristics are very crucial when

piezoelectric materials are used in designing control systems. In addition, PZTs have rigidities comparable to many host structures, including Graphite/Epoxy laminates. Moreover, the dual piezoelectric properties of PZTs patches provide the potential of being used as self-sensing actuators. For sensing applications, mainly PVDFs patches which are available as thin plastic wrap and can be bonded to almost any geometry are used.

Over the last decade piezoelectric materials have found numerous applications ranging from car cigarette lighter, airbag, sensor and microphone to advanced applications as in active fight control[16,17], and Micro Electro Mechanical Systems (MEMS)[18]. Piezoelectric accelerometers are perhaps one of the most common applications of PZTs used in vibration experiments. Piezoelectric materials have been used as smart elements for shape control[19], wave generators[20] and crack detection in laminated composite structures[21]. Prasad *et al*[22] provided some criteria to select piezoelectric materials for smart structures with emphasis on shape control. They also presented some typical applications of piezoelectric materials.

1.3.7 Smart Piezo-laminated structures

Smart laminated structures are created by surface bonding or in situ embedding[23] the piezoelectric patches to the conventional laminated structures. The structure, is then equipped with a controller to create a smart system (See Figure 1.2). The controller is designed to analyze the feedback response from the sensors to command the actuators to

apply localized actuations to alter the system response and control the response of the structure.

The development of smart laminated composite structures using piezoelectric materials may further improve the performance and reliability of the laminated structure.

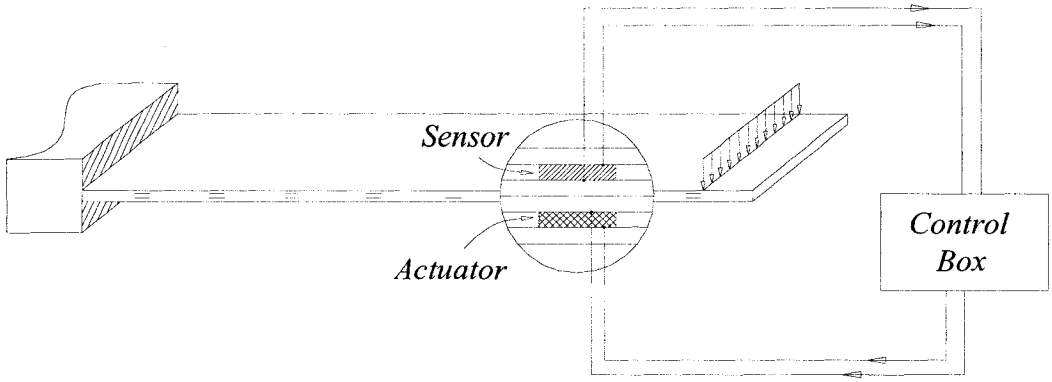

Figure 1.2 Schematic illustration of a smart laminated composite beam

These novel smart composite structures will combine the superior mechanical properties of conventional composite materials, and incorporate the additional inherent capability of piezoelectric layers to sense and adapt their static and dynamic response.

These advanced laminated structures potentially have the capability to compensate the thermal and humidity effects and random loading conditions on structures as well as sense any unpredicted behavior like delamination[24,25] and possibly somehow adapt themselves to perfectly respond to the unforeseen environmental conditions. Smart laminated structures can be designed to actively react to disturbance forces in order to

maintain structural integrity while maintaining or even improving the level of performance.

1.4 Modeling of Smart Laminated Structures

With emerging use of smart laminated structures in aerospace, automotive and civil engineering applications, it is required to develop reliable mathematical tools for the analysis of interaction between induced strain in piezoelectric materials and the composite host structures[26]. The mathematical model should be accurate and computationally efficient as well as capable to account for the electromechanical coupling effects in the structure. In addition, the model should also account for the inhomogeneities in the structure, particularly through the thickness due to application of different materials and geometries in the system.

Various theories, including, Equivalent Single-Layer (ESL) theories, three dimensional and layerwise theories have been developed for the analysis of laminated composite, mainly by improvement of the plate theories. In the following section, the most common mathematical models developed for the analysis of laminated structures integrated with smart materials, particularly piezoelectric materials, are presented.

1.4.1 Equivalent Single-Layer theories (ESL)

The ESL theories assume continuous displacement through the thickness of the laminate. The displacement fields for commonly used ESL theories, Classical Laminated Plate

Theory (CLPT) and First-order Shear Deformation Theory (FSDT) are shown in Figure 1.3.

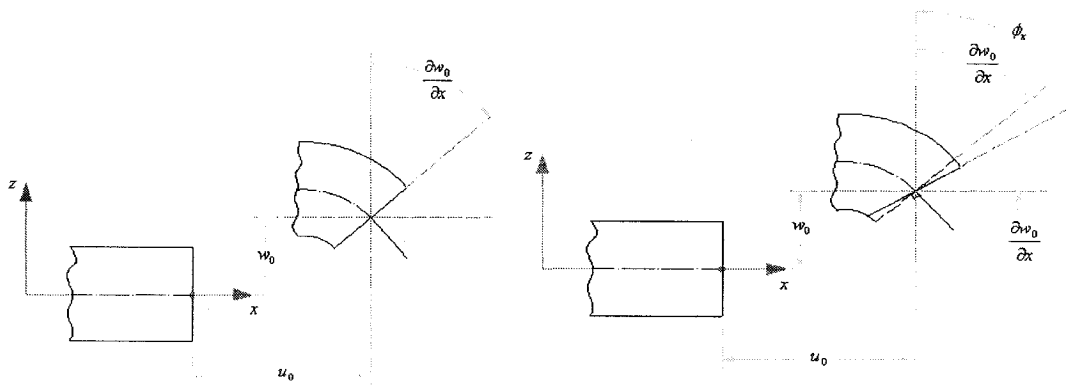

Figure 1.3 Deformation of a transverse normal according to (a) CLPT, (b) FSDT

CLPT theory is based on the Kirchhoff assumption stipulating that the in-plane transverse normal before deformation remains normal after deformation, i.e. the effect of shear deformation is neglected. FSDT is similar to Mindlin theory for isotropic materials and it is defined based on a linear distribution of the in-plane normal and shear stresses over the thickness. Higher-order theories are mainly based on parabolic distribution of transverse shear stress across the plate thickness. In these theories, the material properties of the constituent layers are combined to form a hypothetical single layer whose properties are equivalent to through-the-thickness integrated sum of its constituents. This category of theories has been found to be adequate in predicting global response characteristics of laminates, like maximum deflections, maximum stresses[27,28], fundamental frequencies[29], or critical buckling loads[30].

However, due to simplicity of ESL theories, smart laminated structures have been modeled in the existing works mainly based on ESL theories[31]. Edery-Azulay and Abromovich[32] developed a closed-form solution to investigate the actuation and sensing mechanisms of a shear piezoelectric layer embedded in composite laminated beams for quasi-static deflection. They derived a closed-form solution based on the first-order shear deformation theory for the static deflection of a laminated beam with embedded piezoelectric layers as continuous or distributed patches.

Lee *et al*[33] discussed the transient response of laminated plate with embedded piezoelectric layers using ESL theories. They also investigated the effects of lamination orientations, and piezoelectric position on the vibration response. Reddy[34] developed a finite element formulation for laminated composite plate integrated with sensors and actuators using the most common ESL theories namely, CLPT, FSDT and third-order shear deformation theory (TSDT). The work was basically limited to only actuator mode of piezoelectric. Ghosh and Batra[35] used piezoelectric layers to control the geometric shape of a symmetric laminated plate based on the FSDT. The work also dealt with only the actuation mode of piezoelectric materials. Ray *et al*[36] derived the closed-form solutions for deflection of a simply supported rectangular plate with distributed piezoelectric layers attached on top and bottom surfaces of the plate under sinusoidal loading.

Finite element formulation for laminated composite plates with distributed sensors and actuators has been presented in a few publications[37,38,39]. Suleman and Venkayya[40]

applied CLPT and variational principles to present a finite element formulation for laminated plate with piezoelectric layers. The work was limited to actuation mode of the piezoelectric materials. Ray *et al*[41] extended the application of finite element method in smart structures by considering higher-order shear deformation theory to evaluate the static deflection of laminated composite rectangular plate with PVDF layers. Higher-order theories have been used for analysis of laminated plates with piezoelectric sensor/actuator by Chattopadhyay *et al*[42]. They relaxed the limitation of location of the smart layers by implementing distributed PVDF layers through the thickness. Donthireddy[43] used piezoelectric actuators to control the shape of a laminated beam under static loading based on FSDT. Benjeddou *et al*[44] obtained a closed-form solution for the free vibration of laminated composite plate with bonded piezoelectric layers on top and bottom using FSDT theory. Thirupathi *et al*[45] used a quadri-lateral piezo-laminated shell element with eight nodes to model static deflection of turbine blades. Fernandes and Pouget[46] proposed a model for the displacement analysis of laminated structures using CLPT. They considered the electric potential as a function of thickness coordinates. Combining linear and parabolic distribution in thickness direction for the electric potential, Krommer[47] provided a mathematical model for vibration analysis of laminated beam with embedded piezoelectric layers using CLPT. Yang[48] improved this model by implementing FSDT to determine natural frequencies of the structure.

Knowing that, in general, the values of stiffness of the adjacent layers in the laminates are not equal, continuity of displacement through the thickness, as stated by ESL theories,

results in discontinuity in transverse stress through the thickness, which is contrary to the equilibrium of the inter-laminar stresses as shown in Figure 1.4.

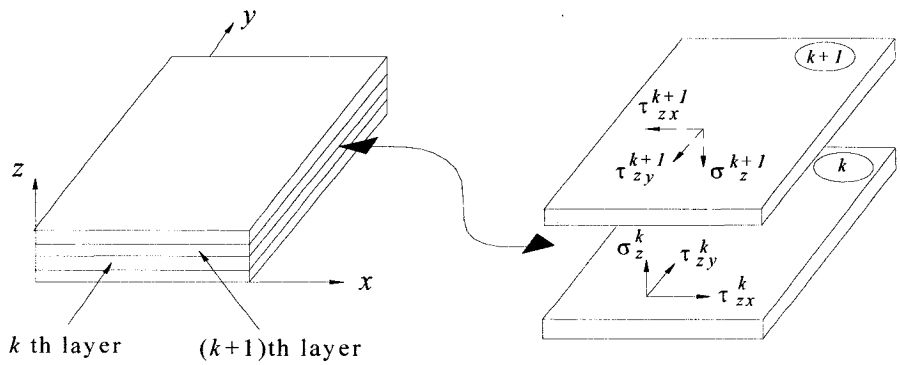

Figure 1.4 Inter-laminar stresses in the laminate

In general, ESL theories provide acceptable results for relatively thin laminate. For thick laminate and laminate with material and/or geometric inhomogeneities, the ESL theories lead to erroneous results for all stresses[49]. In addition to the limitations of ESL theories, it has been indicated that in laminated structures, the presence of inter-laminar stresses near the free edges are significant which may not accurately be determined by ESL theories[50].

Moreover, in smart laminated structures, due to the material and geometric inhomogeneities through thickness, it is required to acquire an accurate evaluation of strain-stress at ply level. The occurrence of inter-laminar stresses at the geometric boundaries such as free-edges, cut-outs, notches, and holes is an important phenomena since high concentration of these stresses may result in delamination cracks at these locations which reduces the strength and stiffness and thus may limit structural life. Inter-laminar stresses can lead to delamination and failure of the laminate at loads that are

much lower than the failure strength predicted by the ESL theories[48]. Accurate determination of the stress state through the thickness of the laminate is therefore, crucial to correctly describe the structural behavior and to prevent it from unpredicted failure. The accurate modeling of inter-laminar stress field in composite laminates requires the displacement field to be piecewise continuous through the thickness direction. This can be achieved by using a three-dimensional model[51,52,53,54] which is computationally expensive. Another alternative is to construct mathematical models based on continuous displacement for each individual layer through the thickness, namely, layerwise displacement model.

1.4.2 Layerwise displacement theories

Reddy[55] developed a layerwise theory based on the piecewise displacement through the laminate thickness. This theory was later modified and improved by him and his collogues to apply for plate bending[56] and buckling[57] analyses. Free vibration analysis of laminated plates has been investigated by layerwise theory in the work done by Nosier *et al*[58]. Layerwise theory has been combined with ESL theories to improve the accuracy of the model for moderately thick layers. Davalos *et al*[59] applied a similar mixed layerwise model for static analysis of laminated beams. Similar model has also been used by Carrera[60] for the analysis of laminated composite plate. Davalos *et al*[61] applied the mixed layerwise theory developed by himself and his co-workers[62] to analyze a plane frame with rectangular laminated sections. Carrera[63] developed a layerwise model by considering an *n*-order expansion for displacement at each ply through the thickness in

order to satisfy the continuity of displacements, transverse shear and normal stresses at the interfaces between consecutive layers.

Kadivar and Samani [64] used layerwise theory to investigate the free vibration of a rotating thick laminate with simply supported boundary conditions. Koo[65] investigated the effects of layerwise in-plane displacements on fundamental frequencies for laminated composite plates. Tahani and Nosier[66] applied layerwise theory to determine the inter-laminar stresses in a rectangular cross-ply laminated plate under pure bending. The work was limited to simply supported boundary conditions. Tahani and Nosier [67] later used the theory to investigate the inter-laminar stresses near the free edges of a cross-ply simply supported laminated plate due to axial extensional loading. David[68] developed a two-dimensional plate theory for the analysis of multilayered piezoelectric plates. This theory was based on a hybrid approach in which the continuity of both mechanical and electrical variables at layer interfaces is satisfied. The proposed model required higher computation compared to the displacement layerwise theory.

Laminated beams with surface bonded/embedded piezoelectric sensor/actuator patches are the specific structures that the accurate calculation of inter-laminar stresses (particularly near free edges) directly affects the functionality of the structure. Exceeding the inter-laminar stresses at these locations may break the bonding between sensor/actuator and composite layer and thus result in the loss of the main functionality, namely, sensing and actuating capability of the smart laminate. Analysis of smart laminated structures requires a mechanics with capability to address the local through-

the-thickness effects, such as the evolution of complicated stress-strain fields in smart composite and interfacial phenomena between the embedded micro-devises and passive composite plies[69]. In attempt to consider the inter-laminar stresses in smart laminated plate, Gao *et al*[70] developed a three dimensional model for the vibration analysis of laminated composite plate with piezoelectric layers. However, the proposed model, like other three-dimensional models, required higher computational effort compared to layerwise models.

In spite of the material (i.e. piezoelectric and composite) and geometric (i.e. discrete patches, bonded/embedded) inhomogeneities in smart laminated composite, very limited works have been reported in the open literature for the analysis of smart laminated structures using layerwise theory and many aspects still remain unexplored. Robbins and Reddy[71] improved the analysis of smart laminated structures by utilizing layerwise displacement theory to investigate the static and dynamic interactions between the piezoelectric actuator and the host laminated beam. The layerwise formulation has the capability to address local through-the-thickness effect, such as the evolution of complicated stress-strain fields in smart composite structures and interfacial phenomena between the embedded micro-devices and passive composite plies in a smart laminate. Due to its excellent capabilities, accuracy and computational efficiency, layerwise formulation has been used by many researchers for a variety of applications.

Donthireddy[72] applied the theory to develop a finite element model for shape control of a composite beam by applying electric potential to piezoelectric actuators. Han and Lee[73]

applied layerwise theory to analyze the free vibration of laminated plate with piezoelectric actuators. Saravanos and Heyliger[74] investigated the effect of electro-mechanical response of piezoelectric sensors and actuators on static deflection of laminated composite beams. Saravanos *et al*[75] investigated the free vibration response of laminated plates with embedded sensors and actuators. Lee and Saravanaos[76] extended this work to incorporate thermal effects for the complete mechanical, electrical, and thermal coupling response of composite beams. This study again was limited to the actuating mode of the piezoelectric materials. They concluded that limited thermal effects could be compensated by applying electrical fields through the piezoelectric. Most recently, Garcao *et al*[77] applied the layerwise theory for vibration analysis of smart laminated plate in actuating mode. This study illustrated the importance of the approximation functions in thickness direction in the accuracy of the results. They provided a comparison between different approximation functions along the thickness direction for static problems. Sunar *et al*[78] developed a finite element model for a smart plate with one piezoelectric layer at the bottom and one magnetoceramic layer at the top to investigate the effect of both electrical as well as magnetic fields in the analysis.

Robbins and Reddy[79] combined the FSDT and layerwise displacement to analyze laminated structures with integrated sensors and actuators. This model was appropriate when each individual layer thickness is relatively thick. Kapuriaet *et al*[80] proposed a one-dimensional model based on FSDT and layerwise theory to approximate electric field though the thickness of laminated beams with piezoelectric elements. Thornburgh *et al*[81]

developed a higher-order formulation to analytically determine the transient response of laminated structures with piezoelectric elements.

One of the goals of the present dissertation is to develop an accurate and efficient finite element modeling of smart laminated beams using layerwise displacement theory with considering full electromechanical effects and interaction between electric potential and mechanical fields.

1.5 Design Optimization of Smart Laminated Structures

Design sensitivity analysis and optimization perhaps are two of the most practical and challenging issues in smart laminated structures due to existing large number of material and geometric parameters as well as loading conditions. The conventional design methodologies lead to very long and expensive procedures which sometimes make the design infeasible. Design optimization techniques have been used in smart laminated structures for various applications. Yan and Yam[82] used bending moment induced by piezoelectric actuator as objective function to determine the optimal thickness of piezoelectric actuators. Same approach was used by Barboni *et al*[83] to determine the optimal size and location of piezoelectric actuator.

The optimal size and location of piezoelectric actuators were determined by introducing a controllability index by Aldraihem *et al*[84]. Frecker[85] reviewed the most recent developments in the field of design optimization. The existing publications in design optimization of smart laminated beams are developed mainly based on ESL theories.

Chee *et al*[86] developed a heuristic algorithm based on ESL higher-order to determine the piezoelectric orientation for shape control of composite beams. In all these works, numerical methods such as finite difference technique have been generally used to determine the gradients of objective and constraints functions. Han and Lee[87] and Yan *et al*[88] employed the genetic algorithm to determine the optimal placement of piezoelectric elements in designing smart isotropic beams.

Design sensitivity analysis for the determination of the gradients of objective and constraints is a critical step in any design optimization procedures. Therefore, it is important to carry out an efficient design sensitivity analysis when the optimization algorithm is to be applied to large structural problems such as aircraft or problems with large number of parameters such as smart laminated structures. In addition, the design sensitivity analysis provides the trends of variation of the design parameters. Thus, it can be used by designer to change the preliminary design and reassess the mathematical model. Therefore, the structural sensitivity analysis can be more than a utility for optimization task and might be used as a useful design tool to evaluate the system response to changing parameters efficiently. Perhaps, parametric study is the most common approach to observe the sensitivity of each factor to desired parameters. Kassegne *et al*[89] applied this approach to investigate the sensitivity of a micro cantilever smart beam for MEMS applications. However, as a large number of parameters exist in smart laminated structures, a solid mathematical formulation for the sensitivity analysis in these structures is required.

Numerical methods are widely used by many researchers to determine the sensitivity gradients. However, in large structural problems and in problems with large number of design parameters, including smart laminated composite structures, numerical evaluation of gradients is computationally expensive. Therefore, efficient analytical evaluation of sensitivity gradients is required. Arora and Haug[90] presented the design sensitivity analysis in structural applications. Later, by progression of numerical methods in structural analysis, this technique was improved for discrete structural systems by Adelman and Haftka[91]. Sedaghati *et al*[92] developed an optimization algorithm using the analytical gradients to minimize the weight of the isotropic beam structures under frequency constraints.

Relatively very few works have been reported on the sensitivity analysis and the determination of the analytical gradients of smart laminated structures. Soares *et al*[93] developed the analytical gradients to be used in an optimization algorithm based on the higher-order finite element displacement theory. Liu and Begg[94] presented the analytical expressions for the design gradients of objective and constraints with respect to the continuous design variables.

To design smart laminated structures for dynamic environment, various factors and parameters should be taken into consideration, including size and locations of sensors/actuators, layer thickness and laminate orientation. This requires a robust design sensitivity analysis and optimization algorithm to determine the optimal design of the structure. Development of design sensitivity formulation and analytical gradients for

various constraints and objective functions in smart laminated composites is another important contribution of this study.

In the present work, the developed analytical gradients are combined with layerwise finite element model to formulate an accurate and efficient design optimization methodology to determine the optimal design of the smart laminated beam for various applications.

1.6 Dynamic Analysis and Vibration Control of Smart Laminated Structures

Smart laminated composite structures have been widely used for aerospace applications such as satellite, and aircraft wings and tails. Excessive vibration in these structures may result in instability and/or poor functionality of the system. Efficiency and accuracy of the dynamic and static responses of smart systems highly depend on the mathematical modeling of the structure and the control strategy. Thus, to achieve the desirable performance and functionality of the smart laminated systems, these two aspects should be thoroughly understood and accurately represented in the modeling. Dynamic analysis[95] and vibration suppression of isotropic structures has been investigated for variety of issues and using various control strategies[96,97].

Blanguernon *et al*[98] developed a piezoceramic element composed of a piezoelectric sensor, a viscoelastic damper and a piezoelectric actuator to control the dynamic response of isotropic beam. Effect of applied electric potential on piezoelectric patches on changing natural frequencies of structures integrated with piezoelectric element has been

investigated by Kim and Jones[99]. Sun and Tong[100] used the frequency response of a beam structure to detect the debonding piezoelectric elements during operation. Analytical studies on active control of isotropic structures using piezoelectric element have been validated by performing experimental works[101,102].

Research works on vibration control of laminated composite structures are very limited[103,104] and still there are many issues that remain unexplored. Liang and Batra[105] studied the effects of embedded piezoelectric patches on natural frequencies of laminated plates. Analysis and design of laminated structures for vibration control requires several aspects to be taken into account, including, modeling of host structures, selecting appropriate sensors and actuators, and designing control mechanism. The mathematical model of the host laminated structure perhaps is one of the most important factors in the efficiency and accuracy of the control mechanism.

Reviewing the available works on vibration control of laminated composite structures reveals that in most of the works, a negative velocity feedback is employed as the controller and the mathematical modeling of the laminated host structure has been performed based on ESL theories, including, classical lamination theory, first-order shear deformation theory[106,107] and third-order shear deformation theory[108,109]. Lim *et al*[110] presented active vibration control for sandwich structure using a three-dimensional finite element model. Analytical solution for active vibration control of laminated beam using damping layer has been studied by Bohua and Huang[111]. Lee *et al*[112] used the most common ESL theories to investigate the transient response of laminated composite structures. They also applied a velocity proportional feedback control for vibration

control purposes. Effect of fiber orientation on vibration control has been investigated by Lin and Nien[113] using a finite element model based on CLPT. This approach was demonstrated experimentally by Gaudenzi *et al*[114] who performed some experimental validation for vibration control based on the velocity feedback control. Chen *et al*[115] investigated the effect of piezoelectric elements on stability of a laminated beam under compression loading[116]. Sethi and Song[117] applied pole placement technique to determine the feedback control gain for vibration control of a composite I-beam with surface bonded piezoelectric sensors/actuators.

In an attempt to improve the efficiency of the smart system in vibration control, Reddy and Barbosa[118] developed a simplified third-order shear deformation theory and combined it with velocity feedback control. Correia *et al*[119] developed a model based on higher-order ESL to represent the mechanical displacement and a layerwise discretization through-the-thickness to represent the electrical behavior of the structure. However, delamination of piezoelectric element has significant effect on vibration control[120,121] requiring a layerwise displacement theory to accurately model the laminated structures for vibration control. Han and Lee[122] used layerwise theory to develop the modal form of laminated plates with piezoelectric actuators.

To design an optimal control mechanism, Linear Quadratic Regulator (LQR) is an efficient approach to determine the optimal feedback gain. In this approach, one may define appropriate weightings for applied voltage and geometry of actuators. In general,

higher weighting for applied voltage requires higher electrical energy and more expensive actuators. Similarly, higher weighting for geometry requires more actuators.

The optimal control based on LQR has been applied for vibration control of many isotropic structures[123]. Bruant *et al*[124] developed a finite element approach based on Kirchhoff's theory and LQR for vibration control of isotropic truss structures. This work was improved recently by Stavroulakis *et al*[125] who used Timoshenko beam theory and LQR theory to suppress the vibration of isotropic beams.

Yousefi-Koma[126] presented an analytical formulation for vibration suppression of isotropic aluminum cantilever beam based on LQR to determine the optimal feedback gain for full state control. Xu and Koko[127] investigated the vibration control of isotropic beam using LQR and commercial finite element software for the analysis of the host structure. Vibration control of sandwich beam using piezoelectric elements and LQR was studied analytically by Hwu *et al*[128]. Most recently, Vasques and Rodrigues[129] presented a comparison between classical and optimal feedback control strategies for beams made of isotropic materials with piezoelectric sensors and actuators.

In the open literature, the optimal control has not been utilized for laminated structures in general, and in particular the layerwise displacement theory has not been used for the mathematical modeling for vibration control. In the present work, optimal control strategy is developed based on a layerwise model to control the vibration of smart laminated beams. The analytical model is validated by performing experimental

investigations. In-house experimental set-up, consisting of a laminated beam integrated with PVDF sensors and piezoceramic actuator, voltage amplifier and controller is designed to demonstrate the functionality of the system and to validate the analytical model.

The vibration analysis of isotropic beams subjected to random excitations has been of considerable importance for several decades. The interest arises from two major sources of random excitations: earthquakes and wind loading on tall buildings, bridges, as well as random excitation on aerospace and automotive structures. The uncertainty in the environmental excitations results in uncertainty in the response behavior. Therefore, it is critically important, especially in aerospace structures, to realize the response of the structure under random external loading. For such sensitive applications, enhanced accuracy in response analysis is possible by modeling the problem with random external loading. The random vibration of elastic systems made of isotropic materials subjected to random loading has been widely discussed in literature[130,131,132,133]. Elishakoff and Zhu[134] developed an improved finite element formulation for isotropic beam subjected to random loading.

Fast growing interests in applications of smart laminated composite in aerospace and automotive structures, arise immediate need to investigate the vibration responses of these new structural systems under random loadings and develop accurate and efficient control strategy to control the dynamic response of smart laminated structures under unpredicted loading conditions. The research works on the influence of random

parameters in laminated composites have been mainly focused on material randomness like fiber orientation and volume fraction and thickness of lamina[135,136,137,138]. There are a large number of important cases when the exciting forces vary in an unpredictable random fashion. In many cases the input excitation is defined in a statistical sense, so that the structural response can also be known in a statistical sense[139]. However, vibration analysis of laminated structures under random excitations is very limited in the open literature and is mainly restricted to application of ESL theories for modeling the laminated structures. Cederbaum *et al*[143] investigated the random vibration of composite laminate using first-order shear deformation theory.

Lin[140] investigated the effect of random loading in buckling analysis of composite structures. Zibdesh and Abu-Hilal[141] discussed the vibration response of a simply supported isotropic beam coated by composite materials under random moving load. Frangopol and Recek[142] applied classical laminate theory to investigate the vibration response of laminated composite plates under random loading. First-order shear deformation theory and a narrow-band noise function have been applied for random vibration analysis of a symmetric cross-ply laminated beam by Librescu and Elishakoff[143] and Cederbaum *et al*[144]. Kang and Harichandran[145] developed a higher-order shear deformation formulation to analyze the vibration response of a laminated plate under random loading.

No specific study has been reported in the open literature to address the response of smart laminated composites under random loading. Therefore, one of the main objectives of the

present research is to conduct a study on the behavior of the smart laminated composite under random excitations.

1.8 Present Work

This work is generally aimed to establish a comprehensive framework for design optimization and vibration suppression of smart laminated structures under both deterministic and random external stimuli. In particular, this work 1) improve the design procedure of smart laminated beams through development of analytical sensitivity analysis and consequently design optimization algorithm, 2) demonstrate the functionality and performance of smart laminated beams under random excitations, 3) demonstrate controllability of smart laminated beams under random loading through designing a linear quadratic regulator controller to suppress the vibration response under random loadings and 4) validate and demonstrate the proof-of-the concepts by performing various open-loop and closed-loop experimental investigation on dynamic response and vibration control of smart laminated beams.

Specifically, the thesis contains the following important components and contributions:

❖ **Mathematical modeling**:

- Development of reliable mathematical modeling for smart laminated beam using layerwise displacement theory.
- Formulating the coupled electro-mechanical interaction between sensors/ actuators and host laminated structure.

❖ **Sensitivity and design optimization**:

- Development of optimization techniques to design smart laminate considering both sensory and actuator effects under different loading condition.
- The discrete analytical gradients of the various design constraints and objective functions with respect to various design variables are determined.
- By combining the developed coupled layerwise finite element model, the developed analytical gradients, and the Sequential Quadratic Programming (SQP) technique, an efficient design optimization algorithm has been developed.
- To determine the most accurate response of the structure, the effect of electro-mechanical coupling has also been taken into account.

❖ **Dynamic analysis of smart laminated beams**:

- In order to reduce the number of degrees of freedom for control purposes, the modal forms of the structural model and sensor and actuator are developed.
- Free vibration response of smart laminated beams is formulated for modal vibration and validated with experimental works.

❖ **Vibration suppression**:

- Linear Quadratic Regulator (LQR) is applied to obtain the optimal control feedback gain.
- To demonstrate the advantages of the present algorithm on dynamic response of smart laminated beams, conventional active control of smart laminated structures based on the classical laminate theory and classical control strategies are also investigated and the results are compared with present algorithm.
- Vibration response under random loading has been studied.

- A control algorithm to suppress the vibration response of the beam under random loading is developed.

❖ **Experimental investigations**:

- A laminated beam with piezoelectric actuator and PVDF sensor is designed and manufactured to investigate the dynamic response of the structure.
- A control algorithm is designed according to LQR controller and implemented in LABVIEW 7.0.
- Experimental investigations for open-loop and closed-loop response of laminated beams with integrated piezoceramic actuator and PVDF sensor are presented.

1.9 Dissertation Organization

The present chapter is aimed to present the motivation and objective of the work, a brief and comprehensive introduction of the concepts and terminologies, and review of the recent pertinent works in the field.

Coupled layerwise finite element modeling of laminated beam integrated with piezoelectric sensors/actuators is developed in Chapter 2. First, the fundamental and governing equations of laminated structures with piezoelectric elements are presented. Then, the displacement field according to layerwise theory is introduced and followed by the variational expression, electromechanical coupling effects and finite element modeling of laminated beam with integrated piezoelectric sensor and actuators. The analytical results are presented to demonstrate the capabilities of the developed model.

Sensitivity analysis of smart laminated beam for static and dynamic applications is presented in Chapter 3. First, the formal sensitivity analysis of the smart laminated beam is presented. Then, the analytical gradients of constraints and objective functions are provided to improve the efficiency and accuracy of the sensitivity analysis.

Chapter 4 dealt with the design optimization of smart laminated beams. The sensitivity analysis and analytical gradients developed in the previous chapter are integrated in Sequential Quadratic Programming (SQP) technique to determine the optimal design of the smart laminated structure under various constraints and objective functions.

Chapter 5 is devoted to vibration control of smart laminated beam under deterministic loadings. Classical and optimal control strategies are developed to actively control the vibration response of the smart laminated beam. The simulation results are then validated by performing an in-house experimental testing to demonstrate the performance and functionality of the developed smart system in real and practical applications.

Vibration suppression of smart laminated beam under random loading is investigated in Chapter 6. The response of the smart system under variety of random excitations, including Gaussian white noise, band limited noise and narrow-band excitation, are studied.

To conclude, a summary of work and major contributions of the dissertation and recommendations for future works are presented in Chapter 7.

CHAPTER 2

ANALYSIS OF SMART LAMINATED BEAMS USING LAYERWISE THEORY

2.1 Introduction

Laminated composite structures with surface bonded/embedded piezoelectric layers are a part of the new generation of adaptive structures. The sensing and actuation capability of piezoelectric layers may further improve the performance and reliability of the laminated structure. These novel smart structures will combine the superior mechanical properties of conventional composite materials, and incorporate the additional inherent capability of piezoelectric layers to sense and adapt their static and dynamic response. Implementing sensing and actuating capabilities leads to strong inhomogeneities through the thickness of smart laminated structures. However, most of existing analytical models are based on Equivalent Single Layer (ESL) theories and use approximate strains through the thickness of the laminate. This approximate representation fails to provide accurate prediction of actuator forces and sensor voltage. In general, ESL theories are inaccurate for both thick laminates and laminates which contain strong inhomogeneities through-the-thickness.

This chapter is devoted to the analysis of laminated composite beams integrated with piezoelectric materials as sensing/actuating elements based on the layerwise displacement theory. Implementing the layerwise approximation through the thickness diminish the limitation of ESL theories and leads to more accurate analysis of smart laminated structures. First, the background concepts of piezoelectric materials are reviewed and then, layerwise approximations for displacement and electric potential are utilized to construct the finite element model for laminated beams integrated with both sensors and actuators as smart elements as shown in Figure 2.1.

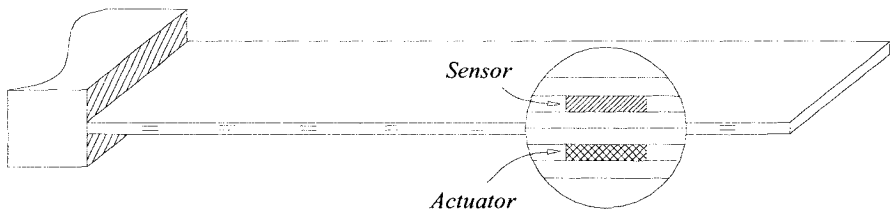

Figure 2.1 Schematic illustration of smart laminated composite beam

The present finite element model incorporates all the aspects of mechanical and electrical responses of smart laminated beams, including the electro-mechanical coupling effect, size and location of piezoelectric sensors/actuators. Variety of numerical illustrations is presented to demonstrate the capabilities and performance of coupled layerwise model for smart laminated beams.

2.2 Governing Equations

In this section, the governing equations of piezoelectric materials based on the linear piezoelectricity[146] are outlined. According to the theory of linear piezoelectricity, *i*) the

equations of linear elasticity are coupled to charge equations of electrostatics through the piezoelectric constants, *ii*) deformation and strains are small, and thus, no distinction is made between the initial and final positions, *iii*) the two way thermopiezoelectric coupling is neglected, which means that, temperature changes due to changes in strains, and electric field are small compared to the magnitude of the thermal load.

The mechanical response of the piezoelectric material is represented by the following equations of motion,

$$\sigma_{ij,i} + f_j = \rho \ddot{u}_j \tag{2.1}$$

while the electrical response is described by the electrostatics equations for the conservation of the electric flux,

$$D_{i,i} = 0 \tag{2.2}$$

where σ_{ij} are the stresses, ρ is the density, f_j are the body forces per unit volume, u_j are the displacements and D_i are electric displacements. Also, i and j indicate the material axes which range from *1* to *3*, superscript dot represents time derivative and subscript comma represents differentiation with respect to spatial coordinates. The variational form of the combined electro-mechanical response of the piezoelectric materials is determined as:

$$\int_V \left(\rho \ddot{u}_i \delta u_i + \sigma_{ij} \delta \varepsilon_{ij} - D_i \delta E_i\right) dV = \int_{A_t} t_i \delta u_i dA + \int_{A_p} Q \delta \psi dA + \int_V f_i \delta u_i dV \tag{2.3}$$

where ε_{ij} represent the strains, E_i represents the electric field, t_i are the surface tractions applied on the surface A_t, Q is the electrical charge applied on the surface A_p of the piezoelectric material, ψ is the electric potential and V represents the whole volume including the piezoelectric and substrate materials. Strains, ε_{ij} considering small deformation are given by

$$\varepsilon_{ij} = \frac{1}{2}(u_{i,j} + u_{j,i}) \tag{2.4}$$

and electric field, E_i is related to the electric potential by

$$E_i = -\psi_{,i} \tag{2.5}$$

2.3 Piezo-laminated Structures

Neglecting the thermal effects, the constitutive equations for an orthotropic lamina with piezoelectric effect are given by

$$\begin{Bmatrix} \sigma_{xx} \\ \sigma_{yy} \\ \sigma_{zz} \\ \tau_{yz} \\ \tau_{xz} \\ \tau_{xy} \end{Bmatrix} = \begin{bmatrix} \overline{C}_{11} & \overline{C}_{12} & \overline{C}_{13} & 0 & 0 & \overline{C}_{16} \\ \overline{C}_{12} & \overline{C}_{22} & \overline{C}_{23} & 0 & 0 & \overline{C}_{26} \\ \overline{C}_{13} & \overline{C}_{23} & \overline{C}_{33} & 0 & 0 & \overline{C}_{36} \\ 0 & 0 & 0 & \overline{C}_{44} & \overline{C}_{45} & 0 \\ 0 & 0 & 0 & \overline{C}_{45} & \overline{C}_{55} & 0 \\ \overline{C}_{16} & \overline{C}_{26} & \overline{C}_{36} & 0 & 0 & \overline{C}_{66} \end{bmatrix} \begin{Bmatrix} \varepsilon_{xx} \\ \varepsilon_{yy} \\ \varepsilon_{zz} \\ \gamma_{yz} \\ \gamma_{xz} \\ \gamma_{xy} \end{Bmatrix} - \begin{bmatrix} 0 & 0 & \overline{e}_{31} \\ 0 & 0 & \overline{e}_{32} \\ 0 & 0 & \overline{e}_{33} \\ \overline{e}_{14} & \overline{e}_{24} & 0 \\ \overline{e}_{15} & \overline{e}_{25} & 0 \\ 0 & 0 & \overline{e}_{36} \end{bmatrix} \begin{Bmatrix} E_x \\ E_y \\ E_z \end{Bmatrix} \tag{2.6}$$

$$\begin{Bmatrix} D_x \\ D_y \\ D_z \end{Bmatrix} = \begin{bmatrix} 0 & 0 & 0 & \bar{e}_{14} & \bar{e}_{15} & 0 \\ 0 & 0 & 0 & \bar{e}_{24} & \bar{e}_{25} & 0 \\ \bar{e}_{31} & \bar{e}_{32} & \bar{e}_{33} & 0 & 0 & \bar{e}_{36} \end{bmatrix} \begin{Bmatrix} \varepsilon_{xx} \\ \varepsilon_{yy} \\ \varepsilon_{zz} \\ \gamma_{yz} \\ \gamma_{xz} \\ \gamma_{xy} \end{Bmatrix} + \begin{bmatrix} \bar{g}_{11} & \bar{g}_{12} & 0 \\ \bar{g}_{12} & \bar{g}_{22} & 0 \\ 0 & 0 & \bar{g}_{33} \end{bmatrix} \begin{Bmatrix} E_x \\ E_y \\ E_z \end{Bmatrix} \tag{2.7}$$

where $\{\sigma\}$ represents the stress vector, $\{D\}$ the electric displacement, $\{E\}$ the electric field, $\{\varepsilon\}$ the strain field, $[\bar{C}]$ the transformed stiffness matrix, $[\bar{e}]$ the transformed piezoelectric coupling matrix and $[\bar{g}]$, the transformed permittivity matrix. The Equations (2.6) and (2.7) can be written in compact form as $\{\sigma\} = [\bar{C}]\{\varepsilon\} - [\bar{e}]^T \{E\}$ and $\{D\} = [\bar{e}]\{\varepsilon\} - [\bar{g}]\{E\}$, respectively. Smart laminated structures are mainly produced as plate structures, thus, can be considered as plane stress conditions.

The stress-strain relation in a plane state of stress are reduced to the following

$$\begin{Bmatrix} \sigma_{xx} \\ \sigma_{yy} \\ \tau_{xy} \end{Bmatrix} = \begin{bmatrix} \bar{Q}_{11} & \bar{Q}_{12} & \bar{Q}_{16} \\ \bar{Q}_{12} & \bar{Q}_{22} & \bar{Q}_{26} \\ \bar{Q}_{16} & \bar{Q}_{26} & Q_{66} \end{bmatrix} \begin{Bmatrix} \varepsilon_{xx} \\ \varepsilon_{yy} \\ \gamma_{xy} \end{Bmatrix} - \begin{bmatrix} 0 & 0 & \bar{e}_{31} \\ 0 & 0 & \bar{e}_{32} \\ 0 & 0 & \bar{e}_{36} \end{bmatrix} \begin{Bmatrix} E_x \\ E_y \\ E_z \end{Bmatrix} \tag{2.8}$$

$$\begin{Bmatrix} \tau_{yz} \\ \tau_{xz} \end{Bmatrix} = \begin{bmatrix} \bar{Q}_{44} & \bar{Q}_{45} \\ \bar{Q}_{45} & \bar{Q}_{55} \end{bmatrix} \begin{Bmatrix} \gamma_{yz} \\ \gamma_{xz} \end{Bmatrix} - \begin{bmatrix} \bar{e}_{14} & \bar{e}_{24} & 0 \\ \bar{e}_{15} & \bar{e}_{25} & 0 \end{bmatrix} \begin{Bmatrix} E_x \\ E_y \\ E_z \end{Bmatrix} \tag{2.9}$$

$$\begin{Bmatrix} D_x \\ D_y \\ D_z \end{Bmatrix} = \begin{bmatrix} 0 & 0 & \bar{e}_{14} & \bar{e}_{15} & 0 \\ 0 & 0 & \bar{e}_{24} & \bar{e}_{25} & 0 \\ \bar{e}_{31} & \bar{e}_{32} & 0 & 0 & \bar{e}_{36} \end{bmatrix} \begin{Bmatrix} \varepsilon_{xx} \\ \varepsilon_{yy} \\ \gamma_{yz} \\ \gamma_{xz} \\ \gamma_{xy} \end{Bmatrix} + \begin{bmatrix} \bar{g}_{11} & \bar{g}_{12} & 0 \\ \bar{g}_{21} & \bar{g}_{22} & 0 \\ 0 & 0 & \bar{g}_{33} \end{bmatrix} \begin{Bmatrix} E_x \\ E_y \\ E_z \end{Bmatrix} \tag{2.10}$$

where $\bar{Q}_{ij}$ are the plane stress-reduced stiffness, provided in Appendix A. The piezoelectric stiffnesses are known in terms of the dielectric constants, [d] and elastic stiffnesses as:

$$[\bar{e}] = [d][\bar{Q}] \tag{2.11}$$

2.3.1 Piezo-laminated beams

In general, two approaches can be used to obtain a beam model: (*1*) from plate model which means neglecting transverse stress, $\sigma_{zz} = 0$ and (*2*) reducing a 3-D model to a 2-D model. In the first approach, in addition to $\sigma_{zz} = 0$, the beam model can be obtained by using Equations (2.8) and (2.9) and considering $\sigma_{yy} = \tau_{yz} = \tau_{xy} = 0$ while assuming $\varepsilon_{yy} \neq \gamma_{yz} \neq \gamma_{xy} \neq 0$. Thus the reduced equation of smart laminated beam can be obtained as:

$$\begin{Bmatrix} \sigma_{xx} \\ \tau_{xz} \end{Bmatrix}^k = \begin{bmatrix} \tilde{Q}_{11} & 0 \\ 0 & \tilde{Q}_{55} \end{bmatrix}^k \begin{Bmatrix} \varepsilon_{xx} \\ \gamma_{xz} \end{Bmatrix}^k - \begin{bmatrix} 0 & \tilde{e}_{31} \\ \tilde{e}_{15} & 0 \end{bmatrix}^k \begin{Bmatrix} E_x \\ E_z \end{Bmatrix}^k \tag{2.12}$$

$$D_z^k = \bar{e}_{31}^k \varepsilon_{xx}^k + \bar{g}_{33}^k E_z^k \tag{2.13}$$

where

$$\tilde{Q}_{11} = \bar{Q}_{11} + \frac{\bar{Q}_{16}\bar{Q}_{26} - \bar{Q}_{12}\bar{Q}_{66}}{\bar{Q}_{22}\bar{Q}_{66} - \bar{Q}_{26}^2}\bar{Q}_{12} + \frac{\bar{Q}_{12}\bar{Q}_{26} - \bar{Q}_{16}\bar{Q}_{22}}{\bar{Q}_{22}\bar{Q}_{66} - \bar{Q}_{26}^2}\bar{Q}_{16} \tag{2.14}$$

$$\tilde{Q}_{55} = \bar{Q}_{55} + \frac{\bar{Q}_{45}^2}{\bar{Q}_{44}} \tag{2.15}$$

$$\tilde{e}_{31} = \left(1 - \frac{\bar{Q}_{12}\bar{Q}_{66} - \bar{Q}_{16}\bar{Q}_{26}}{\bar{Q}_{22}\bar{Q}_{66} - \bar{Q}_{26}^2}\right)\bar{e}_{31} \tag{2.16}$$

In the second approach, a beam model can be obtained by considering a three-dimensional element and eliminating the stress through the width, $\sigma_{yy} = 0$, the in-plane shear stress $\tau_{xy} = 0$ and the transverse shear stress, $\tau_{yz} = 0$. While considering that the corresponding strains $\varepsilon_{yy} \neq \gamma_{yz} \neq \gamma_{xy} \neq 0$. Thus, for a two-dimensional beam element, the constitutive equations in Equation (2.6) reduce to the form:

$$\begin{Bmatrix} \sigma_{xx} \\ \sigma_{zz} \\ \tau_{xz} \end{Bmatrix}^k = \begin{bmatrix} \tilde{C}_{11} & \tilde{C}_{13} & 0 \\ \tilde{C}_{31} & \tilde{C}_{33} & 0 \\ 0 & 0 & \tilde{C}_{55} \end{bmatrix}^k \begin{Bmatrix} \varepsilon_{xx} \\ \varepsilon_{zz} \\ \gamma_{xz} \end{Bmatrix}^k - \begin{bmatrix} 0 & 0 & \bar{e}_{31} \\ 0 & 0 & \bar{e}_{33} \\ \bar{e}_{15} & \bar{e}_{25} & 0 \end{bmatrix}^k \begin{Bmatrix} E_x \\ E_y \\ E_z \end{Bmatrix}^k \tag{2.17}$$

The modified elastic constants $\tilde{C}_{ij}$ are obtained by expanding all the six components of the strain vector in terms of the transformed elastic constants $\bar{C}_{ij}$ and the stress vector σ_{ij} and then eliminating ε_{yy}, ε_{xy} and ε_{yz} from the ensuing equations[147],

$$\tilde{C}_{11} = \bar{C}_{11} + \frac{\bar{C}_{16}\bar{C}_{26} - \bar{C}_{12}\bar{C}_{66}}{\bar{C}_{22}\bar{C}_{66} - \bar{C}_{26}^2}\bar{C}_{12} + \frac{\bar{C}_{12}\bar{C}_{26} - \bar{C}_{16}\bar{C}_{22}}{\bar{C}_{22}\bar{C}_{66} - \bar{C}_{26}^2}\bar{C}_{16} \tag{2.18}$$

$$\widetilde{C}_{13} = \overline{C}_{13} + \frac{\overline{C}_{33}\overline{C}_{26} - \overline{C}_{23}\overline{C}_{66}}{\overline{C}_{22}\overline{C}_{66} - \overline{C}_{26}^2}\overline{C}_{23} + \frac{\overline{C}_{12}\overline{C}_{26} - \overline{C}_{16}\overline{C}_{22}}{\overline{C}_{22}\overline{C}_{66} - \overline{C}_{26}^2}\overline{C}_{36} \tag{2.19}$$

$$\widetilde{C}_{33} = \overline{C}_{33} + \frac{\overline{C}_{36}\overline{C}_{26} - \overline{C}_{23}\overline{C}_{66}}{\overline{C}_{22}\overline{C}_{66} - \overline{C}_{26}^2}\overline{C}_{23} + \frac{\overline{C}_{23}\overline{C}_{26} - \overline{C}_{36}\overline{C}_{22}}{\overline{C}_{22}\overline{C}_{66} - \overline{C}_{26}^2}\overline{C}_{36} \tag{2.20}$$

$$\widetilde{C}_{55} = \overline{C}_{55} - \frac{\overline{C}_{45}^2}{\overline{C}_{55}} \tag{2.21}$$

The modified coefficients $\overline{C}_{ij}$, $\overline{e}_{ij}$ and $\overline{g}_{33}$ are the reduced stiffness, piezoelectric and permittivity coefficients which are given in Appendix A. In practice, for smart laminated beams, the electric field is exerted in thickness direction, z, and it is given as $E_z = V/t$. For all the examples described in the present work the electric field is considered in thickness direction unless otherwise mentioned.

2.3.2 Layerwise theory approximations

In this section the layerwise displacement theory proposed by Reddy[50] for analysis of laminated composite structure which is based on piecewise displacement approximation through the laminate thickness as shown in Figure 2.2 has been applied for the analysis of smart laminated beams integrated with piezoelectric elements.

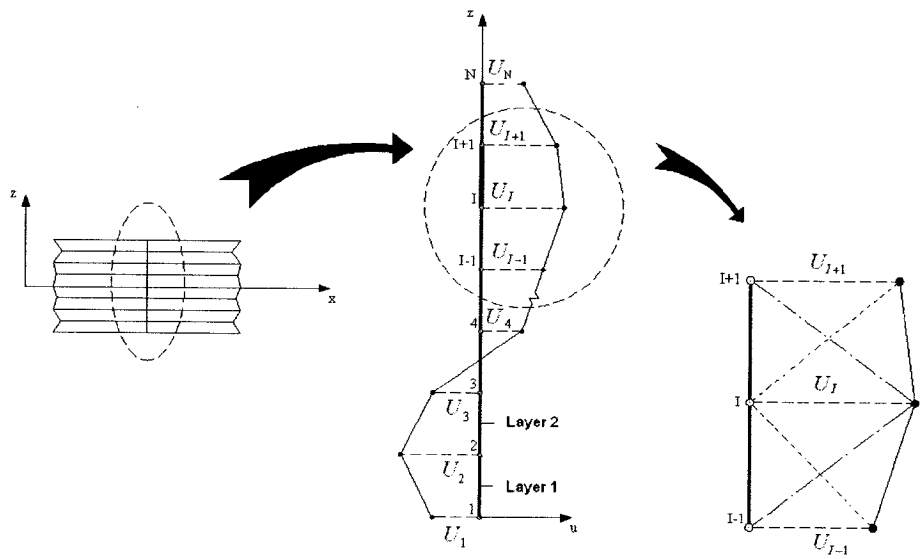

Figure 2.2 Layerwise displacements through the thickness

In deriving the layerwise theory for laminated beam, only axial and through the thickness displacements are assumed. The displacement field and electric potential for a laminated beam based on the layerwise theory are obtained by considering the axial and through-the-thickness displacements as:

$$u(x,z,t)=\sum_{I=1}^{N}U_I(x,t)\Phi^I(z) \tag{2.22}$$

$$w(x,z,t)=\sum_{I=1}^{N}W_I(x,t)\Phi^I(z) \tag{2.23}$$

$$\psi(x,z,t)=\sum_{I=1}^{N}\psi_I^i\Phi^I(z) \tag{2.24}$$

$$\Phi^I(z)=[1-\zeta \quad \zeta] \tag{2.25}$$

where u and w are displacements along x and z-directions, respectively and ψ is the electric potential. N denotes the total number of nodes through the thickness, $\zeta = z/h$, h represents the thickness of each discrete layer. Interpolation functions $\Phi(z)$ are defined between any two adjacent layers. For thin laminate, displacements in z-direction between layers are negligible, so, $w(x,z,t) = W_o(x,t)$. In practical applications, the bottom and upper surfaces of piezoelectric patches are covered with conductive materials which require constant electrical potential at the covered surfaces, so, $\psi_I(x,t) = \psi_I^o(t)$.

Substituting through-the-thickness approximations, Equations (2.22)-(2.24), into the variational form of the equations of motion and the electrostatic equation, Equation (2.3), the generalized beam laminate matrices are obtained as:

$$\sum_{J=1}^{N}\sum_{I=1}^{N}\int_{x}\rho_{11}^{IJ}\ddot{U}^{I}\delta U^{J}dx+\int_{x}\rho_{33}^{IJ}\ddot{W}^{I}\delta W^{J}dx+$$

$$\sum_{J=1}^{N}\sum_{I=1}^{N}\int_{x}(A_{11}^{IJ}\frac{\partial U^{I}}{\partial x}\frac{\partial\delta U^{J}}{\partial x}+B_{13}^{IJ}W^{I}\frac{\partial\delta W^{J}}{\partial x})dx+$$

$$\sum_{J=1}^{N}\sum_{I=1}^{N}\int_{x}(C_{13}^{IJ}\frac{\partial U^{I}}{\partial x}\delta W^{J}+D_{33}^{IJ}W^{I}\delta W^{J})dx+$$

$$\sum_{J=1}^{N}\sum_{I=1}^{N}(D_{55}^{IJ}U^{I}\partial\delta U^{J}+C_{55}^{IJ}\frac{\partial W^{I}}{\partial x}\delta U^{J})dx+$$

$$\sum_{J=1}^{N}\sum_{I=1}^{N}(B_{55}^{IJ}U^{I}\frac{\partial\delta W^{J}}{\partial x}+C_{55}^{IJ}\frac{\partial W^{I}}{\partial x}\frac{\partial\delta W^{J}}{\partial x})dx+ \qquad (2.26)$$

$$\sum_{J=1}^{N}\sum_{I=1}^{N}\int_{x}E_{31}^{IJ}(\psi^{I}\frac{\partial\delta U^{I}}{\partial x}+\frac{\partial\delta U^{I}}{\partial x}\delta\psi^{J})dx-$$

$$\sum_{J=1}^{N}\sum_{I=1}^{N}\int_{x}G_{33}^{IJ}(\psi^{I}\delta\psi^{J}dx=\int_{A_t}t_i\delta U_i dA+\int_{\Gamma_p}Q\delta\psi\,dA$$

The coefficients that are related to the laminate thickness are given by:

$$E_{31}^{IJ}=\sum_{k=1}^{N_p}\left[\int_{z_k}^{z_{k+1}}b\bar{C}_{13}^{k}d_{31}\Phi^{I}(z)\frac{\partial\Phi^{J}(z)}{\partial z}dz\right]$$

$$G_{33}^{IJ}=\sum_{k=1}^{N_p}\left[\int_{z_k}^{z_{k+1}}b\bar{g}_{33}\frac{\partial\Phi^{I}(z)}{\partial z}\frac{\partial\Phi^{J}(z)}{\partial z}dz\right]$$

$$A_{11}^{IJ}=\sum_{k=1}^{N_p}\left[\int_{z_k}^{z_{k+1}}b\bar{C}_{11}^{k}\Phi^{I}(z)\Phi^{J}(z)dz\right]$$

$$A_{55}^{IJ} = \sum_{k=1}^{N_p}\left[\int_{z_k}^{z_{k+1}} b\overline{C}_{55}^{k}\Phi^{I}(z)\Phi^{J}(z)dz\right]$$

$$B_{13}^{IJ} = \sum_{k=1}^{N_p}\left[\int_{z_k}^{z_{k+1}} b\overline{C}_{13}^{k}\frac{\partial\Phi^{I}(z)}{\partial z}\Phi^{J}(z)dz\right]$$

$$B_{55}^{IJ} = \sum_{k=1}^{N_p}\left[\int_{z_k}^{z_{k+1}} b\overline{C}_{55}^{k}\frac{\partial\Phi^{I}(z)}{\partial z}\Phi^{J}(z)dz\right]$$

$$C_{13}^{IJ} = \sum_{k=1}^{N_p}\left[\int_{z_k}^{z_{k+1}} b\overline{C}_{13}^{k}\Phi^{I}(z)\frac{\partial\Phi^{J}(z)}{\partial z}dz\right]$$

$$C_{55}^{IJ} = \sum_{k=1}^{N_p}\left[\int_{z_k}^{z_{k+1}} b\overline{C}_{55}^{k}\Phi^{I}(z)\frac{\partial\Phi^{J}(z)}{\partial z}dz\right] \qquad (2.27)$$

$$D_{55}^{IJ} = \sum_{k=1}^{N_p}\left[\int_{z_k}^{z_{k+1}} b\overline{C}_{55}^{k}\frac{\partial\Phi^{I}(z)}{\partial z}\frac{\partial\Phi^{J}(z)}{\partial z}dz\right]$$

$$D_{33}^{IJ} = \sum_{k=1}^{N_p}\left[\int_{z_k}^{z_{k+1}} b\overline{C}_{33}^{k}\frac{\partial\Phi^{I}(z)}{\partial z}\frac{\partial\Phi^{J}(z)}{\partial z}dz\right]$$

$$\rho_{11}^{IJ} = \sum_{k=1}^{N_p}\left[\int_{-h/2}^{h/2} b\rho^{k}\Phi^{I}(z)\Phi^{J}(z)dz\right]$$

$$\rho_{33}^{IJ} = \rho_{11}^{IJ} \qquad \text{for} \qquad w(x,z,t) = \sum_{I=1}^{N} W_I(x,t)\Phi^{I}(z)$$

$$\rho_{33}^{IJ} = \sum_{k=1}^{N_p}\int_{-h/2}^{h/2} b\rho^{k}dz \qquad \text{for} \qquad w(x,z,t) = W_o(x,t)$$

where $\Phi^{I}(z)$ represent the interpolation functions though the thickness of the beam and ρ^{k} stands for the density of k^{th} layer of the laminate.

2.3.3 Finite element model

Finite element formulation has been obtained by incorporating the local in-plane approximations for the state variables introduced in Equations (2.22-2.23) as follows:

$$U_I = \sum_{i=1}^{Nn} U_I^i(x)\varphi_i(x) \tag{2.28}$$

$$W_I = \sum_{i=1}^{Nn} W_I^i \varphi_i(x) \tag{2.29}$$

$$\psi_I = \sum_{i=1}^{Nn} \psi_I^i \varphi_i(x) \tag{2.30}$$

where Nn is the number of nodes and $\varphi_i(x)$ are the interpolation functions along the length of the beam, respectively. By implementing the in-plane approximations for the state variables into Equations (2.26) and collecting the coefficients of displacements, $\{U\}$, $\{W\}$ and $\{\psi\}$, the following matrix equation for the smart laminated beam can be obtained:

$$\begin{bmatrix} [M_{dd}] & [0] \\ [0] & [0] \end{bmatrix} \begin{Bmatrix} \{\ddot{d}\} \\ \{\ddot{\psi}\} \end{Bmatrix} + \begin{bmatrix} [K_{dd}] & [K_{d\psi}] \\ [K_{\psi d}] & [K_{\psi\psi}] \end{bmatrix} \begin{Bmatrix} \{d\} \\ \{\psi\} \end{Bmatrix} = \begin{Bmatrix} \{F(t)\} \\ \{Q(t)\} \end{Bmatrix} \tag{2.31}$$

where $[K_{dd}]$, $[K_{d\psi}]$, $[K_{\psi\psi}]$and $[M_{dd}]$ are the elastic, piezoelectric, permittivity, and mass matrices, respectively. Elastic stiffness and mass matrices are given by:

$$[K_{dd}]=\begin{bmatrix}[K_{dd}^{11}] & [K_{dd}^{12}]\\ [K_{dd}^{12}]^T & [K_{dd}^{22}]\end{bmatrix},\quad [M_{dd}]=\begin{bmatrix}[M_{dd}^{11}] & [0]\\ [0] & [M_{dd}^{22}]\end{bmatrix} \tag{2.32}$$

where the coefficients of the element matrices are given by:

$$[K_{d\psi}]=\int_0^l([E_{31}][S][S_{,x}])dx \tag{2.33}$$

$$[K_{\psi d}]=[K_{d\psi}]^T \tag{2.34}$$

$$[K_{\psi\psi}]=\int_0^l([G_{33}][S][S])dx \tag{2.35}$$

$$[K_{dd}^{11}]=\int_0^l([A_{11}][S_{,x}][S_{,x}]+[D_{55}][S][S])dx \tag{2.36}$$

$$[K_{dd}^{12}]=\int_0^l([B_{13}][S_{,x}][S]+[D_{55}][S_{,x}][S])dx \tag{2.37}$$

$$[K_{dd}^{21}]=[K_{dd}^{12}]^T \tag{2.38}$$

$$[K_{dd}^{22}]=\int_0^l([A_{55}][S_{,x}][S_{,x}]+[D_{33}][S][S])dx \tag{2.39}$$

$$[M_{dd}^{11}]=\int_0^l([\rho^1][S][S])dx \tag{2.40}$$

$$[M_{dd}^{22}]=\int_0^l([\rho^2][S][S])dx \tag{2.41}$$

where $[S(x)]$ represents the vector of shape functions given by $[S(x)]=[1-\varsigma,\varsigma]$, $\varsigma=x/l$ and subscript comma means derivative with respect to the letter next to comma. Further,

$\{F(t)\}$ and $\{Q(t)\}$ are the applied mechanical load vector and electrical charge vector, respectively. The nodal displacement matrix $\{d\}=\{U,W\}^T$ represents the displacement vector containing axial, $\{U\}$, and transverse, $\{W\}$, displacements and $\{\psi\}$ represents the electric potential. The electric potential vector is written as $\{\psi\}=\{\psi^s,\psi^a\}^T$, where ψ^s and ψ^a represent, respectively the voltage output at the sensor and the voltage imposed on the actuator layer. Equation (2.31) can be expressed in a compact form with the electric potential partitioned into active and sensory components as:

$$\begin{bmatrix}[M_{dd}] & [0]\\ [0] & [0]\end{bmatrix}\begin{Bmatrix}\{\ddot{d}\}\\ \{\ddot{\psi}\}\end{Bmatrix}+\begin{bmatrix}[K_{dd}] & [K^{ss}_{d\psi}]\\ [K^{ss}_{\psi d}] & [K^{ss}_{\psi\psi}]\end{bmatrix}\begin{Bmatrix}\{d\}\\ \{\psi^s\}\end{Bmatrix}=\begin{Bmatrix}\{F_d(t)\}-[K^{sa}_{d\psi}]\{\psi^a\}\\ \{Q^s(t)\}-[K^{sa}_{\psi\psi}]\{\psi^a\}\end{Bmatrix} \tag{2.42}$$

where superscripts s and a stand for partitioned sub-matrices in accordance with the sensory and actuator components, respectively. The left hand side includes the unknown sensor voltage, $\{\psi^s\}$, and the nodal displacements, $\{d\}$. The right hand side includes the applied mechanical load, $\{F_d(t)\}$, applied voltage on the actuator, $\{\psi^a\}$ and the electric charge, $\{Q^s(t)\}$. In open circuit conditions, the electric charge at sensors $\{Q^s(t)\}$ remains constant with time and is assumed to be zero. Therefore Equation (2.42) can also be condensed into the following uncoupled dynamic equations for the structural displacements and sensor voltage, respectively as:

$$[M_{dd}]\{\ddot{d}\} + \left([K_{dd}] - [K^{ss}_{\psi d}][K^{ss}_{\psi\psi}]^{-1}[K^{ss}_{\psi d}]\right)\{d\} = \tag{2.43}$$

$$\{F_d(t)\} + \left([K^{ss}_{d\psi}][K^{ss}_{\psi\psi}]^{-1}[K^{sa}_{\psi d}] - [K^{sa}_{d\psi}]\right)\{\psi^a\}$$

$$\{\psi^s\} = -[K^{ss}_{\psi\psi}]^{-1}\left([K^{ss}_{\psi d}]\{d\} + [K^{sa}_{\psi\psi}]\{\psi^a\}\right) \tag{2.44}$$

2.4 Numerical Examples

This section presents the results from several representative problems. First, the validity and accuracy of the present model is demonstrated by comparison with published results. Secondly, numerous examples are provided to investigate the coupling effects on quasi-static response, effect of actuator voltage on deflection, and sensor location on generated voltage. All the applications are focused on a laminated beam with embedded or surface bonded piezoelectric as sensors and/or actuators. It is pointed out that the piezoelectric properties are measured under stress-free conditions. In these examples the shear piezoelectric effect d_{15} and the axial electric permittivity g_{11} have been neglected.

2.4.1 Validation problem

A cantilever laminated beam made up of two layers of KYNAR piezo-films is considered to investigate the effect of applied voltage on displacement of the beam. This problem was also studied using layerwise theory by Donthireddy and Chandrashekhara[44]. The material and geometric properties are given in Table 2.1.

Table 2.1 Material properties for validation examples[43]

	KYNAR Piezo-film	G-1195 Piezo-ceramic	AS/3501 Graphite/epoxy
$E_1(N/m^2)$	6.85×10^9	63.0×10^9	144.8×10^9
$E_2(N/m^2)$	6.85×10^9	63.0×10^9	9.65×10^9
$G_{12}(N/m^2)$	0.078×10^9	24.8×10^9	7.10×10^9
$G_{13}(N/m^2)$	-	-	7.10×10^9
$G_{23}(N/m^2)$	-	-	5.92×10^9
v_{12}	0.29	0.28	0.3
$d_{31}(m/V)$	22.99×10^{-12}	166.0×10^{-12}	-
$d_{32}(m/V)$	4.6×10^{-12}	166.0×10^{-12}	-
Length (m)	0.08	0.254	0.254
Width (m)	0.01	0.0254	0.0254
Thickness (m)	0.00011	0.0002	0.00127

The effect of applied voltage on the tip deflection of the laminated beam with piezoelectric actuator is given in Figure 2.3. As it is observed the present results are in excellent agreement with the reference.

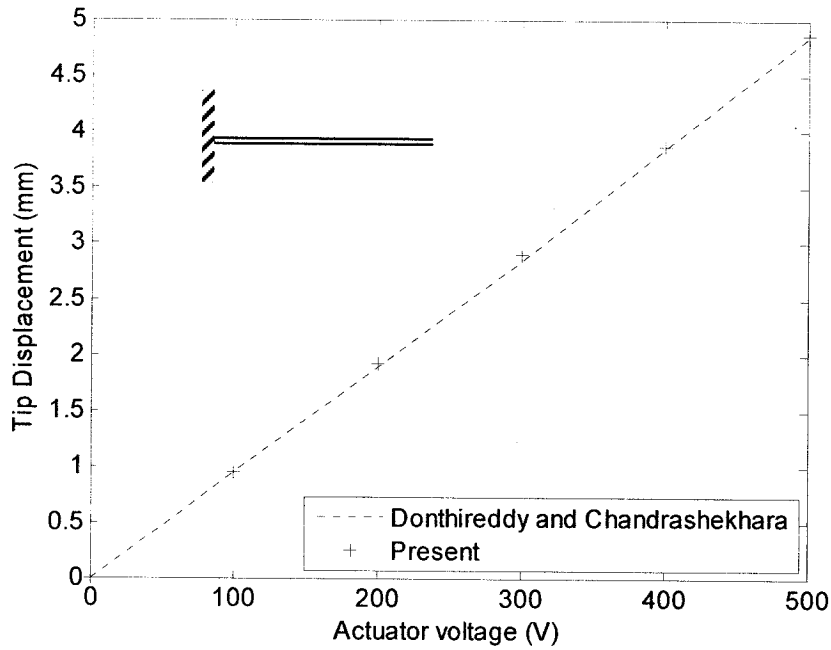

Figure 2.3 Tip deflection of the laminated beam vs actuator voltage

2.4.2 Effect of actuator voltage on deformation of piezo-laminated beam

A cantilever laminated beam with $[0/90]_s$ configuration made of graphite/epoxy (AS/3501) with one layer of piezoelectric (G-1195) actuator bonded on top surface and one layer at the bottom surface with opposite polarity is considered. A uniformly distributed load of $2\times10^3 N/m^2$ is applied on the beam. The material and geometrical properties of graphite/epoxy and piezo-ceramic are given in Table 2.1. The effect of actuator voltage on deflection of the laminated beam with surface bonded piezoelectric actuator is presented in Figure 2.4. As it is realized increasing actuator voltage from 0 to 200 volts reduces the deflection up to 33% at the tip.

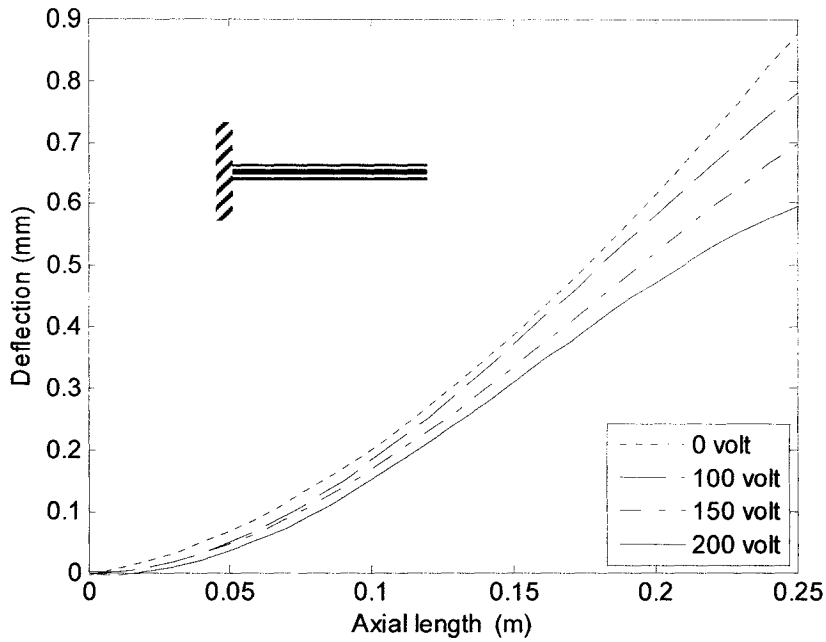

Figure 2.4 Effects of actuator voltage on transverse deflection of a clamped-free beam

The same smart laminated beam but with simply supported boundary conditions is also investigated. Deflection of this simply supported smart composite beam under different applied voltage is provided in Figure 2.5. As it can be realized increasing voltage from 0

to 200 volts can decrease the mid-span beam deflection up to %45. This shows the potential application of piezoelectric actuators to change the response of the system.

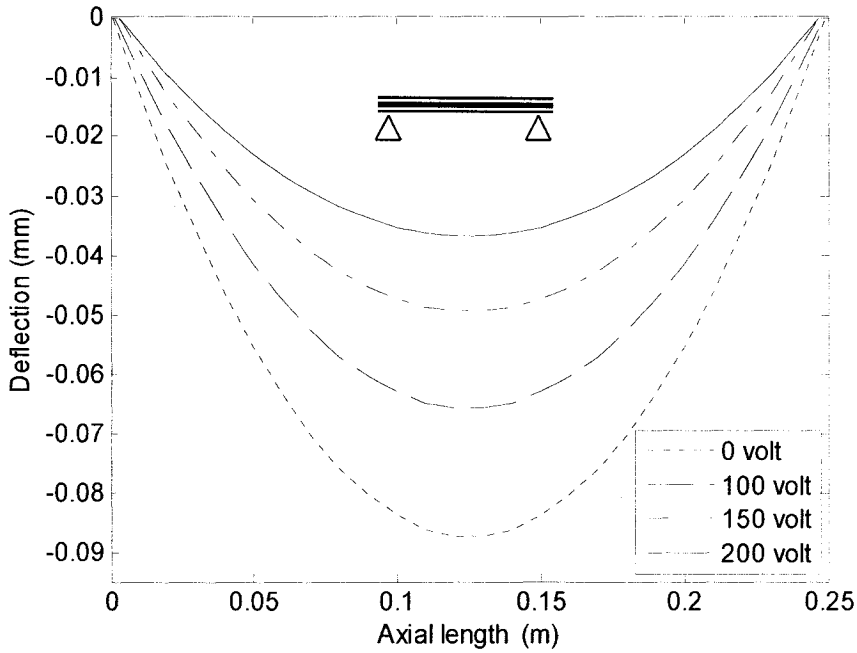

Figure 2.5 Effects of actuator voltage on transverse deflection of a simply supported beam subjected to uniformly distributed load

The effect of laminate configuration is also investigated by considering the laminated beam described in Section 2.4.2 for two cases of $[0/90]_s$ and $[\pm 45]_s$ laminate configurations. Here, the external loading is removed to acquire clear observation of the effect of laminate configuration and actuator voltage on shape control. The responses of the beam under an applied voltage of 150 V is computed and plotted in Figure 2.6. It is observed that laminated beam with $[\pm 45]_s$ experiences higher deflection than $[0/90]_s$ laminate under the same applied voltage. This result was expected since the stiffness of $[\pm 45]_s$ is lower than that of $[0/90]_s$.

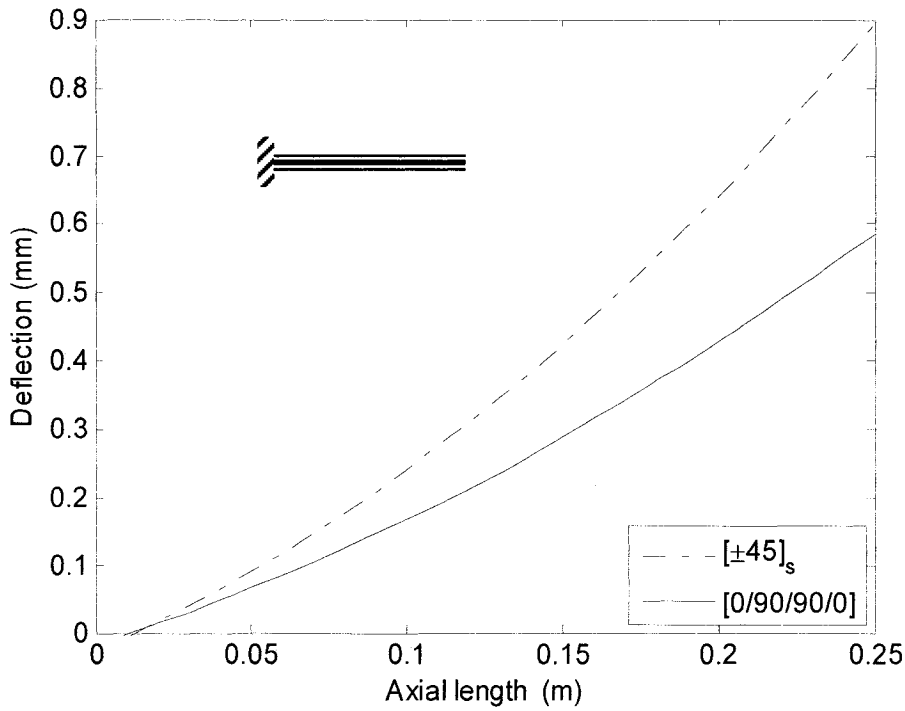

Figure 2.6 Effects of ply orientation on the transverse deflection of a clamped-free beam subjected to an actuator voltage of 150V

The results presented in this section prove the applicability and feasibility of using piezoelectric elements as actuating components in smart laminated structures for shape control.

2.4.3 Effect of electro-mechanical coupling on deflection

To investigate the effect of electro-mechanical coupling on deflection of smart laminated beam, a cantilever smart laminated beam is considered. The thickness of the laminate is 1.524 *mm* which is made from 8 unidirectional layers. The length of the beam is 200 *mm* and the width is 20 *mm*. A point load of 10 *N* is applied at the tip of the beam. Beam is meshed with 10 equally spaced elements. One layer of piezoelectric material of thickness

1.524 *mm* is bonded at the upper surface of the beam. Material properties of the host structure are as:

$E_1 = 126GPa, E_2 = 7.9GPa, G_{12} = 3.4GPa, \rho = 1527Kg/m^3$.

The mechanical and electrical properties of piezoelectric material are given as:

$E = 63GPa,\ \rho = 7600Kg/m^3, d_{31} = d_{32} = -254\times10^{-12} m/V, g_{33} = 15.3\times10^{-10} F/m$

In order to investigate the influence of electro-mechanical coupling on structural stiffness of smart laminated beam, deflection of the beam with and without considering the electro-mechanical coupling is presented in Figure 2.7.

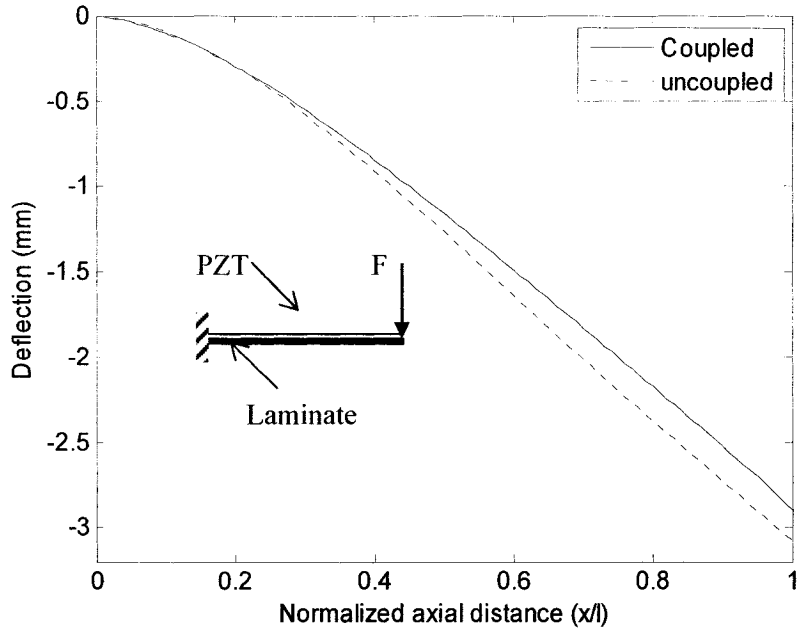

Figure 2.7 Effect of electro-mechanical coupling on displacement

It is observed that considering the coupling effects provide a reduction effect on nodal displacement of the smart laminated beam and it can reduce the tip displacement by about 3.5%. It should be noted that effect of electro-mechanical coupling depends on the total amount of piezoelectric materials used in the smart laminated structure. To have better

understanding, the effect of volume fraction of PZT material on the coupling effect has been investigated. The problem described in Section 2.4.3 has been considered. The thickness and length of the PZT has been selected in such a manner that the minimum thickness and length ratio of PZT and host laminate are 0.1 and the maximum thickness and length ratio are 1 and 0.5, respectively which results in a beam with two equal thickness and equal length parts of PZT and graphite/epoxy. Tip deflection of the beam is normalized by dividing it by the tip deflection obtained without considering electro-mechanical coupling. The effects of volume fraction of piezoelectric elements and host laminated material are provided in Figure 2.8. It is observed that for the volume fraction less than 10 percent the effect of coupling is negligible. The maximum effect of coupling is for 50 percent volume fraction.

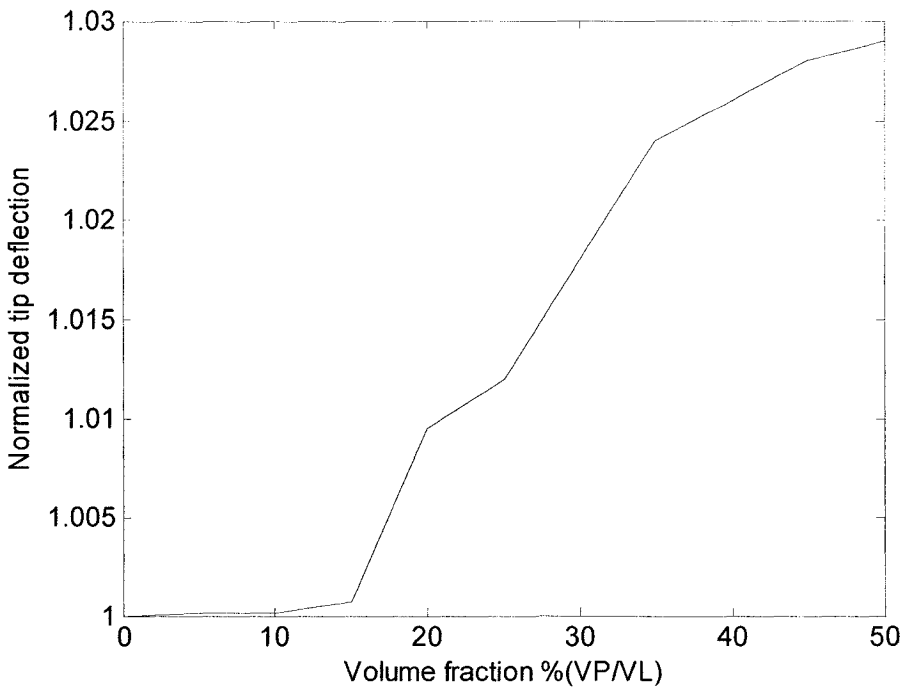

Figure 2.8 Effects of volume fraction of PZT on electro-mechanical coupling

2.4.4 Layerwise theory versus ESL theories

To compare the LayerWise Displacement Theory (LWDT) and Classical Laminated Plate Theory (CLPT), transient response of a cantilever smart laminated beam $[0/90/0]_s$ integrated with one piezoceramic actuator and one PVDF sensor as shown in Figure 2.9 is considered. Sensors and actuator patches are mounted at $l = 4\ cm$ from the fixed end of the beam.

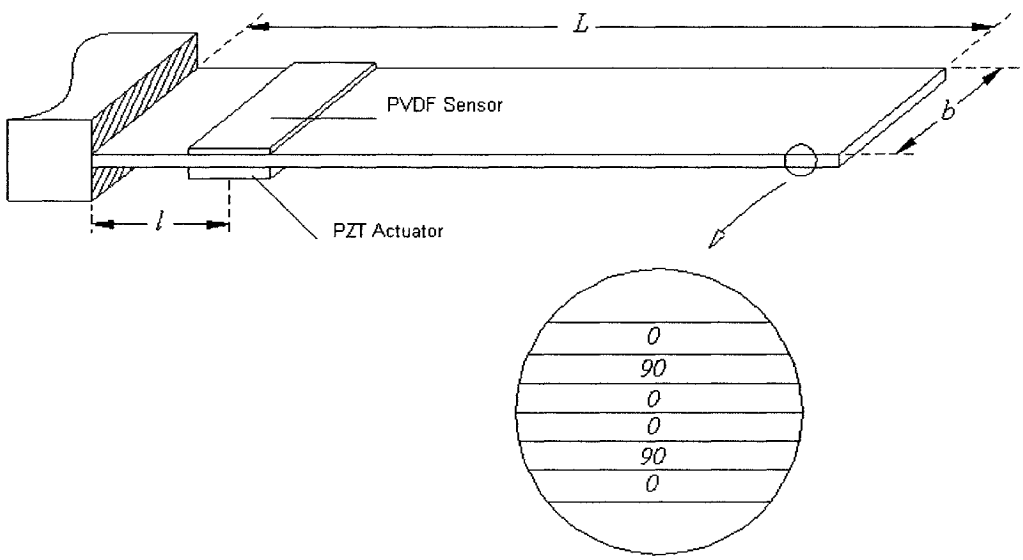

Figure 2.9 Schematic illustration of laminated smart beam

Materials and geometric properties of graphite/epoxy layers, piezoceramic and PVDF patches are given in Table 2.2.

Table 2.2 Material and geometric properties

	Graphite/ Epoxy	Piezoceramic	PVDF
E_1, GPa	98.0	71.4	4.67
E_2, GPa	6.78	71.4	4.80
G_{12}, GPa	3.48	24.8	2.66
ρ, Kg/m^3	1380	7610	1610
d_{31}, m/V	-	-200×10^{-12}	-20×10^{-12}
e_{33}, F/m	-	1501×0^{-10}	1.051×0^{-10}
Length, L, mm	300.0	25.0	25.0
Width, b, mm	30.0	25.0	25.0
Thickness, mm	0.2	0.50	0.0028

The free vibration response of the smart laminated beam for an initial tip displacement of 4 *cm* using CLPT and LWDT are presented in Figure 2.10. It can be realized that CLPT shows lower defection compared to that of LWDT. This result was expected because the CLPT effect of shear strain is neglected and thus it provides higher structural stiffness compared to that of LWDT.

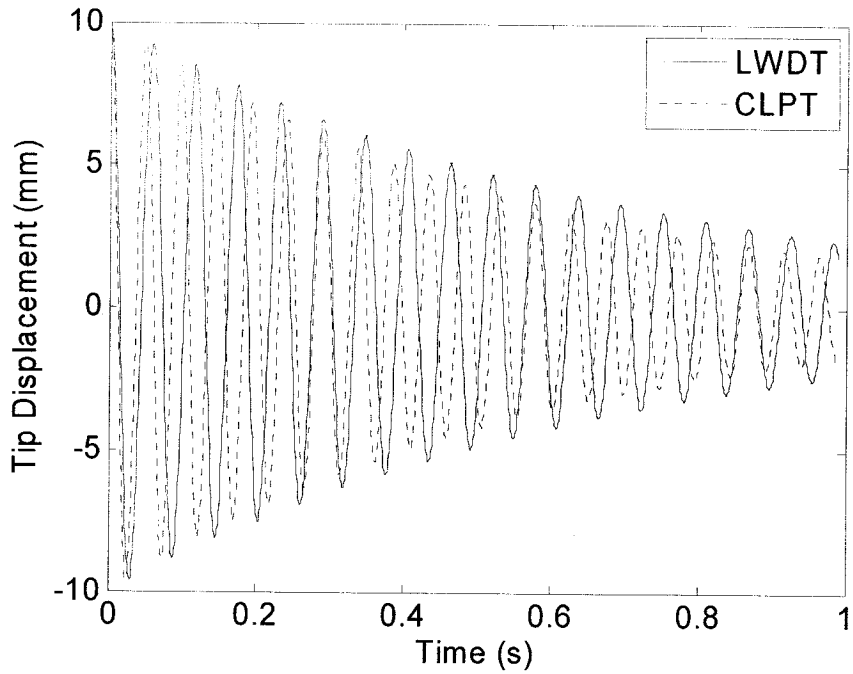

Figure 2.10 Damped response of smart laminated beam using LWDT and CLPT

2.5 Parametric Study on Sensor Voltage

In this section the effects of piezoelectric size and location on generated voltage for a cantilever smart laminated beam are studied. The laminated beam made of nine unidirectional layers of graphite/epoxy is considered. The length of the beam is 20 *cm* and the width is 3 *cm*, and 9 equal-length elements are used to model the beam. In the following sections variety of configurations are considered to study the effect of sensor location in length direction, thickness direction and diagonal direction on generated voltage.

2.5.1 Effect of location of sensor in thickness direction

To investigate the effects of sensor location along the length of the beam, 9 cases are considered and for each case the location of sensor is mounted at one element. In case one, the sensor is considered as the first layer on top surface at the fixed-end, for case nine, the sensor is mounted at the bottom surface at the ninth layer. For other cases, the sensor is replaced with 2^{nd}, 3^{rd},... layers. The voltage generated at sensors for each case has been shown in Figure 2.11. It is worth noting that voltage generated above and below the middle plane is similar. This phenomenon was expected when one recalls that in pure bending and for unidirectional layers, the middle-plane is the neutral plane. However, in case 5, the sensor is placed at the mid layer but the sensor itself has a thickness and the generated voltage is due to deformation of the outer surface of the sensor layer, thus it generates voltage.

The effects of orientation angle on sensor voltage are shown in Figure 2.12. In this case the laminate is not unidirectional. Thus, as one can easily realize the generated voltage is not uniform above and below the middle-plane.

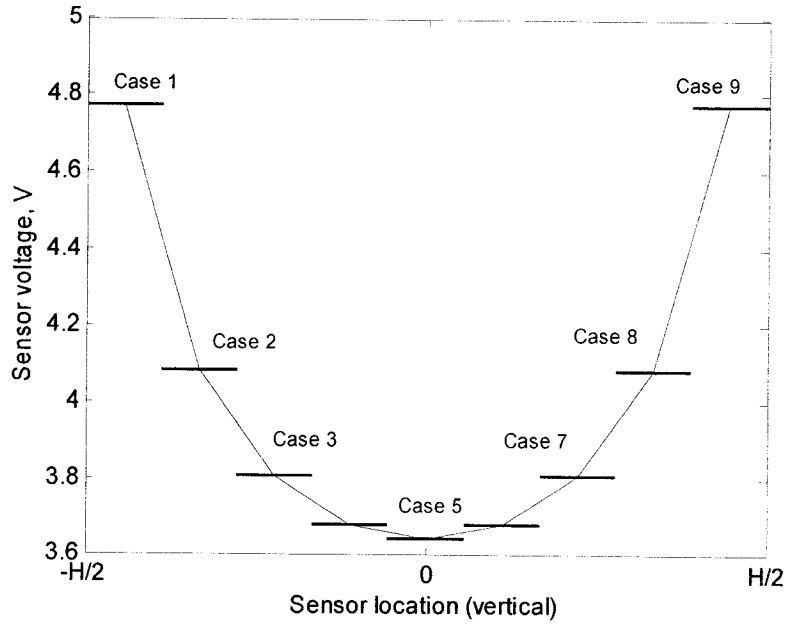

Figure 2.11 Effects of sensor location in thickness direction

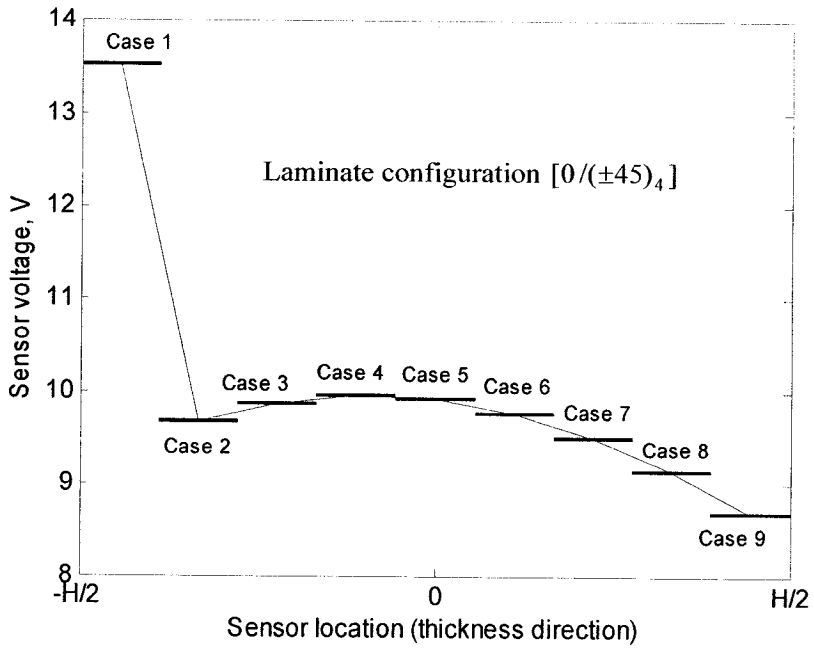

Figure 2.12 Effects of sensor location in thickness direction ply orientation of $[0/(\pm 45)_4]$

2.5.2 Effect of sensor location along the length

As another example, the location of sensor has been changed in axial direction starting from the fixed side moving toward the free end. In case one, the sensor is surface mounted at the first element from the fixed end and for case nine, the sensor location is considered at ninth element at free end, for other cases, the location of sensor is considered at 2^{nd}, 3^{rd}... elements. The material and geometric properties of the beam and the PZT material are similar to that of the problem described in previous section except that the thickness of both graphite/epoxy and PZT are 1.0 *mm* each. The sensor voltage for different lengthwise position is shown in Figure 2.12.

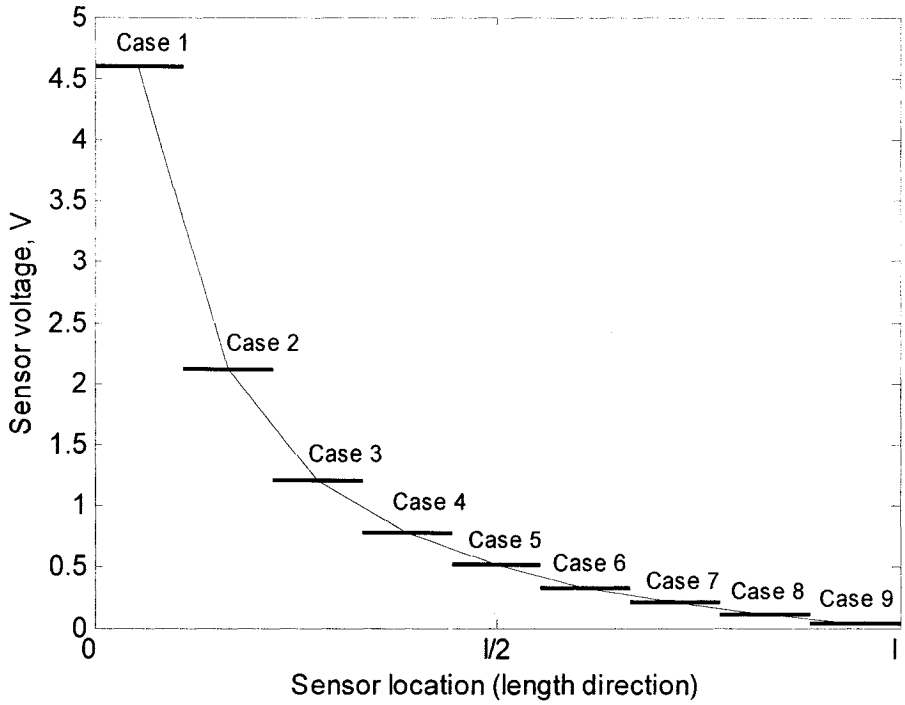

Figure 2.13 Effects of sensor location in axial direction

As expected the voltage decreases gradually when the sensor is moved from the fixed point toward the free end. This result is proportional to the element strain along the length

of the beam. To observe the effect of laminate configuration for this problem, some of the common laminate configurations, namely, $[0/(\pm 45)_4]$, $[0/(0/90)_4]$and $[0_9]$ are considered and the results for tip deflection of the beam are presented in Figure 2.14. One should note that this trend is valid for any laminate. Obviously the magnitude of the sensor voltage will be different.

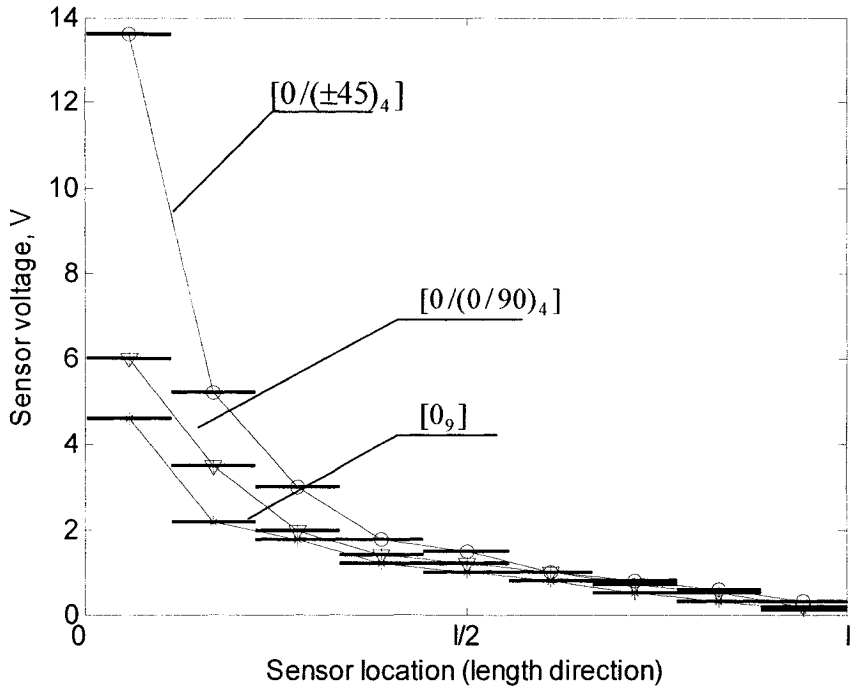

Figure 2.14 Effects of sensor location in axial direction for different ply orientations

2.5.3 Effect of diagonal location of sensor

To complete our study on the effect of sensor location on generated voltage, nine cases of sensor location in diagonal order starting from the most top left element moving toward the most bottom right element are considered. In case one, the sensor is surface mounted at the first element from the fixed end and for case nine, the sensor location is considered

at ninth element at free end and in the ninth layer at the bottom surface, for other cases, the location of sensor is considered at 2nd element and 2nd layer, 3rd element and 3rd layer, and so on. The generated voltages for all the cases are presented in Figure 2.15 where one may observe that these results are similar to that of the generated voltage when changing the sensor in length direction.

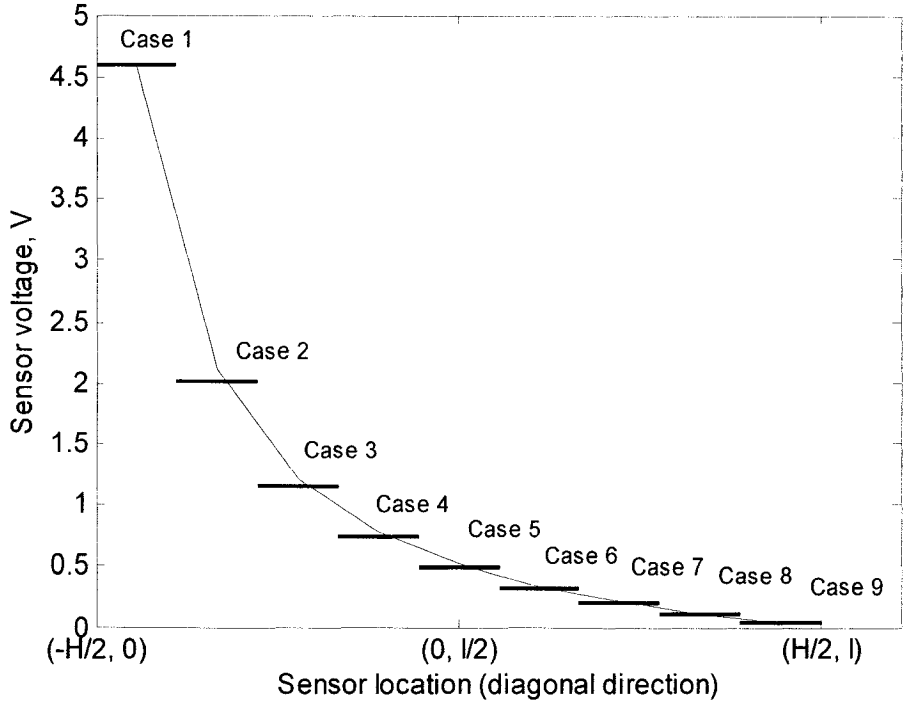

Figure 2.15 Effects of sensor location in diagonal direction

This is due to the high aspect ratio of length and thickness of the structure which makes the length direction the dominant factor in changing the stiffness and in turn strains in sensor elements and finally generated voltage.

2.6 Conclusions

Smart laminated composite beams with bonded/embedded piezoelectric layers as sensors and/or actuators have been investigated based on the layerwise displacement theory. A finite element formulation considering electro-mechanical effects has been developed and validated by comparing the present results with the available published results. The effect of electro-mechanical coupling on the static deformation of smart laminated beams has been investigated. It was realized that effect of electro-mechanical depends on the volume fraction of piezoelectric materials on the host structure and may cause up to 3 % error in tip displacement of a cantilever beam for 50% of volume fraction. In order to demonstrate the applicability and feasibility of the smart laminated beams in shape control, a variety of problems with different laminate configuration and boundary conditions are investigated to observe the influence of applied voltage on static deflection. In sensor mode, effects of sensor location in thickness, length and diagonal directions on generated voltage are also investigated. It was observed that sensor placed at the outer surfaces generate higher voltage, however the amount of generating voltage highly depends on laminate configuration and location of sensor.

CHAPTER 3

SENSITIVITY ANALYSIS OF SMART LAMINATED BEAMS

3.1 Introduction

Design sensitivity analysis and optimization perhaps are two of the most practical and challenging issues in smart laminated structures due to the existing large number of material and geometric parameters as well as loading conditions. The conventional design methodologies lead to very long and expensive procedures which sometime make the design infeasible. Design optimization techniques have been used in smart laminated structures for various applications[85]. Also numerical methods such as finite difference technique have been generally used to determine the gradients of objective and constraints functions. Design sensitivity analysis for the determination of the gradients of objective and constraints is the dominant process in the accuracy and computational time of many design optimization procedures. Therefore, it is very important to carry out an efficient design sensitivity analysis when the optimization algorithm is to be applied to large size structural problems. In addition, the design sensitivity analysis provides the trends of variation of the objective and constraint functions versus design parameters efficiently. Thus, it can be effectively used by designer to change the preliminary design and reassess the mathematical model. Thus, the structural sensitivity analysis can be more than just a utility for optimization task and might be used as a useful design tool to

evaluate the system response to changing parameters efficiently. Numerical methods are widely used by many researchers to determine the sensitivity gradients. However, in large structural problems with large number of design parameters, including smart laminated composite structures, numerical evaluation of gradients may results an inaccurate optimum solution and is also computationally expensive. Therefore, an efficient analytical evaluation of sensitivity gradients is required.

In this chapter, the design sensitivity analysis of laminated structures with surface bonded and/or embedded piezoelectric sensors and actuators is conducted using the finite element model based on the layerwise displacement theory which incorporates the interaction between electrical and mechanical fields. For this purpose, the discrete analytical gradients of the various design constraints and objective functions with respect to the design variables are determined.

3.2 Sensitivity Analysis

In the following section, the analytical stress, displacement and frequency-related gradients of smart laminated beams are developed based on the coupled layerwise finite element formulation presented in Chapter 2. The equations of motion for smart laminated beams have been derived in Chapter 2 and are repeated here in matrix form:

$$[M_{dd}]\{\ddot{d}\} + \left([K_{dd}] - [K^{ss}_{\psi d}][K^{ss}_{\psi\psi}]^{-1}[K^{ss}_{\psi d}]\right)\{d\} =$$

$$\{F_d(t)\} + \left([K^{ss}_{d\psi}][K^{ss}_{\psi\psi}]^{-1}[K^{sa}_{\psi d}] - [K^{sa}_{d\psi}]\right)\{\psi^a\} \tag{3.1}$$

3.2.1 Static problems

For the static case, Equation (3.1) is reduced to:

$$[\hat{K}]\{d\} = \{F(t)\} \tag{3.2}$$

where $[\hat{K}] = [K_{dd}] - [K_{\psi d}^{ss}][K_{\psi\psi}^{ss}]^{-1}[K_{\psi d}^{ss}]$,

and

$$\{F(t)\} = \{F_d(t)\} - \{F^P(t)\} \tag{3.3}$$

where

$$\{F^P(t)\} = -\left([K_{d\psi}^{ss}][K_{\psi\psi}^{ss}]^{-1}[K_{\psi\psi}^{sa}] - [K_{d\psi}^{sa}]\right)\{\psi^a\} \tag{3.4}$$

where $\{F_d(t)\}$ and $\{F^P(t)\}$ represent the mechanical and piezoelectric load vectors, respectively. In actuator mode, and in the absence of the sensors in the structure, the piezoelectric load is reduced to $\{F^P(t)\} = [K_{d\psi}^{sa}]\{\psi^a\}$. It is noted that, the nodal displacement vector, $\{d\}$ is an implicit function of design variable vector, $\{q\} = \{q_1, q_2, ..., q_n\}$ of the system. Stress is also an implicit function of design variables as it is calculated using the nodal displacements. In general, the stress and displacement related constraints can be written in the following form:

$$g_i(\{d\},\{q\}) \le 0 \quad , \quad i = 1,2,...,m \tag{3.5}$$

where m is the number of constraints. Using the chain rule of differentiation, the total derivative of g_i with respect to the jth design variable (q_j) are given as:

$$\frac{dg_i}{dq_j} = \frac{\partial g_i}{\partial q_j} + \left(\frac{\partial g_i}{\partial \{d\}}\right)^T \frac{\partial \{d\}}{\partial q_j} \tag{3.6}$$

where

$$\frac{\partial g_i}{\partial \{d\}} = \left[\frac{\partial g_i}{\partial d_1} \quad \frac{\partial g_i}{\partial d_2} \quad \cdots \quad \frac{\partial g_i}{\partial d_p}\right]^T \tag{3.7}$$

where p is the number of displacement degrees of freedom.

Calculation of $\partial g_i/\partial q_j$ and $\partial g_i/\partial \{d\}$ are generally straight forward. The term $\partial \{d\}/\partial q_i$ is calculated by differentiating both sides of equilibrium Equation (3.2) with respect to q_j:

$$[\hat{K}]\frac{\partial \{d\}}{\partial q_j} = \frac{\partial \{F_d\}}{\partial q_j} + \frac{\partial \{F^P\}}{\partial q_j} - \frac{\partial [\hat{K}]}{\partial q_j}\{d\} \tag{3.8}$$

Since the external mechanical load vector is independent of design variables, we have $\partial \{F_d\}/\partial q_j = 0$. Thus Equation (3.8) can be written as:

$$\frac{\partial \{d\}}{\partial q_j} = [\hat{K}]^{-1}\left(\frac{\partial \{F^P\}}{\partial q_j} - \frac{\partial [\hat{K}]}{\partial q_j}\{d\}\right) \tag{3.9}$$

For a piezoelectric actuator, $\partial \{F^P\}/\partial q_j$ can be determined analytically as

$$\frac{\partial\{F^P\}}{\partial q_j} = \frac{\partial[K_{d\psi}^{sa}]}{\partial q_j}\{\psi^a\} + [K_{d\psi}^{sa}]\frac{\partial\{\psi^a\}}{\partial q_j} \tag{3.10}$$

The gradient of element stiffness matrix, $\partial[\hat{K}]/\partial q_j$ is derived by differentiating all its coefficients with respect to design variables and in principle, it is of the same dimension as matrix $[\hat{K}]$. Considering Equation (3.2), the derivative of stiffness matrix $\partial[\hat{K}]/\partial q_j$ can be described as:

$$\frac{\partial[\hat{K}]}{\partial q_j} = \frac{\partial[K_{dd}]}{\partial q_j} - 2\frac{\partial[K_{d\psi}^{ss}]}{\partial q_j}[K_{\psi\psi}^{ss}]^{-1}[K_{\psi d}^{ss}] + [K_{d\psi}^{ss}][K_{\psi\psi}^{ss}]^{-1}\frac{\partial[K_{\psi\psi}^{ss}]}{\partial q_j}[K_{\psi\psi}^{ss}]^{-1}[K_{d\psi}^{ss}] \tag{3.11}$$

Further, based on Equations (2.33-39), the derivatives of components of Equation (3.11) with respect to the *j*th design variable are also developed as:

$$\frac{\partial[K_{d\psi}]}{\partial q_j} = \int_0^l \left(\frac{\partial[E_{31}]}{\partial q_j}([S][S_{,x}]) + \frac{\partial}{\partial q_j}([S][S_{,x}])[E_{31}] \right) dx \tag{3.12}$$

$$\frac{\partial[K_{\psi\psi}]}{\partial q_j} = \int_0^l \left(\frac{\partial[G_{33}]}{\partial q_j}([S][S]) + \frac{\partial([S][S])}{\partial q_j}[G_{33}] \right) dx \tag{3.13}$$

$$\frac{\partial[K_{dd}^{11}]}{\partial q_j} = \int_0^l \left(\frac{\partial[A_{11}]}{\partial q_j}[S_{,x}][S_{,x}] + \frac{\partial[D_{55}]}{\partial q_j}[S][S] + \frac{\partial[S_{,x}][S_{,x}]}{\partial q_j}[A_{11}] + \frac{\partial[S][S]}{\partial q_j}[D_{55}] \right) dx \tag{3.14}$$

$$\frac{\partial[K_{dd}^{12}]}{\partial q_j} = \int_0^l \left(\frac{\partial[B_{13}]}{\partial q_j}[S_{,x}][S] + \frac{\partial[D_{55}]}{\partial q_j}[S_{,x}][S] + \frac{\partial[S_{,x}][S]}{\partial q_j}[B_{13}] + \frac{\partial[S_{,x}][S]}{\partial q_j}[D_{55}] \right) dx \tag{3.15}$$

$$\frac{\partial[K_{dd}^{22}]}{\partial q_j} = \int_0^l \left(\frac{\partial[A_{55}]}{\partial q_j}[S_{,x}][S_{,x}] + \frac{\partial[D_{33}]}{\partial q_j}[S][S] + \frac{\partial[S_{,x}][S_{,x}]}{\partial q_j}[A_{55}] + \frac{\partial[S][S]}{\partial q_j}[D_{33}] \right) dx \tag{3.16}$$

$$\frac{\partial[K_{dd}^{21}]}{\partial q_j} = \frac{\partial[K_{dd}^{12}]^T}{\partial q_j} \tag{3.17}$$

$$\frac{\partial[K_{\psi d}]}{\partial q_j} = \frac{\partial[K_{d\psi}]^T}{\partial q_j} \tag{3.18}$$

where as mentioned in Chapter 2, $[S(x)]$ represents the vector of shape functions given by $[S(x)] = [1-\varsigma, \varsigma]$, $\varsigma = x/l$ and subscript comma denotes derivative with respect to the letter next to comma.

3.2.2 Dynamic problems

For the free undamped vibration, Equation (3.1) is written as

$$\left([\hat{K}] - \lambda[M]\right)\{d\} = 0 \tag{3.19}$$

where $\lambda(=\omega^2)$ denotes the squared value of natural frequency. The solution of the eigenvalue problem represented by Equation (3.19) consists of k eigenvalues, λ_k, and

corresponding eigenvectors $\{\bar{d}_k\}$. For the k^{th} vibration mode, the sensitivity of natural frequency with respect to changes in the design variable q_j is given by[92]:

$$\frac{d\lambda_k}{dq_j} = \{\bar{d}_k\}^T \left(\frac{\partial[\hat{K}]}{\partial q_j} - \lambda_k \frac{\partial[M]}{\partial q_j} \right) \{\bar{d}_k\} \tag{3.20}$$

where λ_k is the k^{th} natural frequency and $\{\bar{d}_k\}$ is the k^{th} mode shape vector. The gradient of mass matrix can be determined using the coefficients of mass matrix given in Equation (2.40-41) as:

$$\frac{\partial[M^{11}]}{\partial q_j} = \int_0^l \left(\frac{\partial\{\rho^1\}}{\partial q_j}([S][S]) + \frac{\partial[S][S]}{\partial q_j}\{\rho^1\} \right) dx \tag{3.21}$$

$$\frac{\partial[M^{22}]}{\partial q_j} = \int_0^l \left(\frac{\partial\{\rho^2\}}{\partial q_j}([S][S]) + \frac{\partial[S][S]}{\partial q_j}\{\rho^2\} \right) dx \tag{3.22}$$

The gradients of the coefficients corresponding to the laminate thicknesses, $\{A_{55}\}, \{B_{13}\}, \{A_{11}\}, \{D_{55}\}, G_{33}, \{E_{31}\}, \{\rho^1\}$ and $\{\rho^2\}$ can be easily evaluated as these functions are expressed as function of the layer thickness. Assume that the design variable is the thickness of the first layer in the laminate; then the analytical derivative of the coefficients, say for example, $\{A_{55}\}$, is taken which results in a 2×2 matrix. The procedure continues by computing this matrix for 2^{nd}, 3^{rd},...,N^{th} node. Then theses matrices are assembled using the common assembly procedure used in the finite element

method which results in $N \times N$ matrix for $\{A_{55}\}$ with only non-zero components corresponding to the first sub-matrix 2×2 . Similarly, if the thickness of 2nd, 3rd, ..., (*N-1*)th layers are considered as design variables, then $\{A_{55}\}$ becomes a $N \times N$ matrix with only non-zero components corresponding to 2nd, 3rd,..., (*N-1*)th layers, respectively. Similar procedure is applied to compute the analytical derivatives of all the parameters corresponding to $\{B_{13}\}, \{A_{11}\}, \{D_{55}\}, \{G_{33}\}$ and $\{E_{31}\}$ which are given as functions of thickness.

To summarize, using the developed analytical derivatives, the gradients of the element stiffness and mass matrices can be computed. It should be noted that ς are only function of element length. In addition, if the design variables are not functions of the element length, then the second terms in the derivatives given by Equations (3.12) to (3.16) and (3.21) to (3.22) become zero and the analytical gradients are correspondingly simplified.

3.3 Numerical Illustrations

This section presents the results for several representative problems. First, a benchmark problem is considered in order to validate the developed mathematical model for the analytical gradients. Next, several illustrative sensitivity analysis problems are investigated using the developed analytical gradients. All the application examples focus on the laminated cantilever beams with embedded or surface bonded piezoelectric patches as sensors and/or actuators. The properties of the material used for all the examples are given in Table 3.1.

Table 3.1 Material properties for numerical examples

Property	T300/934	Adhesive	PZT
E_1, GPa	126.0	6.9	63.0
E_3, GPa	7.9	6.9	63.0
v_{13}	0.275	0.4	0.28
G_{13}, GPa	3.40	2.46	24.8
$d_{31}(m/V)$	-	-	-166×10^{-12}
$d_{33}(m/V)$	-	-	285×10^{-12}
$d_{15}(m/V)$	-	-	-
$g_{33}(farad/m)$	-	-	11.53×10^{-9}
$\rho(Kg/m^3)$	1527	1662	7600

3.3.1 Sensitivity analysis using analytical gradients and finite difference method

A cantilever beam made of 5 layers of unidirectional graphite/epoxy T300/934 of thickness 1.0 *mm* and one layer of PZT actuator of thickness 1.0 *mm* bonded on the top surface is considered. The objective is to investigate the sensitivity of tip deflection with respect to the layer thickness. The length and width of the beam are given as 20 c*m* and 3 *cm* respectively. The piezoelectric layer is actuated by applying 1.0 *V* electric potential in thickness direction.

In Figure 3.1, the sensitivity of the tip deflection with respect to the laminate thickness (design variable), has been shown based on the developed analytical gradients and compared with that obtained using the finite difference method. As it can be realized insignificant difference exists between the numerical and analytically evaluated tip deflection sensitivity, thus validating the developed analytical gradients. However, determining the gradients using the finite difference method at a specific point requires

repeating the whole procedure at a nearby point whereas analytical formulation directly provides the gradients. For large size structural problems with many design variables, numerical computation of gradients may become significantly computationally expensive. Therefore, analytical gradients provide more efficient and cost saving calculations in design sensitivity and optimization procedures.

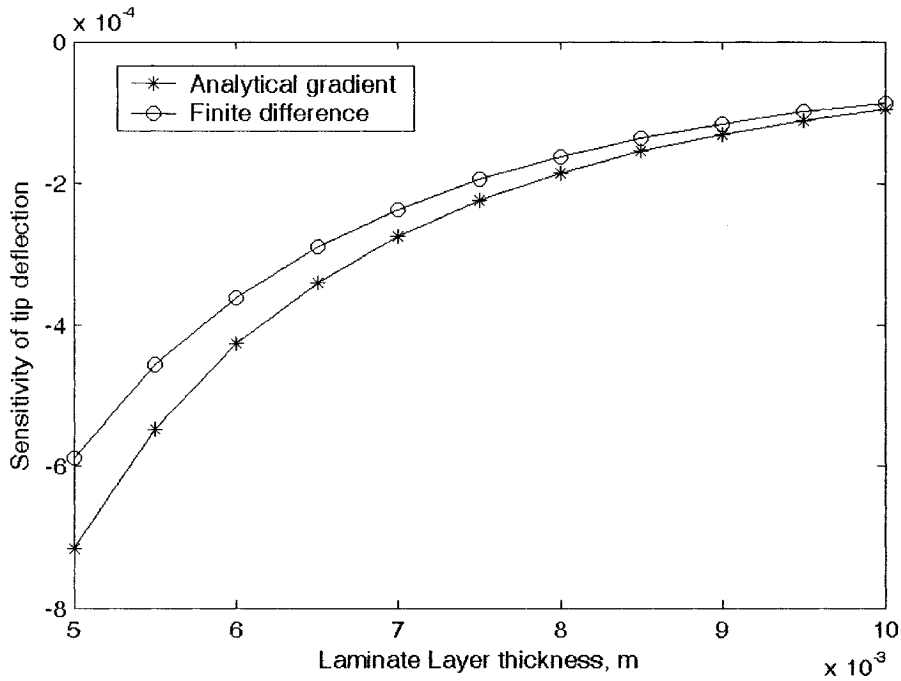

Figure 3.1 Comparison of analytical and finite difference gradients

3.3.2 Sensitivity of deflection with respect to layer thickness

A cantilever beam with similar material and geometric properties as described in Section 3.3.1, made of 4 layers of unidirectional graphite/epoxy T300/934 and one 1.0 *mm* layer of PZT actuator bonded on the top surface is considered to investigate the sensitivity of deflection with respect to the laminate thickness. Sensitivity of the tip deflection with respect to the laminate thickness has been shown in Figure 3.2 for different applied voltages on the actuator.

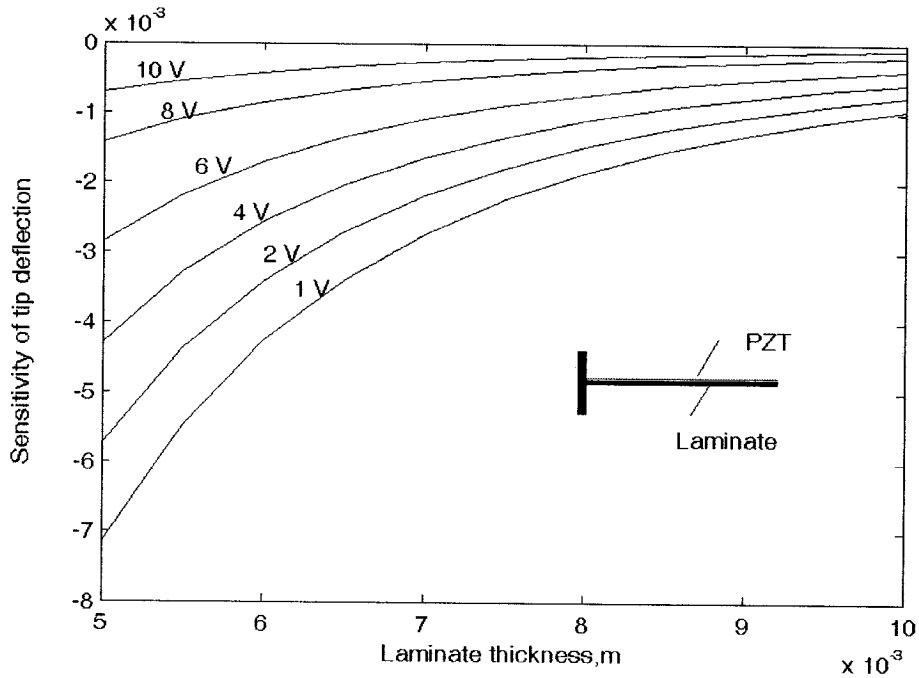

Figure 3.2 Sensitivity of the tip deflection

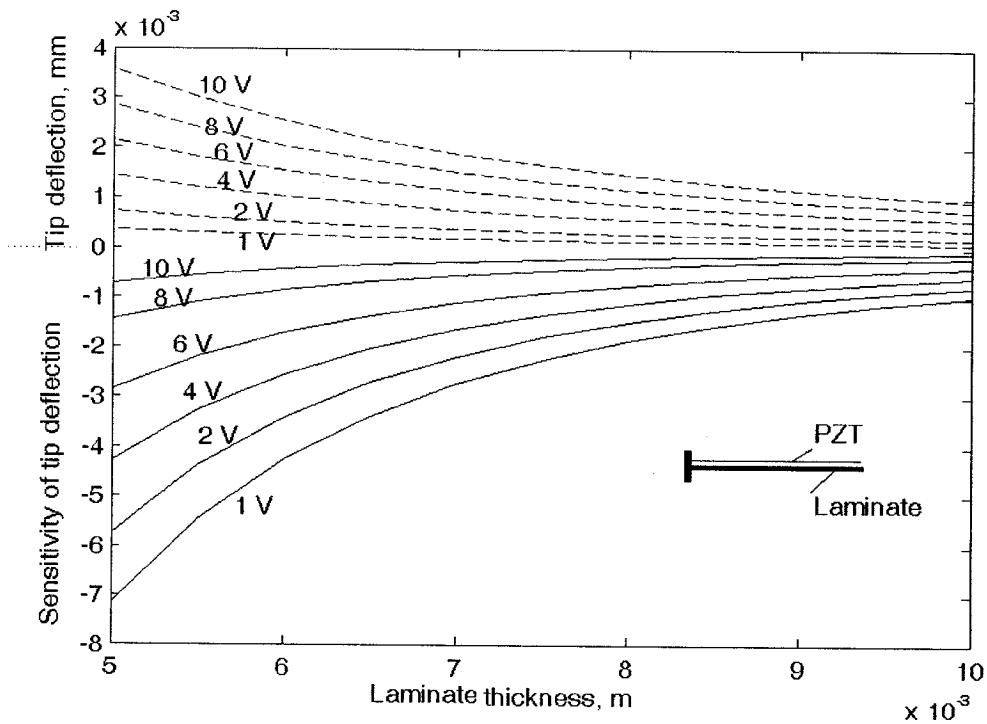

Figure 3.3 Sensitivity of tip deflection and the tip deflection value

The variation of the tip deflection with respect to the laminate thickness is illustrated in Figure 3.3. It is observed that reducing the laminate thickness increases the sensitivity of the tip deflection. Also for a defined laminate layer thickness, increasing the applied voltage reduces the sensitivity of the tip deflection.

Further, the effects of laminate orientation, piezoelectric actuator location and applied voltage on the sensitivity of the tip deflection with respect to the layer thickness are investigated. In Figure 3.4, the sensitivity of the tip deflection is normalized with respect to that of unidirectional laminate. Different laminate orientations have been considered. It is indicated that unsymmetric laminate [0/90/0/90] has the highest sensitivity with respect to the unidirectional and other laminate configurations.

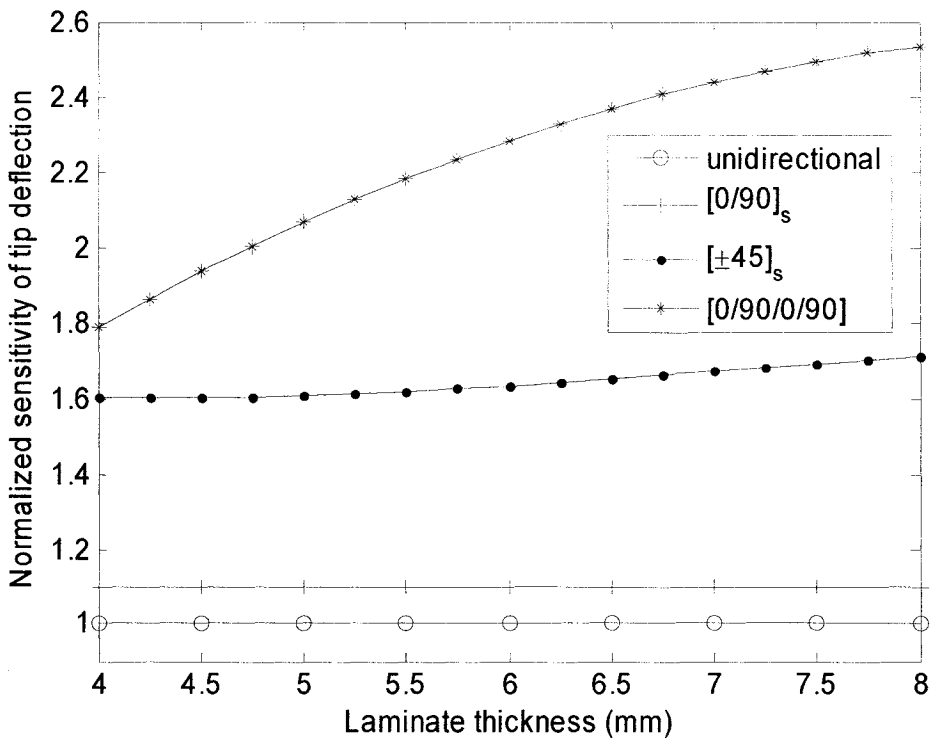

Figure 3.4 Normalized sensitivity of the tip deflection with respect to the laminate thickness

Figure 3.5 presents the effect of actuator location on the sensitivity of the tip deflection. L_p represents the location of PZT patch from the fixed end and L_t is the total length of the beam. The result shows that the unidirectional laminate has the lowest sensitivity compared with the other lamination schemes and unsymmetric laminate [0/90/0/90] presents the highest sensitivity of tip deflection, dw_{tip}/dt .

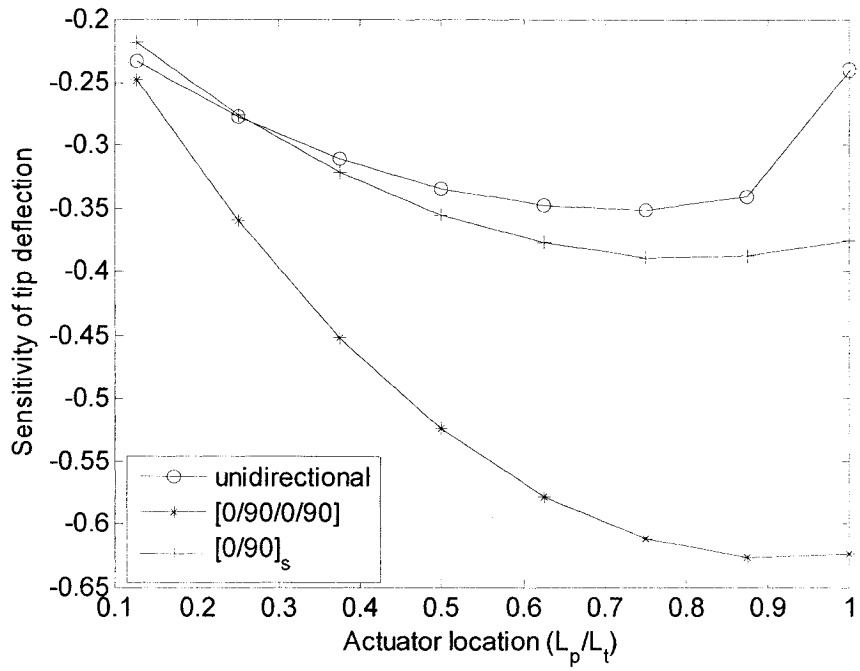

Figure 3.5 Sensitivity of tip deflection with respect to actuator location

Figure 3.6 also shows the effect of applied voltage of PZT actuators on the sensitivity of tip deflection with respect to the layer thickness, dw_{tip}/dt. As it can be realized, the value of tip sensitivity increases linearly by increasing the applied voltage for all laminate configurations. The unsymmetric cross ply laminate scheme [0/90/0/90], shows the highest sensitivity and the unidirectional laminate the lowest one.

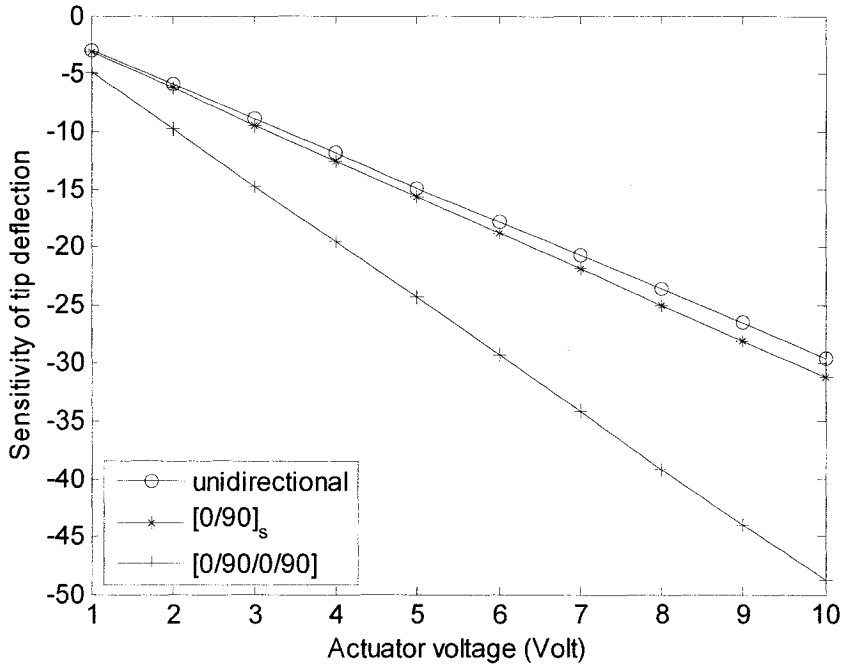

Figure 3.6 Sensitivity of the tip deflection versus actuator voltage for different laminate configurations

3.3.3 Sensitivity of beam mass with respect to layer thickness

The sensitivity of the beam mass with respect to the layer thickness can easily be determined by analytical gradient. Since the mass is a linear function of layer thickness, its gradient with respect to layer thickness is a constant value. The sensitivity of mass with respect to layer thickness can be obtained by differentiating the summation of volumes of the graphite/epoxy layers multiplied by density of the material with respect to layer thickness. Similarly sensitivity of mass with respect to piezoelectric layers is obtained by differentiating the summation of volumes of piezoelectric layers multiplied by the density of piezoelectric material with respect to piezoelectric layer thickness. For the cantilever beam described in Section 3.3.1 with one layer of piezoelectric layer

bonded on top surface, sensitivity of mass with respect to the thickness of the composite layer (graphite/ epoxy T300/934) is 41.6 and sensitivity of the mass with respect to the thickness of piezoelectric layer is 45.1. In the case that we have two piezoelectric layers in the laminate, sensitivity of mass with respect to the laminate layer is 33.3 and with respect to the piezoelectric layer is 91.2. Figure 3.7 presents the effect of ratio of PZT volumes and graphite/epoxy volumes ($V_{PZT}/V_{composite}$) to the sensitivity of mass with respect to the layer thickness. This concludes that the mass of the structure is more sensitive to the changes in PZT layers compared with the changes in the graphite/epoxy layers. At the coincidence point $V_{PZT}/V_{composite} = 0.18$, both PZT and graphite/epoxy show an equal effect on the sensitivity of mass with respect to the layer thickness.

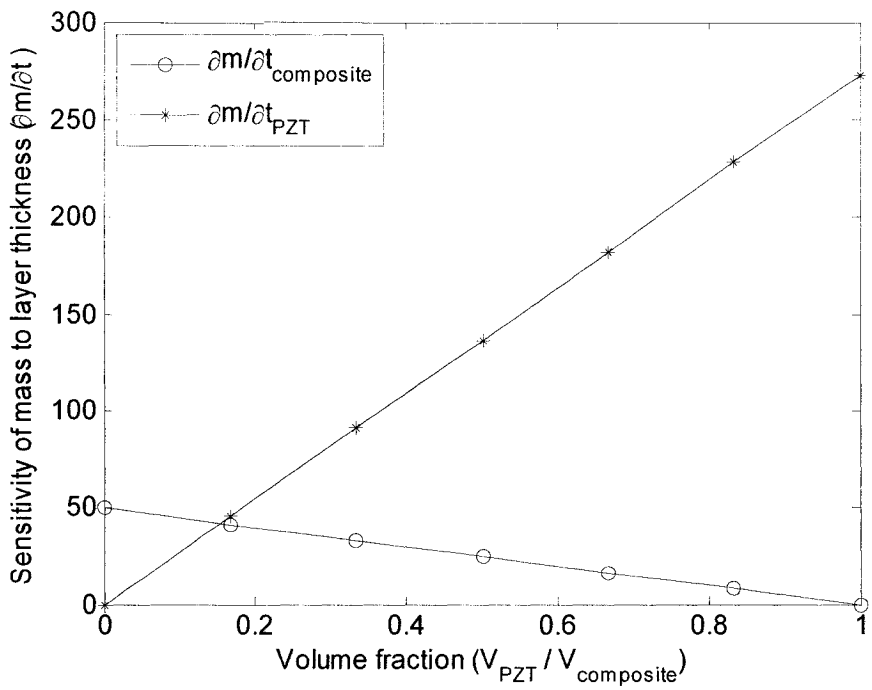

Figure 3.7 Sensitivity of mass with respect to volume ratio of composite material and PZT

3.4 Conclusions

Analytical sensitivity formulation has been developed for smart laminated composite beams with bonded/embedded piezoelectric layers as sensors and/or actuators have been investigated based on the layerwise displacement theory. A systematic sensitivity analysis based on the developed analytical gradients of various constraints and objective functions has been presented.

The design sensitivity analysis provides the trends of variation of the design parameters and can be used by designer to change the preliminary design and obtain the desired design without performing long and expensive optimization procedures. Accuracy and efficiency of the presented algorithm have been demonstrated through numerical examples.

CHAPTER 4

DESIGN OPTMIZATION OF SMART LAMINATED BEAMS

4.1 Introduction

Design optimization perhaps is one of the most important issues in smart laminated structures due to the presence of large number of material and geometrical parameters as well as loading conditions. The conventional design methodology (Figure 4.1) is an ad-hoc procedure which typically results in a non-optimal design solution. The designer's experience plays an important factor in the success of the design process which may sometimes be very computationally expensive.

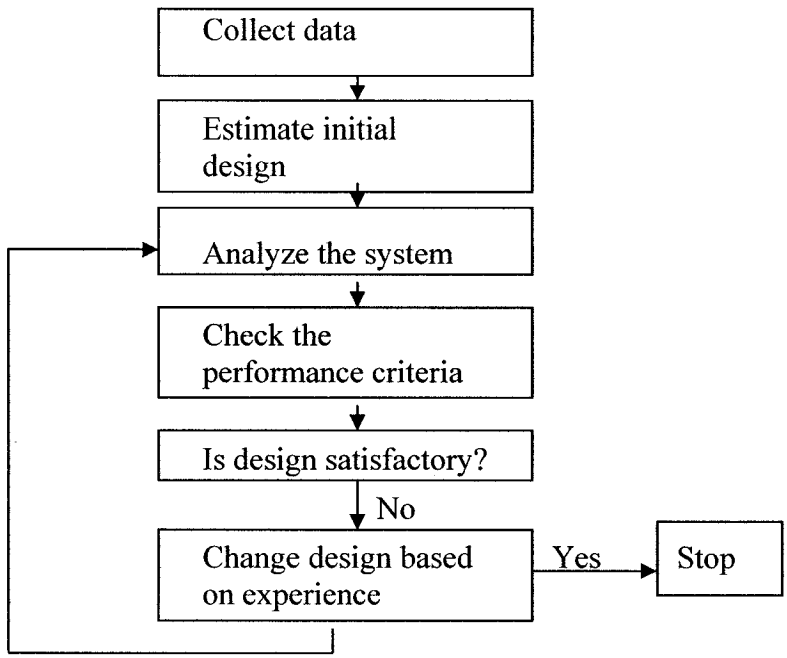

Figure 4.1 Conventional design process

However, in formal design optimization, processes are performed following a systematic manner to achieve the optimal design. The typical optimum design process is shown in Figure 4.2.

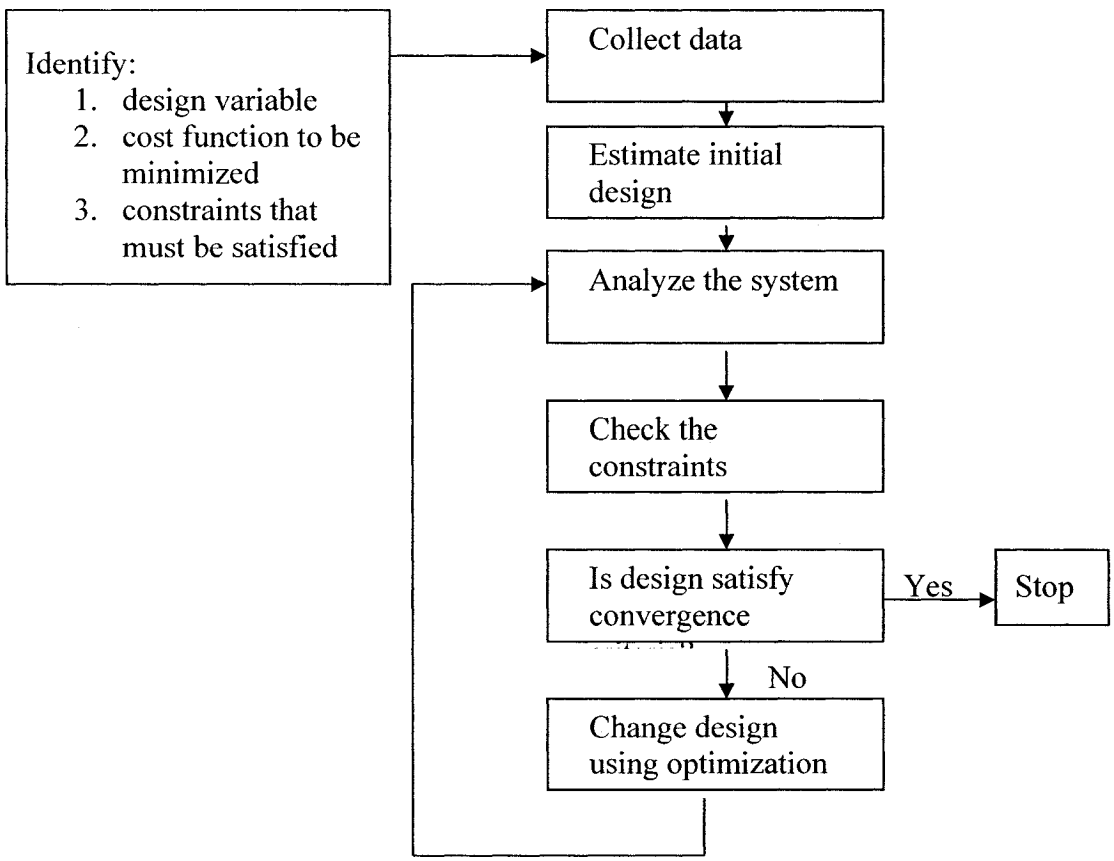

Figure 4.2 Optimum design process

In this chapter, an efficient design optimization algorithm has been developed by combining the coupled layerwise finite element model presented in Chapter 2, sensitivity and analytical gradient developed in Chapter 3, and optimization technique based on the Sequential Quadratic Programming (SQP) technique to obtain the optimal design of the

structure. Various objectives and constraints are considered. Illustrative examples are presented to demonstrate the methodology.

4.2 Design Optimization Algorithm

In order to determine the optimal design of laminated beam with integrated piezoelectric actuators, one of the most powerful methods of the gradient based optimization techniques, namely the Sequential Quadratic Programming (SQP) method has been implemented. For more details of the procedure, one may consult the books written by Arora[148] and Fletcher[149]. Here the most essential issues of the SQP technique have been reviewed. The main idea is to generate a Quadratic Programming (QP) problem based on the quadratic approximation of the Lagrangian function described as:

$$L(\{q\},\lambda) = f(\{q\}) + \sum_{i=1}^{m} \lambda_i . g_i(\{q\}) \tag{4.1}$$

where $\{q\}$, g_i and λ_i are design variable vector, constraints and Lagrange multipliers, respectively. It should be noted that the bound constraints have been expressed as inequality constraints in derivation of the Lagrangian in Equation (4.1). The SQP implementation consists of three main steps: (*i*) a QP Sub-problem solution; (*ii*) a line search and objective function calculation, and (*iii*) updating of the Hessian matrix of the Lagrangian function given by Equation (4.1). The procedure proceeds by solving a QP sub-problem at each major iteration.

The solution of the QP sub-problem generates an estimate of the Lagrange multiplier, λ, and a search direction vector $\{d\}$ in each iteration k, which is used to form a new iteration as:

$$\{q\}_{k+1} = \{q\}_k + \alpha_k \{\mathrm{d}\}_k \tag{4.2}$$

The step length parameter α_k, should be determined by using an appropriate line search technique (one-dimensional minimizations) in order to produce a sufficient decrease in the merit function. At the end of the one-dimensional minimization, the Hessian of the Lagrangian, required for the solution of the next positive definitive quadratic programming problem, is updated using the Broyden-Fletcher-Goldfarb-Shanno (BFGS) updated formula.

For the solution of QP sub-problem, the algorithm requires computing the gradient of both constraints and objective function at each iteration. Gradients are typically evaluated using the finite difference method. It has been shown that the analytical gradients may lead to an accurate optimal result efficiently.

It should be noted that the non-linear mathematical programming optimization techniques such as SQP may find the local minima instead of the global one. In other words, they may get trapped into the local optima, without having a mechanism to climb out of it. Thus, these methods may fail to discover the global optimum. In this study, to alleviate this problem, optimization algorithm has been executed for multitude of random initial points in an attempt to catch the global optimum point.

In the following examples the design variable vector $\{q\} = \{t_1, t_2, ..., t_{n+n_p}\}$ is considered as the vector of thicknesses of composite layers and piezoelectric actuators unless otherwise specified.

4.3 Numerical Examples

This section presents the results for several representative problems. The effects of various design variables on the design objective and constraints are also investigated. All the applications focus on a laminated cantilever beam with embedded or surface bonded piezoelectric sensors and/or actuators. The properties of the material used for all the example applications are given in Table 4.1.

Table 4.1 Material properties for numerical examples

Property	NCT/301	Adhesive	PZT
E_1, GPa	144.34	6.9	63.0
E_3, GPa	9.85	6.9	63.0
ν_{13}	0.28	0.4	0.28
G_{13}, GPa	4.34	2.46	24.8
$d_{31}(m/V)$	-	-	-166×10^{-12}
$d_{33}(m/V)$	-	-	285×10^{-12}
$d_{15}(m/V)$	-	-	-
$g_{33}(farad/m)$	-	-	11.53×10^{-9}
$\rho(Kg/m^3)$	1385	1662	7600

4.3.1 Optimal design for static problem

A smart laminated beam with 2 unidirectional layers of graphite/epoxy NCT/301 and of 30 *cm* length and 3 *cm* width are considered to investigate the effect of developed analytical gradients on the efficiency of optimization procedure. Five piezoelectric

actuator patches, made of PZT and of size $3\times3\,cm^2$ are bonded at the upper surface which covers half of the whole length of the beam and another five similar patches are bonded at bottom surface as shown in Figure 4.3. One may note that in physical model, the five PZT patches can be considered as one element as the applied voltage is equal for all the patches. Mechanical and electrical loadings are: a 100 N point load applied at the tip of the beam and a 240 V electric potential applied through the thickness at the actuators. It is desired to determine the optimal design of the layer thickness of both piezoelectric and composite materials in order to minimize the mass of the beam while restricting the tip deflection to be lower than 0.2 *mm*.

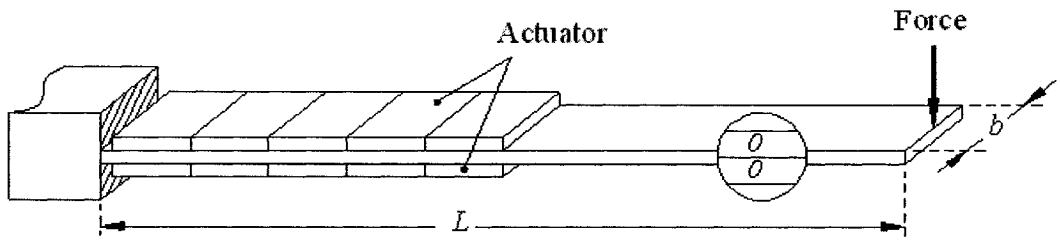

Figure 4.3 Schematic illustration of piezo-laminated cantilever beam

The variation of mass in optimization process is presented versus number of iterations and number of objective function evaluations in Figure 4.4 and 4.5, respectively. The optimal thicknesses for piezoelectric patches and composite material are found to be 0.1 *mm* and 11.7 *mm*, respectively. Using the optimal layer thicknesses, the tip displacement at optimal point is obtained as 0.189 *mm*.

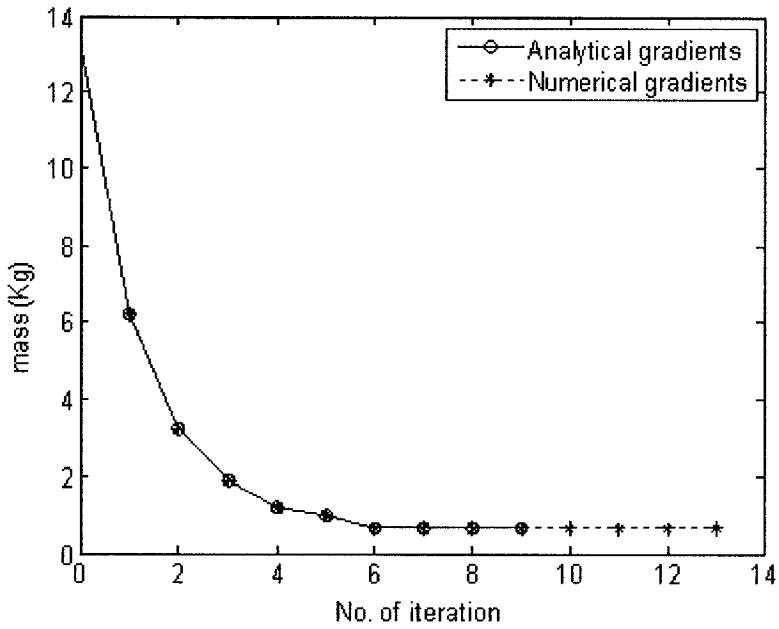

Figure 4.4 Iteration history for mass of the smart composite beam versus number of iteration in optimization process

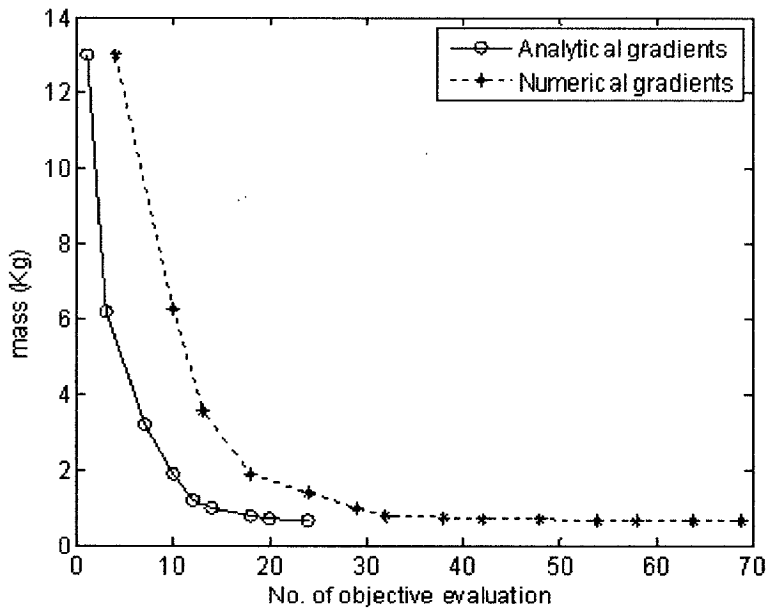

Figure 4.5 Iteration history for mass of the smart composite beam versus number of objective function evaluation in optimization process

Using analytical gradients, the optimal design has been obtained after 9 iterations and 24 function evaluations while using finite difference gradients the same results have been obtained after 13 iterations and 68 function evaluations thus confirming the design optimization process can be conducted more efficiently by using analytical gradients. It is worth noting that this result has been obtained for a simple problem with only two design variables. In large structural problems with many numbers of design variables and constraints, using analytical gradients may dramatically improve the efficiency of the design optimization procedure.

4.3.2 Optimal thicknesses of sensor and actuator

In this example, two $3\times 3\,cm^2$ patches of piezoelectric material are attached on top of the laminated beam as sensing device and another two piezoelectric patches are attached to the bottom of the laminated beam as actuating devices. The laminate consists of six layers of 0.125 *mm* thick graphite/epoxy and is configured as$[0/90/0]_S$. The length and width of the beam are (L = 0.3 *m*) and (b = 0.03 *m*), respectively. The beam is meshed with 10 equal-length elements and PZT patches are bonded at the location of the first two elements as shown in Figure 4.6. PZT actuators are excited by 100 *V* electric potential.

The objective of this problem is to obtain the thicknesses of both sensors and actuators to minimize the mass of the beam while satisfying constraints on tip deflection (to be greater than 0.1 *mm*) and generated voltage at sensors (to be grater than 5 volts). The optimal solution has been obtained only after 2 iterations and found to be 0.5 *mm* thickness for both sensors and actuators. The optimal mass is 11.3 gr.

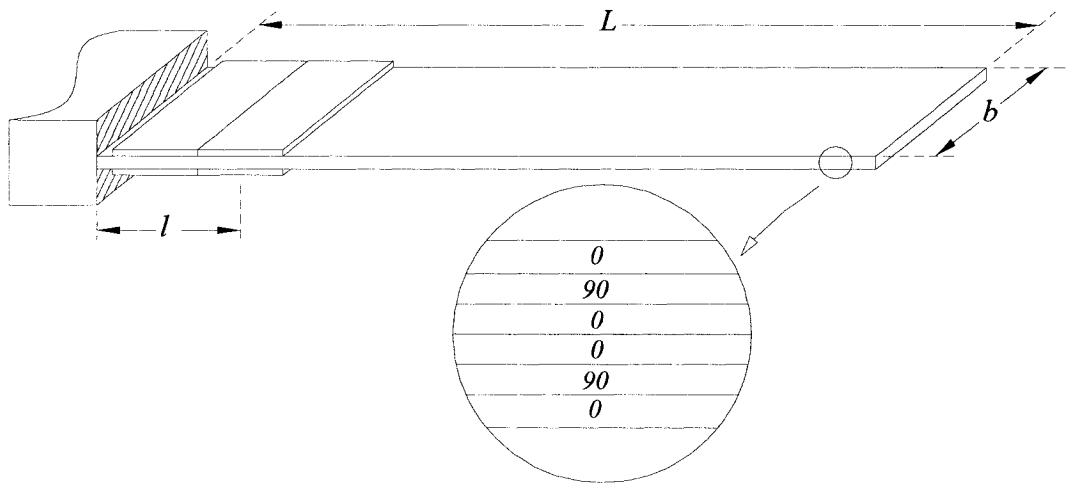

Figure 4.6 Schematic illustration of piezo-laminated cantilever beam

It should be noted that different initial points have been selected to confirm the global optimality of the solution. This optimal configuration results in 0.177 *mm* tip deflection and 6.0 *V* electric potential generated at the sensors. It is noted that the accuracy of voltage generated in sensors is of great interest in shape control application, since it is used to evaluate the deflection and in turn to compute the actuator voltage required to control the nodal displacements.

4.3.3 Displacement control while monitoring inter-laminar stresses

The laminated beam described in example 4.3.2 is considered to investigate displacement control while monitoring inter-laminar stresses between layers. The beam is meshed with ten equal-length finite elements where the actuator patches are considered at the first three finite elements. Material and geometric properties are given in Table 4.1. It is desired to achieve the minimum mass of the beam while having 2 *mm* tip deflection. The

inter-laminar stresses between layers are also monitored not to exceed 1 *MPa*. The applied voltage is limited between 1 and 100 volt. The layer thicknesses are limited between 0.125 *mm* (lower limit), which is typical for graphite/epoxy lamina, and 20 *mm* (upper limit). The thicknesses of PZT patches are also limited between 0.2 *mm* and 20 *mm*. The optimization problem is cast into the following form:

$$f = \sum_{j=1}^{N_{PZT}} b\rho_j^{PZT} t_j^{PZT} + \sum_{i=1}^{N} b\rho_i^c t_i^c \rightarrow \min.$$

Subject to

$$u_{tip} = 2.0\,mm,$$

$$(\tau_{xz})_{layer} \leq 1\,MPa$$

$$1.0V \leq \psi^a \leq 100\,V,$$

$$0.1\ mm \leq t^c \leq 20.0\,mm,$$

$$0.1\ mm \leq t^{PZT} \leq 20.0\,mm$$

The thicknesses of composite and PZT layers as well as the applied voltage are determined for laminate configurations, $[0/90]_{3T}$, $[\pm 45]_{3T}$ and $[\pm 30]_{3T}$. The results are provided in Table 4.2 in which one can realize that configuration $[\pm 45]_{3T}$ requires higher layers thickness and lower actuating voltage than that of the $[0/90]_{3T}$ and $[\pm 30]_{3T}$. This is due to the lowest stiffness of configuration $[\pm 45]_{3T}$. Consequently, configuration $[\pm 30]_{3T}$ needs lower layer thickness and higher actuating voltage than that of $[0/90]_{3T}$.

Table 4.2 Optimal layer thickness (mm) and PZT voltage (volt)

Laminate	Layer thickness, *mm*						Top	Bottom	Voltage
	L_1	L_2	L_3	L_4	L_5	L_6	PZT	PZT	
$[0/90]_{3T}$	0.10	0.10	0.888	0.889	0.889	0.887	0.10	0.887	72.2
$[\pm 45]_{3T}$	0.10	0.10	0.913	1.110	0.963	0.897	0.10	0.897	66.33
$[\pm 30]_{3T}$	0.10	0.10	0.10	0.810	0.790	0.887	0.10	0.887	91.5

Iteration procedure leading to the optimal mass for different laminate configurations is provided in Figure 4.7. As it was expected from the conclusion derived from the results provided in Table 4.2, the minimum mass is obtained for $[\pm 30]_{3T}$ and configurations $[0/90]_{3T}$ and $[\pm 45]_{3T}$ are in the second and third ranks.

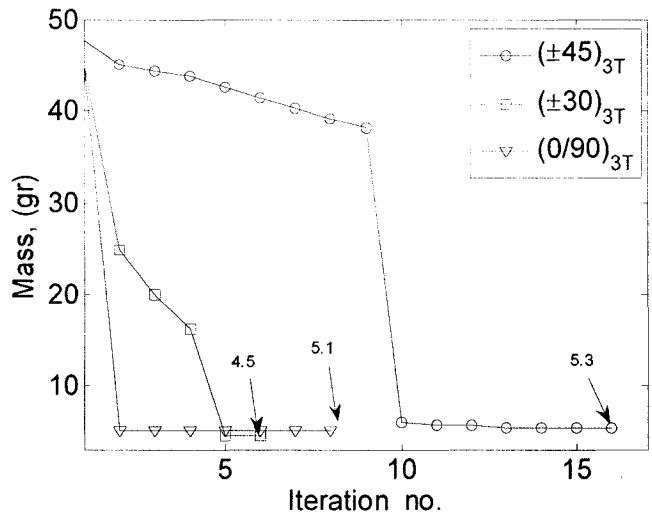

Figure 4.7 Iteration history to minimize the mass

The inter-laminar stresses corresponding to the optimal design are provided in Figure 4.8. It is indicated that inter-laminar stresses between the laminate layers and piezoelectric

layers are higher than the inter-laminar stresses between host layers. This is due to the higher value of shear stiffness for piezoelectric materials.

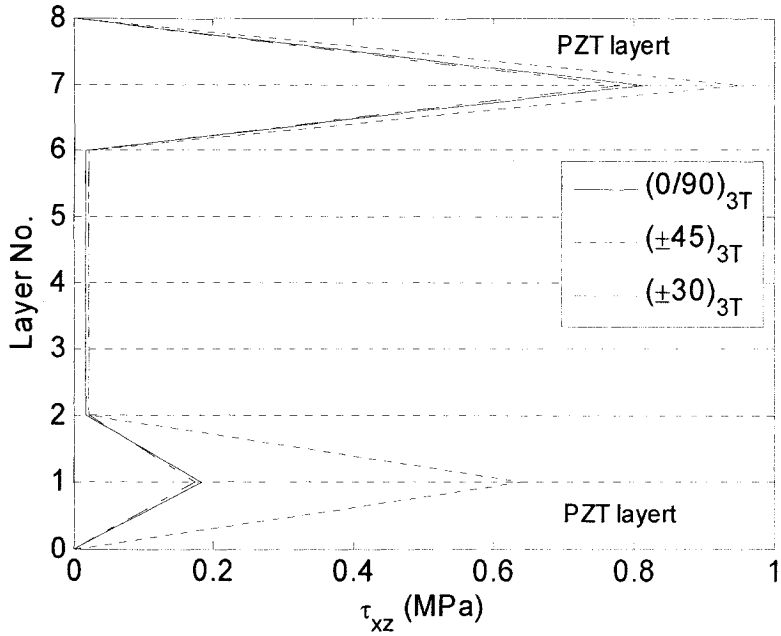

Figure 4.8 Optimal inter-laminar stresses

This result is of great importance in designing smart laminated beam since the force applied by the PZT actuators usually is very small. In terms of manufacturing, the bonding between piezoelectric elements and host structure should be well treated in order to prevent detaching of actuators from the composite layers.

In addition, the applied voltage should be kept in a safe region for PZT ceramics. It is observed that the optimal thickness of the upper and lower PZT patches greatly depends on the lamination orientation and applied voltage. It should be noted that monitoring inter-laminar stress in optimization procedure using ESL theories is not straight forward and also not accurate. However, the finite element method based on the layerwise theory

provides inter-laminar stresses that are very close to the results obtained using three dimensional finite element method[13]. Therefore, finite element method based on the layerwise theory is an efficient (in terms of computation) and accurate (compared to 3D analysis) analysis tool in the design optimization procedure.

4.3.4 Optimal design with frequency constraint

The smart laminated beam described in Section 4.3.1 is again considered here with 4 layers and sequence configuration of $[0/90]_s$ to determine the optimal thickness of composite layers to minimize the mass under frequency constraints, while the thickness of both sensors and actuators is 0.5 *mm*. The first three natural frequencies of the beam are monitored not to exceed 40, 215 and 680 *Hz*, respectively. The optimal design for layer thickness is obtained and given in Table 4.3 considering with and without electromechanical coupling effect in the finite element model. It is observed that performing optimization technique may reduce the total mass of the beam by 28 percent when neglecting the effect of electro-mechanical coupling in the analysis. Considering electro-mechanical effect in the finite element model may decrease the optimum mass by 34 percent.

Table 4.3 Optimal layer thickness with frequency constraint

	Layer thickness, *mm*	Total mass, *gr*	% Reduced mass
Initial design	1.0	82.0	0.0
Optimal (no coupling)	0.59	58.55	28.65
Optimal (coupling)	0.54	56.0	34.14

The optimal layer thicknesses for both PZT patches and composite material are determined using the finite difference and analytical gradients and are presented in Figure

4.9. It is observed that the results obtained using analytical gradients and finite difference methods are in very good agreement.

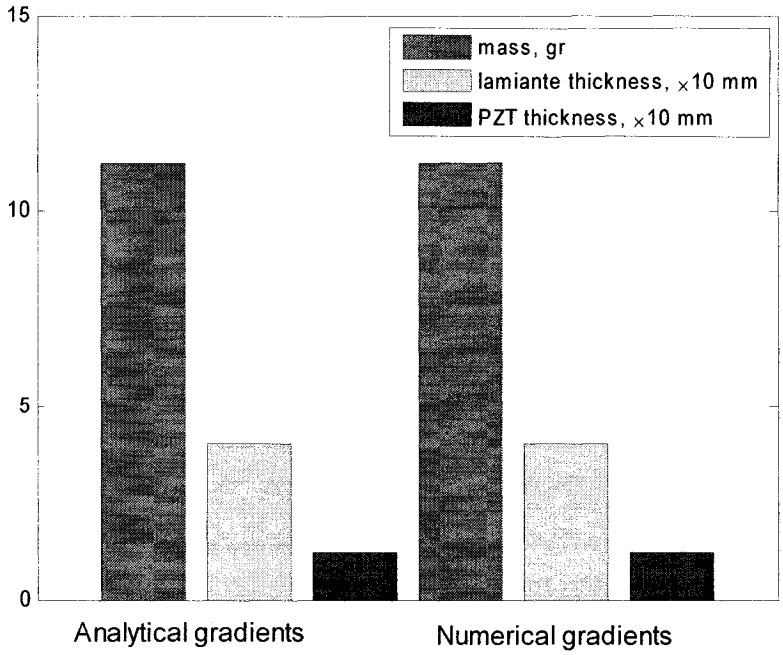

Figure 4.9 Optimal design of piezo-laminated beam under frequency constraints

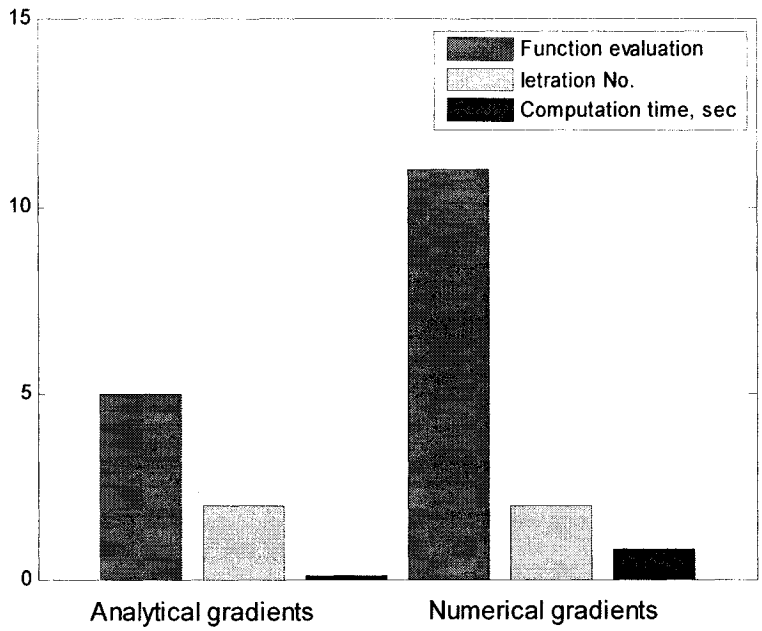

Figure 4.10 Number of iteration, function evaluation and computational time in optimal design of piezo-laminated beam under frequency constraints

However, as shown in Figure 4.10 significant reduction in computational efforts is achieved using analytical gradients in the optimization procedure.

4.3.5 Effect of boundary conditions and PZT patches on optimal design

In order to investigate the effect of boundary conditions and location of PZT patches on the optimal design of the smart laminated beam, the beam described in the Section 4.3.1 is again considered except that the PZT patches are located in two different cases as shown in Figure 4.11. The laminate configuration, geometric and material properties are considered similar to the example in Section 4.3.1. Both cases are modeled with 10 finite element meshes. In case I, the five PZT patches are attached in the first five meshes. In case II, the five PZT patches are distributed along the length of the beam by equal distance. All the PZT patches are subjected to +240 V at the upper surface and -240 V at lower surface.

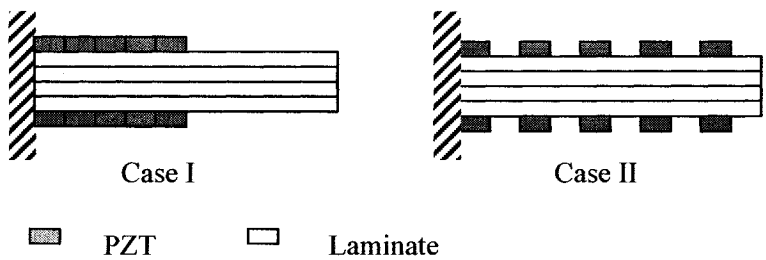

Figure 4.11 schematic illustrations of different cases of smart laminated beam

The optimization problem is defined as the following:

minimize (*mass of the beam*) subject to , $(\omega_1 \quad \omega_2 \quad \omega_3) \geq (40 \quad 215 \quad 680) Hz$

where ω_i represent the natural frequency of the beam.

The optimization problem has been solved for simply supported, clamped free and clamped-clamped boundary conditions and with different PZT locations, namely case I and case II. The results are provided in Table 4.4. It is observed that for all boundary conditions under investigation, the optimal mass for case I is lower than that of case II. This effect is mainly due to the higher stiffness of the beam configured with case I. Also, the results indicate that, the beam with clamped–free boundary requires the higher value of mass to satisfy the required constraints while the clamped-clamped boundary condition requires the lowest value of mass.

Table 4.4 Optimal design of smart laminated beam under frequency constraint

	Clamped-free			Simply-support			Clamped-clamped		
	TL	TP	Mass,g	TL	TP	Mass,g	TL	TP	Mass,g
Case I	6.7	1.0	42.6	3.8	1.0	2.72	2.47	1.0	2.00
Case II	6.9	1.0	43.7	3.9	1.0	2.77	2.57	1.0	2.06

*TL: thickness (*mm*) of individual layer of the laminated beam, TP: Thickness (*mm*) of PZT patches

4.3.4 Optimal design for vibration control

A cantilever laminated beam with 4 layers $[(0/90)_s]$ each of 0.125 *mm* thickness is considered. The length and width of the beam are given as 0.33 *m* and 0.0254 *m*, respectively. One piezoelectric actuator ($16.5 \times 25 \times 0.8 mm^3$) is attached on the top surface at 0.05 *m* from the fixed end of the beam. The free end of the beam is initially displaced by 10 *mm*. It is desired to determine the minimum electric potential desired to suppress the transient vibration in a controlled manner. It is required to reduce the settling time to 0.5 seconds by applying electric potential to the actuators. The optimization problem is

minimization of the control effort in time interval 0 to T. The problem is cast into the following standard format:

$$\min f = \int_0^T V^2(t)dt$$

$$\text{subject to,} \qquad w(T) = 0, \qquad |V(t)| \le V_a \tag{4.4}$$

where T is the allowable time to suppress the motion and is assumed to be 2 sec, V_a is the maximum applied voltage on the actuators (1000 V), and w represents the transverse displacement of the beam.

Figure 4.11(a) shows the initial response of the laminated beam and the response of the system after the optimum voltages given in Figure 4.10(b) are applied to the system. It is observed that by performing the optimization, the settling time is reduced from 2.5 seconds to 0.5 seconds. In Figure 4.12(a), the iteration history of the performance function (control effort) is shown. In the second iteration, the control effort is jumped to its maximum level and after six iterations is converged to its minimum value which is about 10000 V^2.sec.

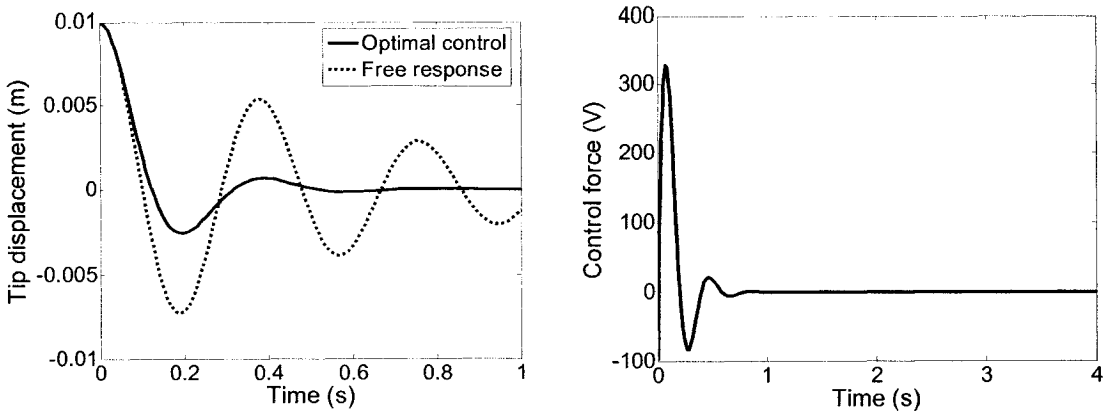

(a) (b)

Figure 4.11 (a) Vibration suppression using optimal electric potential, (b) Optimal voltages applied at actuators

Initial and optimal control forces are presented in Figure 4.12(b) where one may realize a significant reduction in the first peak. Obviously the difference is a relative value and it depends on the initial design.

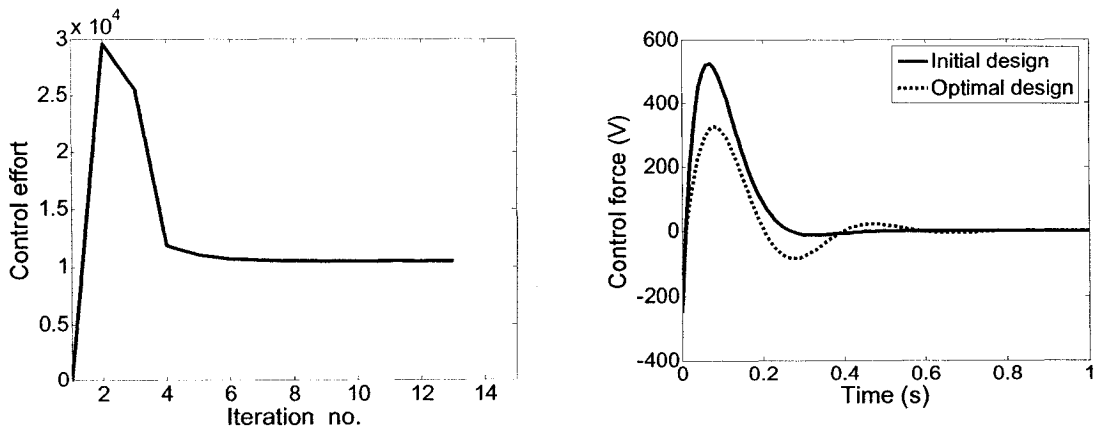

Figure 4.12 (a) Performance history for the optimal control, (b) initial and optimal control forces

Further, the effects of laminate configuration and location of actuator are investigated. The same smart laminated beam is considered except that the laminate configuration and location of the actuator are changed for different cases. In the first case, the actuator, A, and sensor, S, are attached at the lower and upper surfaces, respectively $[S/(0/90)_s/A]$. For the second case, the actuator is embedded inside the laminate, as, $[S/0/90/A/90/0]$. In the third case, the effect of laminate configuration is studied by making a smart laminated beam as $[S/(\pm 45)_s/A]$.

For all cases the design variable is actuator force and the constraint is 0.5 seconds settling time. In Figure 4.13 the optimal tip response and the optimal control force of the laminated beam with different configurations are presented. As it is observed from Figure 4.13(a), the settling time for all the cases is 0.5 seconds as was prescribed in optimization problem. Figure 4.13(b) indicates that the laminated beam configured as $[S/(\pm 45)_s/A]$ requires higher value of control force in order to suppress the vibration in 1 sec. This value is slightly reduced for the laminate configuration $[S/0/90/A/90/0]$. This is due to the change in stiffness matrices and piezoelectric force applied by the actuator.

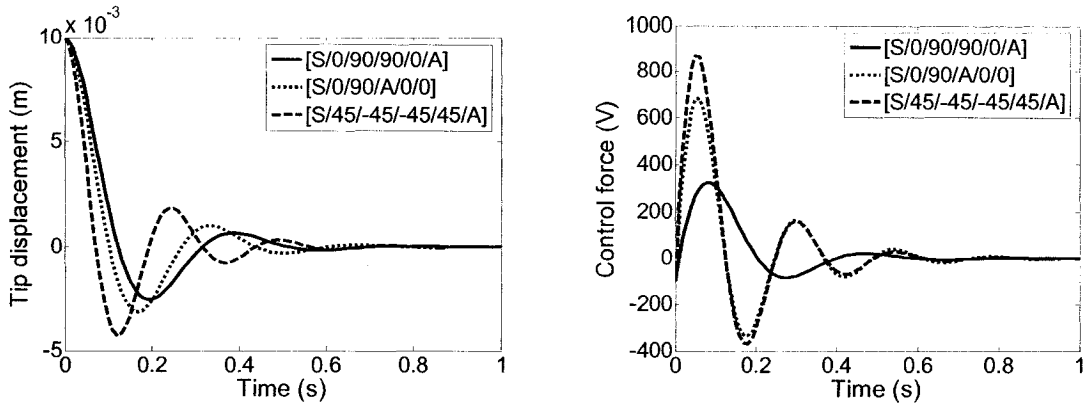

(a) (b)

Figure 4.13 Effects of laminate configuration and location of actuator on (a) vibration suppression using optimal electric potential, (b) optimal voltages applied at actuators

4.4 Conclusions

The coupled layerwise finite element formulation, and the analytical gradients have been combined with Sequential Quadratic Programming technique to develop an efficient and accurate optimization algorithm. In static case, nodal displacement and inter-laminar stresses are considered as constraints to minimize the mass. In dynamic problems, natural frequencies are monitored as design constraints for eigenvalue problem and minimization of control effort is considered for transient vibration. It has been revealed that the use of analytical gradients in optimization procedure results in significant reduction in computational efforts in terms of iteration numbers as well as function evaluations required to converge to the optimal result. The effect of boundary conditions and location of piezoelectric elements on the optimal design of the smart laminated beam under frequency constraints are also investigated. It is indicated that the beam with clamped-free boundary condition requires the higher value of mass in order to satisfy the

frequency constraints. Consequently, the beams with simply supported and clamped-clamped boundary conditions require the lower value of mass.

The layerwise approximation for displacements through the thickness of the laminates provides more accurate results for in-plane strain and stress distributions and inter-laminar stresses. Therefore, the optimal designs of smart laminated structures based on the layerwise approach are more reliable than that of the equivalent single layer theories.

CHAPTER 5

OPTIMAL VIBRATION CONTROL OF SMART LAMINATED BEAMS

5.1 Introduction

Laminated composite structures have been widely used for aerospace applications such as satellite, and aircraft wings and tails. Excessive vibration in these structures may result in instability and/or poor functionality of the system. In order to control the stability of the laminated structures during operation, the concept of smart laminated structures has been recently attracted by many researchers. These novel structures consist of the laminated structures as the host structure, smart materials with capability to serve as sensor and/or actuator, and the control mechanism. Excellent sensing and actuating capabilities of piezoelectric materials make them the most practical smart materials to integrate with laminated structures. This smart system is now, equipped with a control mechanism to provide an active vibration control. Active vibration control is refereed to the procedure of suppressing vibration response of the structure through an automatic modification of the system structural response.

Efficiency and accuracy of the dynamic and static responses of smart systems highly depend on the mathematical modeling of the structure and the control strategy. Thus, to

achieve the desirable performance and functionality of the smart laminated systems, these two aspects should be thoroughly understood and accurately represented in the modeling. In this chapter, the coupled layerwise displacement theory developed in Chapter 2 has been utilized to model the smart laminated structure. Finite element model based on the layerwise theory typically results in large number of degrees of freedom. In order to reduce the number of degrees of freedom for control purposes, the modal forms of the structural model and sensor and actuator are developed. Linear Quadratic Regulator (LQR) is then applied to obtain the optimal control feedback gain. Open-loop and closed-loop investigations have been performed and the results are compared with those obtained based on the classical laminate theory and classical control strategies. Experimental investigations have also been conducted to validate the simulation results.

5.2 Structural Modeling

As shown in Chapter 2, finite element model based on the layerwise theory can be effectively used to evaluate the generated voltage in sensor of the smart system. This observation greatly influences the feedback control design where the actuating force is determined using the sensor output. Slight change in sensor output may lead to significant change in actuator input as it is amplified by a gain factor.

Most of the smart laminated systems are developed based on velocity feedback control where the sensor output current is used to detect strain rate (velocity signal) generated in the structure due to external forces, however the output current may need to be amplified by a gain factor of the order of 10^{10} in order to be measured. In addition, in many

practical cases velocity signal is not accessible or is expensive to measure due to number of sensors, current amplifier, etc. Thus, the sensors are used to detect the displacement signal, and then, are differentiated using a numerical approach to determine the velocity signal. Numerical differentiation of displacement signal usually adds noise to the signal which may significantly affect the controller functionality. Thus, inaccuracy in the sensor input may significantly influence the performance of the smart system. To ensure the highest accuracy and efficiency of the functionality of the smart laminated system, in the present work, layerwise displacement theory is utilized to develop the mathematical model of the smart structure.

Considering that in the sensor layers the converse piezoelectric effect is negligible, the equations of motion and electrostatic, (2.43) and (2.44) are reduced to:

$$[M_{dd}]\{\ddot{d}\}+[\hat{K}_{dd}]\{d\}=\{F_d(t)\}-[K^{sa}_{d\psi}]\{\psi^a\} \tag{5.1}$$

$$\{\psi^s\}=-[K^{ss}_{\psi\psi}]^{-1}\left([K^{ss}_{\psi d}]\{d\}\right) \tag{5.2}$$

where $[\hat{K}_{dd}]=[K_{dd}]-[K^{ss}_{\psi d}[K^{ss}_{\psi\psi}]^{-1}[K^{ss}_{\psi d}]$.

5.3. Vibration Control

Formulating the smart laminated beams using the layerwise finite element model leads to a large number of degrees of freedom. On the other hand, vibration control is mainly

concerns of controlling the specific vibration modes, practically the fundamental mode. Thus, in this section the modal form of the governing equations are presented.

5.3.1 Modal form

Assuming a modal form with n vibration modes, the transverse displacement vector can be written as the modal summation in the form[150]:

$$\{d\} = \sum_{r=1}^{n} \{q_r\}\eta_r(t) = [q]\{\eta\} \tag{5.3}$$

where $[q]$ is the modal shape matrix. Substituting Equation (5.3) into Equations (5.1) and (5.2) and use the orthogonality of mass as $[q^T][M][q]=1$ and stiffness as $[q^T][K][q]=[\omega^2]$, leads to:

$$\{\ddot{\eta}\} + [\omega^2]\{\eta\} = [q]^T[F] - [q]^T[K_{d\psi}^{sa}]\{\psi^a\} \tag{5.4}$$

$$\{\psi^s\} = -[K_{\psi\psi}^{ss}]^{-1}\left([K_{\psi d}^{ss}][q][\eta]\right) \tag{5.5}$$

If structural damping is also taken into account, Equation (5.4) may be written as

$$\{\ddot{\eta}\} + [2\xi\omega]\{\dot{\eta}\} + [\omega^2]\{\eta\} = [q]^T[F] - [q]^T[K_{d\psi}^{sa}]\{\psi^a\} \tag{5.6}$$

where according to Rayleigh modal damping, $[2\xi\omega]$ is a diagonal matrix representing the damping of the structures and ξ is a vector of modal damping factors.

5.3.2 State space model

The state vector x is defined as

$$\{x\} = \{\{\eta\}, \{\dot{\eta}\}\}^T \tag{5.7}$$

Now using Equation (5.7), the state space form of Equation (5.6) can be written as the following:

$$\{\dot{x}\} = [A]\{x\} + [B]\{u_c\} + \{f\} \tag{5.8}$$

$$\{\psi^s\} = \{y\} = [C]\{x\} \tag{5.9}$$

where $\{u_c\}$ represents the actuating control force, $\{f\}$ is load force vector generating the primary excitation force and the remaining coefficients are given by

$$[A] = \begin{bmatrix} [0] & [I] \\ [-\omega^2] & [-2\xi\omega] \end{bmatrix}, \qquad [B] = \begin{bmatrix} [0] \\ -[q]^T[K^a_{d\psi}] \end{bmatrix}, \qquad \{f\} = \begin{Bmatrix} \{0\} \\ [q]^T\{F\} \end{Bmatrix}$$
$$[C] = [-[K^{ss}_{\psi\psi}]^{-1}[K^{ss}_{\psi d}][q] \quad [0]] \qquad \{u_c\} = \{\psi^a\} \tag{5.10}$$

5.3.3 Classical control

The most common approach in controlling the vibration of smart laminated structures is output feedback control in which the sensors outputs are amplified and directly fed back to the piezoelectric actuators. The control voltage is given by

$$\{u_c\} = -[G]\{\psi^s(t)\} \tag{5.11}$$

where $[G]$ is a feedback control matrix defined according to the control law. Substituting Equation (5.9) into (5.11) and the resultant into Equation (5.8), the closed-loop system state is given by

$$\{\dot{x}\} = ([A] - [B][G][C])\{x\} \tag{5.12}$$

Equation (5.12) indicates that the gain matrix $[G]$ modifies the closed-loop system dynamic. Therefore, this approach can attenuate the vibration by transferring the initial poles of the system to higher damped ones.

The velocity feedback control is the most common control law utilized in vibration suppression of smart laminated structures. In this approach, the piezoelectric sensors are utilized as strain rate detectors[151] where the output current of the sensors is measured, amplified and fed back to actuator through multiplication by a control gain. This approach is called C*onstant Gain Velocity Feedback* control (CGVF). The control gain is selected based on the desired output response such as settling time and maximum amplitude of the response. The given control gain is then utilized to determine the required control voltage. If the control voltage exceeds the maximum allowable voltage applied on the actuator, the design should be repeated using a new control gain. It is worth noting that, most of commercial piezoelectric patches are applied within the electric field of 300 V/mm[131]. Exceeding that voltage may result in depolarization of the

piezoelectric material and consequently leads to loss of functionality of the smart structures.

To investigate the CGVF control, a symmetric laminated beam $[0/90/0]_s$ integrated with one piezoceramic actuator and one PVDF sensor as shown in Figure 2.9 is considered to determine the closed-loop response of the system. Sensors and actuator patches are mounted at 4 *cm* from the fixed end of the beam. Material and geometric properties of graphite/epoxy layers, piezoceramic and PVDF patches are given in Table 2.2.

The closed-loop vibration response of the smart laminated beam for an initial tip displacement 4 cm and the required control voltage for constant gain of G = 1000, 2000, 4000, and 6000 are provided in Figure 5.1. It is expected, increasing the feedback gain results in faster vibration suppression as shown in Figure 5.1. However, it requires higher actuator voltage which may exceed the maximum allowable actuator voltage as shown in Figure 5.2. Thus, designing the optimal controller requires a trial-and-error procedure and trade off between vibration response of the structure and the actuating voltage of the actuators.

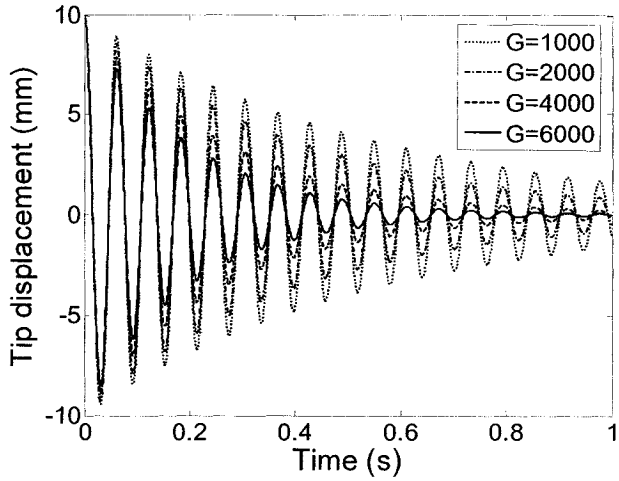

Figure 5.1 Tip displacement (a) and control voltage

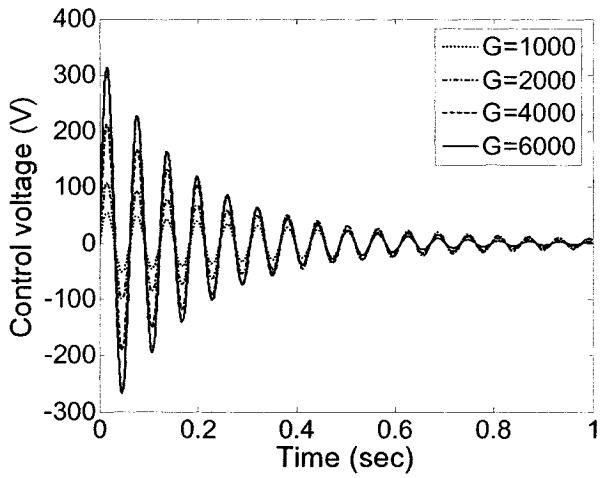

Figure 5.2 Control voltage of laminated smart beam using CGVF

To design control algorithm according to CGVF, one may encounter various difficulties: *i*) Results similar to Figure 5.1 might be obtained for all the possible location/size of sensors/actuators and control gains to find the optimum combination for the desired vibration response. *ii*) This approach does not include well defined criteria to find the optimum value for the size, location and control gain. Thus, designing control algorithm

based on the classical control strategies, including CGVF, for vibration control of smart laminated beams requires very long and time consuming effort.

5.3.3 Optimal control

The optimal control system is designed based on the state feedback control law. The Linear Quadratic Regulator (*LQR*) is a control algorithm employed here to determine the optimal feedback gain. In *LQR*, the feedback gain, K_{sc} is chosen to minimize a quadratic cost function of the form subject to the system equation

$$J = \frac{1}{2}\int_0^\infty \left(\{x\}^T[Q]\{x\} + \{u_c^T\}[R]\{u_c\}\right)dt \tag{5.13}$$

where $[Q]$ is a symmetric semi-positive definite and $[R]$ is a positive definite weighting matrices, and are selected to provide suitable performance. The relative magnitudes of $[Q]$ and $[R]$ are selected so as to trade off the requirements on minimizing vibration energy against the requirements on minimizing control energy. In general, a larger $[Q]$ puts higher demand on control voltage, and a larger $[R]$ puts more limits on applied control force.

State feedback control requires that

$$\{u_c\} = -[K_{sc}]\{x\} \tag{5.14}$$

where the feedback gain $[K_{sc}]$ is determined by solving the following matrix Riccati equation[132] .

$$[A]^T[P]+[P][A]-[P][B][R]^{-1}[B]^T[P]+[Q]=0 \tag{5.15}$$

where $[P]$ is an auxiliary matrix. The control gain is then obtained by

$$[K_{sc}]=[R]^{-1}[B]^T[P] \tag{5.16}$$

For details of *LQR* control, one may consult the book written by Kirk[152].

Compared to classical control strategies, optimal control provides a systematic criterion to determine the optimum feedback control gain. Once the weighting matrices corresponding to control voltage and vibration energy are selected, then remaining procedure is a standard optimization algorithm based on minimizing the cost function defined by Equation (5.13).

5.4 Numerical and Experimental Works

In this section both open-loop and closed-loop responses of smart laminated beams have been simulated and compared with experimental results. A proof-of- concept smart laminated composite beam has been fabricated. First, the experimental open-loop response of smart laminated beam is determined to obtain the actual damping coefficient of the system. Then, the closed-loop response of the beam using the *LQR* controller is determined to validate the performance and functionality of the structural and control

model. The second case aims to provide a numerical insight on application of *LQR* optimal control on a laminated composite beam with integrated piezoelectric sensor (top) and actuator (bottom). The effects of location of sensors and actuators and that of laminate configurations are also investigated in this simulation study.

5.4.1 Experimental open-loop response

The experimental set-up consists of a symmetric laminated beam $[0/90/0]_s$ as the host structure; one piezoceramic actuator (BM 500, Sensor Technology Ltd.) and one PVDF sensor (28UM FILM W/NICU, Measurement Specialties) bonded at outer surfaces of the beam, a home built voltage amplifier with capacity to supply ± 200 Volts, a data acquisition board (NI-6220, National Instruments) and a PC computer loaded with LABVIEW® 7.0 as the controller. The schematic and physical experimental set-ups are shown in Figures 5.3 and 5.4 respectively. Material and geometric properties of graphite/epoxy layers, piezoceramic and PVDF patches are given in Table 5.1. It should be noted that the material properties of graphite/epoxy are verified through standard tensile and DMA tests, provided in detail in Appendix B and C.

Table 5.1 Material and geometric properties

	Graphite/ Epoxy	Piezoceramic	PVDF
E_1, GPa	98.0	71.4	4.67
E_2, GPa	6.78	71.4	4.80
G_{12}, GPa	3.48	24.8	2.66
ρ, Kg/m^3	1380	7610	1610
d_{31}, m/V	-	$-200x10^{-12}$	$-20x10^{-12}$
e_{33}, F/m	-	$150x10^{-10}$	$1.05x10^{-10}$
Length, *mm*	300.0	25.0	25.0
Width, *mm*	30.0	25.0	25.0
Thickness, *mm*	0.2	0.50	0.0028

For simulation purpose, the structure is meshed with 15 equal-length elements along the length of the beam. In thickness direction each physical layer, including piezoelectric materials, are considered as one numerical layer to develop layerwise finite element model. To obtain the free vibration response of the laminated smart beam, the tip of the beam is dislocated 4 cm and then suddenly released. Sensor output is fed directly to the data acquisition board and the time response is obtained using LABVIEW® 7.0 as shown in Figure 5.5.

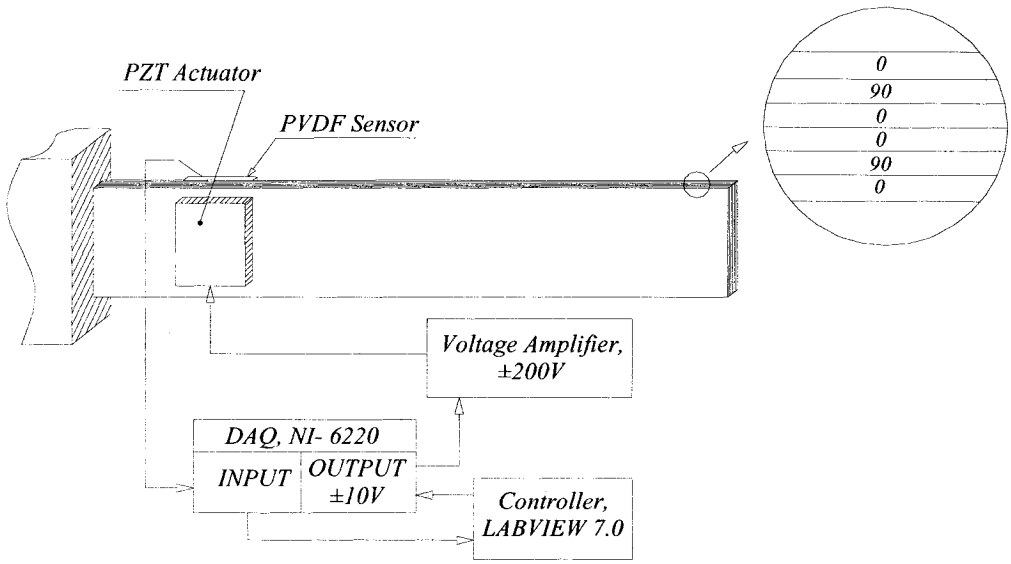

Figure 5.3 Schematic set-up of the test for vibration control of laminated beam

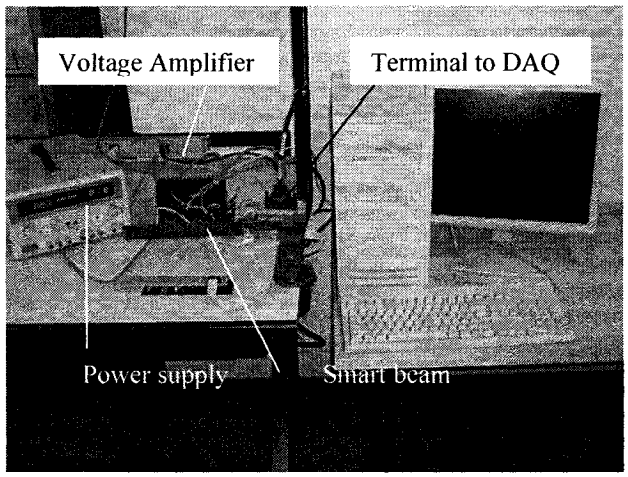

Figure 5.4 Experimental set-up for vibration control of laminated beam

Using the experimental response of the beam shown in Figure 5.5, it is noted that 31 cycles are realized in the time interval (0.069-1.969) seconds. Therefore, the natural frequency of the system is determined as: $\omega_1 = 31/(1.969 - 0.069) = 16.3\,Hz$ which is in very good agreement with the natural frequency obtained using finite element analysis based on the layerwise theory ($\omega_1 = 16.37\,Hz$). Using the same time interval, the damping coefficient is determined by computing the logarithmic decrement as: $\delta = 1/32 \ln(2.526/0.1858) = 0.0842$ and the damping factor is determined as: $\xi_1 = \delta/2\pi = 0.0134$. The experimental value of damping coefficient is of great importance to design the control strategy, since this value directly affects the state matrices.

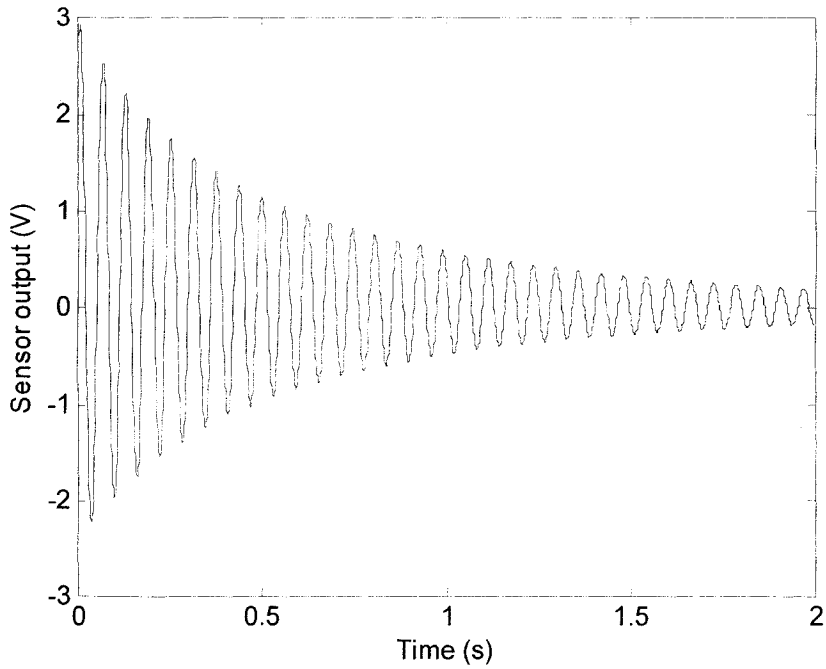

Figure 5.5 Experimental open-loop sensor output of cantilever beam with 4.0 *cm* initial displacement

In addition, damping coefficient of laminated smart beam is influenced by many factors, including, laminate configuration, material and geometric properties, and location of sensors/ actuators, requiring testing of individual cases to determine the accurate damping factor.

Now using the experimental damping coefficient in the finite element model, the open-loop response of the system is obtained and compared with that of the experimental. Figures 5.6 and 5.7 show the comparison between the experimental and simulation of sensor output voltage in open-loop condition for 1 second and 2 second time response, respectively. As it can be realized good agreement exists between the simulation and experimental results.

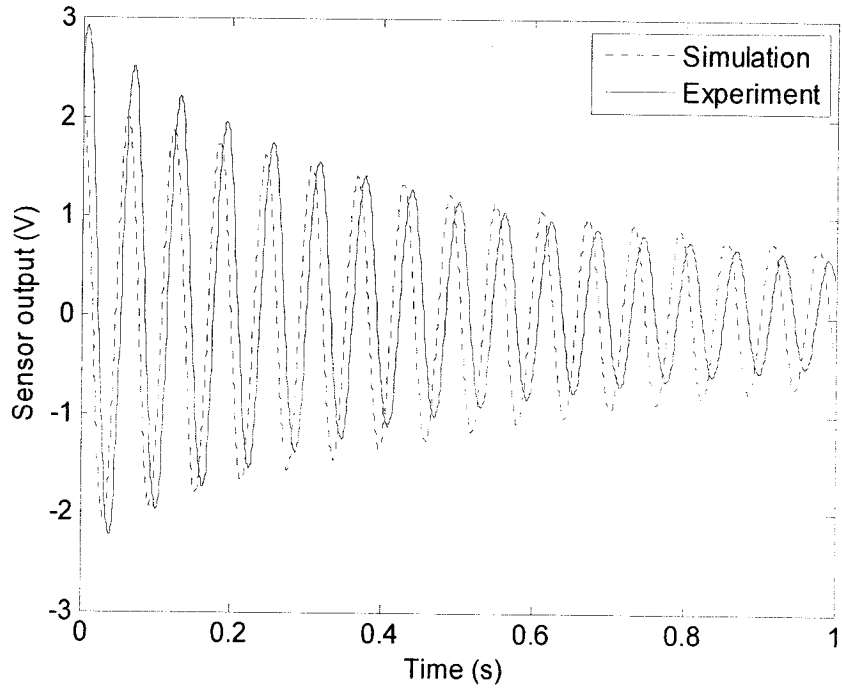

Figure 5.6 Simulation and experimental open-loop sensor output voltage of cantilever beam with 4.0 *cm* initial displacement for 1 sec time response

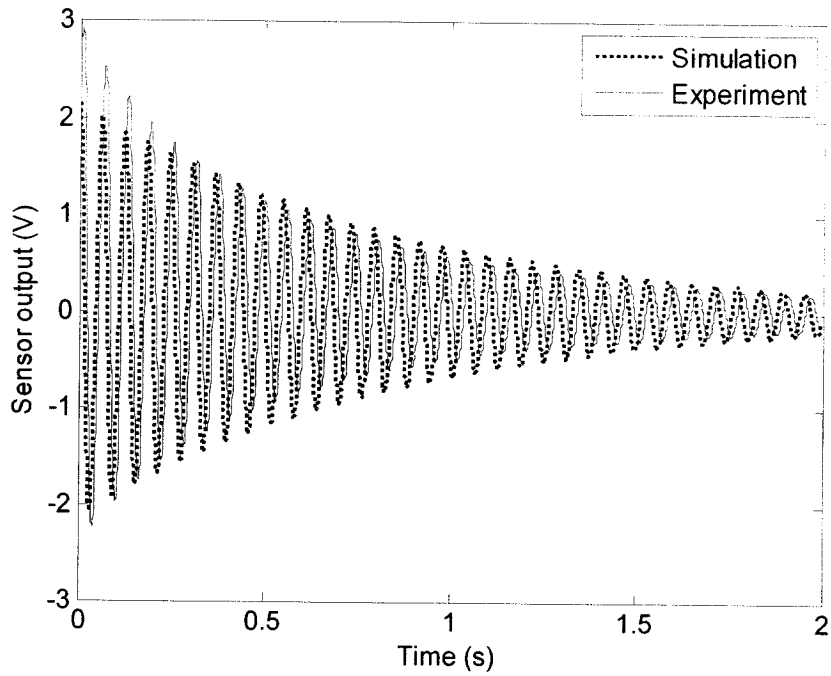

Figure 5.7 Simulation and experimental open-loop sensor output voltage of cantilever beam with 4.0 *cm* initial displacement for 2 sec time response

To design the feedback control using *LQR*, appropriate selection of the weighting matrices [*Q*] and [*R*] plays a vital role. To have better understanding, the effects of [*Q*] and [*R*] on vibration response and control voltage are investigated first.

The smart laminated beam described in Section 5.4.1 is again considered. The value of [*R*] matrix is assumed to vary between 1 to 3 in the *LQR* procedure described in Section 5.3.3, while the value of [*Q*] is kept constant as $[Q] = 10^7 I_{2\times 2}$. Equations (5.15) and (5.16) are solved using MATLAB® software to determine the feedback gain according to each [*R*] value.

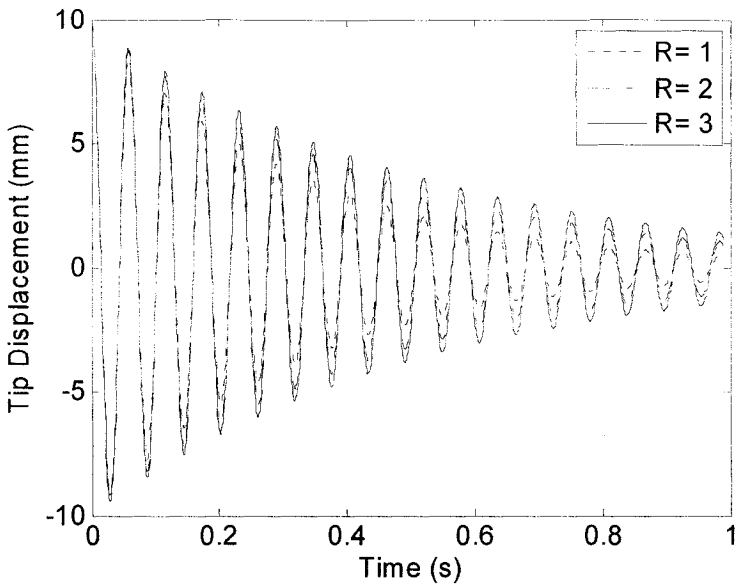

Figure 5.8 Effect of [*R*] matrix on tip displacement

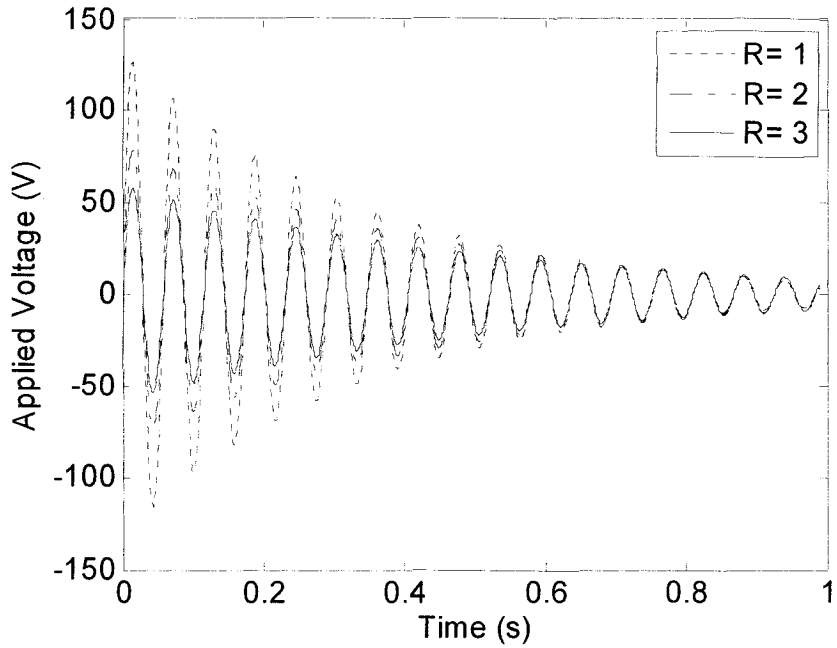

Figure 5.9 Effect of [R] matrix on applied control voltage

One should note that the order of matrix [R] is determined according to the number of actuators used in the system. In the present example, only one actuator is utilized thus requiring a single value for matrix [R]. Similarly, the order of matrix [Q] is determined according to the order of state variable vector, $\{x\}$, which is defined by the number of vibration modes considered in the control system. In this study controller has been designed to suppress the fundamental vibration mode.

The effect of using this matrix [R] on tip displacement and the generated control voltage applied on actuator are demonstrated in Figure 5.8 and 5.9, respectively. As is can be seen, increasing the value of [R] decreases the required electric voltage but on the other hand increasing the vibration settling time. It should be noted that to save computational time, a relatively large the time step is

Next, the value of $[R]$ is kept constant as $R = 1.3$ and the value of $[Q]$ matrix is changed as $(10^7, 10^8, 10^9)I_{2\times2}$. The effect of changing $[Q]$ matrix on vibration response and control voltage is shown in Figures 5.10 and 5.11, respectively.

It is observed that increasing the value of $[Q]$ results in decreasing the settling time from one side, however increasing the applied control voltage from other side.

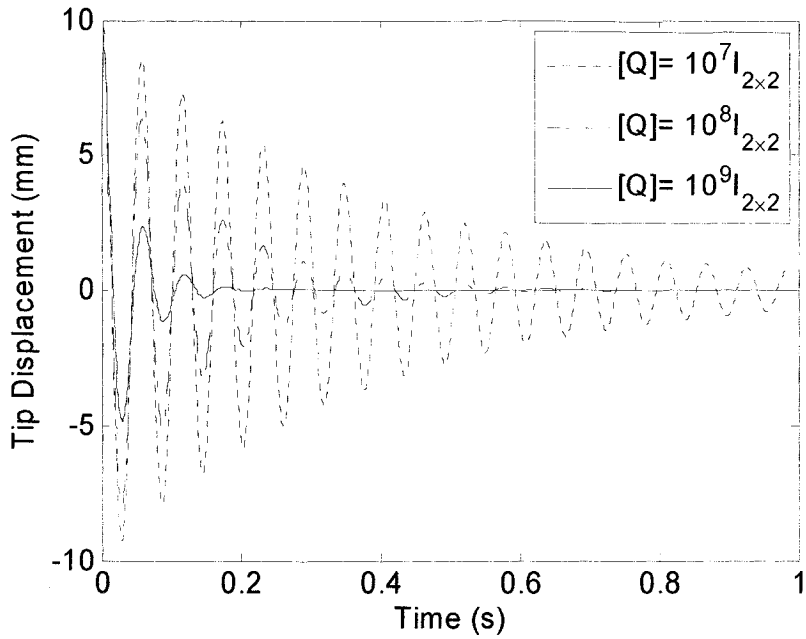

Figure 5.10 Effect of $[Q]$ matrix coefficient on tip displacement

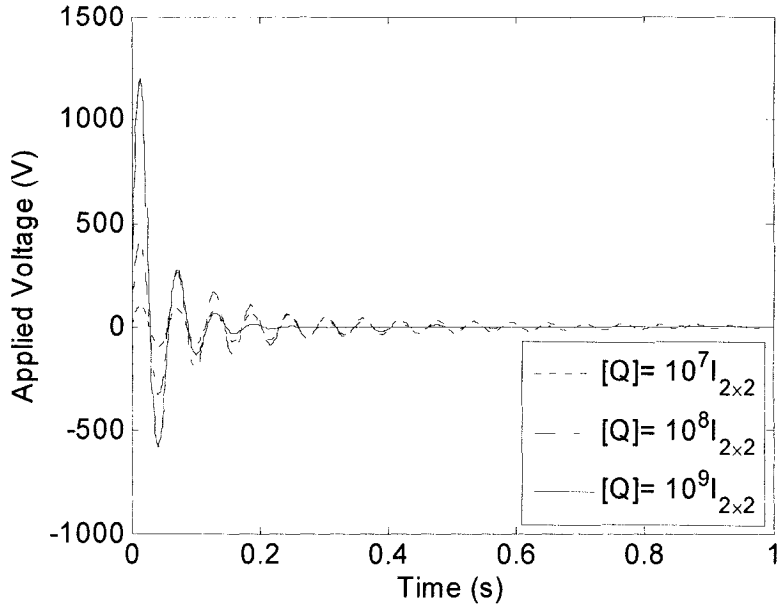

Figure 5.11 Effect of $[Q]$ matrix coefficient on applied voltage

5.4.2 Experimental closed-loop response

Considering the effects of $[Q]$ and $[R]$ on control algorithm in smart systems presented in Section 5.4.1, the weighting matrices utilized are: $[Q]=1\times10^{7}I_{2\times2}$ and $R=1.3$ and the feedback gain is determined as: $[K_{sc}]=[0.049\quad 1557]$. According to this value, the velocity state has a major impact on feedback gain. However, we have utilized only one sensor and measured its output voltage which is proportional to displacement. To measure the velocity state, it is required to take numerical differentiation of the displacement values. Although this method may generate noisy signal, but it is acceptable for validation purposes. In addition, it uses only one sensor to determine both displacement and velocity signals.

To demonstrate the control strategy, the set-up described in Section 5.4.1 has been used. A push button is simulated in the LABVIEW® to activate the controller. A 4.0 *cm* initial displacement has been applied at the tip of the beam and the beam is suddenly released. After 1.0 second, the controller is activated to damp out the vibration. As it is observed in Figure 5.12, once the controller is activated, the amplitude is significantly reduced. After 0.2 second of controller activation the vibration is suppressed to about 3% of its steady state response. Figure 5.13 provides a comparison between simulation response with *LQR* controller and the experimental response. One may realize that good agreement exists between experimental and simulation results. However, due to the effect of measurement and system noise, a steady noisy signal, as long as the controller is activated, remains in the system even after the vibration is suppressed.

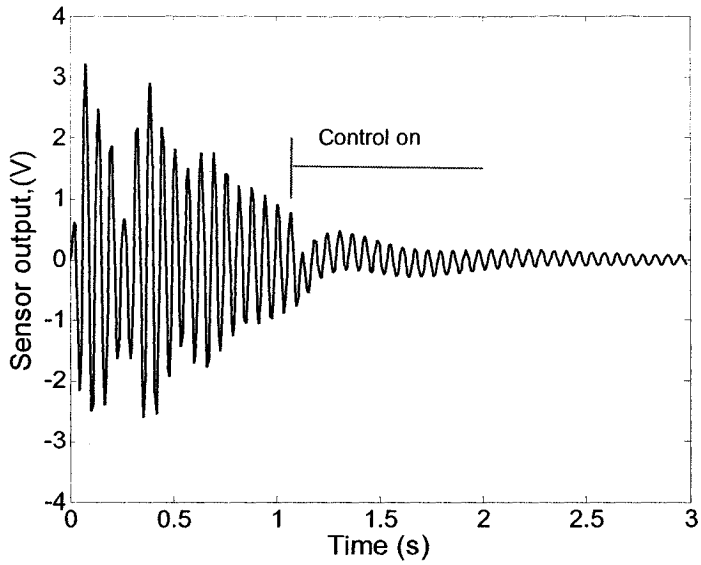

Figure 5.12 Experimental closed-loop sensor output of cantilever beam with 4.0 *cm* initial displacement

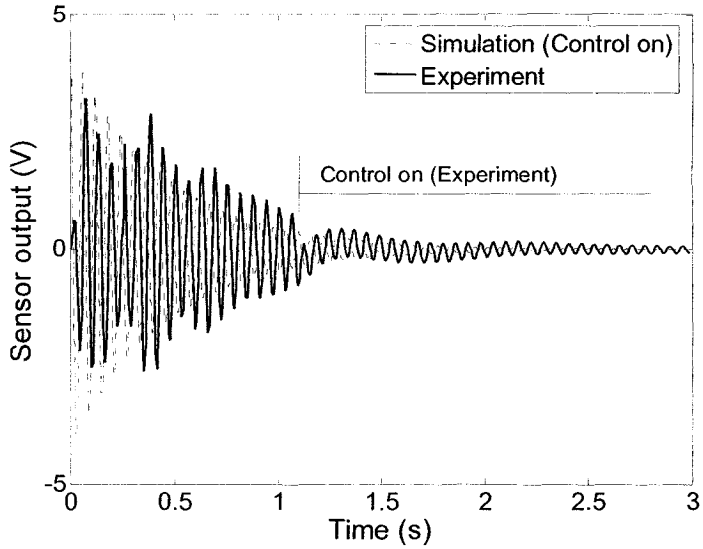

Figure 5.13 Comparison between the experimental and simulated closed-loop sensor output voltage of cantilever beam with 4.0 *cm* initial displacement

The open-loop and closed-loop experimental responses of the smart laminated beam are presented in Figure 5.14 in which one may realize 50 % reduction in the settling time when control is on.

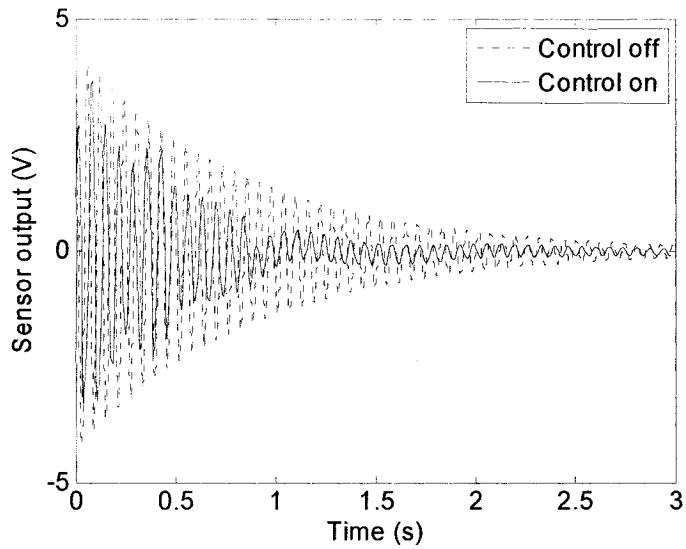

Figure 5.14 Comparison between the experimental open-loop and closed-loop sensor output voltage of cantilever beam with 4.0 *cm* initial displacement

In order to examine the influence of *LQR* algorithm on controlling the vibration modes, the frequency response of the smart laminated beam is presented in Figure 5.15 and 5.16 It should be noted that in the experimental beam, only one sensor is utilized to control the first mode of vibration. As it can be seen, the developed control mechanism has significant impact on controlling the first vibration mode. It should be considered that controlling the higher modes requires more sensors/ actuators or more complicated mathematical modeling of the smart system.

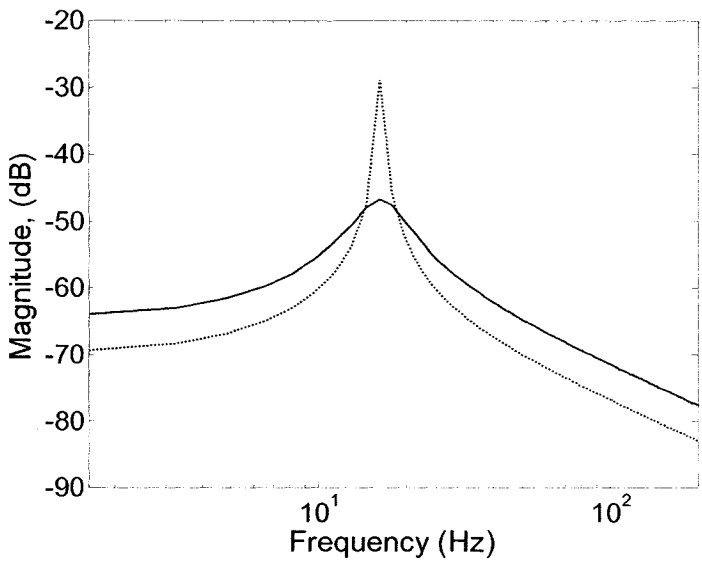

Figure 5.15 Frequency response of the smart laminated beam generalized modal coordinate; open-loop (dotted line), closed-loop (solid line)

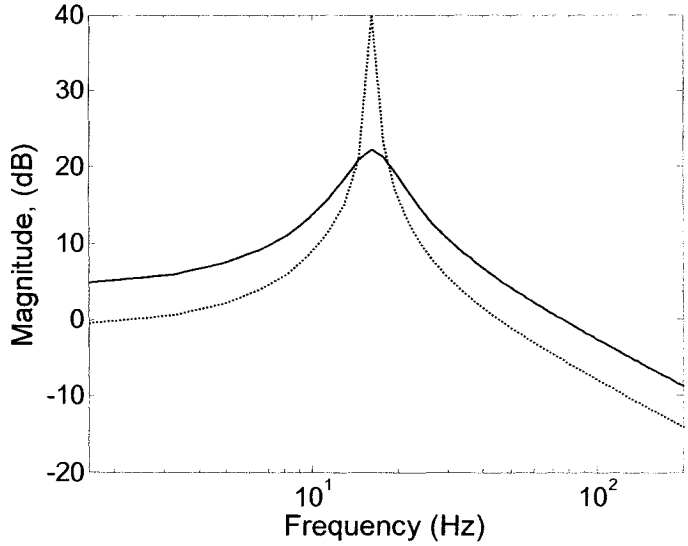

Figure 5.16 Frequency response of the smart laminated beam; open-loop (dotted line), closed-loop (solid line); sensor output

5.4.3 Effect of laminate configuration on optimal control

The smart laminated cantilever beam studied in Section 5.4.1 is considered. The first two natural frequencies of this structure are identified to be: $\omega_1 = 16.31\,Hz$ and $\omega_2 = 102.0\,Hz$, respectively, and the corresponding damping ratios are determine as $\xi_1 = 0.0113$ and $\xi_2 = 0.16$.

In order to determine the feedback control gain using *LQR*, the matrices [*Q*] and [*R*] are selected as $[Q] = 2\times10^7 I_{4\times4}$, $[R] = 1.3$. Using the given numerical values, the feedback control gain, [K_{sc}], has been determined as: $[K_{sc}] = [0.79 \quad -57.1 \quad -2645 \quad -38.7]$. An initial displacement of 10 mm is applied at the tip of the beam. Different laminate configurations, [*PS/(0/90/0)$_s$/PA*], [*PS/(±30/0)$_s$/PA*], [*PS/(±45/0)$_s$/PA*] are investigated (*PS* and *PA* stand for sensor and actuator, respectively). The closed-loop vibration

response and corresponding applied control for each laminate configuration is obtained and presented in Figures 5.17 and 5.18, respectively. It is indicated that [*PS/(0/90/0)$_s$/PA*] has the fastest deflection suppression. Correspondingly, [*PS/(±30/0)$_s$/PA*] *and* [*PS/(±45/0)$_s$/PA*] have the second and third positions. In terms of applied control voltage at the actuator, the magnitudes are similar for all configurations except that there are delays between each configuration. To make a better comparison, the decay envelopes and the frequency responses for various laminate configurations are plotted in Figures 5.19 and 5.20, respectively. To save computational time, a relatively big time step is used to plot theses graphs which cause sharp edges; however, it is sufficiently demonstrate the effect of laminate configurations in time responses.

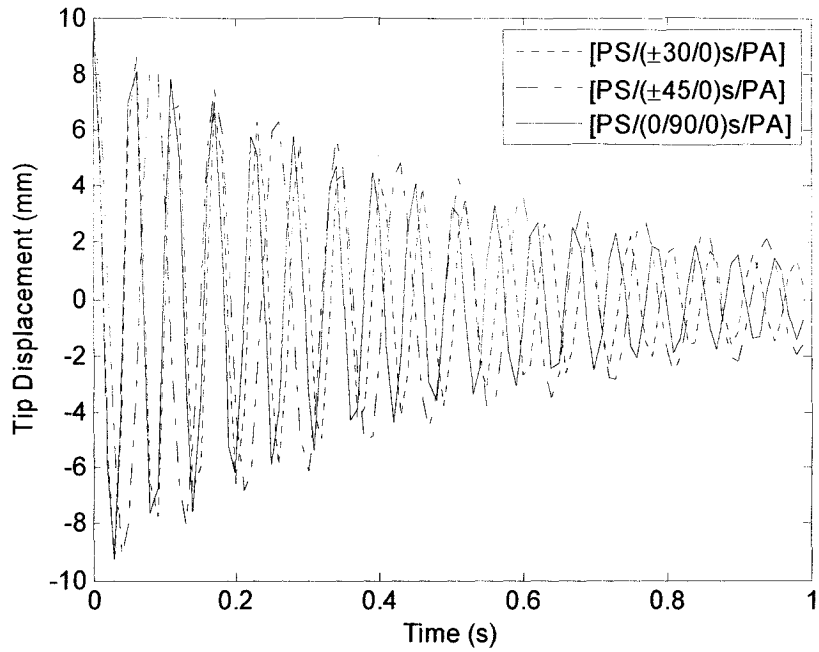

Figure 5.17 Tip displacement for different ply orientations

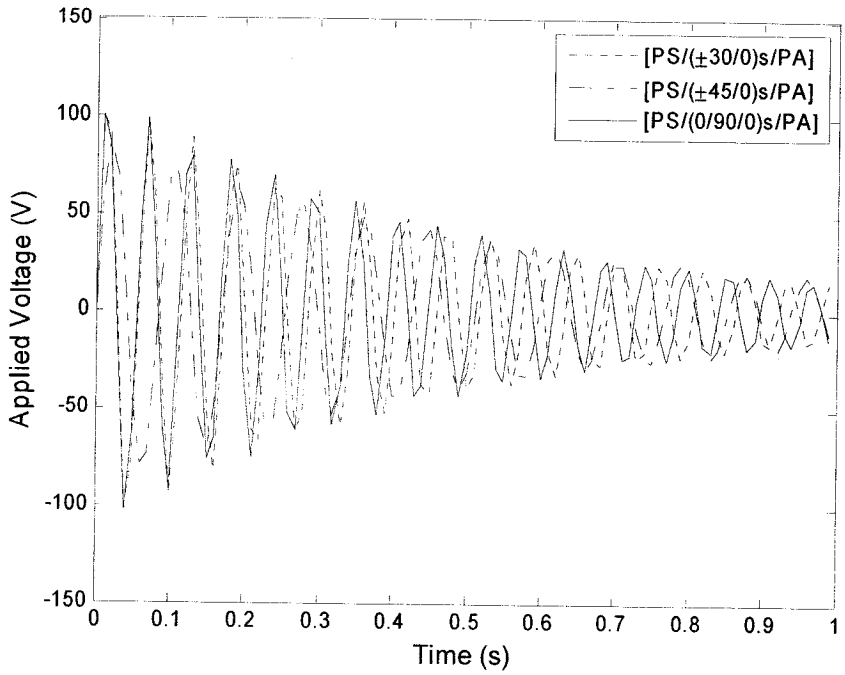

Figure 5.18 Applied control voltage for different ply orientations

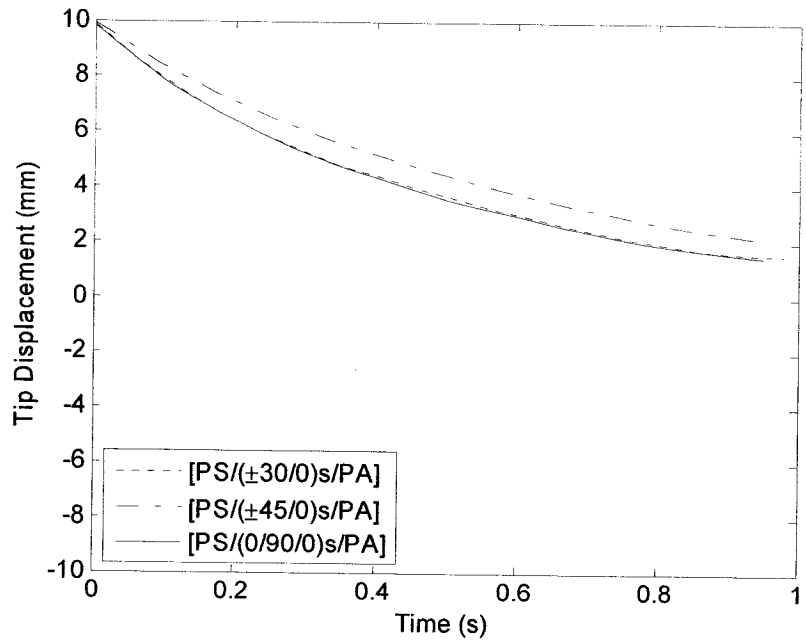

Figure 5.19 Family of decay envelopes for various laminate configurations

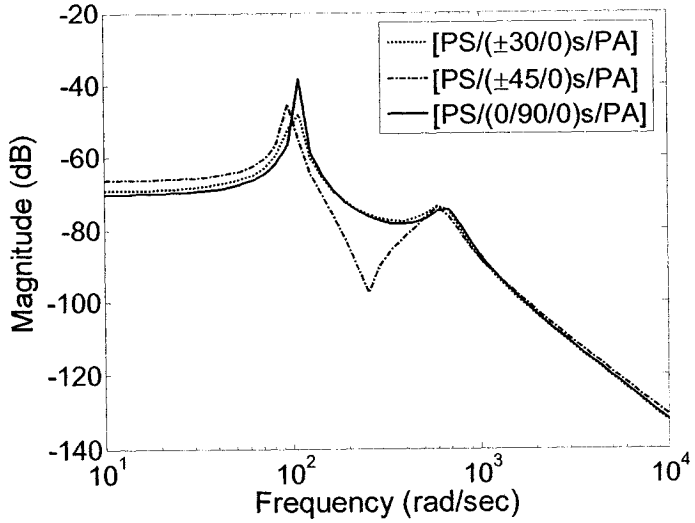

Figure 5.20 Frequency response for various laminate configurations

The relation between settling time ($\pm 3\%$ of steady state response) and control force has also been investigated. In general, as the settling time increases, the control voltage decreases as shown in Figure 5.21.

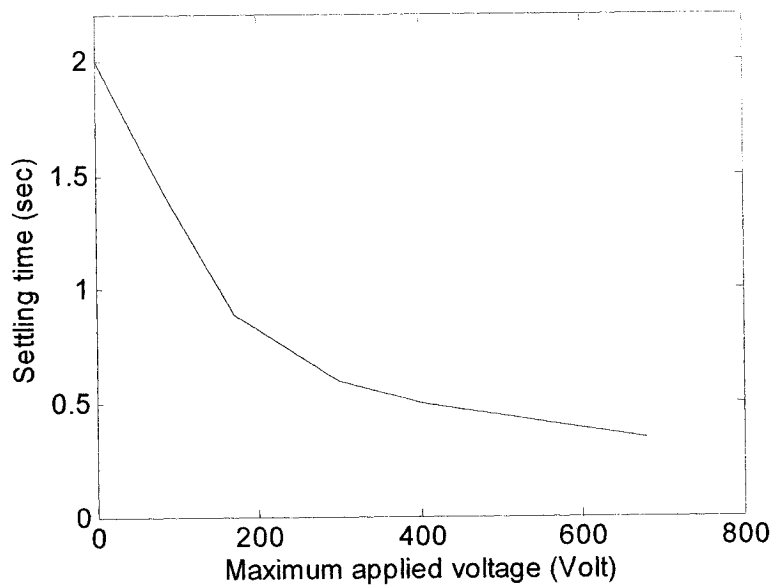

Figure 5.21 Maximum control voltage vs. settling time

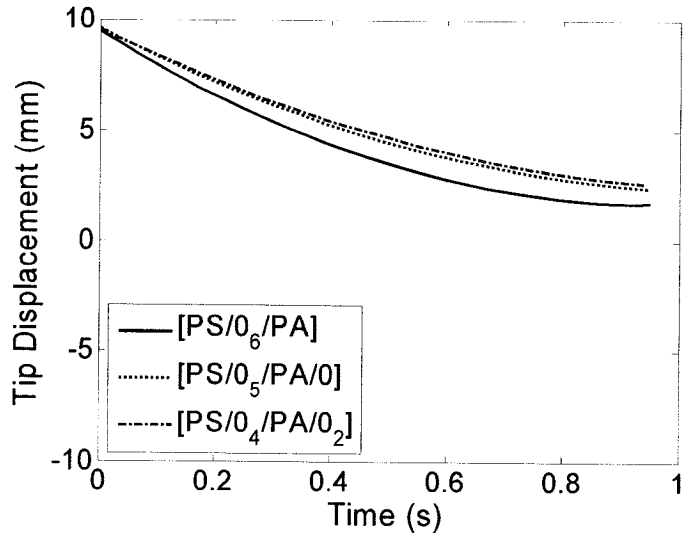

Figure 5.22 The decay envelope for different through the thickness locations of actuators

Another important factor in vibration control of laminated structures is the location of the embedded piezoelectric actuator through the thickness. To investigate the effect of piezoelectric actuator location through the thickness, the smart laminated beam described in Section 5.4.1 is investigated but the laminate configuration is assumed unidirectional. The location of actuator has been changed from outer surface (layer 8) to inner layers in succession (5 and 3). The decay envelopes for various configurations are plotted in Figure 5.22. It is observed that as the smart material layer is moved farther from the mid-plane the suppression time decreases as expected due to the moment effect caused by smart layer actuations.

Figure 5.23 and Figure 5.24 show the vibration response and corresponding control voltage for two different locations of piezoelectric actuator through the thickness, respectively. It is noted that in order to remove the effect of changing elastic stiffness due to different laminate orientations, the laminate is considered as unidirectional. As it can

be realized the relocation of piezoelectric actuator patch from the 3rd inner layer to the top layer significantly reduces the settling time; however, it increases the control voltage significantly.

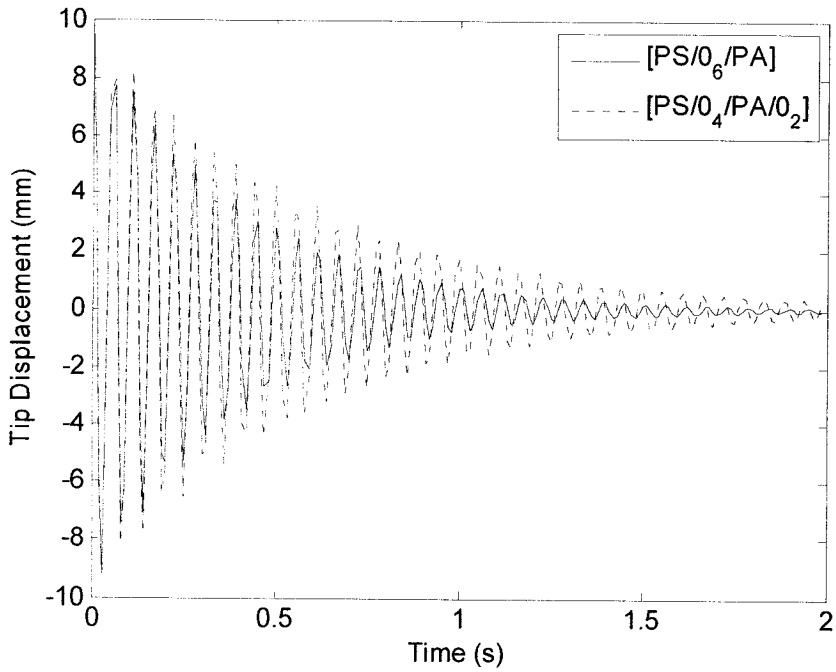

Figure 5.23 The effect of actuator location on tip displacement for two different through the thickness location of the actuator in unidirectional laminate configuration

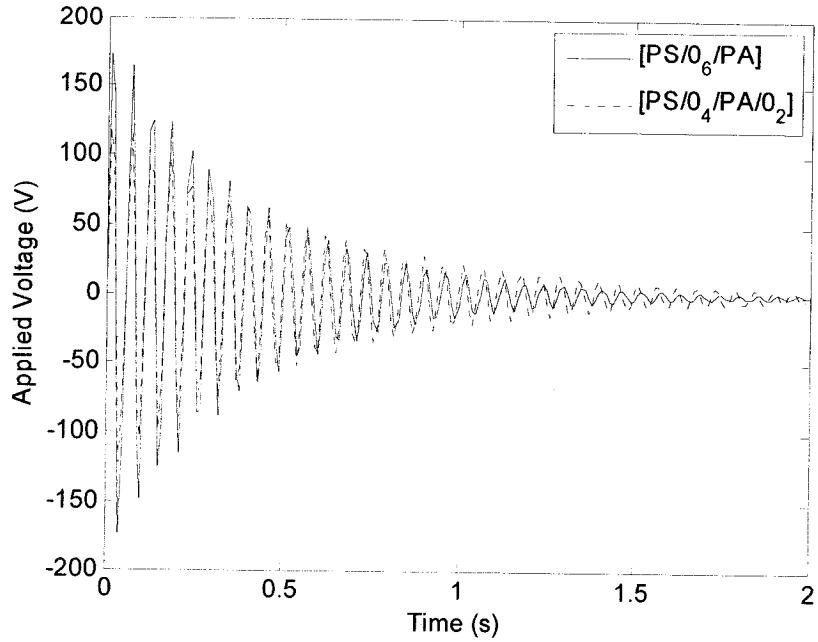

Figure 5.24 The effect of actuator location through the thickness in unidirectional laminate configuration the control actuator voltage

In another investigation, the configuration $[PS/(0/90/0)_s/PA]$ is considered and the actuator element is relocated from the outer surface to the 3rd layer from top. The tip displacement and the corresponding control actuator voltage are shown in Figures 5.25 and 5.26, respectively. The same conclusion made for unidirectional configuration can also be drawn for $[PS/(0/90/0)_s/PA]$ configuration. It is worth noting that in non-unidirectional configurations, when relocating actuator through the thickness, one should take special care to achieve similar ply orientation for the host composite ply. For example if one removes one layer with 90 degree and place an actuator instead of it, then, the stiffness of the structure will change and the effect of actuator location can not be pronounced.

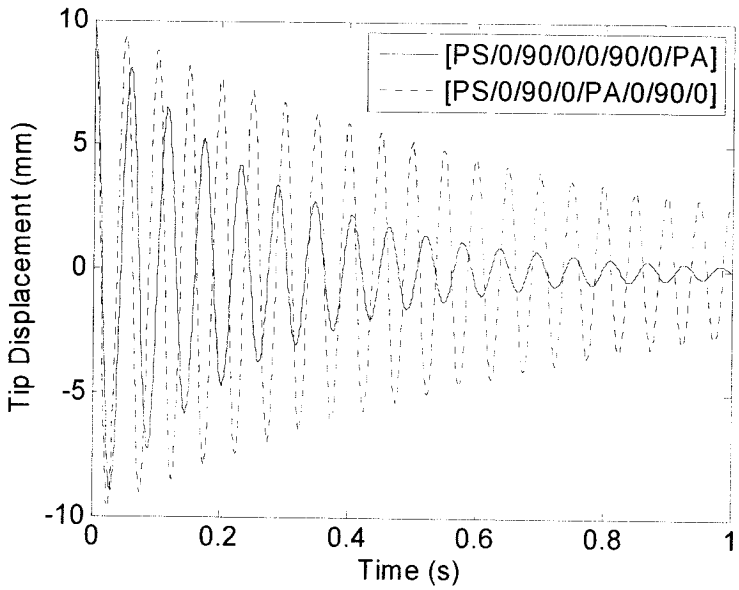

Figure 5.25 Effect of actuator location through the thickness on tip displacement in non-unidirectional laminate configuration

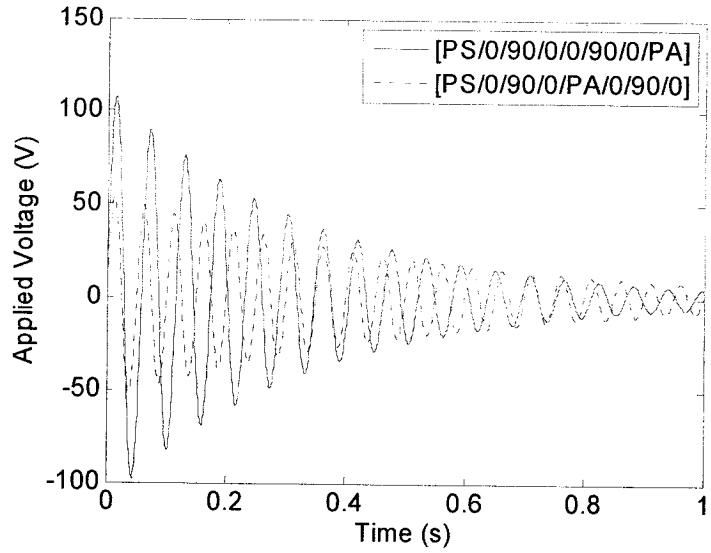

Figure 5.26 Effect of actuator location through the thickness on the applied control voltage in non-unidirectional laminate configuration

5.6. Conclusions

Vibration control of smart laminated structure has been performed using optimal control strategy. A finite element model based on the layerwise displacement theory which incorporates the electromechanical coupling effect has been developed to efficiently and accurately obtain the response of the system. The smart system consists of laminated composite beam as the host structure, piezoceramic actuator and PVDF sensor. Utilizing the layerwise displacement theory, the modal form of both sensors and actuators has been developed. The state space model of the active laminated beam is then used to design the control system. Full state feedback controller based on Linear Quadratic Regulator (*LQR*) is designed to suppress the vibration of the smart laminated beam. Dynamic response of the smart laminated beam according to classical laminate theory and layerwise displacement theory has been investigated to demonstrate the accuracy of layerwise theory in vibration suppression. Numerical illustrations have been presented to discuss the classical control strategies versus the optimal control. The effects of laminate configuration, locations of sensors and actuators and weighting matrices on controlled response of the smart system have also been investigated. An experimental set-up consisting of a laminated beam, one piezoceramic actuator bonded on the top surface and one PVDF sensor mounted on bottom surface has been developed to determine the open-loop response of the system. Experimental damping coefficient of the smart system has been determined and utilized to develop state space model. Based on *LQR* controller, an experimental feedback controller has been designed and employed to determine the closed-loop response of the system. It is indicated that optimal control strategy significantly improves the vibration response of the structure. In practice, the system is

very sensitive to changing the values of feedback gain requiring an accurate formulation for mathematical modeling of the system. Utilizing layerwise theory for vibration control purpose provides high accuracy (compared to equivalent single-layer theories) and reasonable efficiency (compared to 3D models). In addition, this model can be applied at the same time to monitor the inter-laminar stresses between the layers, particularly between the actuator patches and the laminated host structure.

CHAPTER 6

VIBRATION SUPPRESSION OF SMART LAMINATED BEAMS UNDER RANDOM LOADING

6.1 Introduction

To date, the majority of works on modeling and vibration control of smart laminated composite structures assumed deterministic loading conditions, where the applied forces are known. However, many of the laminated composite structures are exposed to randomly varying dynamic loading, such as aircraft components (due to turbulence, acoustic pressure, or rough burning engines), and marine structures in which the variation of such loading cannot be determined exactly. It is only possible to make probabilistic statements about the variation of response. In order to design smart laminated structures for realistic engineering applications, an in-depth understanding of the dynamic response of the smart system under random excitations is of great importance. In this chapter the spectral characteristics of response of smart laminated beam under stationary random loading, for which the statistical properties are time-independent is studied. First, fundamental concepts of random vibration analysis are reviewed. Then, dynamic response of the smart laminated system under random excitation is investigated. An optimal control algorithm based on Linear Quadratic Regulator (*LQR*) is designed to actively suppress the vibration of the system. Numerical examples are presented to demonstrate the rationally and validity of the active control model.

6.2 Random Vibration Analysis

A random signal is defined by the probability of the variable X to take a specific value of x and is shown as $P_X(x)$ and characterized as[133]:

.

$$0 \le P_X(x) \le 1, \qquad \sum_{all\,x} P_X(x) = 1 \tag{6.1}$$

The function that describes the distribution of probability density over the sample space of random variable, X, is called the *probability density function* (PDF) and is designated $f_X(x)$. Thus, to find the probability of X occurring between a and b, $f_X(x)$ is integrated from a to b:

$$P(a \le X \le b) = \int_a^b f_X(x)dx \tag{6.2}$$

Mean value: The mean value, μ_X, is the average value. It is also called as *expected value* and shown as $E[X]$. For discrete systems, the mean value is calculated by adding each possible value of X multiplied by its probability:

$$\mu_X = E[X] = \sum_X x_i P_X(x_i) \tag{6.3}$$

For continuous systems, summation is replaced by integration and $P_X(x_i)$ is replaced by $f_X(x)dx$. The mean value may also be thought as the first moment of PDF.

Variance: The variance is defined as:

$$\sigma_X^2 = E[(X - \mu_X)^2] \tag{6.4}$$

The expected value of the square of X, $E[X^2]$, is known as the mean-square value and its square root is called as the *Root-Mean-Square*, or RMS, value. If the mean of X is zero, then the mean-square value is equal to the variance σ_X^2 and the RMS is equal to the standard deviation, σ_X.

Gaussian distribution: Many of the real-world random phenomena are approximated with Gaussian or normal distribution. The probability density function of the Gaussian process is given by

$$f_X(x) = \frac{1}{\sqrt{2\pi}\sigma_X} \exp\left[-\frac{1}{2}\left(\frac{x-\mu_X}{\sigma_X}\right)^2\right] \quad , \quad -\infty < x < \infty \tag{6.5}$$

The Gaussian distribution is completely defined by its mean value and standard deviation and it is symmetrical about its mean value. Also, all derivatives and integrals of a Gaussian process are Gaussian processes.

Correlation function: If a random process consists of two individual processes, then the expectation of their simultaneous occurrence is called as *correlation* function. Further, if

the correlation of a random process is measured with itself at two different times, $X(t_1)$ with $X(t_2)$, then this correlation is called *autocorrelation* function and is defined as:

$$R_X(t_1,t_2) = E[X(t_1)X(t_2)] = \int_{-\infty}^{\infty} \int_{-\infty}^{\infty} x_1 x_2 f_{X(t_1)X(t_2)}(x_1,x_2)dx_1 dx_2 \tag{6.6}$$

Power spectral density function: A random process is essentially a non-periodic process and can be represented by the sum of individual harmonic processes:

$$X(t) = \sum_{k=1}^{m} X_k(t) = \sum_{k=1}^{m} (A_k \cos\omega_k t + B_k \sin\omega_k t) \tag{6.7}$$

When m goes to infinity, the autocorrelation function of this process may be represented as Fourier cosine transform:

$$R_X(\tau) = E[X(t)X(t+\tau)] = \sigma_X^2 \int_0^{\infty} g(\omega)\cos(\omega\tau)d\omega \tag{6.8}$$

The Fourier transform of the autocorrelation function is called the *spectral density* function, $S_X(\omega)$ can be defined as:

$$S_X(\omega) = \frac{1}{2\pi} \int_{-\infty}^{\infty} R_X(\tau)e^{-i\omega\tau}d\tau \tag{6.9}$$

and using inverse Fourier transform we have:

$$R_x(\tau) = \int_{-\infty}^{\infty} S_X(\omega) e^{i\omega\tau} d\omega \tag{6.10}$$

If the mean value is equal to zero, then the area under the spectral density function is equal to the variance:

$$R_X(\tau = 0) = \sigma_X^2 = \int_{-\infty}^{\infty} S_X(\omega) d\omega \tag{6.11}$$

In analog spectral analyzers, the waveform, represented by current $i(t)$ or voltage $v(t)$, is iteratively filtered to a signal with only a single frequency. The filtered signal's mean-square value is then measured and plotted. Since, i^2 and v^2 are proportional to the average power dissipated in a resistive load, this is called the "power" at that frequency. In practice, it is impossible to develop a physical filter that outputs only a single frequency; the output is actually a signal that contains many frequencies but is dominated by frequencies within a narrow bandwidth, Δf. Thus, the measured power is divided by the width of the band, Δf, making a units i^2 per unit frequency or v^2 per unit frequency. Hence, $S_X(\omega)$ is called *Power Spectral Density* (PSD) which is basically estimating how the total power is distributed over frequencies from a finite record of a stationary data sequence[153], and provides information on the characteristics of mechanical parts under study.

Another two practical issues are: changing the units of frequency from radian per second to cycles per second, or Hertz and discarding the negative frequencies. If the first change is applied then,

$$S_X(f) = 2\pi S_X(\omega) \tag{6.12}$$

If the negative frequencies are neglected then, the one-sided spectral density, $G_X(\omega)$ is given by

$$G_X(\omega) = 2S_X(\omega) \qquad \omega \geq 0 \tag{6.13}$$

And if both changes are applied, the spectral density is called engineering spectral density function and is represented by

$$W_X(f) = 4\pi S_X(\omega) \qquad \omega, f \geq 0 \tag{6.14}$$

White-noise: White noise is the simplest random process and is one of the most practical representations for many engineering random process. It is defined by a constant spectral density for all frequencies:

$$S_X(\omega) = S_0, \qquad -\infty < \omega < \infty \tag{6.15}$$

The spectral density function for white-noise process using mathematical spectral density function as well as engineering spectral density function is shown in Figure 6.1 where the terms W_O and W_X are corresponding to the engineering spectral density function in which only the positive values for frequency are considered.

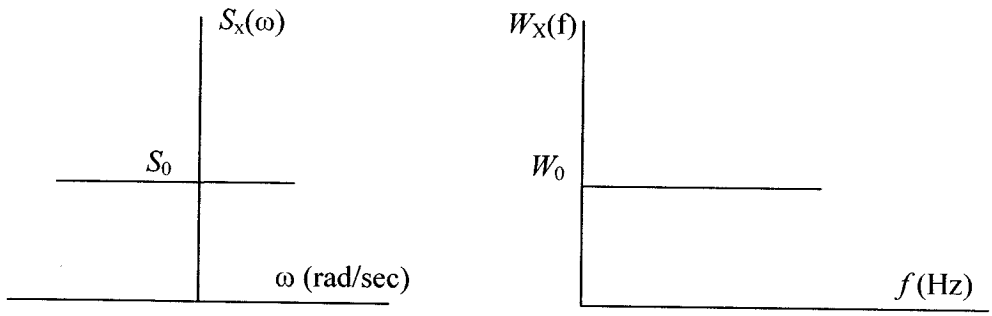

Figure 6.1 Spectral density function for white-noise process

White-noise is physically impossible; however, many of practical random excitations, including aerospace structures[154] can be approximated as white-noise for limited frequency intervals.

Random vibration of single and multi degree of freedom systems:

Response of a single degree of freedom system under random excitation can be described as[158]:

$$S_X(\omega) = |H(\omega)|^2 S_F(\omega) \tag{6.16}$$

where $H(\omega)$ represents the transfer function of the system and $S_F(\omega)$ is the PSD of the random excitation force. For multi-degree of freedom system, the response is given by

$$[S_X(\omega)] = [H(\omega)][S_F(\omega)][H^*(\omega)]^T \tag{6.17}$$

where '*' represents the complex conjugate. $H_{ij}(\omega)$ represent the transfer function for coordinate i due to force at coordinate j. Similarly, $S_{X_{ij}}(\omega)$ is the PSD of response of coordinate i due to force at coordinate j. For more details for the background on random process, one may consult the books written by Wirsching *et al*[155], Newland[156] and Yang[157].

6.3 Response of the Smart Laminated Beam to Random Excitation

In this section the response of the smart laminated beam to different random excitations are studied. Following the finite element formulation of a smart laminated beam using layerwise displacement theory described in Chapter 2, the equation of motion under a random excitation can be expressed as

$$[M_{dd}]\{\ddot{d}\}+[C]\{\dot{d}\}+[\hat{K}]\{d\}=\{F_d(t)\}+[K^{sa}_{d\psi}]\{\psi^a(t)\} \tag{6.18}$$

where $\{F_d(t)\}$ represents the external force vector generating the primary excitation. The vector $\{\psi^a(t)\}$ is the control force applied to the system. The matrix $[K^{sa}_{d\psi}]$ defines the location of the actuators and also converts the applied electric field to the mechanical force. The remaining matrices in the equation we introduced in Chapter 2.

As mentioned before layerwise theory leads to the large number of degrees of freedom in finite element model. Thus, using direct method to construct transfer function is not

efficient for many practical cases. In fact, when dealing with vibration problems, usually the effect of the first few modes is dominant. Using the modal expansion $\{d(t)\} = [q]\{\eta(t)\}$, and substituting in Equation (6.18), the equations of motion take the following form

$$[I]\{\ddot{\eta}(t)\} + [D]\{\dot{\eta}(t)\} + [\Omega]\{\eta(t)\} = [q]^T\{F_d(t)\} + [q]^T[K_{d\psi}^{sa}]\{\psi^a(t)\} \tag{6.19}$$

where $[D] = diag[2\xi_j\omega_j]$, $[\Omega] = diag[\omega_j^2]$, for $j = 1,2...,n$, and $[q]$ is the normal mode matrix of the smart structure. ω_j and ξ_j are the jth-order natural frequency and damping ratio, respectively. The response of this system to arbitrary loading can be obtained using the impulse response function. Using the mode superposition method, the response of the jth degree of freedom in modal coordinates is obtained as:

$$\eta_j(t) = \int_0^t (\{q\}_j^T\{F_d(\tau)\} + \{q\}_j^T[K_{d\psi}^{sa}]\{\psi^a(\tau)\})h_j(t-\tau)d\tau \tag{6.20}$$

where

$$h_j(t) = \frac{1}{\varpi_j}\exp(-\xi_j\omega_j t)\sin\varpi_i \tag{6.21}$$

where $\varpi_j = \omega_j(1-\xi_j^2)^{1/2}$

The autocorrelation function matrix of the modal coordinates can be obtained from Equation (6.20) as

$$[R_\eta(\varepsilon)] = E\left[\{\eta(t)\}\{\eta(t+\varepsilon)\}^T\right] = \int_0^\infty \int_0^\infty [h(\tau)][R_P(\tau-\tau_1+\varepsilon)][h(\tau_1)]^T d\tau d\tau_1 \tag{6.22}$$

where $[R_\eta(\varepsilon)]$ is the correlation function matrix for the modal displacement response of the smart system. $[R_P(\tau-\tau_1+\varepsilon)]$ represents the correlation function matrix of the total force $\{P\}$ given by

$$\{P\} = [q]^T\{F_d(t)\} + [q]^T[K_{d\psi}^{sa}]\{\psi^a(t)\} \tag{6.23}$$

By performing the Fourier transformation on $[R_\eta(\varepsilon)]$, the power spectral density matrix of the displacement response $[S_\eta(\omega)]$ is determined as

$$[S_\eta(\omega)] = [H_\eta(\omega)][S_P(\omega)][H_\eta^*(\omega)]^T \tag{6.24}$$

where $[S_P(\omega)]$is a diagonal matrix representing the power spectral function matrix of $\{P(t)\}$ and its diagonal terms represent the spectral density functions of each coordinate of S_{η_i}. $[H_\eta(\omega)]$is the frequency response function matrix of the structure and $[H_\eta^*(\omega)]$is its conjugate matrix. The *j*th component of $[H_\eta(\omega)]$is given by

$$H_{\eta_j}(\omega) = \frac{1}{\omega_j^2 - \omega^2 + 2\mathrm{i}\xi_j\omega_j\omega} \quad , \mathrm{i} = \sqrt{-1} \tag{6.25}$$

The mean-square response of the jth coordinate is given by

$$E[\eta_j^2(t)] = 2\int_0^\infty S_{\eta_j}(\omega)d\omega \tag{6.26}$$

For more details on spectral analysis, one may consult the book written by Goldman[158].

6.4 Active Control of Smart Structure under Random Excitations

In this section both the classical and optimal control strategies are utilized to develop closed-loop response of the smart laminated system under a variety of random loading conditions, including, Gaussian white-noise, band-limited and narrow-band processes.

To study the active control of smart laminated structures as discussed in Chapter 5, the equations of motion is formulated in the state space form. The modal state vector $\{x\}$ is defined as:

$$\{x\} = \{\{\eta\}, \{\dot{\eta}\}\}^T \tag{5.7}$$

Now using the state variable matrix given by Equation (5.7), the state space form of Equation (6.19) can be written as the following:

$$\{\dot{x}\} = [A]\{x\} + [B]\{\psi^a\} + \{f_d\} \tag{6.27}$$

where $\{\psi^a\}$ represents the actuating control force and $\{f_d\} = \{\{0\} \quad [q]^T\{F_d\}\}^T$. The relation for sensor output given by Equation (5.9),

$$\{\psi^s\} = \{y\} = [C]\{x\} \tag{5.9}$$

The remaining coefficients are given by Equation (5.10) as

$$[A] = \begin{bmatrix} [0] & [I] \\ [-\omega^2] & [-2\xi\omega] \end{bmatrix}, [B] = \begin{bmatrix} [0] \\ -[q]^T [K_{d\psi}^{sa}] \end{bmatrix}, [C] = [-[K_{\psi\psi}^{ss}]^{-1}[K_{\psi d}^{ss}][q] \quad [0]] \tag{5.10}$$

In the following sections, the classical and optimal control (*LQR*) methods are utilized to develop feedback control gain.

6.4.1 Classical control

To design a controller in classical control method, the sensors output are amplified and directly fed back to the piezoelectric actuators. The control voltage is given by

$$\{\psi^a\} = -[G]\{\psi^s(t)\} \tag{6.28}$$

where $[G]$ is a feedback control matrix defined according to the control law. Substituting Equation (6.28) into (6.27), the closed-loop system state is given by

$$\{\dot{x}\} = ([A] - [B][G][C])\{x\} + \{f_d\} \tag{6.29}$$

Performing Laplace transform and replacing s with $j\omega$, the frequency response function for the closed-loop system can be obtained in steady state form as

$$H(j\omega) = \left(j\omega I - ([A] - [B][G][C])\right)^{-1} \tag{6.30}$$

Substituting the Equation (6.30) into Equation (6.24), the power spectral density for closed-loop system can be obtained.

6.4.2 Linear quadratic regulator

In full state control method, the actuating voltage is determined as

$$\{\psi^a\} = -[K_{sc}]\{x\} \tag{6.31}$$

where $[K_{sc}]$ is the optimal feedback gain, determined in Chapter 5. Substituting Equation (6.31) into Equation (6.27) the closed-loop state equation is obtained as

$$\{\dot{x}\} = ([A] - [B][K_{sc}])\{x\} + \{f_d\} \tag{6.32}$$

and the frequency response function in state space form is determined as

$$H(j\omega) = \left(j\omega I - ([A] - [B][K_{sc}])\right)^{-1} \tag{6.33}$$

Substituting Equation (6.33) into Equation (6.23) the power spectral density of response of the smart laminated structure can be determined.

For active control, the control force is induced to the actuators to respond to the disturbance occurred due to random excitations. Thus, to design an efficient control mechanism, it is of significant importance to know how the actuator forces correlate with applied external random forces. The correlation functions of external force $F_d(t)$, and actuator force $F_A(t)$, are defined as

$$R_{F_d F_A}(\tau) = E[F_d(t)F_A(t+\tau)] \tag{6.34}$$

A numerical magnitude of correlation between $F_d(t)$ and $F_A(t+\tau)$ can be determined by introducing the correlation coefficient, $\rho_{F_d F_A}$, defined as

$$\rho_{F_d F_A} = \frac{\sigma_{F_d F_A}}{\sigma_{F_d}\sigma_{F_A}} \tag{6.35}$$

where σ_{F_d} and σ_{F_A} represent the standard deviation of external random force $F_d(t)$, and actuator force $F_A(t)$ respectively, and $\sigma_{F_d F_A}$ is the covariance of the external and actuator forces which indicates the deviations of $F_d(t)$ and $F_A(t)$, from their centroid and is given by

$$\sigma^2_{F_dF_A} = E[F_dF_A] - \mu_{F_d}\mu_{F_A} \tag{6.36}$$

Here, μ_{F_d} and μ_{F_A} represent the mean value of external random force and the mean value of applied actuator force, respectively. Values of $\sigma_{F_dF_A} \cong 0$ indicate that the two signals tend not to vary together. It should be noted that since the units of external force and actuator force are different, the covariance $\sigma_{F_dF_A}$ should be normalized to remove the units of measurements.

The values of $\rho_{F_dF_A} = \pm 1$ indicate there is perfect correlation, and $\rho_{F_dF_A} = 0$, means there is no correlation between the external force and the control force.

6.5 Numerical Examples

A smart laminated beam with $[PS/(0/90/0)_s PA]$ configuration with clamped-free boundary condition is considered in this section to study the response of the smart laminated system to random excitation. The length and width of the beam are, 30 *cm* and 3 *cm*, respectively. The material properties for composite lamina, piezoceramic and PVDF are provided in Section 5.5.1. The first three natural frequencies of this system are, respectively, 17.93 *Hz*, 105.98 *Hz* and 276.07 *Hz*. As it is realized the three natural frequencies are enough separated to be considered independently. Thus, in this section the optimal controller is designed to suppress the vibration at the fundamental frequency of the system under random loading.

6.5.1 Response to a Gaussian white noise

The smart laminated beam is exposed to a random excitation approximated as Gaussian white noise with zero mean value, variance of 95.0 N^2 and standard deviation of 9.70 N as shown in Figure 6.2. The input random signal is considered to generate a realistic displacement in the system and to show the performance of the control algorithm for vibration suppression. The LQR control algorithm is utilized to control the response of the system. The cost function coefficients are considered as $Q = 2 \times 10^9 I_{2\times 2}$ and $R = 1.3$.

Time responses for open-loop and closed-loop are obtained and shown in Figure 6.3. As it is indicated, applying LQR control significantly suppresses the vibration response of the system.

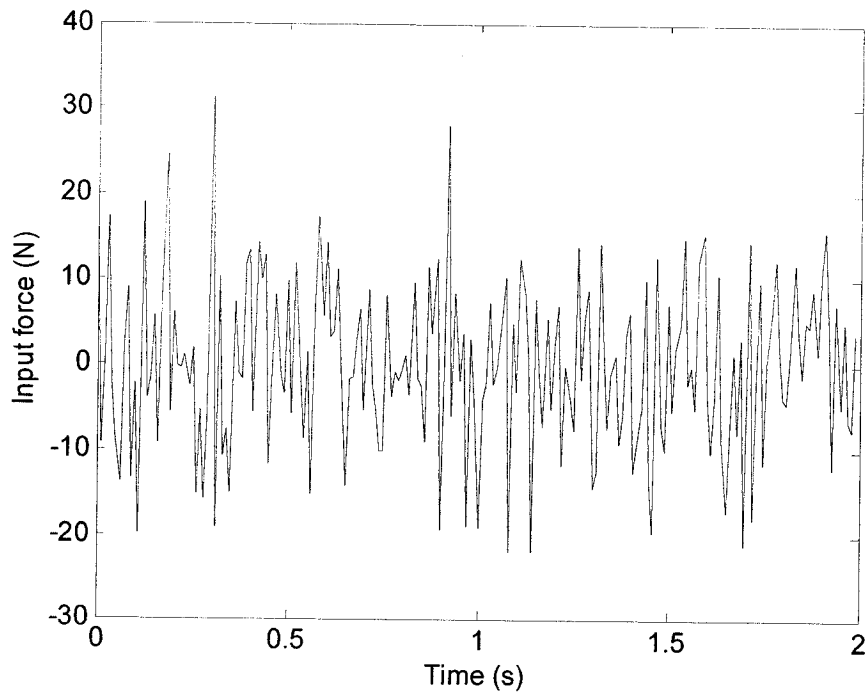

Figure 6.2 Input applied force approximated as Gaussian white noise

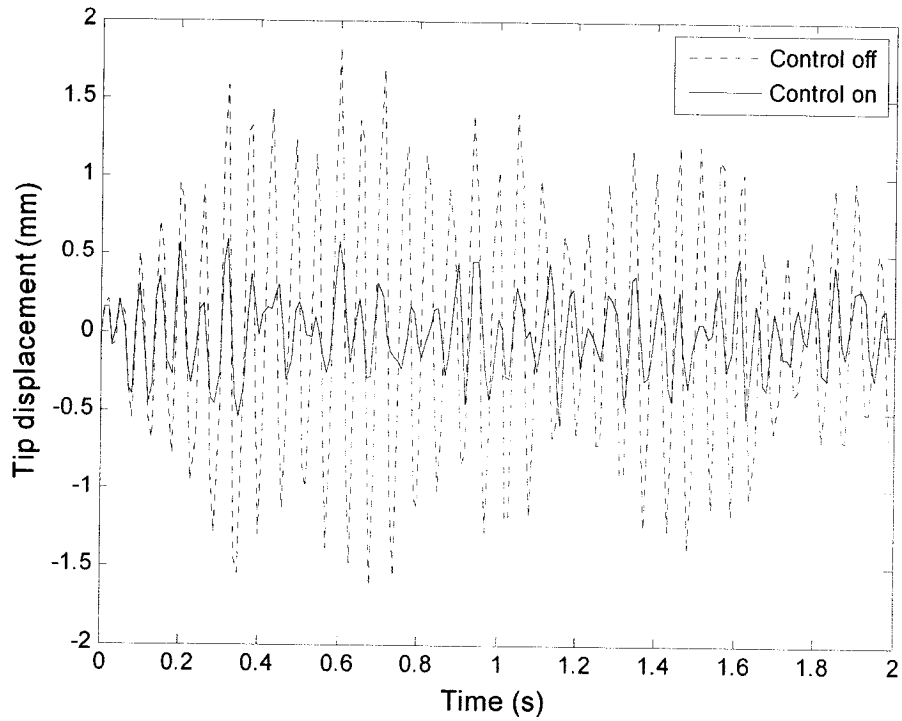

Figure 6.3 Response of the smart laminated beam under applied white noise

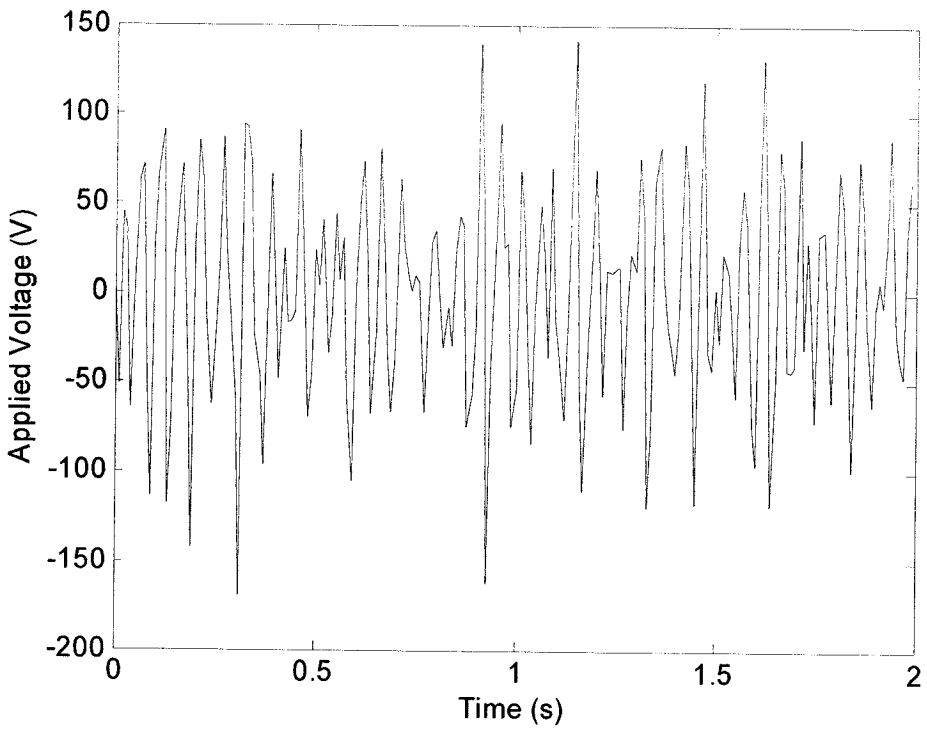

Figure 6.4 Actuator voltage required to suppress the vibration

The required applied control voltage on the actuator is also provided in Figure 6.4 where one can realize that the maximum actuator voltage never exceeds the maximum allowable voltage (150 V). The variance of the actuator voltage is 3417 V^2 and its standard deviation and mean value are 58.5 V and 0.25 V, respectively. The power spectral density of the tip displacement for the smart laminated beam is provided in Figure 6.5. It can be realized that most of the power of the actuating signal is concentrated at the frequency close to the fundamental natural frequency of the system. This result was expected since the maximum deformation is close to the fundamental natural frequency. Thus, most of the actuating energy supplied by the actuator is consumed at this frequency.

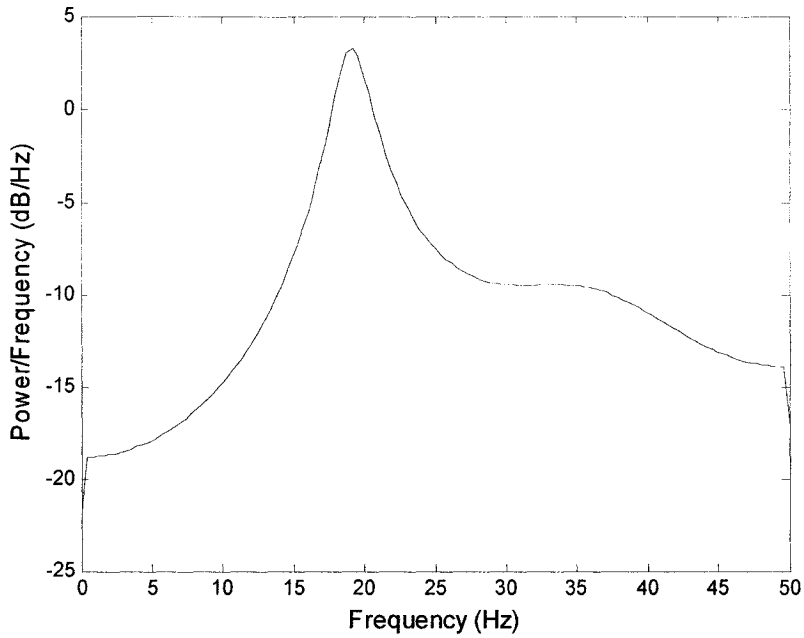

Figure 6.5 PSD of actuator voltage

To design an active control system to efficiently suppress the vibration response of the smart laminated system under random excitation, it is very important to have good

correlation between the external random force and the actuating applied force. The correlation coefficient for the above example is found to be $\rho_{F_d F_A} = 0.658$. It should be noted that for a deterministic sinusoidal external force, the correlation coefficient is 0.998.

The correlation coefficient depends on laminated configuration, piezoelectric location and weighting factors in LQR control design. In the following, the effects of the above parameters on correlation coefficient between input random force and actuating force are investigated. For all the cases, the Gaussian white noise excitation shown in Figure 6.2 utilized. Keeping a constant value for weighting factor $R = 1.0$ in LQR and changing the value of weighting factor Q, the correlation coefficients for different laminate configurations are computed and provided in Table 6.1. It should be noted that there is always a time shift between the primary external force and the applied actuating force. In this case, the results provided in Table 6.1 are determined when the actuator signal is shifted for $\Delta t = 0.01s$ to the origin.

However, we may compute the correlation coefficient at the time when both external and applied actuating forces are available, (i.e. after $t = 0.02s$). Similar results are computed for correlation coefficient after $t = 0.02s$ and provided in Table 6.2.

Table 6.1 Effect of weighting factor $[Q]$ on correlation coefficient at ($\tau = 0$) for different laminate configurations

Laminate configurations							
$[PS/0_6/PA]$		$[PS/(0/90/0)_s/PA]$		$[PS/\pm 30/0)_s/PA]$		$[PS/\pm 45/0)_s/PA]$	
$Q\times 2$	$\rho_{F_dF_A}$	$Q\times 2$	$\rho_{F_dF_A}$	$Q\times 2$	$\rho_{F_dF_A}$	$Q\times 2$	$\rho_{F_dF_A}$
$10^7 I_{2\times 2}$	0.271	$10^7 I_{2\times 2}$	0.271	$10^7 I_{2\times 2}$	0.312	$10^7 I_{2\times 2}$	0.350
$10^8 I_{2\times 2}$	0.450	$10^8 I_{2\times 2}$	0.451	$10^8 I_{2\times 2}$	0.471	$10^8 I_{2\times 2}$	0.494
$10^9 I_{2\times 2}$	0.684	$10^8 I_{2\times 2}$	0.685	$10^9 I_{2\times 2}$	0.694	$10^9 I_{2\times 2}$	0.711

Table 6.2 Effect of weighting factor $[Q]$ on correlation coefficient at ($t = 0.02s$) for different laminate configurations

Laminate configurations				
$[PS/0_6/PA]$		$[PS/(0/90/0)_s/PA]$	$[PS/\pm 30/0)_s/PA]$	$[PS/\pm 45/0)_s/PA]$
$Q\times 2$	$\rho_{F_dF_A}$	$\rho_{F_dF_A}$	$\rho_{F_dF_A}$	$\rho_{F_dF_A}$
$10^7 I_{2\times 2}$	-0.0393	-0.0241	-0.0371	-0.1639
$10^8 I_{2\times 2}$	-0.0913	-0.0900	-0.1051	-0.1480
$10^9 I_{2\times 2}$	-0.1361	-0.1383	-0.1510	-0.1470

As it can be realized, increasing the value of $[Q]$ improves the correlation coefficient between the random excitation and applied actuating voltage. This is basically due to the fact that higher value of $[Q]$ demands more power of actuating force which correlate better with input signal. On the other hand, for the same value of $[Q]$, the correlation coefficient is the highest for the laminate configuration $[PS/(\pm 45)/0)_s/PA]$ compared to other three configurations.

It is worth noting that by increasing the value of $[Q]$ to $2\times10^{13}\times I_{2\times2}$, the value of $\rho_{F_dF_A}$ will approach 0.999 (for $\tau = 0$) which is a perfect correlation between input random force and applied actuating force. On the other hand, Table 6.2 indicates negative and lower values for the correlation coefficients as in this case the actuating force is not shifted, but the origin of computation is shifted to the point where both external and applied forces are available. The lower and negative value is due to the phase shift between the external and applied forces. However, increasing the value of $[Q]$ dramatically increases the required actuating voltage. Using the magnitude of $[Q] = 2\times10^{9}\times I_{2\times2}$ in *LQR* results in 157 volts actuating voltage which is the maximum practical amount for the present example. Applying higher voltage to the actuator requires more powerful voltage amplifier and higher quality of piezoceramic actuators.

Next, the value of $[Q] = 2\times10^{9} I_{2\times2}$ is kept constant and the value of $[R]$ is changed form 1 to 3 to investigate its effect on the correlation coefficient for different laminate configurations. Table 6.3 provides the value of $\rho_{F_dF_A}$ for similar laminate configurations

described in Table 6.1. From Table 6.3, one can realize that increasing the value of weighting matrix $[R]$ reduces the value of correlation coefficient which is identical to the results obtained in Chapter 5 showing that increasing the value of $[R]$ requires weaker signal for actuating voltage. In general, one may conclude that the weaker is actuating voltage, the higher correlation exists between the actuating voltage and input random signal. Similar investigation is conducted when the correction coefficient is computed at $t = 0.02s$ and the results are provided in Table 6.4. For this case, the actuating force is not shifted, but the origin of computation is shifted to the point where both external and applied forces are available. The lower and negative value is due to the phase shift between the external and applied forces.

Table 6.3 The effect of weighting factor $[R]$ on correlation coefficient at $(\tau = 0)$ for different laminate configurations

Laminate configurations							
$[PS/0_6/PA]$		$[PS/(0/90/0)_s/PA]$		$[PS/\pm 30/0)_s/PA]$		$[PS/\pm 45/0)_s/PA]$	
R	$\rho_{F_dF_A}$	R	$\rho_{F_dF_A}$	R	$\rho_{F_dF_A}$	R	$\rho_{F_dF_A}$
1.0	0.684	1.0	0.685	1.0	0.694	1.0	0.711
2.0	0.614	2.0	0.616	2.0	0.628	2.0	0.643
3.0	0.572	3.0	0.574	3.0	0.577	3.0	0.603

Table 6.4 The effect of weighting factor $[R]$ on correlation coefficient at $(t = 0.02s)$ for different laminate configurations

Laminate configurations				
$[PS/0_6/PA]$		$[PS/(0/90/0)_s/PA]$	$[PS/\pm 30/0)_s/PA]$	$[PS/\pm 45/0)_s/PA]$
R	$\rho_{F_dF_A}$	$\rho_{F_dF_A}$	$\rho_{F_dF_A}$	$\rho_{F_dF_A}$
1.0	-0.136	-0.138	-0.151	-0.164
2.0	-0.128	-0.130	-0.145	-0.162
3.0	-0.121	-0.123	-0.138	-0.159

The effect of actuator location on correlation coefficient is also investigated for a unidirectional laminated beam. The location of actuator is changed from the bottom surface toward the inside layers. Table 6.5 provides the correlation coefficients for different actuator locations through the thickness when $\tau = 0$. Similarly, Table 6.6 is computed based on the $t = 0.02s$. Once again, one may realize that when $t = 0.02s$, the corresponding values are negative and lower compared to that of $\tau = 0$ which is as explained before due to the phase change. It is observed that when the actuator is surface mounted at bottom surface, the correlation coefficient is the highest and when we move toward the middle plane this value reduces. As mentioned in Chapter 5, when the actuator is surface mounted at the bottom surface the generating moment is the highest which results in stronger control signals leading to the higher values for correlation coefficients.

Table 6.5 Effect of actuator location through the thickness on the correlation coefficient at $(\tau = 0)$

Correlation coefficient	Actuator location through the thickness		
	$[PS/0_6/PA]$	$[PS/0_5/PA/0]$	$[PS/0_4/PA/0_2]$
$\rho_{F_d F_A}(\tau = 0)$	0.658	0.532	0.529

Table 6.6 Effect of actuator location through the thickness on the correlation coefficient for different laminate $(t = 0.02\,s)$

Correlation coefficient	Actuator location through the thickness		
	$[PS/0_6/PA]$	$[PS/0_5/PA/0]$	$[PS/0_4/PA/0_2]$
$\rho_{F_d F_A}(t = 0.02\,s)$	-0.134	-0.114	-0.112

(note that after middle-plane the pattern will repeat.)

The statistical properties of structural controlled response of the smart laminated beam under the input white noise random force (Figure 6.1) and for different laminate configurations are provided in Table 6.7.

Table 6.7 Effect of laminate configurations on statistical properties of tip displacement of the smart beam for closed-loop control

Laminate configuration	Statistical properties of tip displacement		
	μ_{tip}, mm	σ_{tip}, mm	σ_{tip}^2, mm^2
$[PS/(0)_6/PA]$	0.0006	0.240	0.058
$[PS/(\pm 30)/0)_s/PA]$	0.0007	0.248	0.0616
$[PS/(\pm 45)/0)_s/PA]$	0.0008	0.257	0.066
$[PS/(0/90/0)_s/PA]$	0.0006	0.242	0.058

The effects of actuator location on the statistical properties of structural controlled response are provided in Table 6.8.

Table 6.8 Effect of the actuator location on statistical properties of tip displacement of the smart beam for closed-loop control

Laminate configuration	Statistical properties of tip displacement		
	μ_{tip}, *mm*	σ_{tip}, *mm*	σ_{tip}^2, *mm*^{2}
$[PS/(0)_6/PA]$	0.00058	0.241	0.0583
$[PS/0_5/PA/0]$	0.00053	0.179	0.0321
$[PS/0_4/PA/0_2]$	0.00043	0.178	0.0317

In the previous examples the random input signal was available in time domain, however, in many practical engineering applications only the stochastic characteristic, usually power spectral density function, of the input random excitation is given.

In the following study a Gaussian white noise with given $PSD_P = 40\,dB$ and zero mean value is considered to investigate the displacement response of the smart laminated beam. The displacement is also converted to decibel (dB) which commonly used for PSD plots. Figure 6.6 shows the open-loop and closed-loop of the PSD of the system response for the first mode. It is indicated that the maximum value of the PSD at natural frequency of the system is reduced by almost 25% when the LQR controller is applied to the smart system. Figure 6.7 presents the effect of control mechanism on the first two vibration modes under random excitation. As one can realize, the developed optimal control can successfully suppresses the vibration of both mode one and mode two. However, it has much higher effect on controlling the vibration of the first mode than the second mode. This is basically due to the fact that control system has been designed based on the fundamental mode. It means the control system is developed to control the fundamental vibration mode of the smart system.

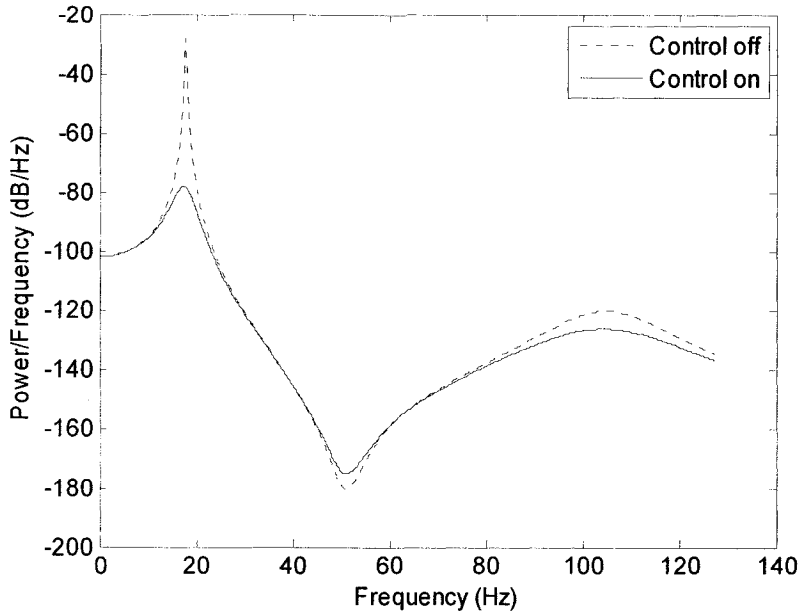

Figure 6.6 PSD for smart laminated beam using control-on /off; first mode

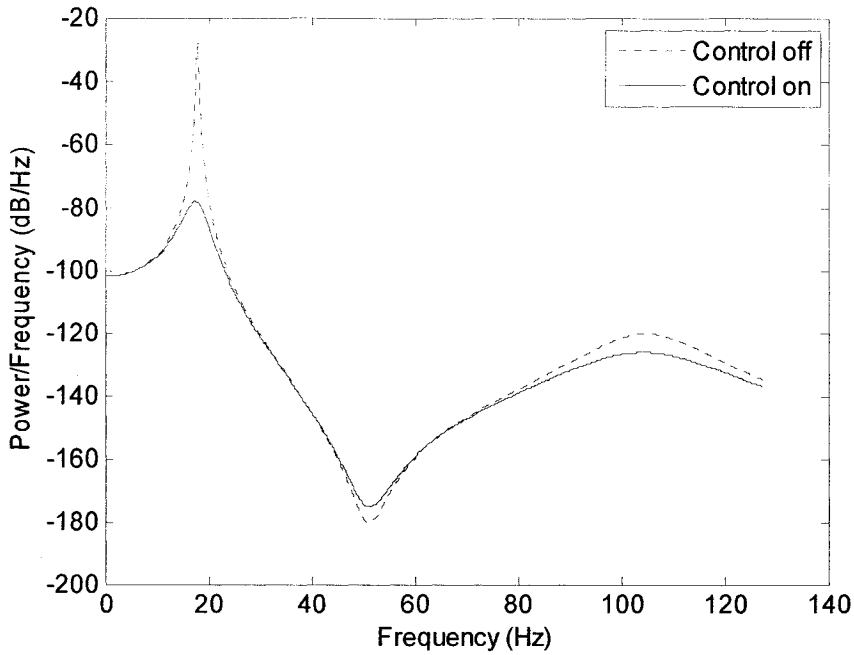

Figure 6.7 PSD for smart laminated beam using control-on /off; the first two modes

6.5.2 Effect of laminate configuration on the PSD of the optimal closed-loop response

The effect of laminate configuration on the PSD of the system response under the same Gaussian white-noise random loading with a PSD of, 40 dB is studied in this section. Figure 6.8 shows the PSD of response of the smart system for different laminate configurations. It is realized that the power consumption for the smart systems with configurations $[PS/(0/90/0)_s/PA]$ and $[PS/(0)_6/PA]$ are almost the same but lower than that of smart systems with laminate configurations $[PS/(\pm 30/0)_s/PA]$ and $[PS/(\pm 45/0)_s/PA]$. It is interesting to note that the configurations have higher amount of power concentrated at frequencies below the first natural frequency.

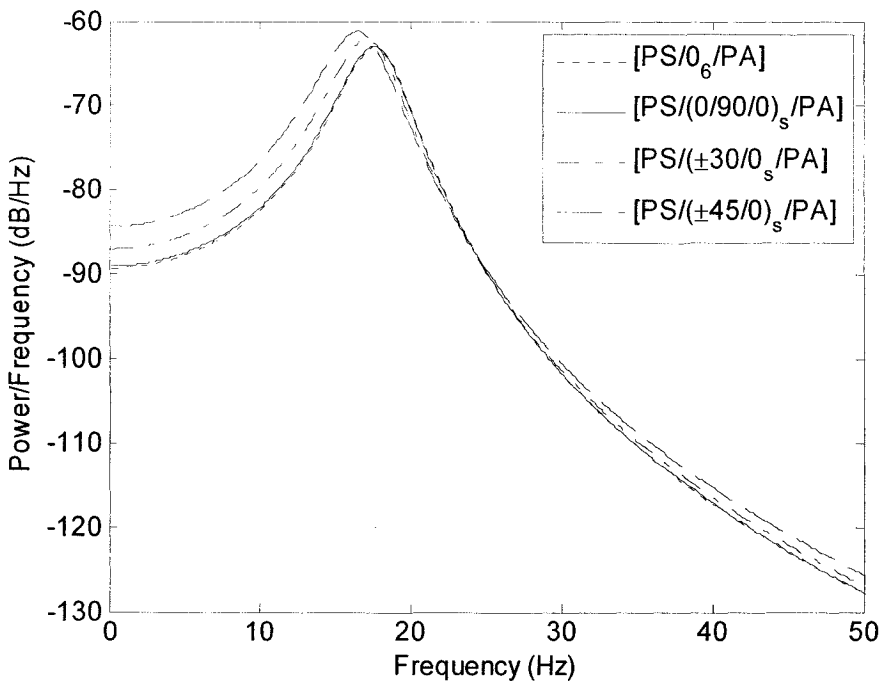

Figure 6.8 Effect of laminate configuration on PSD of optimal closed-loop response

Effect of actuator location through the thickness of the smart laminated system is also investigated for configurations considered in the study of vibration response in time domain, namely, $[PS/(0)_6/PA]$, $[PS/0_5/PA/0]$ and $[PS/0_4/PA/0_2]$ for a known PSD of the input white-noise excitation of 40 dB. The PSD of the response of the system is provided in Figure 6.9. It is observed that the peak value of the PSD is almost equal for all cases, however, when the actuator is surface mounted the overall energy consumption for the given frequency interval is higher than that of the other two cases. This is due to the fact that when the actuator is mounted on the upper surface the generating moment is higher, and it remains higher for all frequencies in the domain. Obviously, the energy corresponding to the configuration $[PS/0_5/PA/0]$ is higher than that of the configuration $[PS/0_4/PA/0_2]$ since the former is closer to the outer surface.

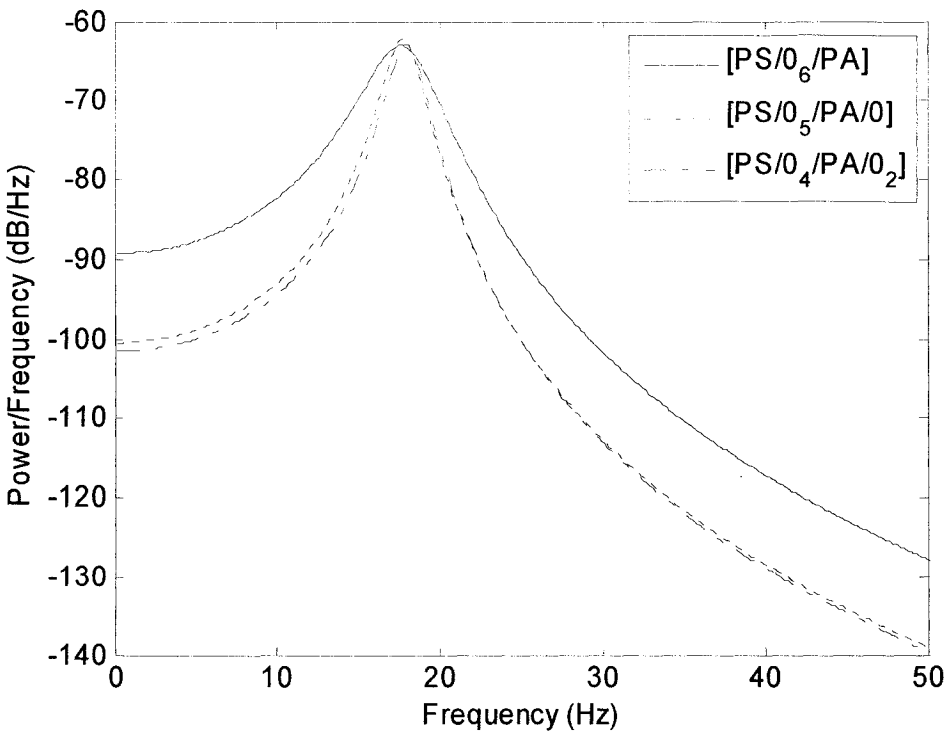

Figure 6.9 Effect of location of actuator on PSD of optimal closed-loop response

The effect of collocated and uncollocated sensor/actuator pairs on optimal vibration control is also investigated in the following example. Two cases of uncollocated sensor/actuator pairs are considered as shown in Figure 6.10.

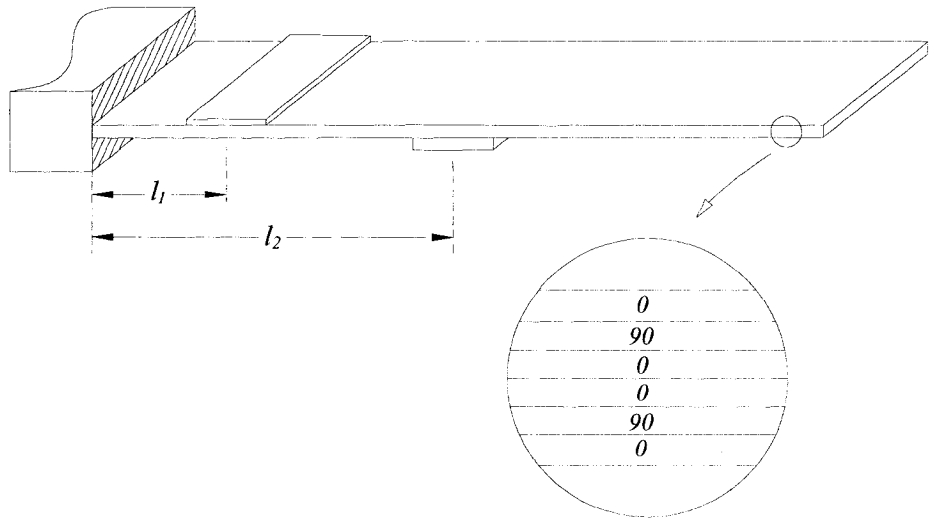

Figure 6.10 Smart laminated beam with uncollocated sensor/actuator pairs

In case I, the sensor is mounted on top surface at $l_1 = 3\,cm$ from the fixed end and the actuator is bonded on bottom surface at $l_2 = 6\,cm$ from the fixed end. In case II, the actuator is bonded at $l_2 = 8\,cm$ from the fixed end on the bottom surface, and the location of sensor is kept the same as that of the case I.

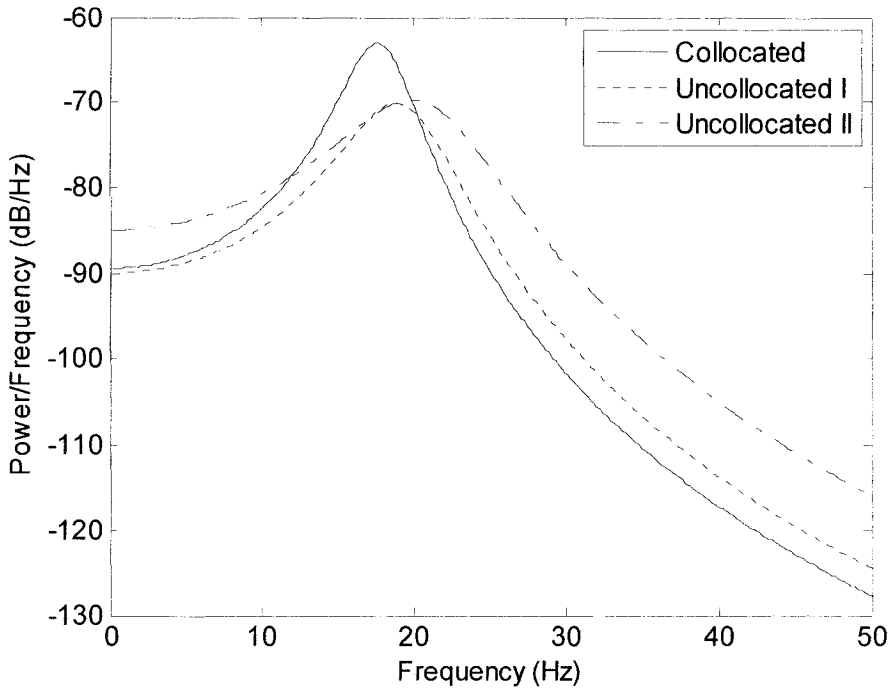

Figure 6.11 Effect of collocated and uncollocated PZT pair on the response of the smart beam

Figure 6.11 shows that for collocated sensor/actuator pairs, the peak of power is higher than uncollocated pairs and occurs at the lower frequency. As the actuator is shifted away from the sensor location, the peak of power occurs at higher frequency and becomes more distributed through all the frequencies in the domain.

6.5.3 Response to a band limited excitation

Band limited random process is defined as random process whose spectral density is uniform for all frequencies between frequency interval (ω_1, ω_2) as shown in Figure 6.12. The spectral density function of band limited random process can be defined as:

$$S_X(\omega)=\begin{cases} S_O & \omega_1<|\omega|<\omega_2 \\ S_O/2 & |\omega|=\omega_1,\omega_2 \\ 0 & otherwise \end{cases} \tag{6.36}$$

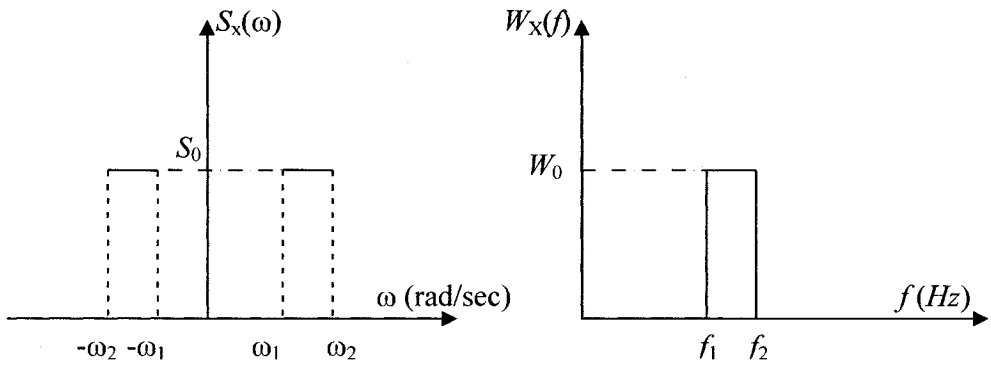

Figure 6.12 Spectral density of a band limited random process

To study the vibration response of the smart system for band limited excitation, smart laminated beam described in Section 6.4.2 has been exposed to a random excitation with PSD of 200 dB which is concentrated in the frequency range between 10 and 30 *Hz*. A *LQR* controller with properties similar to that of the section 6.4.2 is considered to suppress the vibration response. The power spectral density of system without and with control is presented in Figure 6.13. It is indicated that the power consumption at the peak is reduced from -10 dB for free response to -70 dB in controlled response. This leads to about 17 % reduction in RMS of the response when the control system is activated.

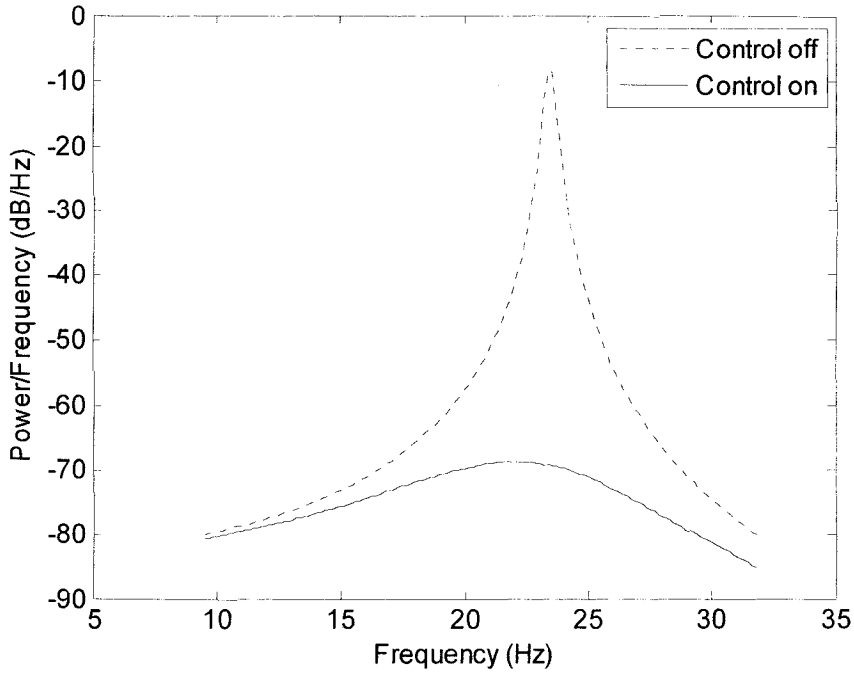

Figure 6.13 Spectral density of smart system under band limited random load

Once again the effect of laminate configuration on the power spectral density for a band limited excitation is investigated and the PSD of the response is provided in Figure 6.14. The same conclusion derived for the effect of laminate configuration on power spectral density for white-noise can be conceived for band limited excitation also.

It is observed that for laminate configurations with lower stiffness, namely, $[PS/(\pm 30/0)_s/PA]$ and $[PS/(\pm 45/0)_s/PA]$ the PSD is shifted to the left, toward the lower frequency range compared to the configurations with higher stuffiness, $[PS/(0/90/0)_s/PA]$ and $[PS/(0)_6/PA]$ which is due to the lower value of natural frequency for these configurations.

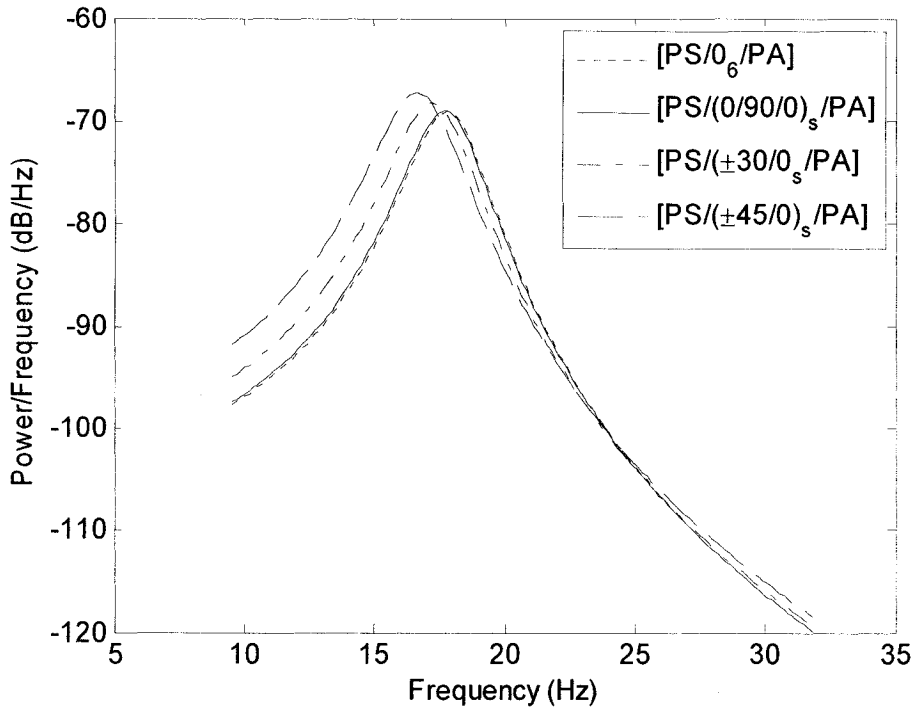

Figure 6.14 Effect of laminate configuration on PSD under band limited random loading

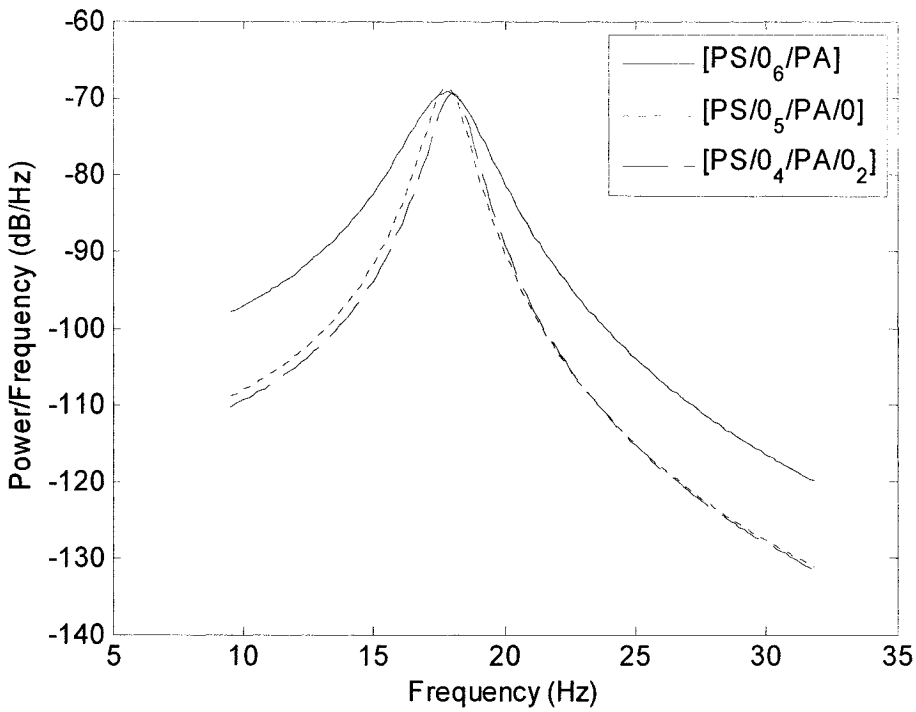

Figure 6.15 Effect of actuator location on PSD under band limited random loading

The effect of actuator location on the vibration response to band limited excitation is also investigated considering the same configurations given for the analysis of the response under the white-noise, namely, $[PS/0_6/PA]$, $[PS/0_5/PA/0]$ and $[PS/0_4/PA/0_2]$. The PSD of the response for different laminate configurations is shown in Figure 6.15. Here, a similar conclusion achieved for the effect of actuator location under white-noise can be drawn. When the actuator is mounted at outer surface the overall energy in the frequency domain is higher compared to that of the configuration in which the actuator is inside the laminate toward the middle plane.

6.5.4 Response to narrow-band excitation

Narrow-band process is a stationary random process whose realizations (samples) are close to being sinusoidal oscillations of some fixed frequency ω_o, for time interval equal to a large number of periods $2\pi/\omega_o$. Clearly such a process has a zero mean value[159]. The spectral density of a narrow-band process is negligible everywhere except in a narrow frequency band.

$$\omega_o - \frac{\Delta\omega}{2} \le \omega \le \omega_o + \frac{\Delta\omega}{2}, \quad \Delta\omega \prec 0 \tag{6.37}$$

The spectral density function for a narrow-band process is impulsive and is defined as:

$$S_X(\omega) = \sigma_X^2 [0.5\delta(\omega + \omega_o) + 0.5\delta(\omega - \omega_o)] \tag{6.38}$$

The spectral density of a narrow-band process is shown in Figure 6.16 where one may realize that $S_o = 1/2\sigma_x^2$.

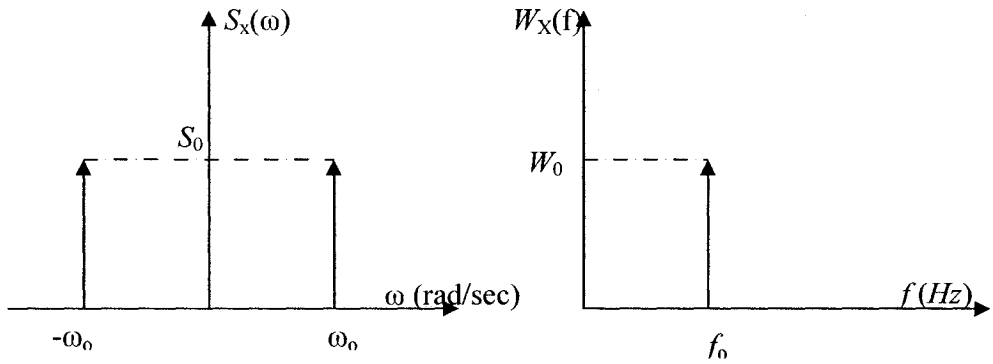

Figure 6.16 Spectral density of a band limited excitation random process

A random excitation with narrow-band frequency between (15-20 *Hz*) is applied to the smart laminated beam described in Section 6.4.3. The spectral density function of this loading can be realized as an impulse at the middle of frequency interval. The spectral density of the open-loop and closed-loop responses of the smart system is provided in Figure 6.17. It can be realized that PSD of the closed-loop system is significantly reduced compared to the PSD of open-loop system. The autocorrelation of the open-loop and closed-loop response to a narrow-band excitation is also provided in Figure 6.18 where once again the similar conclusion is obtained.

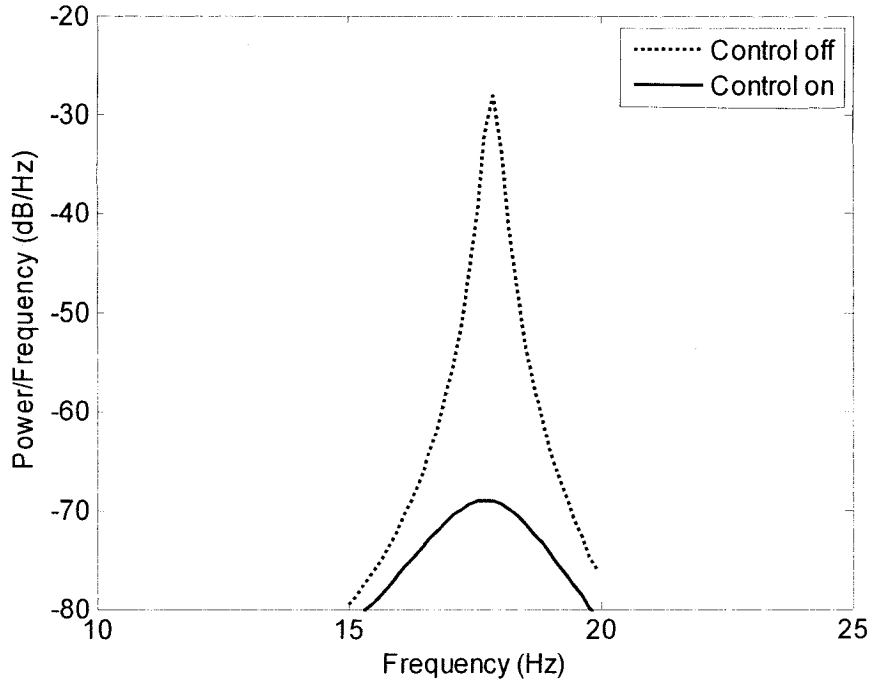

Figure 6.17 Spectral density of a narrow-band random process with frequency close to natural frequency

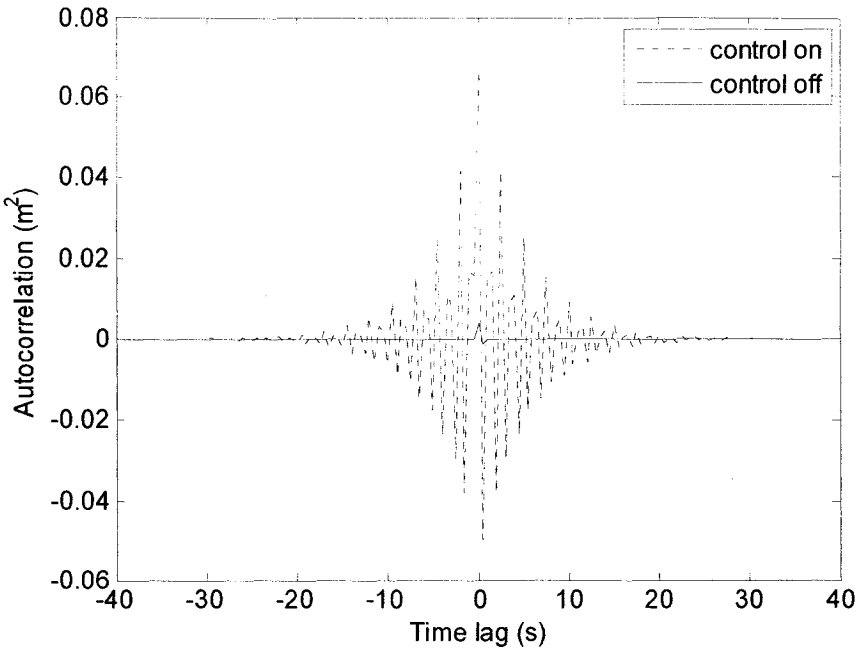

Figure 6.18 Auto-correlation of response to a narrow-band random input

Narrow-band process is of great importance for aerospace structures to simulate operating environments. In practice, recorders are mounted at points of interest in the structure to measure the vibration of the structure. Typically, the output of sensors is monitored as a function of time. This signal is then analyzed in frequency bands, and the spectrum at different time are plotted. A typical example of the vibration data is shown in Figure 6.21. However, such a spectrum is too complicated to be used as test spectrum, thus, usually, the envelope of this spectrum is considered. For conservative test, i.e., the test is more sever than the environment, one may use curve *A* and for over estimate environment, curve *B* may also be considered for under estimate design[157].

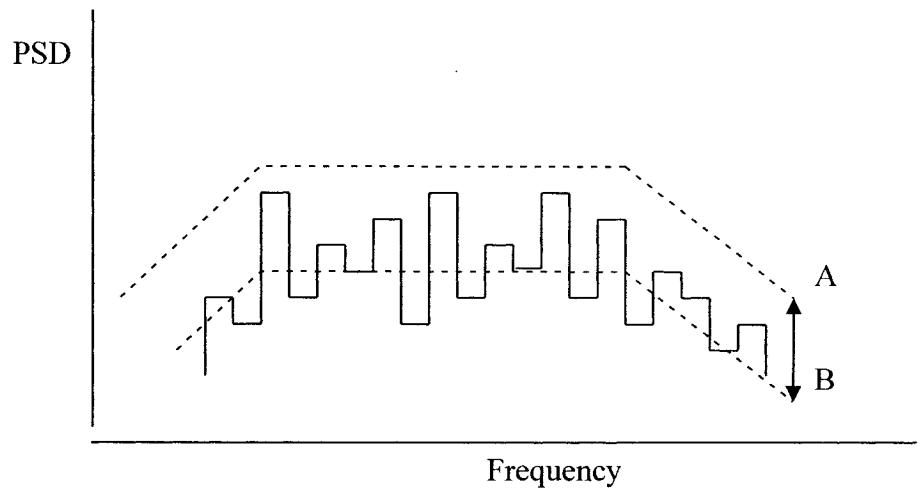

Figure 6.19 Typical narrow-band vibration spectrum for aerospace structures

Here, the vibration for the open-loop and closed-loop responses of smart laminated beam subjected to a typical envelope spectrum is studied. The material and geometric properties of the smart laminated structure are those provided for the problem described in Section 6.4.2. The laminate configuration is assumed to be $[PS/(0/90/0)_s/PA]$. The

upper and lower envelopes of the power spectral density are given in Figure 6.22. The frequency range is considered from 1 *Hz* to 20 *Hz* to cover the frequencies below and slightly beyond the fundamental frequency of the system. The power spectral densities of the response of the smart beam subjected to both upper envelope *A* and lower envelope *B* are shown in Figure 6.23. The open-loop and closed loop responses are provided to demonstrate the performance of the controlled system for typical and practical random loading conditions. It is observed that for both envelopes the power is well distributed though the frequency range. However, as it was expected the peak value is occurred at the natural frequency of the system.

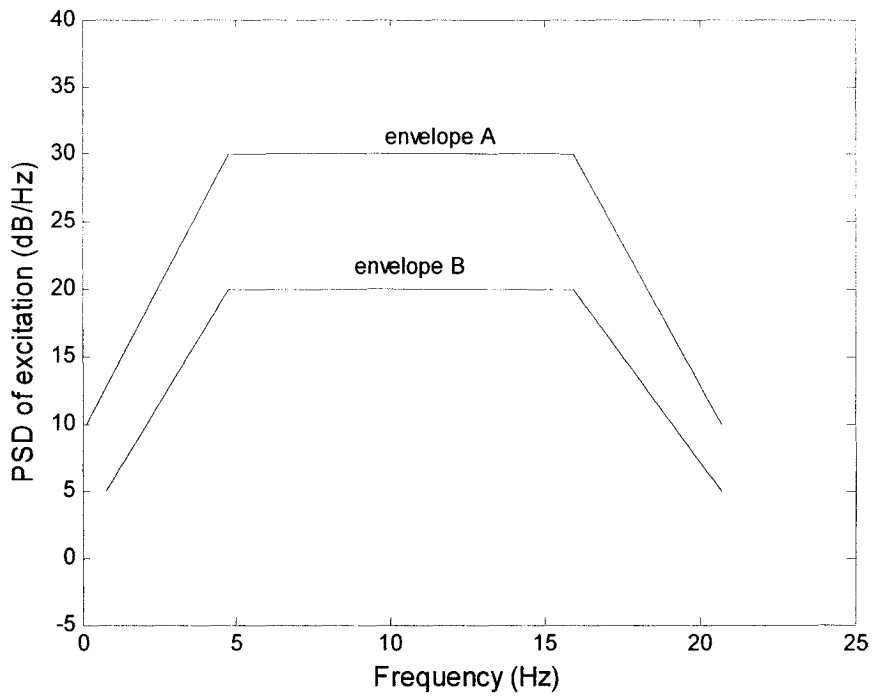

Figure 6.20 Spectral density of a typical input aerospace random process

The effect of laminate configuration of the system subjected to random input force given by envelope A is presented in Figure 6.24.

As it can be realized, the configuration $[PS/(\pm 45/0)_s/PA]$ has the highest peak level which occurs at lower frequencies compared to other configurations. The configurations with higher stuffiness, $[PS/(0/90/0)_s/PA]$ and $[PS/(0)_6/PA]$ provide lower level of power consumption. These conclusions are similar to corresponding results obtained for the smart system subjected to white-noise. The important feature is that for all cases the power spectral density is evenly distributed in the frequency range and the peak which occurs at the fundamental natural frequency is effectively suppressed when control is on.

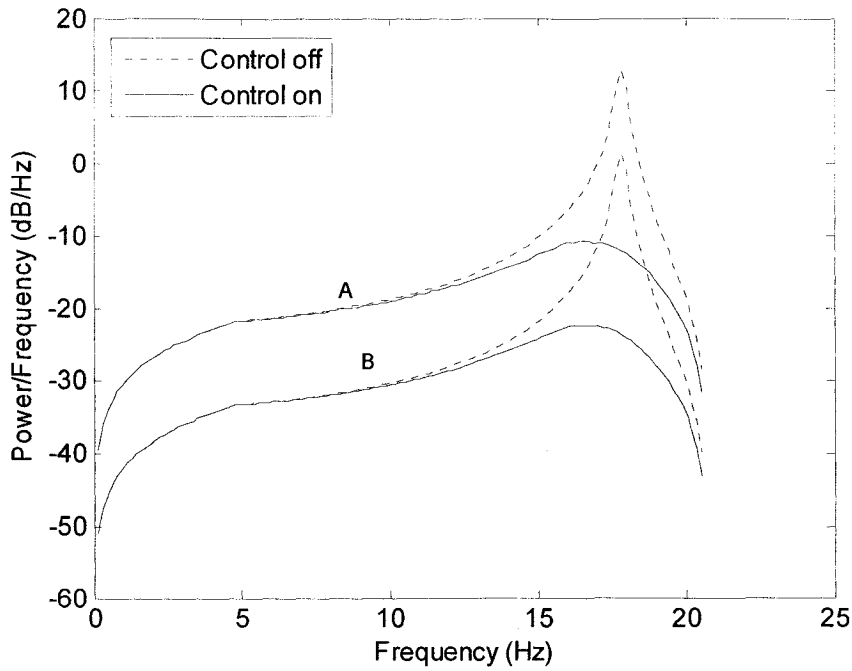

Figure 6.21 Spectral density of a the response under envelope A and B

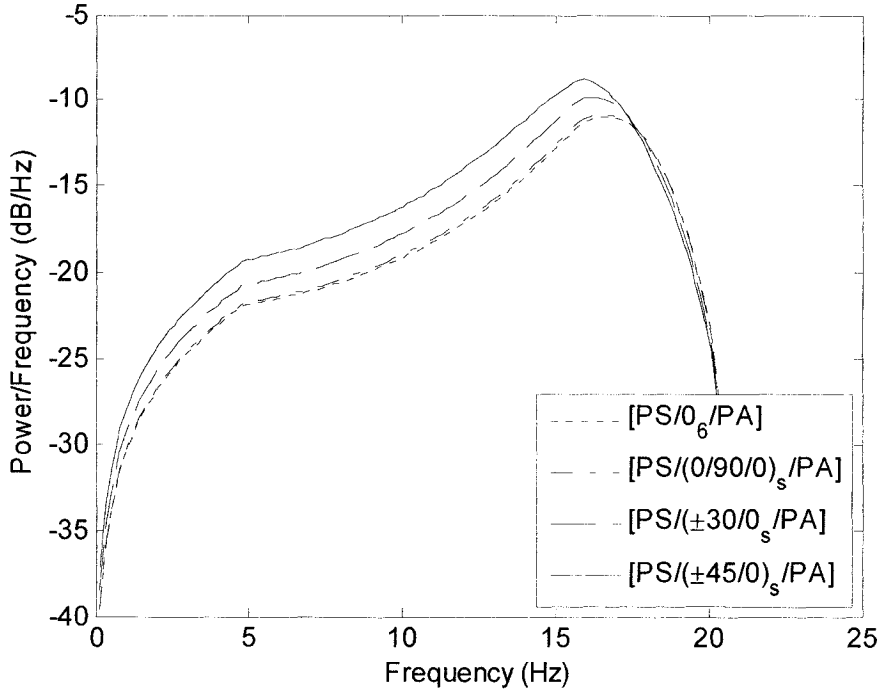

Figure 6.22 Effect of laminate configuration on the response due to envelope A

The effect of actuator location on the power spectrum of the smart system subjected to envelope A is also presented in Figure 6.25. Three different locations through the thickness are considered as: $[PS/(0)_6/PA]$, $[PS/0_5/PA/0]$ and $[PS/0_4/PA/0_2]$.

Here, a conclusion similar to the one achieved for the effect of actuator location under a white-noise is obtained. When the actuator is mounted at outer surface, the overall energy in the frequency domain is higher compared to configuration in which the actuator is inside the laminate toward the middle plane.

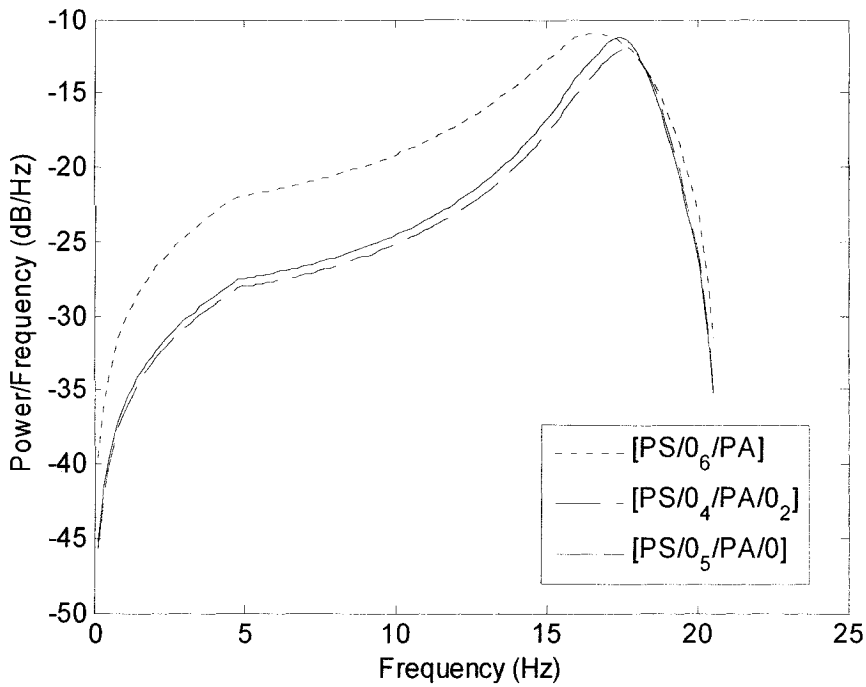

Figure 6.23 Effect of actuator location on the response due to envelope A

6.6 Conclusions

In this chapter random vibration of smart laminated beams has been investigated. The response of a laminated beam with surface mounted/embedded sensor and actuator subjected to Gaussian white-noise has been investigated. A control algorithm utilizing linear quadratic regulator and layerwise displacement finite element formulation has been developed to actively suppress the vibration of the system under random excitations. The stochastic properties of the time response of the smart system for the closed-loop system have also been determined. To demonstrate the correlation between the input random force and the applied actuator voltage, the correlation coefficients for variety of case studies, including those with laminate configuration changes and actuator location

changes through the thickness have been provided. It is concluded that for all cases, the developed control model can significantly suppress the vibration response of the system.

The study is further proceeded in frequency domain by considering band limited and narrow band processes. Power spectral density of the displacement response of the system subjected to a known input power spectral density of the excitation has been computed. Using the developed LQR controller the closed-loop response in frequency domain has been investigated. The effects of laminate configuration and actuator location through the thickness as well as along the length of the beam we also considered.

The chapter is completed by considering typical envelopes of narrow-band random process, usually used for aerospace applications, to determine the open-loop and closed loop responses of the smart system. The study has been performed to investigate the effects of laminate configuration and actuator location through the thickness of the structure. It was observed that the developed control system successfully suppresses the vibration response of the system for the input envelopes.

CHAPTER 7

CONCLUSIONS AND RECOMMENDATIONS

7.1 Conclusions

A comprehensive framework is presented for design optimization and vibration control of laminated composite beams integrated with piezoelectric sensors and actuators. A layerwise displacement approximation is utilized to account for the strong material and geometric inhomogeneities through the thickness and to provide the static and dynamic responses of the smart laminated structures accurately and efficiently. Effect of electro-mechanical coupling due to the presence of piezoelectric elements in the structure is taken into account to develop the finite element model of the system. Parametric studies are conducted to investigate the effects of sensor location through the thickness and along the length of the beam on generated voltage at the sensors. Effect of electro-mechanical coupling is also demonstrated in numerical illustration for static problems.

Sensitivity analysis for different parameters is conducted through development of analytical gradients for static and dynamic applications. Utilizing the developed sensitivity analysis and analytical gradients, a design optimization algorithm based on Sequential Quadratic Programming technique is developed to determine the optimal design of smart laminated beams for a variety of objective functions, including mass minimization, and maximization of actuator performance, subjected to different constraint functions, including displacement and inter-laminar stresses as well as

frequency constraints. It is indicated that a cantilevered laminated beam with sensors and actuators mounted at the outer surface close to the fixed end provides the highest actuating force and highest sensor voltage.

The developed optimal model of the smart laminated beam is further investigated for dynamic response under deterministic loadings. A Linear Quadratic Regulator is developed to obtain the optimal feedback control gain to actively control the smart laminated system. An in-depth study is performed to investigate the influences of laminate configuration, sensor/actuator location through the thickness and along the length on open-loop and closed-loop vibration responses of the system. It is shown that the *LQR* controller can significantly reduce the settling time of the response with reasonable actuating voltage. A proof-of-concept smart laminated composite beam is fabricated and an in-house experimental set up is designed to validate the mathematical model and to demonstrate the functionality and performance of the control algorithm. The results obtained from the experimental set-up are in good agreement with the simulation model.

Random vibration analysis is performed to investigate the response of the smart laminated system under random loading. Different random processes, including Gaussian white-noise, band limited and narrow-band random processes are considered. An optimal control mechanism based on the Linear Quadratic Regulator is developed to suppress the vibration response of the smart system subjected to random excitations. Influences of laminate configuration and actuator location through the thickness are taken into account

to obtain the closed-loop response of the system. It is observed that the developed controller provides significant effect on reducing the level of the power spectral density of the displacement response.

The major components of the work and important observations are summarized as follows:

❖ Mathematical modeling:

- Development of finite element modeling for smart laminated structures using the layerwise displacement theory.
- Incorporation of the coupled electro-mechanical interaction between sensors/ actuators and host laminated structure in the finite element model.

Finite element models based on the layerwise displacement model provides higher accuracy (compared to Equivalent Single Layer theories) and higher efficiency (compared to 3D models). This model is capable to account for all material and geometric inhomogeneities through thickness which is very common in smart laminated structures. The parametric studies in this part of the work indicate that for a smart laminated beam, placing the sensor at the outer surface close to the constraint nodal displacement generates higher voltage. Similarly, placing actuator at the outer surface provides higher actuating force. The location of actuator along the length is related to desired nodal displacements.

❖ Sensitivity analysis:

- Formulation of the sensitivity analysis algorithm for smart laminated beams concerning static and dynamic problems.

- Development of the discrete analytical gradients of the various design constraints and objective functions with respect to the design variables.

It is shown that utilizing analytical gradients significantly reduces the computational effort required for sensitivity analysis. Further, for thin laminated beam, deflection and the mass of the beam are more sensitive to changing the thickness and volume of piezoceramic actuator than the thickness of the composite layers. However, when the volume fraction of piezoceramic and composite is about 20%, the sensitivity of both components on displacement are very close.

❖ Design optimization:

- By combining the developed coupled layerwise finite element model, the developed analytical gradients, and the Sequential Quadratic Programming (*SQP*) technique, an efficient design optimization algorithm has been developed.
- Numerical examples are provided to determine the optimal designs of the smart laminated beams for different objectives and constraint functions.

It is proved that utilizing analytical gradients can significantly improve the design optimization process based on *SQP* algorithm. Using analytical gradients may reduce the number of iterations required to achieve the optimal design by up to 35 % for a typical smart laminated beam problem. In addition, the number of function evaluation required to complete the design optimization process is reduced by up to 65%. This conclusion is highly pronounced for large scale design optimization problem and/or problems with large number of design variables, including smart laminated structures.

❖ Dynamic analysis of smart laminated beams:

- In order to reduce the number of degrees of freedom for control purposes, the modal forms of the structural model and sensor and actuator are developed.
- Formulating the governing equations of smart laminated beam into the state space forms to be implemented in modern control strategies is completed.

Development of modal forms of the equations provides the possibility to investigate specific modes of vibration instead of performing the long and expensive computations to run for all nodal displacements. Further, state space form provides the opportunity to utilize many available well-defined modern control strategies.

❖ Vibration suppression:

- Linear Quadratic Regulator (*LQR*) is applied to obtain the optimal control feedback gain.
- To demonstrate the advantages of the present algorithm on dynamic response of smart laminated beams, conventional active control of laminated smart structures based on the classical laminate theory and classical control strategies are also investigated and the results are compared with present algorithm.
- Vibration response under random loading has been determined.
- Developed a control algorithm to suppress the vibration response of the structures under random loading.

Utilizing *LQR* controller can significantly reduce the settling time for the first mode of vibration without exceeding the maximum allowable actuator voltage. Placing the sensor and actuator at the outer surfaces and collocated along the length close to the fixed end (cantilever boundary condition) provides the minimum settling time. In addition,

increasing actuator voltage reduces the settling time for free vibration. In random loading problems, application of *LQR* controller can significantly reduce the power spectral density of the response.

❖ Experimental investigations:

- A laminated beam with piezoceramic actuator and PVDF sensor is designed and manufactured to investigate the dynamic response of the structure.
- A control algorithm is designed according to *LQR* controller and implemented in LABVIEW 7.0.
- Experimental investigations for open-loop and closed-loop responses of smart laminated beams are presented.

Experimental works successfully demonstrates the functionality and performance of the smart laminated beam for vibration control. In addition, experimental results established a strong platform to validate the mathematical model and results obtained from simulations.

7.2 Relevant Publications

Based on the conclusions and results obtained from the present work, the following articles are prepared and published/submitted in refereed journals/conferences:

- **Zabihollah**, **A.**, Ganesan, R. and Sedaghati, R., "Sensitivity Analysis and Design Optimization of Smart Laminated Beams Using Layerwise Theory", Journal of Smart Materials and Structures, 15(1), 2006.
- **Zabihollah**, **A.**, R. Sedaghati, R. Ganesan, "Active vibration suppression of smart laminated beams using layerwise theory and optimal control strategies", Journal of Smart Materials and Structures, 2007, in process.
- **Zabihollah**, **A.**, Sedaghati, R. Ganesan, R., 2005, "Optimal Design of Smart Laminated Beams Using Layerwise Theory", Proceeding of 8th Cansmart Meeting

International Workshop on Smart Materials and Structures, October 13-14, 2005, Toronto, Ontario, Canada.

- **Zabihollah, A.**, Sedaghati, R., Ganesan, R., 2006, "Design Optimization of Smart Laminated Composite Beams using Layerwise Theory", Proceeding of III European Conference on Computational Mechanics Solids, Structures and Coupled Problems in Engineering C.A. Mota Soares et.al. (eds.) Lisbon, Portugal, 5–8 June 2006.

- **Zabihollah, A.**, Sedaghati, R., Ganesan, R., "Sensitivity Analysis and Optimization of Smart Laminated Beams by Layerwise Theory", Proceeding of The Eighth International Conference on Computational Structures Technology, Las Palmas de Gran Canaria, Spain, 12-15 September 2006.

- **Zabihollah, A.**, Ganesan, R., Sedaghati, R., "Optimal vibration control of active laminated beam using unimorphic piezoceramic elements and LQR controller", Proceeding of 9th Cansmart Meeting International Workshop on Smart Materials and Structures, October 12-13, 2006, Toronto, Ontario, Canada.

- **Zabihollah, A.**, Ganesan, R., Sedaghati, "Optimal vibration control of smart laminated beams using layerwise theory", Proceeding of 21st Canadian Congress of Applied Mechanics CANCAM 2007, June 3-7, Toronto, Canada,

- **Zabihollah, A.**, Sedaghati, R., Ganesan, R., "Sensitivity analysis and design optimization of smart laminated beams using layerwise theory", Presented in Centre for Applied Research on Polymers and Composites, CREPEC, 2005, University of Montreal, Montreal, Canada.

- **Zabihollah, A.**, Ganesan, R., Sedaghati, R., "Vibration control of laminated smart structures: Experimental approaches", Presented in Centre for Applied Research on Polymers and Composites, CREPEC, 2006, Ecole de Technologie Superior, Montreal, Canada.

7.3 Recommendations for Future Works

The present work established a framework for design and application of smart laminated beams for vibration suppression applications. This work can be extended and improved for the following aspects:

Structural elements: Design other smart laminated structural elements such as plates and shells as well as structural components with variable thickness.

Mathematical modeling: To improve the accuracy of mathematical model for thin structure, effect of geometric non-linearity should also be taken into consideration. Smart laminated structures are very sensitive to temperature and humidity, thus, the effect of thermo-electro-mechanical coupling should be considered when the structure is being used in moderately high temperature.

Smart materials: Application of other type of smart materials such MR fluids in laminated structures should also be investigated.

Experimental works: In order to achieve the highest level of confidence and reliability, more experimental work is required to demonstrate functionality and performance of smart laminated system for real applications. Particularly, functionality of the smart system under different random excitations is of great importance.

Design optimization: Application of other design optimization techniques such as genetic algorithm should be investigated to improve the efficiency of the design optimization procedure and to facilitate the procedure of designing smart laminated structures. In addition, for smart laminated plate and shell structures, design optimization procedure should be thoroughly conducted to determine the optimal location of the multi sensors/actuators to control the different modes of vibrations.

REFERENCES

[1] Bertholet, J. M., *Composite Materials; Mechanical Behavior and Structural Analysis,* Springer Verlag, New York, 1999.

[2] Zhou, X., "Modeling of Piezoceramics and Piezoelectric Laminates Addressing Complete Coupling and Hysteresis behavior", PhD Dissertation, 2002, Arizona State University.

[3] Newnham, R. E., and Ruschau, G.R., "Smart Electroceramics", *Journal of the American Ceramic Society,* Vol. 74(3), 1991, 463-480.

[4] Yong K. H., Parka, H. K., Leeb, S. Q., Moon, K. S., Vangac, R. R. and Levyc, M., "Design and Performance of a Self-sensing, Self-actuating Piezoelectric Monomorph with Interdigitated Electrodes", Proceedings of the SPIE International Conference on Opto-mechatronic Actuators, Sensors and Control, SPIE, Philadelphia, Vol. 5602, 2004, 210-217.

[5] Qian, W., Liu, G. R., Chun, L. and Lam, K. Y., "Active Vibration Control of Composite Laminated Cylindrical Shells via Surface-bonded Magnetostrictive Layers", *Smart Materials and Structures,* Vol. 12, 2003, 889–897.

[6] Pratt, J., and Flatau, A. B., "Development and Analysis of a Self-sensing Magnetostrictive Actuators Design", *Journal of Intelligent Materials Systems and Structures*, Vol. 6(5), 1995, 639-648.

[7] Winslow, W. M., "Induced Vibration of Suspensions", *Journal of Applied Physics*, Vol. 20, 1945, 1137-1140.

[8] Kamath, G. M. and Werley, N. M., "Development of ER Fluid Based Actuator for Rotorcraft Flexbeam Applications", Proceeding of SPIE North American

conference on smart materials and structures, San Diego, CA, Feb. 27-Mar 3, 1995, 120-133.

[9] Ashour, O., Rogers, C. A., "MagnetoRhelogical Fluids: Materials, Characterization, and Devices." *Journal of Intelligent Material Systems and structures*, Vol. 7, 1996, 123-130.

[10] Yalcintas, M. and Dai, H., "Vibration Suppression Capabilities of Magnetorheological materials based adaptive structures", *Smart Material and Structures*, Vol. 13, 2004, 1–11.

[11] Encyclopedia Britannica, Piezoelectricity, Encyclopedia Britannica Inc., Chicago, IL.1994.

[12] Mason, W., *Piezoelectric Crystals and Their Applications to Ultrasonic*, D. Van Nostrand Co., New York, 1950.

[13] Wang, Z. L., and Kang, Z. C., *Functional and Smart Materials: Structural Evolution and Structure Analysis*, Plenum Press, New York, 1998.

[14] Srinivasan, A.V. and McFarland, D. M., *Smart Structures: Analysis and Design*, Cambridge University Press, New York, 2001.

[15] Fripp, M. and Hagood, N., "Comparison of Electrostrictive and Piezoceramic Actuators for Vibration Suppression", Proceedings of the SPIE, North American conference on smart structures and materials, San Dieago, CA, Feb.26-March 3, 1995.

[16] Leeks, T. J. and Weisshaar, T. A., "Optimization of Unsymmetric Actuators for Maximum Panel Deflection Control", Proceedings of the SPIE, North American

conference on smart structures and materials, San Dieago, CA, Feb.26-March 3, 1995.

[17] Crawley, E. F., and de Luis, J., "Use of Piezoelectric Actuators as Elements of Intelligent Structures", *AIAA Journal,* Vol. 25(10), 1987, 1373-1385.

[18] Ikuta, K. T., and Hirose, S., "A Tiny Silent Linear Cybernetic Actuator Driven by Piezoelectric Device with Electromagnetic Clamp", Proceedings of the IEEE, Robotic and Actuation Society Conference on MicroElectroMechanical Systems, Travemunde, Germany, Feb.4-7, 1992, IEEE publishing, 232-237.

[19] Eisenberger, M. and Abramovich, H., "Shape Control of Non-symmetric Piezolaminated composite beams", *Composite Structures,* Vol. 38(1-4), 1997, 565-571.

[20] Paget, C. A., Levin, K. and Delebarre, C., "Actuation Performance of Embedded Piezoceramic Transducer in Mechanically Loaded Composites", *Smart Materials and Structures,* Vol. 11, 2002, 886–891.

[21] Yan, Y. J. and Yam, L. H., "Online Detection of Crack Damage in Composite Plates using Embedded Piezoelectric Actuators/Sensors and Wavelet Analysis", *Composite Structures,* Vol. 58, 2002, 29–38.

[22] Prasad, E. S., Waechter, D. F., Blacow, R. G., King, H. W. and Yaman, Y., " Application of Piezoelectrics to Smart Structures", Proceedings of II ECCOMAS THEMATIC Conference on Smart Structures and Materials, C.A. Mota Soares et al. (Eds.) Lisbon, Portugal, July 18-21, 2005.

[23] Paradies, R. and Ruge, M., "In Situ Fabrication of Active Fiber Reinforced Structures with Integrated Piezoelectric Actuators", *Smart Materials and Structures,* Vol. 9, 2000, 220–225.

[24] Tan, P. and Tong, L. "A Delamination Detection Model for Composite Beams using PFRC Sensor/Actuator", Composites Part A: Applied Science and Manufacturing, Vol. 35(2), 2004, 231-247.

[25] Perel, V.Y. and Palazotto, A. N., "Finite Element Formulation for Dynamics of Delaminated Composite Beams with Piezoelectric Actuators", *International Journal of Solids and Structures,* Vol. 39, 2002, 4457–4483.

[26] Mollenhauer, D.H. and Griffen, O.H., "Induced Strain of Actuation of Surface Bonded Piezoceramic Patches: A Numerical and Experimental Study", *Journal of Intelligent materials systems and structures,* Vol.5, 1994, 335-362.

[27] Abararcar, R. B. and Cunniff, P. F., "The Vibration of Cantilevered Beam of Fiber Reinforced Materials", *Journal of Composite Materials*, Vol. 6, 1972, 504-516.

[28] Chandrashekhara, K., Krishnamurthy, K. and Roy, S., "Free Vibration of Composite beams including Rotary Inertia and Shear Deformation", *Composite Structures*, Vol. 14, 1990, 269-279.

[29] Khedeir, A. A. and Reddy, J. N., "Free Vibration of Cross-ply Laminated Beams with Arbitrary Boundary Conditions", *International Journal of Engineering*, Vol. 32(12), 1994, 1971-1980.

[30] Green A. E., Naghdi, P. M., "A Theory of Laminated Composite Plates", *Journal of Applied Mathematic,* Vol. 29(1), 1982, 35–46.

[31] Reddy, J. N., "On Laminated Composite Plates with Integrated Sensors and Actuators", *Engineering and Structures,* Vol. 21, 1999, 568-593.

[32] Lucy, E. A. and Abramovich H., "A Piezoelectric Actuation and Sensing Mechanism-closed Form Solutions", *Composite Structures,* Vol. 64, 2004, 443-453.

[33] Lee, S. J., Reddy, J. N., Rostam-Abadi, F., "Transient Analysis of Laminated Composite Plates with Embedded Smart-material Layers", *Finite Elements in Analysis and Design*, Vol. 40(5-6), 2004, 463 – 483.

[34] Reddy, J. N., "On Laminated Composite Plates with Integrated Sensors and Actuators", *Engineering Structures*, Vol. 21, 1999, 568-593.

[35] Ghosh, K. and Batra, R.C., "Shape Control of Plates using Piezoelectric Elements", *AIAA Journal,* Vol. 33, 1995, 1354-1357.

[36] Ray, M. C. Bhattacharya, R. and Samanta, B., "Exact Solutions for Static Analysis of Intelligent Structures", *AIAA, Journal*, Vol. 31(9), 1993, 1684-1691.

[37] Kyu, H. S., Keilers, C. and Chang, F. K., "Finite Element Analysis of Composite Structures Containing Distributed Piezoelectric Sensors and Actuators", *AIAA Journal*, Vol. 30, 1992, 772-776.

[38] Hwang, W. S. and Park, H. C., "Finite Element Modeling of Piezoelectric Sensors and Actuators", *AIAA Journal*, Vol. 31(5), 1993, 930-937.

[39] Detwiler, D. T., Shen, M. H. H. and Venkayya, V. B., "Finite Element Analysis of Laminated Composite Structures Containing Distributed Piezoelectric Actuators and Sensors", *Finite Elements in Analysis and Design*, Vol. 20, 1995, 87-100.

[40] Suleman, A., Venkayya, V. B., "A Simple Finite Element Formulation for a Laminated Composite Plate with Piezoelectric Layers", *Journal of Intelligent Material Systems and Structures,* Vol. 6, 1995.

[41] Ray, M. C., Battacharyya, R. and Samanta, B., "Static Analysis of an Intelligent Structure by the Finite Element Method", *Computers and Structures*, Vol. 52(4), 1994, 617-631.

[42] Chattopadhyay, A., Li, J.and Gu, H., "Coupled Thermo-Piezoelectric-Mechanical Model for Smart Composite Laminates", *AIAA Journal*, Vol. 37(12), 2003, 1633-1638.

[43] Donthireddyand, P. and Chandrashekhara, K., "Modeling and Shape Control of Composite Beams with Embedded Piezoelectric Actuators", *Composite Structures*, Vol. 35, 1996, 237-244.

[44] Benjeddou, A., Deu, J. F. and Letombe, S., "Free Vibrations of Simply-supported Piezoelectric Adaptive plate: An Exact Sandwich Formulation", *Thin-walled Structures*, Vol. 40, 2002, 573-593.

[45] Sridhar, R. T., Seshu, P. and Naganathan, N. G., "A Finite Element Static Analysis of Smart Turbine Blades", *Smart Materials and Structures*, Vol. 6, 1997, 607-615.

[46] Fernandes, A. and Pouget, J., "An Accurate Modeling of Piezoelectric Multi-layer Plates", *European Journal of Mechanics A/Solids*, Vol. 21, 2002, 629–651.

[47] Krommer, M., "Piezoelastic Vibrations of Composite Reissner–Mindlin-type Plates", *Journal of Sound and Vibration*, Vol. 263, 2003, 871–891.

[48] Yang, J. S., "Variational Formulations for the Vibration of Piezoelectric Plates", *Applied Mechanics*, Vol. 45(6), 1993, 639-651.

[49] Reddy, J. N., *Mechanics of Laminated Composite Plates, Theory and Analysis*, CRC Press, New York, 1997.

[50] Tahani, M. and Nosier, A., "A Edge Effects of Uniformly Loaded Cross-ply Composite Laminates", *Materials and Design*, Vol. 24, 2003, 647-658.

[51] Desai, Y. M., Ramtekkar, G. S. and Shah, A. H., "Dynamic Analysis of Laminated Composite Plates using a Layer-wise Mixed Finite Element Model", *Composite Structures*, Vol. 59, 2003, 237-249.

[52] Liew, K. M., Jordan, Z., Zhang, C. L. and Meguid, S.A., "Three-dimensional Analysis of the Coupled Thermo-piezoelectro-mechanical Behavior of Multilayered Plates using the Differential Quadrature Technique", *International Journal of Solids and Structures*, Vol. 42, 2005, 4239–4257.

[53] Senthil, S. V. and Batra, R. C., "Cylindrical Bending of Laminated Plates with Distributed and Segmented Piezoelectric Actuators/Sensors", *AIAA Journal*, Vol. 38(5), 2003, 857-867.

[54] Reddy, J. N, and Cheng, Z. Q., "Three-Dimensional Solutions of Smart Functionally Graded Plates", *Journal of Applied Mechanics*, Vol. 68, 2001, 234-241.

[55] Reddy, J. N., "A Generalization of Two-dimensional Theories of Laminated Composite Plates". *Communication Applied Numerical Methods*, Vol. 3, 1987, 173-180.

[56] Reddy, J. N., Barbero, E. J. and Teply, J. L., "A Plate Bending Element Based on a Generalized Laminate Plate Theory". *International Journal of Numerical Methods in Engineering*, Vol. 28, 1989, 2275-92.

[57] Barbero, E. J., "On a Generalized Laminate Theory with Application to Bending, Vibration, and Delamination Bucking in Composite Laminates". PhD dissertation, Department of Engineering Mechanics, VPI & SU, Blacksburg, VA, 1989.

[58] Nosier, A., Kapania, R. K and Reddy, J. N., "Free Vibration Analysis of Laminated Plates using a Layerwise Theory", *AIAA Journal*, Vol. 13(12), 1993, 2335 –2346.

[59] Davalos, J.F., "Analysis of Laminated Beams with a Layer-wise Constant Shear Theory", *Composite Structure*, Vol. 28(3), 1994, 241-253.

[60] Carrera, E., "Evaluation of Layerwise Mixed Theories for Laminated Plates Analysis", *AIAA Journal*, Vol. 36(5), 2003, 830-839.

[61] Davalos, J. F., "A Layerwise Beam Element for Analysis of Frames with Laminated Sections and Flexible Joints", *Finite Element in Analysis and Design*, Vol. 19(3), 1995, 181-194.

[62] Clinton, Y. K., Tong, C., L. and Steven, G. P., "A Mixed Model for Composite Beams with Piezoelectric Actuators and Sensors", *Smart Materials and Structures,* Vol. 8, 1999, 417-432.

[63] Carrera, E., "Mixed-layerwise Models for Multilayered Plates Analysis", *Composite Structures*, Vol. 43, 1998, 57-70.

[64] Kadivar, M. H. and Samani, K., "Free Vibration of Rotating Thick Composite Cylindrical Shells using Layerwise Laminate Theory", *Mechanics Research Communications*, Vol. 27(6), 62000, 79-684.

[65] Koo, K. N., "Vibration and Damping Analysis of Composite Plates using Finite Element with Layerwise In-plane Displacements", *Computers and Structures*, Vol. 80, 2002, 1393-1398.

[66] Tahani, M. and Nosier, A., "Edge Effects of Uniformly Loaded Cross-ply Composite Laminates", *Materials and Design*, Vol. 24, 2003, 647–658.

[67] Tahani, M. and Nosier, A., "Three-dimensional Inter-laminar Stress Analysis at Free Edges of General Cross-ply Composite Laminates", *Materials and Design*, Vol. 24, 2003, 121–130.

[68] Claire, O. D., "Multilayered Piezoelectric Refined Plate Theory", *AIAA Journal*, Vol. 41(1), 2003, 90-99.

[69] David, A. S. and Viuini, A. J., "Structural Integrity of Composite Laminates with Interlaced Actuators", *Smart Material sand Structures*, Vol. 3, 1994, 71-79.

[70] Gao, J. X., Shen, Y. P. and Wang, J., "Three Dimensional Analysis for Free Vibration of Rectangular Composite Laminates with Piezoelectric Layers", *Journal of Sound and Vibration*, Vol. 213(2), 1998, 383-390.

[71] Robbins, D. H. and Reddy, J. N., "Analysis of Piezoelectrically Actuated Beams using a Layerwise Displacement Theory", *Composites and Structures*, Vol. 41(2), 1991, 265-279.

[72] Donthireddy, P. and Chandrashekhara, K., "Modeling and Shape Control of Composite Beams with Embedded Piezoelectric Actuators", *Composite Structures,* Vol. 35, 1996, 237-244.

[73] Hung, H. J. and Lee, I., "Analysis of Composite Plates with Piezoelectric Actuators for Vibration Control using Layerwise Displacement Theory", *Composites Part B,* Vol. 29, 1998, 621-632.

[74] Saravanos, D. A. and Heyliger, P. R., "Coupled Layerwise Analysis of Composite Beams with Embedded Piezoelectric Sensors and Actuators *Journal of Intelligent Materials Systems and Structures,* Vol. 6, 1995, 350-363.

[75] Saravanaos, D.A., Heyliger, P. R. and Hopkins, D. A., "Layerwise Mechanics and Finite Element for the Dynamic Analysis of Piezoelectric Composite Plates" *International Journal Solids Structures*, Vol. 34(3), 1997, 359-378.

[76] Lee, H. J. and Saravanaos, D.A., "Couples Layerwise Analysis of Thermo-piezoelctric Composite Beams", *AIAA Journal*, Vol. 34(6), 1996.

[77] Garcao, S. J. E., Soares, C. M. M., Soares, C. A. M. and Reddy, J.N., "Analysis of Laminated Adaptive Plate Structures using Layerwise Finite Element Models", *Computers and Structures*, 2004, in press.

[78] Sunar, M., Al-Garni, A. Z. Ali, M. H. and Kahraman, R., "Finite Element Modeling of Thermopiezomagnetic Smart Structures", *AIAA Journal*, Vol. 40(9), 2002, 1846-1851.

[79] Robbins, D. H. and Reddy, J. N., "An Efficient Computational Model for The Stress Analysis of Smart Plate Structures", *Smart Materials and Structures*, Vol. 5, 1996, 353–360.

[80] Kapuria, S., Dumir, P.C. and Ahmed, A., "An Efficient Coupled Layerwise Theory for Dynamic Analysis of Piezoelectric Composite Beams", *Journal of Sound and Vibration*, Vol. 261, 2003, 927–944.

[81] Thornburgh, R. P., Chattopadhyay, A. and Ghoshal, A., "Transient Vibration of Smart Structures using a Coupled Piezoelectric-mechanical Theory", *Journal of Sound and Vibration*, in press.

[82] Yan, Y. J., Yam, L. H., "Mechanical Interaction Issues in Piezoelectric Composite Structures", *Composite Structures*, Vol. 59, 2003, 61–65.

[83] Barboni, R., Mannini, A., Fantini, E. and Gaudenzi, P., "Optimal Placement of PZT Actuators for the Control of Beam Dynamics", *Smart Materials and Structures*, Vol. 9, 2000, 110–120.

[84] Osama J. A., Singh, T. and Wetherhold, R. C., "Optimal Size and Location of Piezoelectric Actuator/Sensors: Practical Considerations", *Journal of Guidance, Control, and Dynamics*, Vol. 23(3), 2000, 509-515.

[85] Frecker, M. I., "Recent Advances in Optimization of Smart Structures and Actuators", *Journal of Intelligent Materials and System Structures*, Vol. 14, 2003, 207-216.

[86] Chee, C., Tong, L. and Steven, G. P., "Piezoelectric Actuator Orientation Optimization for Static Shape Control of Composite Plates", *Composite structures*, Vol. 55, 2002, 169-184.

[87] Han, J. H. and Lee, I., "Optimal Placement of Piezoelectric Sensors and Actuators for Vibration Control of a Composite Plate using Genetic Algorithms", *Smart Materials and Structures*, Vol. 8,1999, 257–267.

[88] Yang, Yaowen, Jin, Zhanli and KiongSoh, Chee, "Integrated Optimal Design of Vibration Control System for Smart Beams using Genetic Algorithms", *Journal of Sound and Vibration*, Vol. 282, 2005, 1293–1307.

[89] Kassegne, S., Madou, M., Whitten, R., Zoval, J., Mather, E., Sarkar, K., Dalibor H. and Maity, S., "Design Issues in SOI-Based High-Sensitivity Piezoresistive Cantilever Devices", Proceeding of SPIE, 2005, San Diego.

[90] Arora, J. S., *Introduction to Optimization Design*, New York, McGraw-Hill, 1989.

[91] Adelman, H. M. and Haftka, R. T., "Sensitivity Analysis of Discrete Structural Systems", *AIAA Journal*, Vol. 24(5), 1986, 823-829.

[92] Sedaghati, R. Suleman, A., Tabarrok, B., "Structural Optimization with Frequency Constraints Using the Finite Element Force Method", *AIAA Journal*, 40 (2), 2003, 382-388.

[93] Soares, C. M. M., Soares, C. A. M. and Correia, V. M. F., "Optimal Design of Piezo-laminated Structures", *Composite Structures*, Vol. 47(1–4), 1999, 625–634.

[94] Liu, X. and Begg, W., "Sensitivity Analysis of Smart Structures", *Computer Methods in Applied Mechanical Engineering*, Vol. 163, 1998, 311-322.

[95] Yang, S. M. and Lee, Y. J., "Modal Analysis of Stepped Beams with Piezoelectric materials", *Journal of Sound and Vibration*, Vol. 176(3), 1994, 289-300.

[96] Bailey, T. and Hubard, J. E., "Distributed Piezoelectric-polymer Active Control of a Cantilever Beam", *Journal of Guidance, Control and Dynamics*, Vol. 8, 1985, 605-611.

[97] Gaudenzi, P., Carbonaro, R. and Barboni, R., "Vibration Control of an Active Laminated Beam", *Composite Structures*, Vol. 38(1-4), 1997, 413-420.

[98] Blanguernon, A., Leneand, F., Bernadou, M., "Active Control of a Beam using a Piezoceramic Element", *Smart Materials and Structures*, Vol. 8, 1999, 116–124.

[99] Kim, S. J. and Jones, J. D., "Quasi-static Control of Natural Frequencies of Composite Beams using Embedded Piezoelectric Actuators", *Smart Materials and Structures*, Vol. 4, 1995, 106-112.

[100] Sun, D. and Tong, L., "Closed-loop Based Detection of Debonding of Piezoelectric Actuator Patches in Controlled Beams", *International Journal of Solids and Structures*, Vol. 40, 2003, 2449–2471.

[101] Pankaj, K. L. and Seshul, P., "Experimental Studies on Active Vibration Control of a Beam Using Hybrid Active/Passive Constrained Layer Damping Treatments", *Journal of Vibration and Acoustics*, Vol. 127, 2005, 515-518.

[102] Dong, Xing-Jian, Meng, G. and Peng, Juan-Chun, "Vibration Control of Piezoelectric Smart Structures Based on System Identification Technique: Numerical simulation and experimental study", *Journal of Sound and Vibration*, in press.

[103] Hwang, W. S., Hwang, W. and Park, H. C., "Vibration Control of Laminated Composite Plate with Piezoelectric Sensor/Actuator: Active and Passive Control Methods", *Mechanical Systems and Signal Processing*, Vol. 8(5), 1994, 571-583.

[104] Pradhan, S. C., Lam, T. Y., and Reddy, J. N., "Control of Laminated Composite Plates using Magnetostrictive Layers", *Smart Materials and Structures*, Vol. 10, 2001, 657-667.

[105] Liang, X. Q. and Batra, R. C., "Changes in Frequencies of a Laminated Plate Caused by Embedded Piezoelectric Layers", *AIAA Journal*, Vol. 35(10), 1673-1674.

[106] Subramanian, P., "Vibration Suppression of Symmetric Laminated Composite Beams", *Smart Materials and Structures*, Vol. 11, 2002, 880-885.

[107] Chandrashekhara, K., and Agrawalm A. N., "Active Vibration Control of Laminated Composite Plates using Piezoelectric Devices: a Finite Element Approach", *Journal of Intelligent Material System and Structures*, Vol. 4(4), 1993, 496-507.

[108] Wang, S. Y., Quek, S. T. and Ang, K. K. "Vibration Control of Smart Piezoelectric Composite Plates", *Journal of Smart Materials and Structures*, Vol. 10, 2001, 637-644.

[109] Zhou, X., Chattopadhyay, A., and Gu, H., "Dynamic Responses of Smart Composites Using a Coupled Thermo-Piezoelectric-Mechanical Model", *AIAA Journal*, Vol. 38(10), 2003, 1939–1948.

[110] Lim, Young-Hun, Vasundara, V. V. and Varadan, V. K., "Closed Loop Finite Element Modeling of Active Structural Damping in the Frequency Domain", *Smart Materials and Structures*, Vol. 6, 1997, 161–168.

[111] Sun, B. and Da, Huang, "Vibration Suppression of Laminated Composite Beams with a Piezoelectric Damping Layer, *Composite Structures*, Vol. 53, 2003, 437-447.

[112] Lee, S. J., Reddy, J. N. and Rostam-Abadi, F., "Transient Analysis of Laminated Composite Plates with Embedded Smart-material Layers", *Finite Element in Analysis and Design*, in press.

[113] Lin, J. C., Nien, M. H., "Adaptive Control of a Composite Cantilever Beam with Piezoelectric Damping-modal Actuators/Sensors", *Composite Structures*, Vol. 70, 2005, 170–176.

[114] Gaudenzi, P., Carbonaro, R. and Benzi, E., "Control of Beam Vibrations by Means of Piezoelectric Devices: Theory and Experiments", *Composite Structures,* Vol. 50, 2000, 373-379.

[115] Chen, L. W., Lin, C. Y. and Wang, C. C., "Dynamic Stability Analysis and Control of a Composite Beam with Piezoelectric Layers", *Composite Structures,* Vol. 56, 2002, 97–109.

[116] Sloss, J. M., Bruch, J.C., Sadek, I. S. and Adali, S., "Piezo Patch Sensor/Actuator Control of the Vibrations of a Cantilever under Axial Load", *Composite Structures*, Vol. 62, 2003, 423–428.

[117] Sethi, V. and Song, G., "Pole-Placement Vibration Control of a Flexible Composite I-beam using Piezoceramic Sensors and Actuators", *Journal of Thermoplastic Composite Materials*, Vol. 19, 2006, 293-307.

[118] Reddy, J. N. and Babosa, "On Vibration Suppression of Magnetostrictive Beams", *Smart Materials and Structures*, Vol. 9, 2000, 49-58.

[119] Correia, P., Cristovao, I. F. and Soares, M. M. Soares, C. A. M. and Herskovits, J., "Active Control of Axisymmetric Shells with Piezoelectric Layers: A Mixed Laminated Theory with a High order Displacement Field", *Computers and Structures*, Vol. 80, 2002, 2265–2275.

[120] Tylikowski, A., "Effects of Piezoactuator Delamination on The Transfer Functions of Vibration Control Systems", *International Journal of Solids and Structures*, Vol. 38, 2001, 2189-2202.

[121] Sun, D., Tong, L. and Atluri, S.N., "Effects of Piezoelectric Sensor/Actuator Debonding on Vibration Control of Smart Beams", *International Journal of Solid and Structures*, Vol. 38, 2001, 9033-9051.

[122] Han, J. H. and Lee, I., "Analysis of Composite Plates with Piezoelectric Actuators for Vibration Control using Layerwise Displacement Theory", *Composites Part B*, 29B, 1998, 621-632.

[123] Narayanana, S., Balamurugan, V., "Finite Element Modeling of Piezolaminated Smart Structures or Active Vibration Control with Distributed Sensors and Actuators", *Journal of Sound and Vibration*, Vol. 262, 2003, 529–562.

[124] Bruant, I., Coffigal, G., Lene, F. and Verge, M., "A Methodology for Determination of Piezoelectric Actuator and Sensor Location on Beam Structures", *Journal of Sound and Vibration*, Vol. 243(5), 2001, 861-882.

[125] Stavroulakis, G. E., Foutsitzi, G., Hadjigeorgiou, E., Marinova, D. and Baniotopoulos, C. C., "Design and Robust Optimal Control of Smart Beams with Application on Vibrations Suppression", *Advances in Engineering Software,* Vol. 36, 2005, 806–813.

[126] Yousefi-Koma, A., Active Vibration Control of Smart Structures using Piezoelements, Ph.D. Thesis, 1997, Carleton University.

[127] Xu, X. S. and Koko, T. S., "Finite Element Analysis and Design of Actively Controlled Piezoelectric Smart Structures", *Finite Element in Analysis and Design*, in press.

[128] Chyanbin, H., Chang, W.C. and Gai, H. S., "Vibration Suppression of Composite Sandwich Beams", *Journal of Sound and Vibration* , Vol. 272, 2004, 1–20.

[129] Vasques, C. M. A and Rodrigues, J. D., "Active Vibration Control of Smart Piezoelectric Beams: Comparison of Classical and Optimal Feedback Control Strategies", *Computers & Structures*, Vol. 84, 2006, 1402-1414.

[130] Meirovitch, L. *Analytical Methods in Vibrations*, London: Collier-Machmillan, 1967.

[131] Soong, T. T., Grigoriu, M., *Random Vibration in Mechanical and Structural Systems*, Prentice-Hall, Englewood Cliff, N. J., 1993.

[132] Balakrishanan, A. V., *Introduction to Random Process in Engineering*, John Wiley and Sons Inc., New York, 1995.

[133] Wirsching, P., H., Paez, T. L. and Ortiz, K., *Random Vibration: Theory and practice*, John Wiley and Sons Inc. New York, 1995.

[134] Elishakoff, I., Zhu, L., "Random Vibration of Structures by Finite Element Method", *Computational Methods in Applied Mechanical Engineering*, Vol. 105, 1993, 359-373.

[135] Onkar, A. K. and Yadav, D., "Non-linear Response Statistics of Composite Laminates with Random Material Properties under Random Loading", *Composite Structures,* Vol. 60(4), 2003, 375-383.

[136] Wu, W. F., Cheng, H. C. and Kang, C.K., "Random Field Formulation of Composite Laminates", *Composite Structures*, Vol. 49(1), 2000, 87-93.

[137] Sigh, B. N. Yadav, D. and Iyengar, N. G. R., "Free Vibration of Laminated Spherical Panels with Random Material Properties", *Journal of Sound and Vibration*, Vol. 244(2), 2001, 321-338.

[138] Lin, S. C., "Reliability Predictions of Laminated Composite Plates with Random System Parameters", *Probabilistic Engineering Mechanics*, Vol. 15, 2000, 327–338.

[139] Cederbaum, G., Elishakoff, I., Aboudi, J. and Librescu, L., *Random Vibration and Reliability of Composite Structures*, Technomic Publishing Company, Inc., PN, 1992.

[140] Lin, S. C., "Buckling Failure Analysis of Random Composite Laminates Subjected to Random Loads", *International Journal of Solids and Structures*, Vol. 37, 2000, 7563-7576.

[141] Zibdesh, H. S. and Abu-Hilal, M., "Stochastic Vibration of Laminated Composite Coated Beam Traversed by a Random Moving Load", *Engineering Structures,* Vol. 25, 2003, 397-404.

[142] Frangopol, D. M. and Recek, S., "Reliability of Reinforced Composite Laminated Plates", *Probability Engineering Mechanics*, Vol. 18, 2003, 119-137.

[143] Librescu, L. and Elishakoff, I., "Response of Laminated Plates to Non-stationary Random Excitation", *Structural Safety*, Vol. 6, 1998, 99-113.

[144] Cederbaum, G. Librescu, L. and Elishakoff, I., "Random Vibration of Laminated Plates Modeled Within the First-order Shear Deformation Theory", *Composite Structures*, Vol. 12, 1989, 97-111.

[145] Kang, J. and Harichandran, R. S., "Random Vibration of Laminated FRP Plates with Material Non-linearity using Higher-order Shear Theory", *Journal of Engineering Mechanics*, Vol. 125(9), 1999, 1081-1088.

[146] Tiersten, H. F., *Linear Piezoelectric Plate Vibration*, Plenum Press, New York, 1969.

[147] Kassegne, S. K. and Reddy, J. N., "A Layerwise Shell Stiffener and Stand-Alone Curved Beam Element", *Asian Journal of Structural Engineering*, Vol. 2(1-2), pp 1-14, 1997.

[148] Arora, J. S., *Introduction to Optimization Design*, McGraw-Hill, New York, 1989.

[149] Fletcher, R., Practical *Methods of Optimization; 2nd ed.*, Wiley-Interscience, New York, 1987.

[150] Thomson, W., T., *Theory of Vibration with Applications, 4th ed.* Englewood Cliffs, N.J. : Prentice Hall, 1993.

[151] Peng, X. Q., Lam, K. Y. and Liu, G.R., "Active Vibration Control of Composite Beams with Piezoelectric: a Finite Element Model with Third Order Theory", *Journal of Sound and Vibration*, Vol. 209(4), 1998, 635-650.

[152] Kirk, *Optimal Control Theory: An Introduction,* Prentice-Hall, Englewood Cliffs, N.J., 1970.

[153] Stoica, P. and Randolph L., *Moses Introduction to Spectral Analysis*, Prentice Hall, Upper Saddle River, N.J. 1997.

[154] Lyon, R. H, *Random Noise and Vibration in Space Vehicles*, Shock and Vibration Information Center, U.S. Dept. of Defense, Washington, 1967.

[155] Wirsching, P. H., Thomas, L. P. and Ortiz, K., *Random Vibration: Theory and Practice*, John Wiley and Sons Inc., New York, 1995.

[156] Newland, D. E., *An Introduction to Random Vibrations, Spectral & Wavelet Analysis*, Lonman Scientific & Technical, New York, 1993.

[157] Yang, C.Y., *Random Vibration of Structures*, John Wiley and Sons Inc., New York, 1986.

[158] Goldman, S., *Vibration Spectral Analysis, 2nd ed.*, Industrial Press Inc., New York, 1999.

[159] Stratonovich, R. L., *Topics in the Theory of Random Noise*, Volume I, Gordon and Breach, New York, 1967.

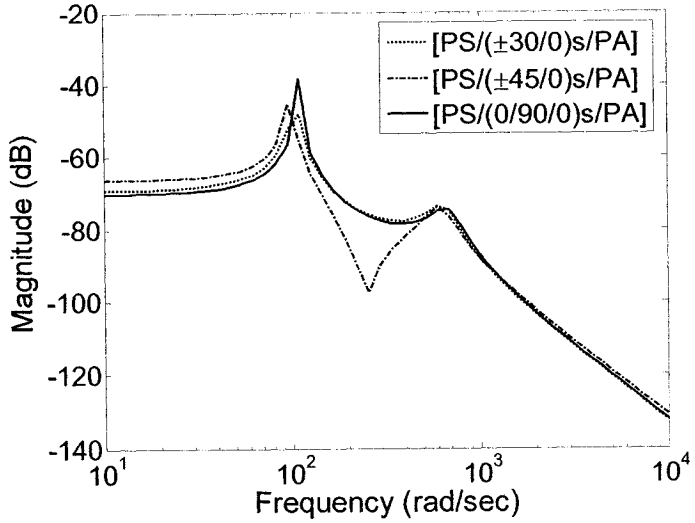

Figure 5.20 Frequency response for various laminate configurations

The relation between settling time ($\pm 3\%$ of steady state response) and control force has also been investigated. In general, as the settling time increases, the control voltage decreases as shown in Figure 5.21.

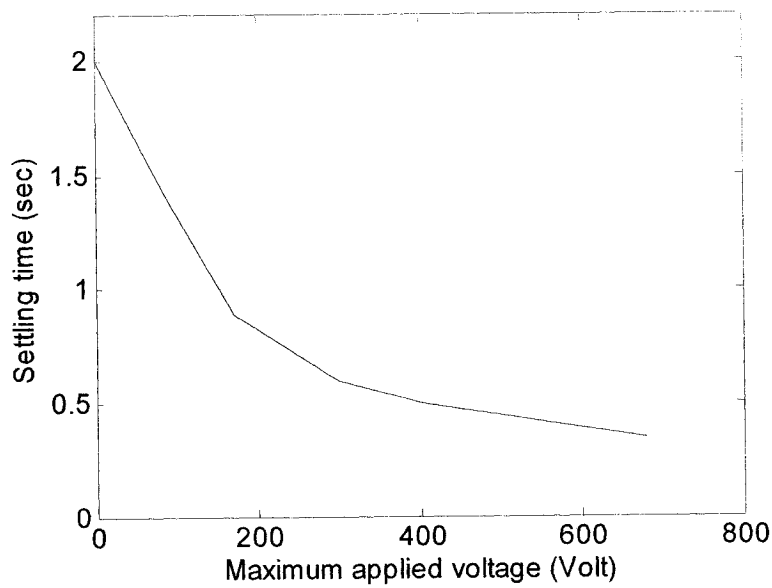

Figure 5.21 Maximum control voltage vs. settling time

$$\begin{aligned}
\bar{e}_{31} &= e_{31}c^2 + e_{32}s^2 & \bar{e}_{32} &= e_{31}s^2 + e_{32}c^2 \\
\bar{e}_{36} &= (e_{31} - e_{32})cs & \bar{e}_{14} &= (e_{15} - e_{24})cs \\
\bar{e}_{24} &= e_{24}c^2 + e_{15}s^2 & \bar{e}_{15} &= e_{15}c^2 + e_{24}s^2, \quad \bar{e}_{25} = (e_{15} - e_{24})cs
\end{aligned} \tag{A.3}$$

The dielectric constants in global coordinates are given by:

$$\begin{aligned}
g_{xx} &= g_{11}c^2 + g_{22}s^2 \\
g_{yy} &= g_{11}s^2 + g_{22}c^2 \\
g_{xy} &= (g_{22} - g_{11})sc
\end{aligned} \tag{A.4}$$

where $c = Cos\theta$, $s = Sin\theta$

Relation of $[e]$ as function of $[d]$ and $[Q]$ is given by:

$$\begin{bmatrix} 0 & 0 & e_{31} \\ 0 & 0 & e_{32} \\ 0 & 0 & 0 \end{bmatrix}_k = \begin{bmatrix} 0 & 0 & d_{31} \\ 0 & 0 & d_{32} \\ 0 & 0 & 0 \end{bmatrix}_k \begin{bmatrix} Q_{11} & Q_{12} & 0 \\ Q_{12} & Q_{22} & 0 \\ 0 & 0 & Q_{66} \end{bmatrix}_k \tag{A.5}$$

APPENDIX B: Preparation of Specimen of Smart Laminated Beam

The procedure of preparation of smart laminated beams is described in detail in the Figures B1-B.8.

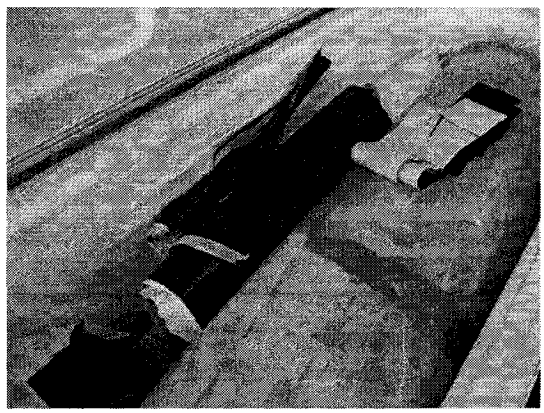

Figure B.1 Selecting the composite preparage from freezer

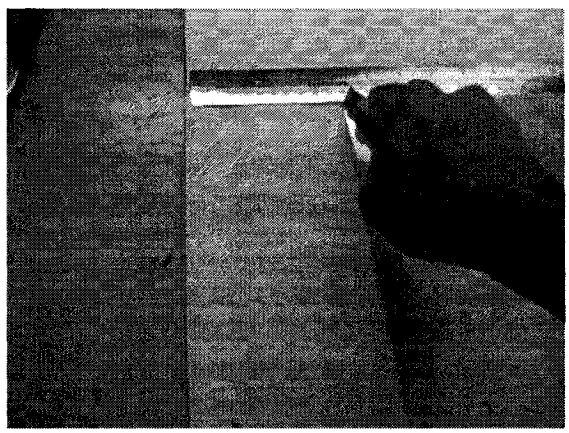

Figure B.2 Cutting the layers according to desired laminate figuration

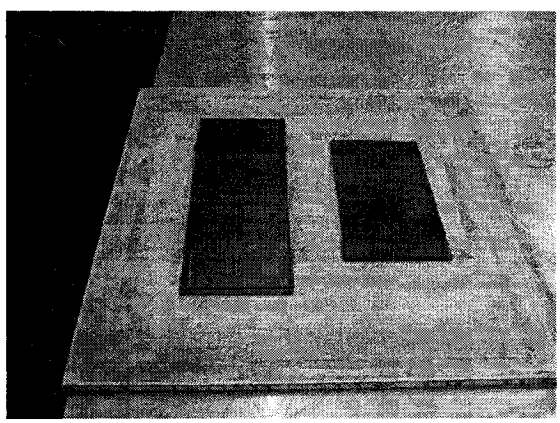

Figure B.3 Hand lay up and making the laminate

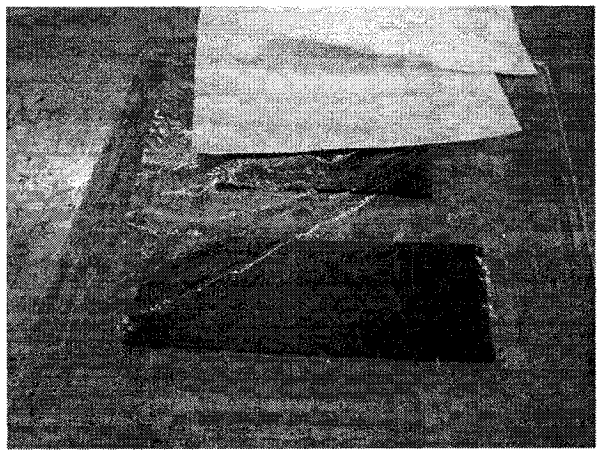

Figure B.4 Putting the releasing plastic and bleeders

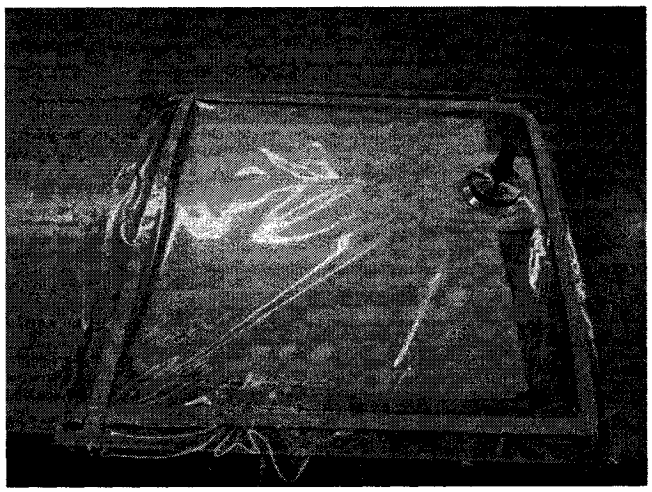

Figure B.5 Sealing bag and putting the vacuum valve

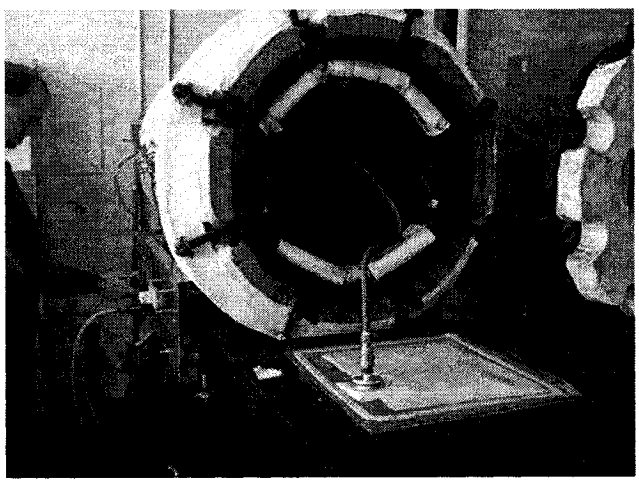

Figure B.6 Vacuum the bag before putting in autoclave

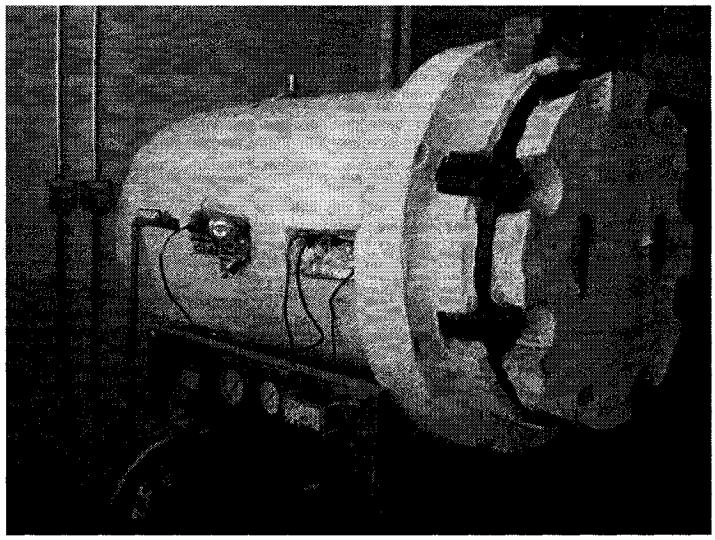

Figure B.7 Putting in autoclave

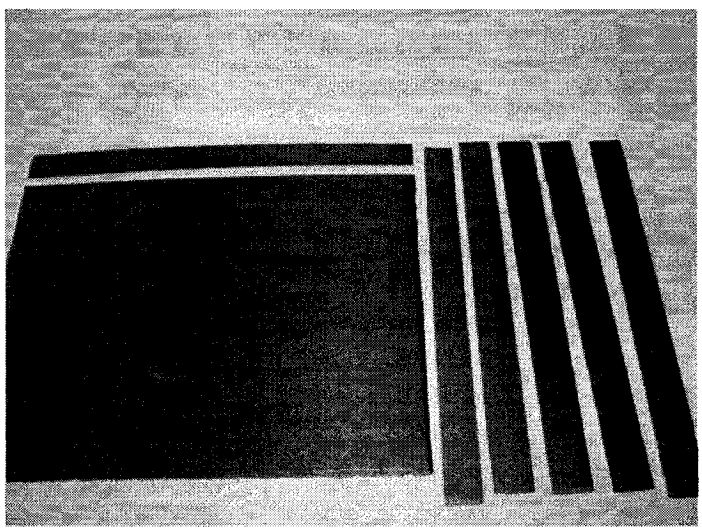

Figure B.8 Cutting the laminated plates to make beams

APPENDIX C: Testing Composite Material

Composite materials are degrades in time, thus to validate a very accurate mathematical model such as layerwise displacement theory, it is very important to use accurate values of material properties. Therefore, the composite materials are tested to determine the elastic modulus. In this order, two common machine are utilized, DMA and MTS machines. In the following both test are described.

Dynamic Mechanical Analyzer (DMA):

The Du Pont 983 Dynamic Mechanical Analyzer (DMA) is a highly sophisticated mechanical module that can be used with the Du Pont 9900 thermal analyzer running at least version 6.0 software. The 983 DMA is an instrument that offers a rapid and sensitive means to simultaneously obtain an elastic modulus (stiffness) and a mechanical damping (toughness) for the materials. The 983 DMA module measures changes in the viscoelastic properties of materials resulting from changes in temperature, frequency and time. There are four modes of operations: resonant frequency, fixed frequency stress relaxation and creep. Each of these modes measures different aspect of the viscouelastic properties.

Test specimen for this machine are 3 laminated beam ($1\times 5 cm^2$) with four layer 0 orientation to determine E_1 and 3 specimen of the same size with 90 degree orientation to determine E_2.

Principle of operation:

The sample is clamped in between two parallel arms and is deformed under a constant stress, oscillating stress or a constant strain, depending on the experiment mode. The behavior of the sample under this deformation is monitored by a linear variable displacement transducer (LVDT).

When operating DMA 983, in fixed mode, the sample and arms form a compound system, the system is oscillate under a fixed frequency using a sinusoidal driver signal. The sample displacement is monitored by LVDT and the lag between the driver signal and the LVDT is the phase angle. The phase angle the driver signal are used to calculate the storage, loss modulus and tan delta of the sample. Some of the most desired results of the test are given as: E': flexure storage modulus, E'': flexure loss modulus, G': shear storage modulus, G'': shear loss modulus.

Figures C.1 and C.2 shows results of DMA for E1 andE2.

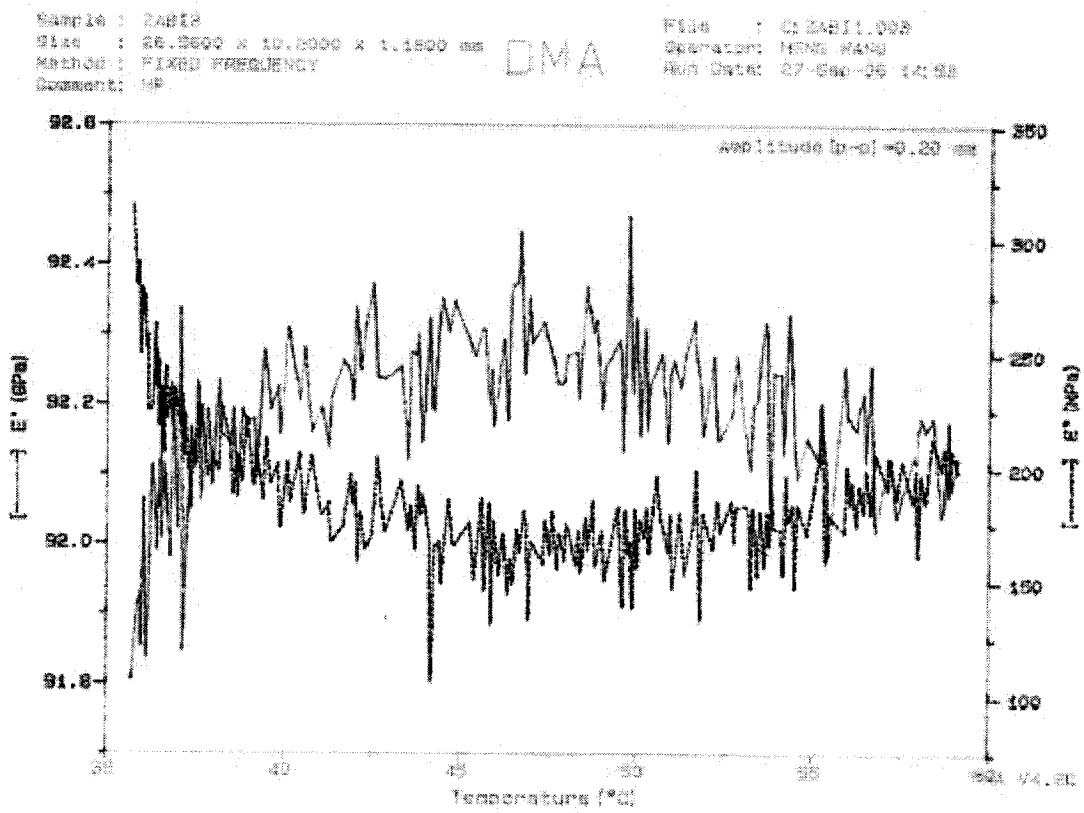

Figure C.1 Result of DMA (dynamic mechanical analyzer for E1 (sample is 6 layers 0)

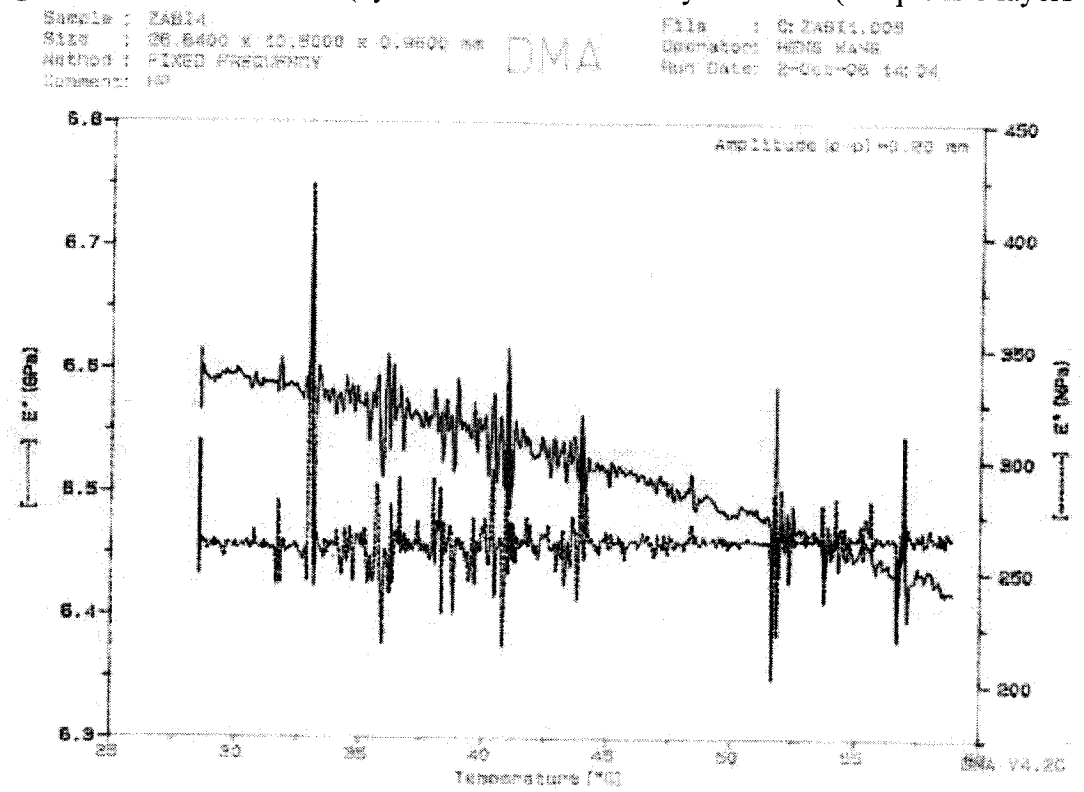

Figure C.2 Result of DMA (dynamic mechanical analyzer for E2 (sample is 6 layers 90)

Tensile test:

Three test specimens have been prepared according to standard ASTM, the griping force is set to 14 Mpa and rate is set to 100N/sec.

Specimen # 1: 122.25x15.5x1,

Specimen #2:122.34x15.6x1.02,

Specimen #3:122.5x15.3x1.02

The procedure of test is described in detail in Figures C 3-C10.

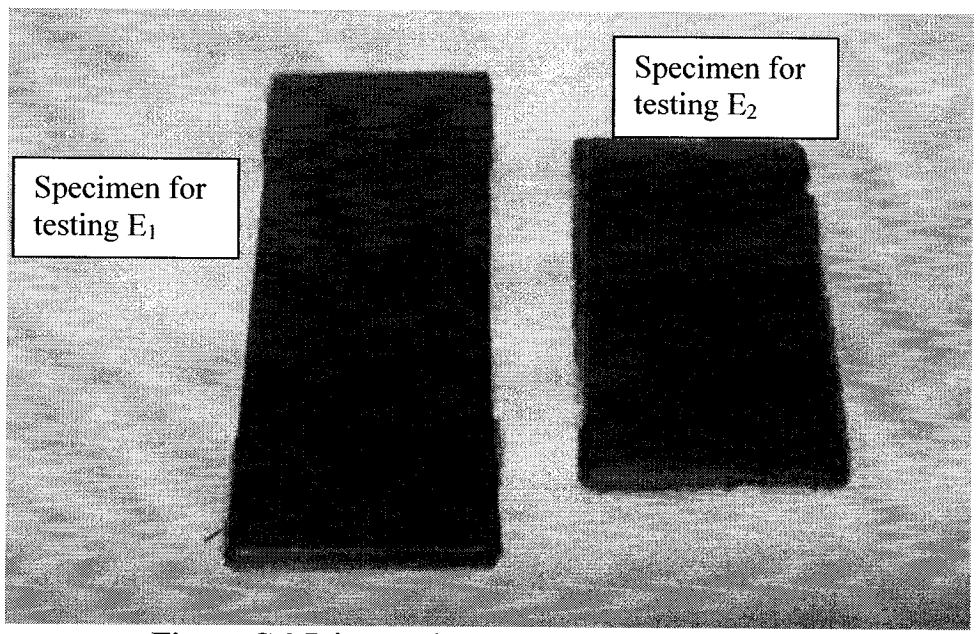

Figure C.3 Primary plate prepared for test specimen

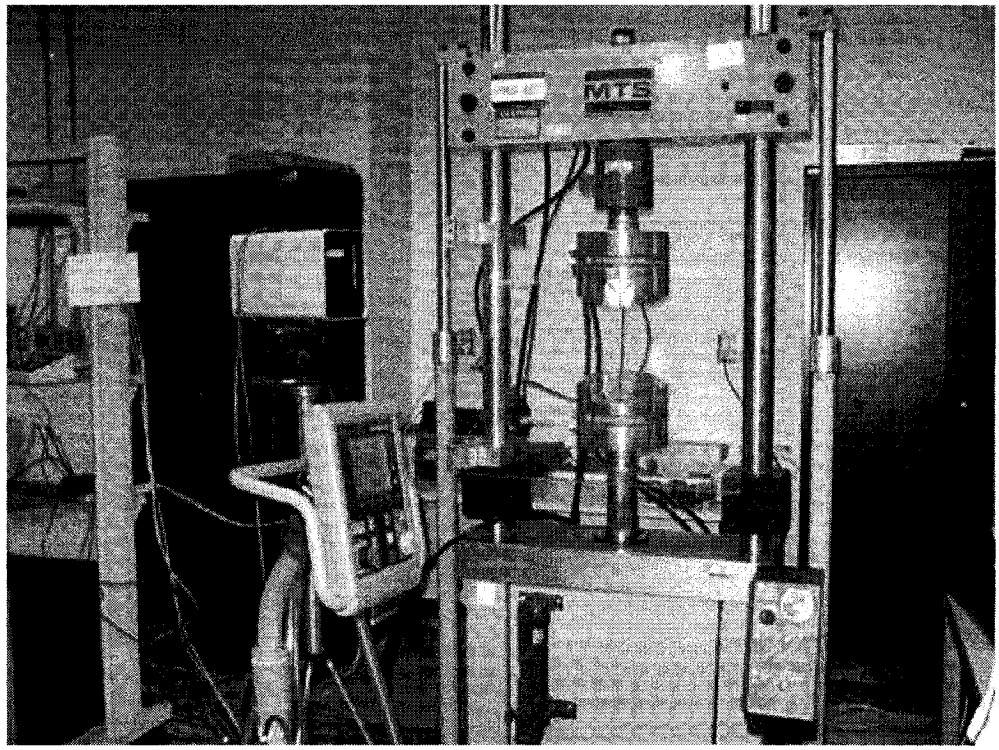

Figure C.4 MTS machine

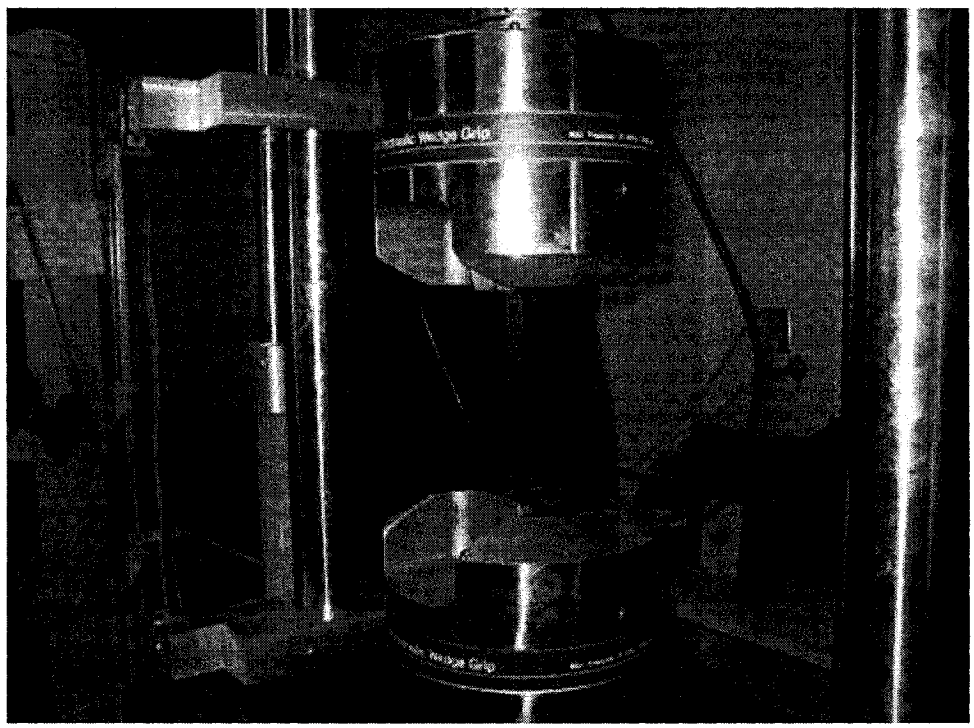

Figure C.5 The specimen is clamped in MTS machine

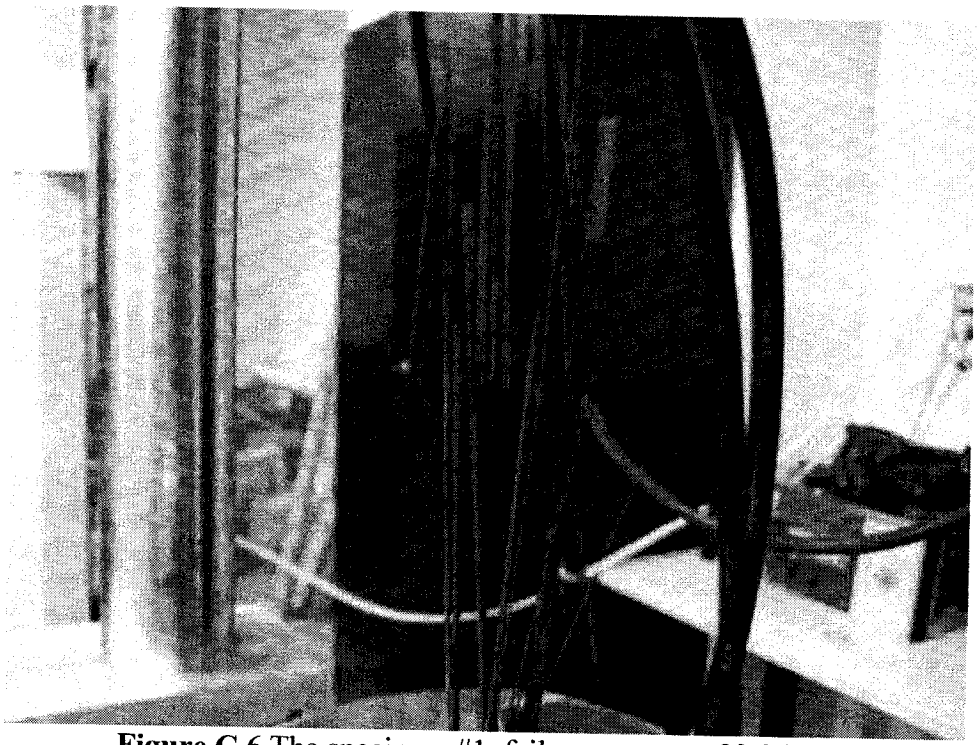

Figure C.6 The specimen #1, failure occurs at 32.061KN

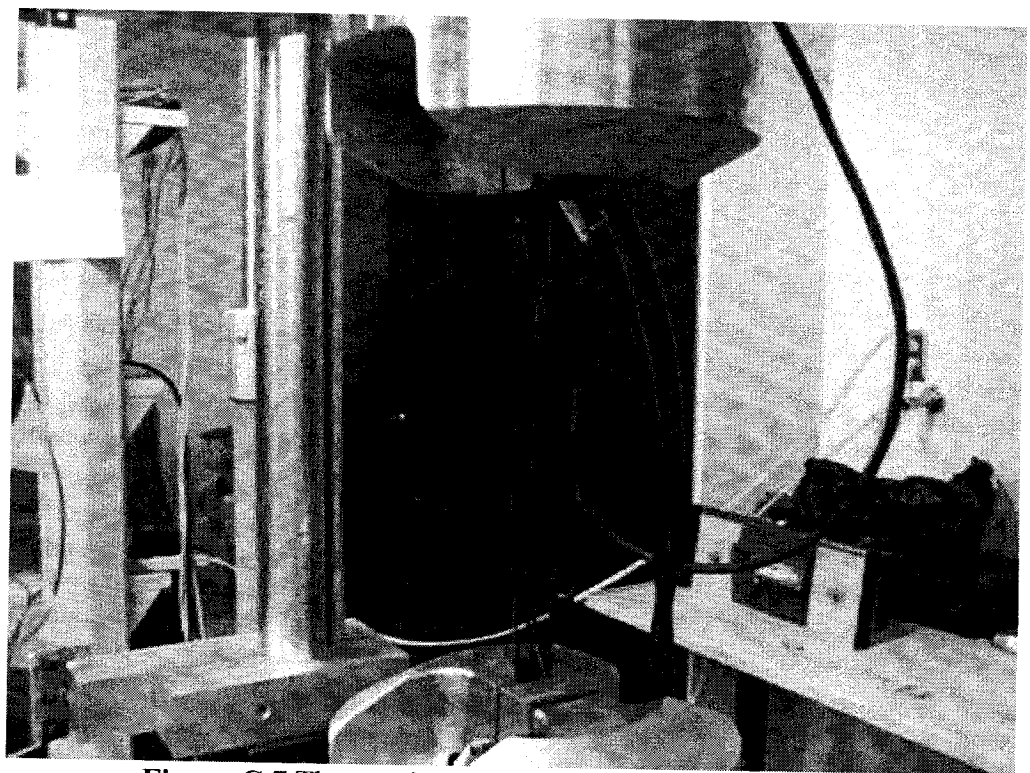

Figure C.7 The specimen #3, failure occurs at 28.292KN

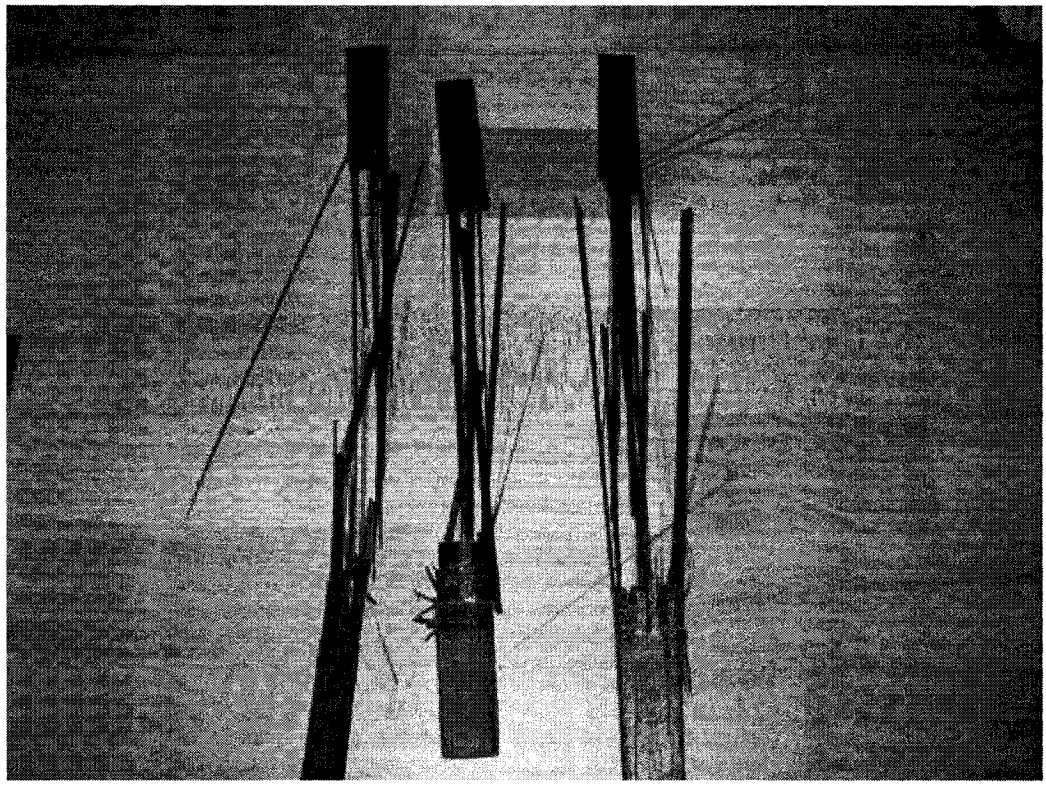

Figure C.8 The specimen failure: #1:32.061KN, #2: 29.218KN, #3: 28.292KN

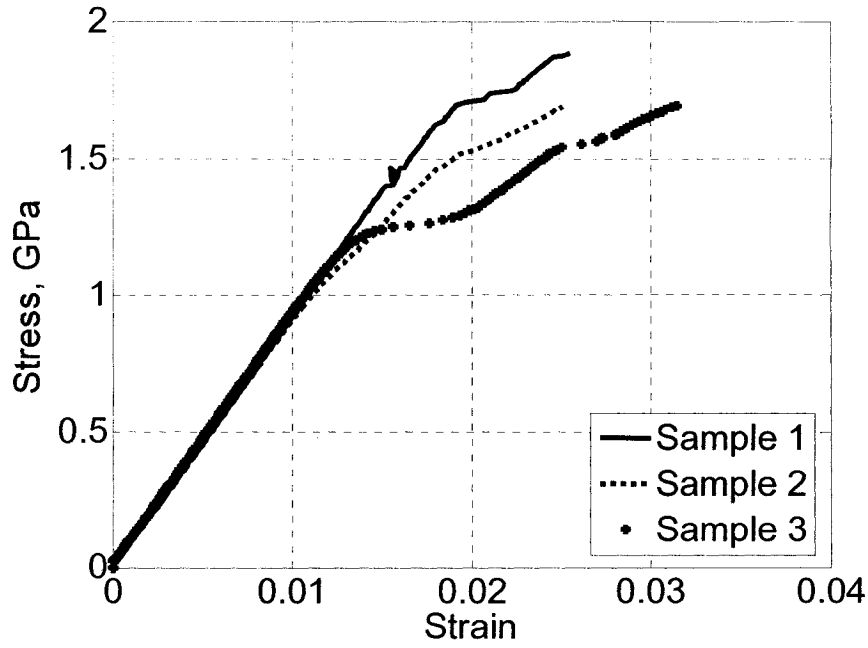

Figure C.9 Stress-strain relation for unidirectional (0^{o}) samples

APPENDIX D: Experimental Works

In this section a brief description of the experimental works and some helpful tips and techniques are provided.

Step 1: Cutting PVDF sensor element

Cut $2 \times 2\, cm^2$ from the corner of the PVDF sheet as shown in Figure D.1. Pay attention to the orientation of the polling direction. Also, one should take care when handling PVDF material, it should be handled wearing vinyl gloves because oily finger may results in localized oxidation and changes to the surface resistively. PVDF sensors used in this work are piezofilm with 28 μm and two sided electrodes (Measurement Specialties Inc., 1000 Lucas way, Hampton, VA, 23666). More technical information about the sensors can be obtained from www.piezofil.com

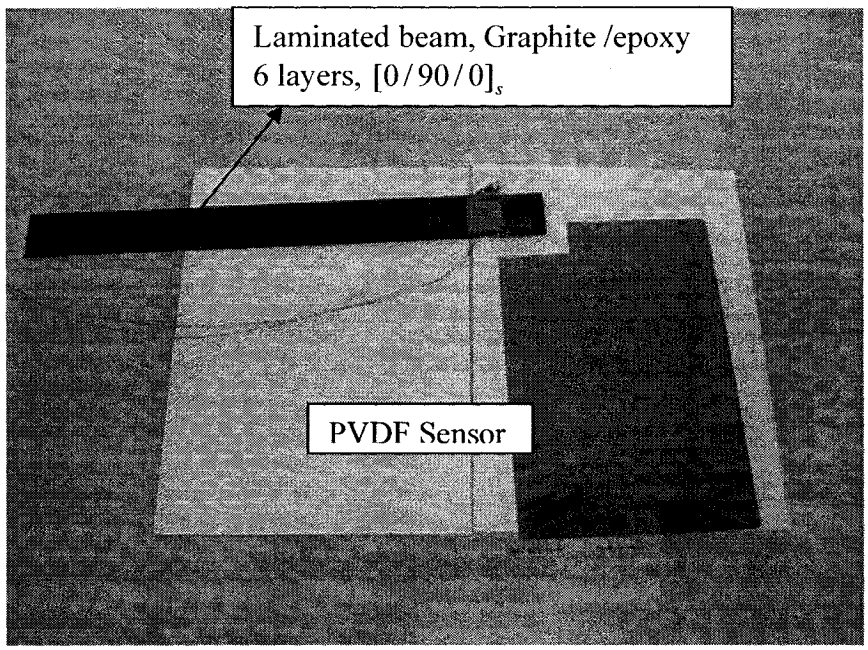

Figure D.1 Cutting PVDF sensor and bonding to the beam

Step 2: Bonding Sensor to the laminated beam

Use non-conductive epoxy glue to make a perfect bonding between sensor and the host structure. Connecting electrodes are chosen a thin strip of copper for higher accuracy. Connecting wires is also 5 μm diameter. To protect the sensor connection, an extra tape is used to cover the arrangement and keep that in place. (Figure D. 2)

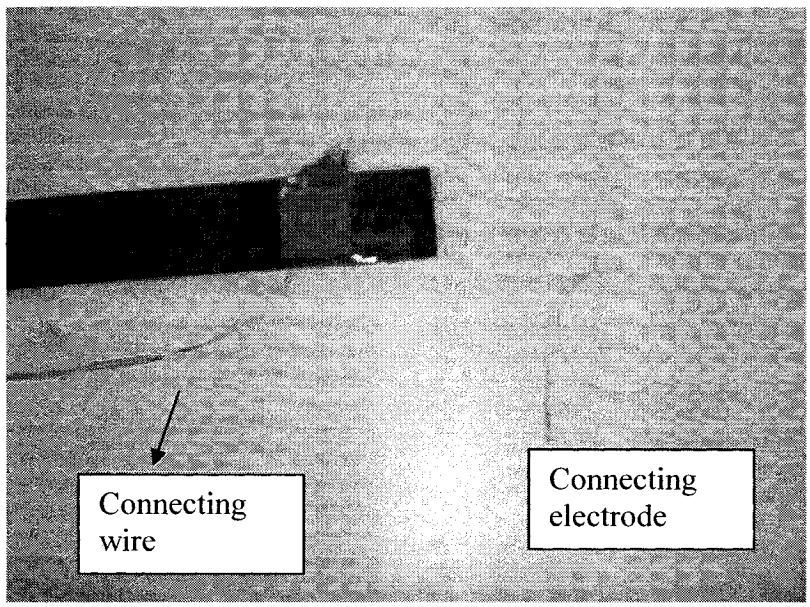

Figure D.2 Bonding electrode to output

Step 3: Mounting PZT actuator

Use non-conductive epoxy glue to mount the PZT material. Since the electrodes should be connected to both sides of the PZT, electrodes should be mounted before gluing the element to the host beam. (Figure D.3). It should be noted that PZT materials are very brittle and should be handled with more care.

PZT Actuators used in this work are BM500, $1\times1 in^2$ ("Sensor Technology Limited", PO Box 97, Collingwood, Ontario, Canada) with $\rho = 7650 Kg/m^3$ and thickness of 0.3 mm and $d_{31} = -160\times10^{-12}\ C/N$. For other information one may visits www.sensortech.ca

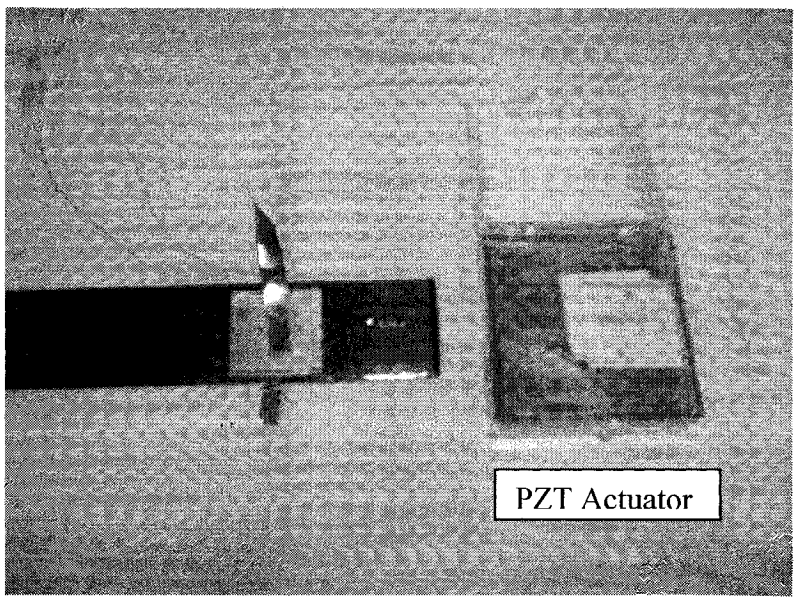

Figure D.3 Mounting piezoceramic actuator to the beam

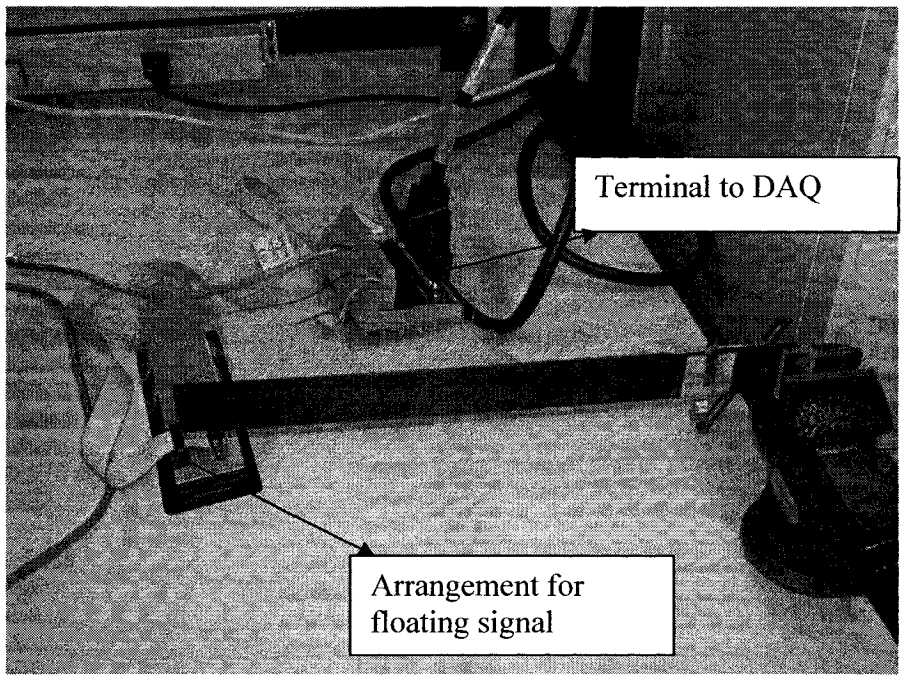

Figure D.4 Boundary conditions and wire connections

Step 4: Connecting to the DAQ board

Connect the input and output connections according to the DAQ manual instruction. In order to acquire a better signal from sensor, an arrangement of resistors, according to the DAQ manual is required.

Since the maximum output voltage from the DAQ board is ± 10 volts, but the voltage required to actuate the PZT is about ± 200 volts, we need a voltage amplifier. An in-house voltage amplifier is designed using a high voltage amplifier (Figure D.5). It is composed of a commercial minatory high voltage amplifier provided by EMCO (± 200 V http://www.emcohighvoltage.com/), cooling parts and connecting board. However, this voltage amplifier requires a external power supply. (DC Power supply, GW-Dual Tracking with 5 V fixed Model: GPC-303D).

Figures D. 6 and D. 7 show the physical and schematic ready to test set ups. The first experiment is performed in open-loop to achieve the natural frequency and damping factor of the smart laminated system. The block diagram of this test for LABVIEW 7 software is given in Figure D.8.

After performing the open-loop properties of the system and validating the mathematical modeling, variety of closed loop have been performed for different purposes. A typical closed-loop block diagram is provided in Figure D. 9.

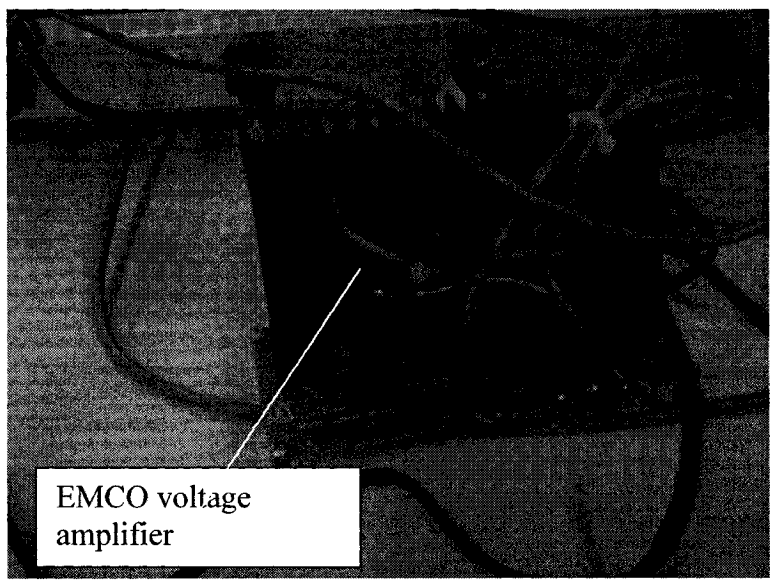

Figure D.5 In-house voltage amplifier

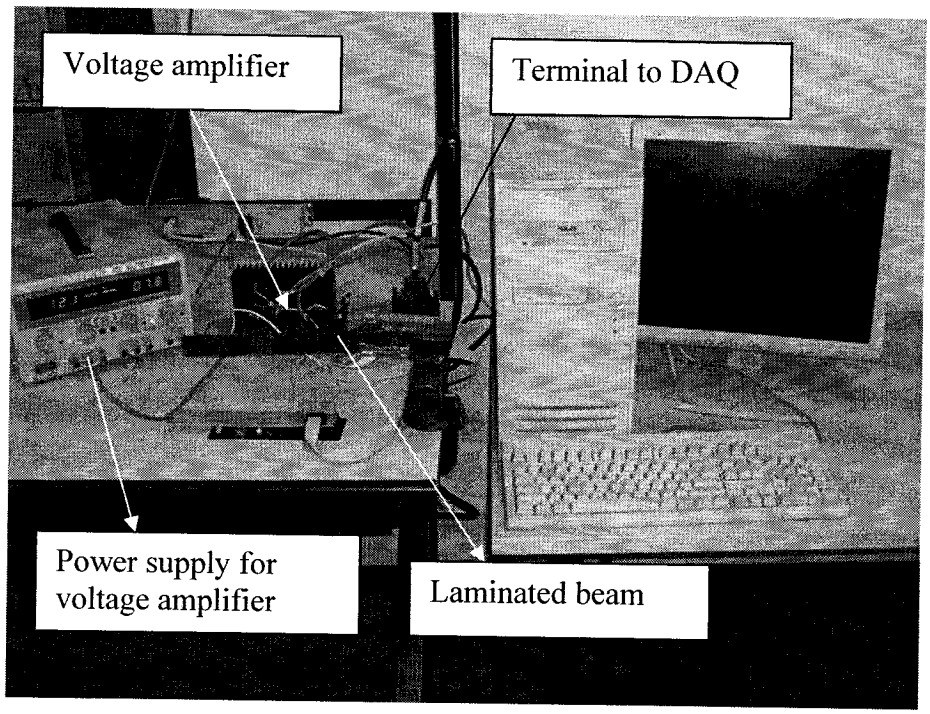

Figure D.6 Ready to test

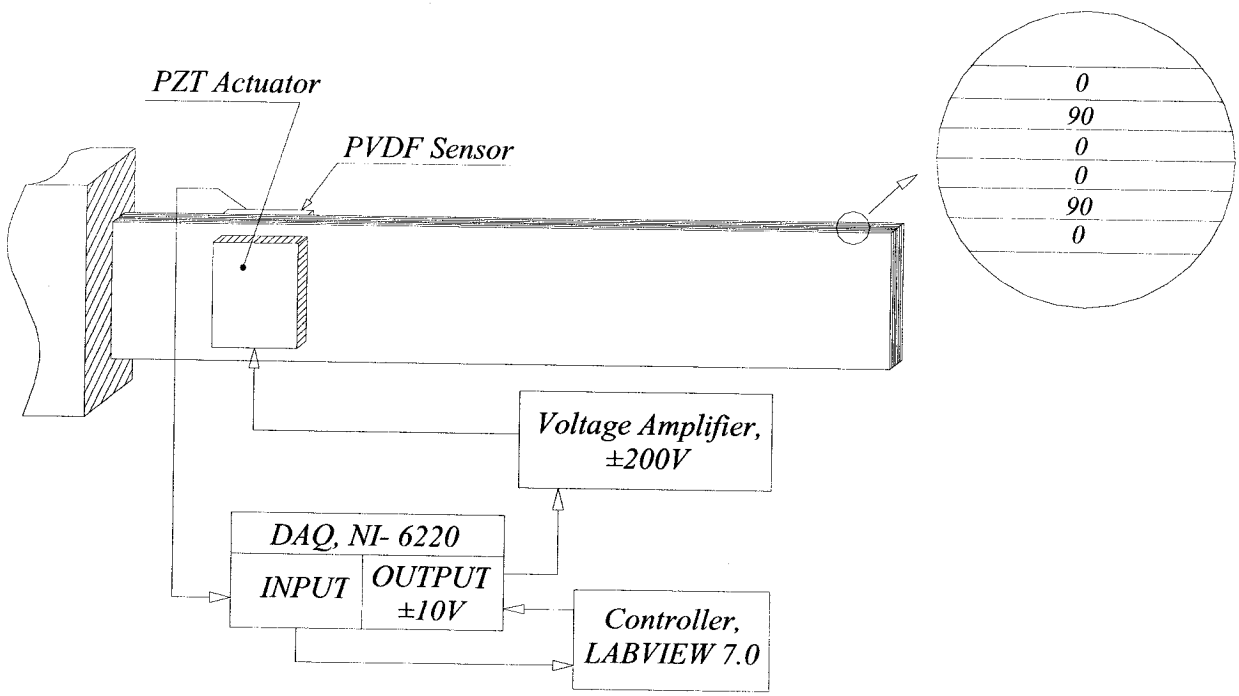

Figure D.7 Schematic experimental set up

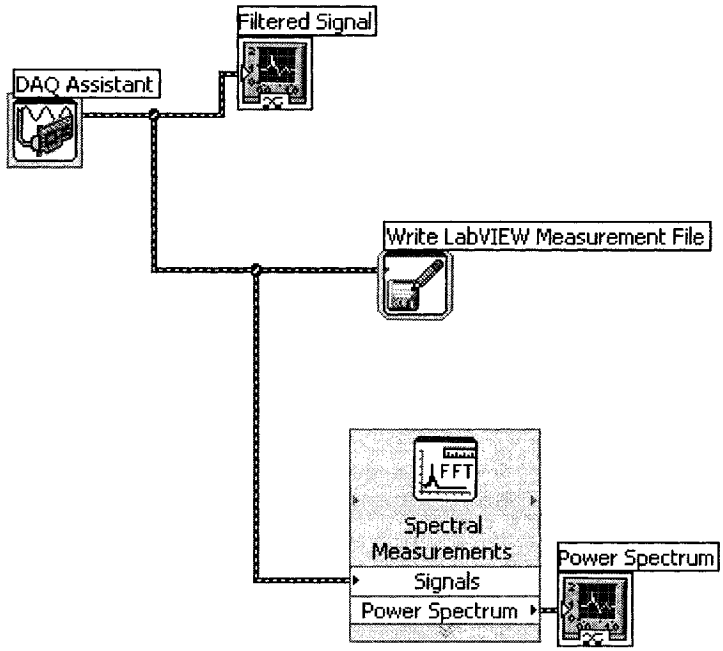

Figure D.8 Open-loop block diagram

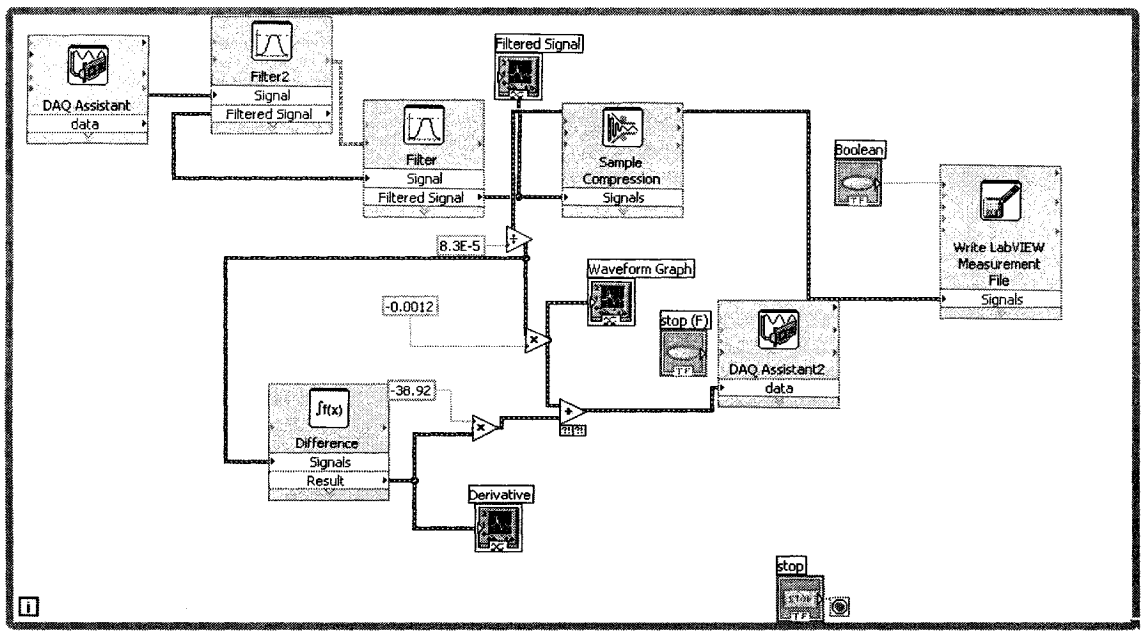

Figure D.9 Closed-loop block diagram